EFFECTS OF PROCESS VARIABLES AND MICROSTRUCTURES

ON PROPERTIES OF ELECTROSLAG WELDMENTS

Srivathsan Venkataraman
B.Sc., University of Madras, India, 1973
B.E., Indian Institute of Science, India, 1976

A dissertation submitted to the faculty
of the Oregon Graduate Center
in partial fulfillment of the
requirements for the degree
Doctor of Philosophy
in
Materials Science

November, 1981

The dissertation "Effects of Process Variables and Microstructures on Properties of Electroslag Weldments" by Srivathsan Venkataraman has been examined and approved by the following Examination Committee:

William E. Wood, Thesis Advisor
Professor

Jack H. Devletian
Associate Professor

Nicholas G. Eror
Associate Professor

Lynwood Swanson
Professor

DEDICATION

I dedicate this work to Mrs. Ellen Sharma (1898-1978), a great educator and social worker of Madras, India. I was able to reach this highest goal of my life mainly because of her love, care, and kind sponsorship.

ACKNOWLEDGEMENT

I express my appreciation and sincere thanks to Dr. W. E. Wood for his valuable guidance and encouragement throughout this work. I also thank Drs. N. G. Eror, J. H. Devletian, D. F. Barofsky, and L. Swanson for their efforts in planning my Ph.D. program and examining my dissertation.

My sincere appreciation goes to Dr. D. G. Atteridge for his helpful advice during this work, as well as the Battelle Northwest Laboratories staff for their assistance in weld impact toughness testing. I also thank M. Coffey and the ESCO Corporation for their help in spectrographic chemical analyses of welds.

I express my gratitude for the extensive help I received from R. B. Turpin, M. Scholl, D. K. Johnsen, Dr. K. H. Khan and Dr. P. A. Molian during this work. My sincere thanks to Ms. N. A. Fick and Mrs. B. P. Ryall for their assistance in the preparation of this dissertation.

I acknowledge the U. S. Department of Transportation for sponsoring this research work.

TABLE OF CONTENTS

LIST OF TABLES

LIST OF FIGURES

Page

ABSTRACT

Effects of Process Variables and Microstructures
on Properties of Electroslag Weldments

Srivathsan Venkataraman, Ph.D.
Oregon Graduate Center, 1981

Supervising Professor: William E. Wood

Electroslag weldments, while economically attractive, exhibit low

impact toughness and lack of reliable non-destructive inspectability.

The purpose of this investigation was to improve the reliability and

integrity of electroslag weldments through control of welding process

variables, improvements in as-welded microstructure and weld metal alloy

additions.

The influence of process variables including electrode position,

slag level, welding current, voltage, guide tube geometry and joint

spacing on A588 structural steel consumable guide electroslag weldments

were investigated. Plate grounding and electrode positioning were criti-

cal to control the weld symmetry, and proper slag level maintenance was

necessary to control the process stability and weld microstructure. The

welding current vs. wire feed rate relationship was influenced by the

guide tube design and joint spacing, and the use of a winged guide tube

enabled lower welding voltages. The high current/narrow gap/winged guide

tube weld provided a 50% reduction in specific heat input and heat

affected zone width and a 67% reduction in weld time.

Grain refinement in the as-welded condition was achieved by shield-

ing the consumable guide tube with either a mullite or fused quartz

sleeve combined with a supplemental vibration of the consumable guide tube in the case of mullite. Several other weld puddle agitation techniques were also studied. A hypothesis for the grain refinement mechanism is presented.

Alloy additions were made through either elemental wires welded on to the guide tube or alloyed filler electrodes. Weld metal alloy additions provided a better control over the proeutectoid ferrite films bordering grain boundaries in standard welds.

Both standard and fatigue precracked CVN toughness tests were carried out for several electroslag welds. Standard electroslag welds possessed least toughness at mid-thickness weld centerline location (4 ft.lbs. at 0°F). Crack propagation along proeutectoid ferrite films was observed. High current/narrow gap welds posted an improvement in mid-thickness weld centerline toughness (11 ft.lbs. at 0°F). Both grain refined and alloyed welds showed limited variations in toughness across their width. The high current/narrow gap weld made with chromium and molybdenum alloyed filler wire possessed much improved mid-thickness weld centerline toughness (17 ft.lbs. at 0°F).

Optical, scanning and transmission electron microscopy were carried out for weld microstructure evaluations.

1. INTRODUCTION

The electroslag welding (ESW) process was developed originally in the Paton Electric Welding Institute, USSR, in the early 1950's.[1] Later, countries such as Czechoslovakia (Bratislava Institute of Welding) and Belgium (Arcos Corporation) made further contributions to the development of the process[2] and the welding technique was introduced into the United States in 1959 by the Arcos Corporation.[3] Since then, the process has been used in heavy structure fabrications, which includes bridges. In the mid-1970's, several bridge failures occurred in service and their study revealed that brittle fracture initiated at the electroslag welded joints. Based on those facts, the Federal Highway Administration prohibited the use of the electroslag weldments on main structural tension members on any federally-aided projects.[4] This thesis research has established the fundamental relationships between process variables, microstructure and properties of electroslag welds in A588 structural steel.

ESW is a joining method in which a molten slag melts the filler metal and the surfaces of the work to be welded. The molten weld pool is shielded by the molten slag, which moves along the full cross section of the joint as the weld progresses. The process is initiated by an electric arc between the electrode and the bottom of the joint. Powder flux is then added and melted by the heat of the arc. Once a layer of the molten slag is established (1.5 to 2 inches), the arc stops and the welding current (500-700A) passes from the electrode through the slag by

electrical conduction. The passage of the current provides the necessary heat for fusion.

The ESW process requires a large heat input accompanied by slow cooling, when compared to other welding processes. To assist the extraction of this large quantity of heat evolved during the process, water cooled copper shoes are used on both sides of the plates being welded. In addition to heat extraction, these shoes contain the molten pool during welding and provide the final weld contour. Usually, electroslag welds are prepared in the vertical or the near vertical direction. The welding technique utilizes a starting sump and a runoff block to eliminate defects associated with the initiation and the termination of the process.

There are two types of ESW. They are conventional ESW and consumable guide ESW. The conventional ESW system utilizes a non-consumable contact tube to direct the electrode into the molten slag pool (Figure 1). The contact tube is maintained at about 2 inches above the slag pool surface. The entire welding head along with cooling shoes is moved upward at a predetermined rate consistent with the welding speed.

The consumable guide electroslag welding system uses a tube to guide the welding electrode into the slag pool (Figure 2). At the start, the guide tube is positioned with its tip at about 1-1/2 inches above the bottom of the joint. As the name implies, the guide tube is consumed into the weld pool as the weld progresses. This method involves no moving parts except the welding electrode.
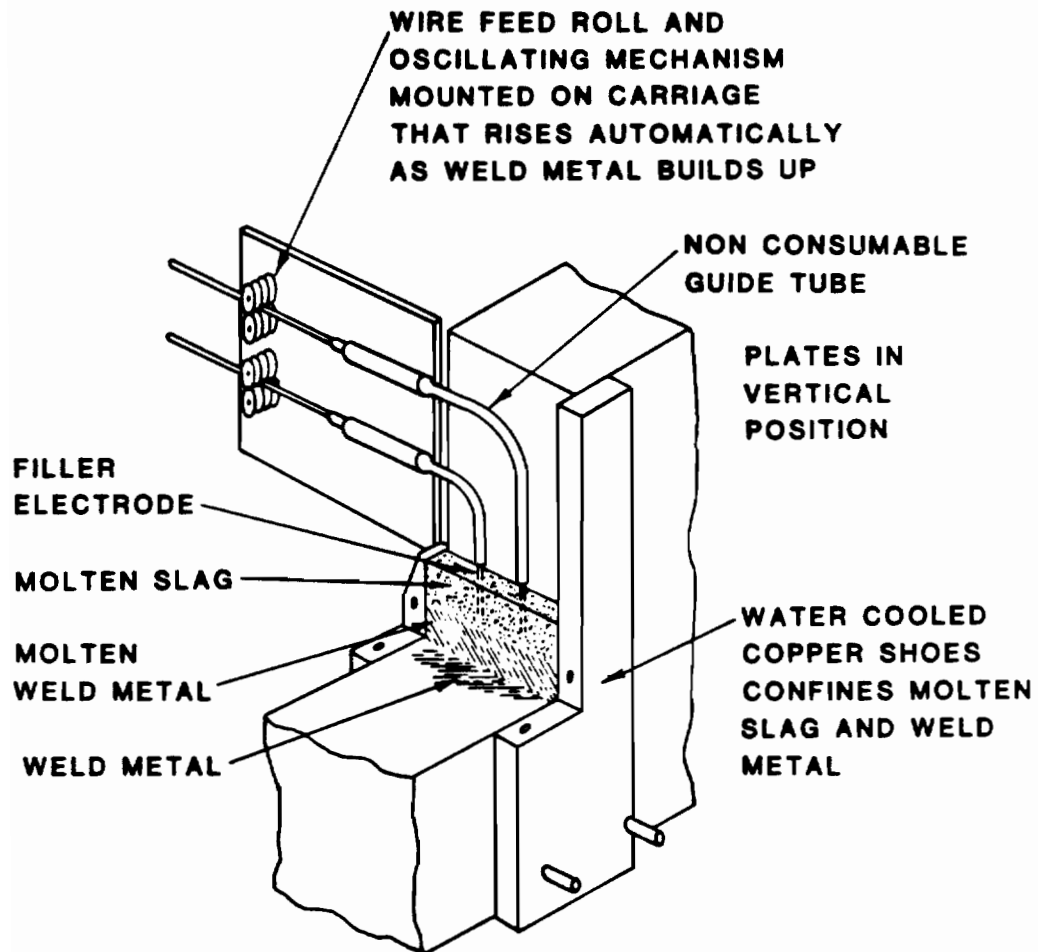
Figure 1.   SCHEMATIC REPRESENTATION OF CONVENTIONAL ELEC-
TROSLAG WELDING PROCESS (NON-CONSUMABLE GUIDE).
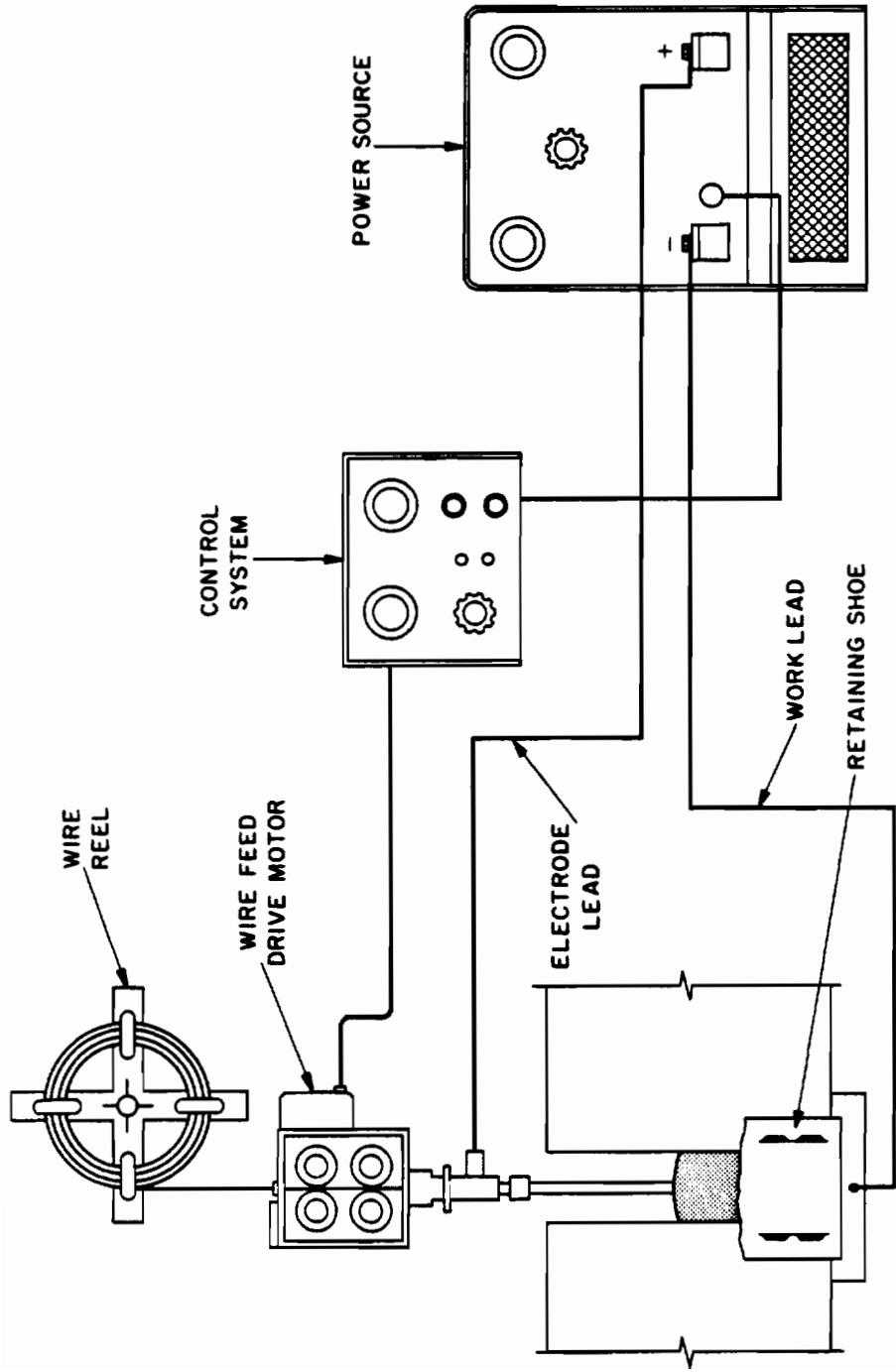
Figure 2. SCHEMATIC REPRESENTATION OF CONSUMABLE GUIDE ELECTROSLAG WELDING PROCESS.

ESW provides great savings in manpower, time and welding consumables, especially for welding thicker sections. Sections several inches in thickness can be welded in a single pass by selecting a suitable number of electrodes and/or electrode oscillation. The sections being welded do not require any edge preparation; the weld pool size, the high heat input, and welding speed eliminate the necessity for preheating. As the process is associated with a slow weld cooling rate, the distortion involved is minimal when compared to other processes. The slag/metal reaction involved in the process provides sound, "defect-free" welds, if properly controlled.

Despite these advantages, there are certain problems associated with the process. Once initiated, the process has to be completed without interruption. Intermittent stopping produces serious defects at restart locations. The large heat input associated with the process results in a coarse cast structure in the weld metal with anisotropic mechanical properties. In addition, the grain orientation and segregation lead to hot cracking near the center of the weldment. The prolonged thermal cycles in the base metal adjacent to the fusion line produces a coarse-grained heat affected zone which is more susceptible to brittle fracture than the parent material. In addition, the coarse structure of the weld metal and the heat affected zone inhibits reliable non-destructive testing of the weldments.

Many of these problems may be solved if the fundamental factors that control these features are understood. First of all, the successful application of the ESW process depends strongly on the ability to produce

sound, defect-free welds. Process variables such as voltage, current, slag depth, root gap, guide tube geometry, heat input, etc., control the weld quality more critically than anticipated in the past and a thorough understanding of the influence of each of these variables on the weld quality is essential.

Also, anisotropic weld properties result from microstructural variations in the weld fusion and heat affected zones (HAZ). The refinement of the coarse cast structure of the weld metal and the reduction of the coarse grained HAZ width will aid in improving the mechanical properties and non-destructive evaluation. Alloy additions to the weld metal will also enhance the properties by altering the weld microstructure.

This investigation studied the influence of these variables on both weld microstructures and properties, and to determine the process conditions that consistently produce reliable, sound electroslag welds with improved mechanical properties.

1.1. Background

ESW of thick section materials requires a large heat input in comparison to other welding processes. Both low heating and cooling rates result in a long dwell time at high temperatures. These features account for the complex HAZ and weld metal microstructures present in electroslag weldments.

The HAZ can be divided into two regions, namely, the coarse grain zone formed in the base metal immediately adjacent to the fusion line, and the fine grain zone found at a distance from the fusion line (Figure

3).   In mild steel, the coarse-grain HAZ consists of large equiaxed

grains bounded by a proeutectoid ferrite network. The grain interior

is normally made up of Widmanstatten structure.[2,5] A bainitic structure

has been reported in this region for A588 materials.[6] This coarse-grain

HAZ structure formation is due to the thermal cycle experienced in the

base metal adjacent to the fusion line during welding. This zone is

heated well above AC_3 temperature, which results in complete transforma-

tion to austenite. Extensive growth of these austenite grains occurs

due to the long dwell time at high temperatures which is at a maximum

near the fusion line. Upon cooling, ferrite is nucleated in the interior

as well as the boundaries of the large austenite grains. The matrix

ferrite grows in an acicular morphology (Widmanstatten structure) prior

to the initiation of pearlite transformation. The resulting microstruc-

ture is coarser than the starting structure of the base metal[2] and may

vary according to the base metal chemistry.

The weld metal consists of a coarse columnar grain (CCG) zone loca-

ted on the weld periphery. In this zone, the grains grow mainly in the

direction of the heat flow. As the CCG zone develops, the heat removal

becomes increasingly retarded and at a certain distance from the fusion

boundary, a more refined thin columnar grain (TCG) structure is achieved.

These are the two major structural zones usually observed in electroslag

welds made using water-cooled copper shoes (Figure 3).   In welds made

using shoes with no supplemental cooling provisions, an additional equi-

axed grain structure may be present at the weld center. Under certain
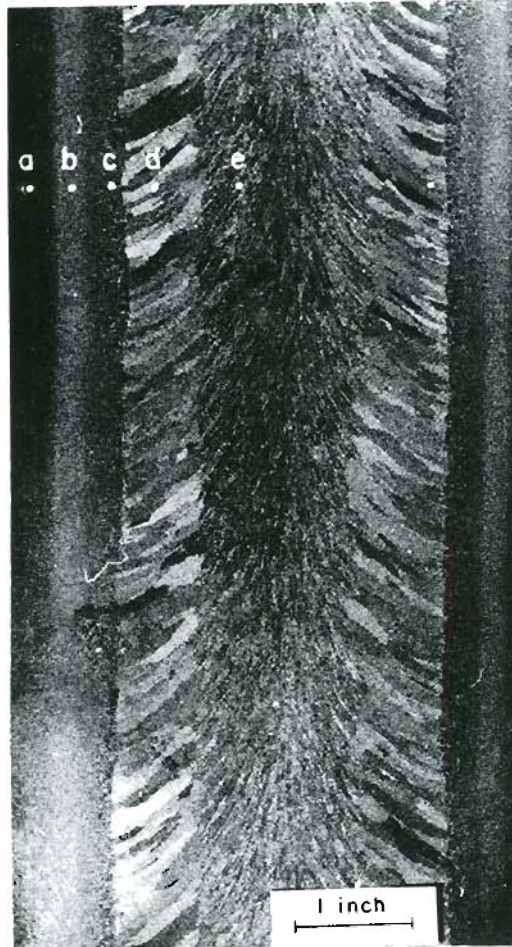
Figure 3. STANDARD ES WELD MACROSTRUCTURE INDICATING VARIOUS STRUCTURAL ZONES PRESENT

a. Base Metal   b. HAZ 2   c. HAZ 1   d. Coarse Columnar Grain Zone   e. Thin Columnar Grain Zone

process conditions, only one morphology may exist. Welds made with low current and voltage and with high thickness of base metal per electrode may contain only CCGs. On the other hand, welds with minimum penetration may consist solely of TCGs.[5]

The structure of the weld is, to a great extent, determined by the chemical composition and conditions governing the solidification of the weld pool. The temperature, the volume of the weld pool, the holding time of the melt at this temperature, the direction and the intensity of the heat removal, the intensity of the agitation of the liquid metal, etc., control the weld metal grain size.[5] Since grain growth occurs perpendicular to the surface of the weld pool (direction of the heat flow), the radial-axial grain growth results. The weld center consists of TCGs oriented parallel to the welding direction. Both coarse and thin columnar grains are bordered by proeutectoid ferrite films and the grain interior consists of a Widmanstatten structure. Transverse solute bands are also observed in most electroslag weldments.[7] The columnar grains change neither their orientation nor their shape while growing across these bands of chemical inhomogeneity.

The complex, directional microstructure of electroslag welds is governed by several process variables and the weld metal chemistry. The structure directionality also results in anisotropic weld metal mechanical properties. The influence of these variables on both the weld structure and properties, as reported by previous investigators, will be presented in the following sections.

1.1.1. Process Variables. Although the large heat input associated
with ESW process is a major concern, the total weld heat input is not of
primary significance in determining the weld characteristics. The in-
teraction of the electrical variables, namely current, voltage and re-
sistance as well as the influence of factors such as geometry, electrode
types and positioning, slag depth, guide tube geometry, welding speed,
weld pool agitation, and material being welded determine final character-
istics of the weld. Variations in one or more of these conditions may
result in significant spatial variations in weld properties. Hence, com-
plete understanding of the influences of these variables on the weld
characteristics is necessary to produce welds with consistent structure
and properties.

1.1.1.a. Current, Voltage and Resistance. In standard prac-
tice, electroslag welding is performed using a constant voltage-dc power
supply. In this system, current and electrode feed rate are interdepen-
dent and increasing the electrode feed rate increases the welding current.
Several investigators[8-10] have found a linear relation between the current
and electrode feed rate at a fixed voltage, but Frost et al.[11] have re-
ported that at constant voltage, the current is proportional to the
square root of the electrode feed rate. Irrespective of the current--
electrode feed rate relationship, the current rise is slower than the
rise in the electrode feed rate. This leads to a decrease in unit power
input with increasing electrode feed rate.[2,5,11,12] Since the heat for
the welding process is obtained from resistance heating of the slag (I^2R),

the voltage and the current should be selected carefully to provide the proper unit input power. For example, a higher voltage is required when using low wire feed rates.[5]

Jones et al.[13] have suggested that, for a particular slag composition, the weld morphology is controlled by the current and voltage. According to their "most direct current path" assumption, there are two possible modes of current transfer occurring in ESW. Current is transferred from the electrode sides to plate edges and from the tip of the electrode to the bottom of the pool.

For a fixed current and varying voltages, the effective resistance is relatively large at a high voltage assuming an ohmic model. This will occur with a short electrode extension into the slag, and a majority of the heat will be generated near the top of the slag pool, much of which may be lost by radiation. Further voltage increases will eventually result in arcing at the slag surface.

On the other hand, at a relatively low voltage, ohmic behavior requires a much lower effective resistance. This leads to electrode extension nearly to the bottom of the slag pool. In this case, most of the current will then flow from the tip of the electrode to the bottom of the slag pool which provides the maximum heat generation at the bottom of the slag pool. As a result, less heat is available for base metal penetration.

Finally, with the voltage midway between the extremes, the electrode will extend a moderate distance into the slag pool, and the heat will be

primarily generated in the central region of the slag pool. The portion of the current flowing from the side of the electrode to the side of the slag pool will provide the heat for base metal penetration.

Hence, both voltage and current influence the heat distribution. Two major characteristics influenced by these variables are the shape and the size of the molten weld pool. The shape is expressed by the term "form factor". The base metal dilution (BMD) or the weld penetration indicates the weld pool size.

The form factor of an electroslag weld is defined as the ratio between the width and the depth of the weld pool and the weld grain orientation is determined by the shape of the weld pool. Welds possessing a low form factor in which grains meet butt end to butt end at the weld center are less resistant to hot cracking. Welds with medium and high form factors have a grain structure meeting at an acute angle at the weld center and are most resistant to hot cracking.[5] Welds made at higher voltages and lower currents possess high form factors while those made at low voltages and high currents possess low form factors. As a result, welds made using high current (high speed welds) are prone to centerline cracking.[14]

The BMD, expressing the size of the weld pool as well as the proportion of the base metal in the weld metal, is determined from the relation

$$\text{Percent BMD} = \frac{b_w - b_g}{b_w} (100)$$

where b_w is the width of the weld, which is taken as the mean value of

the measurements at the edges and at the center of the weld, and b_g is

the initial spacing between the plates being welded.[5] The voltage in-

fluence on BMD is pronounced at medium voltages. At higher voltages,

the heat transfer efficiency is reduced and, as a result, the BMD de-

creases. At lower voltages, the BMD again decreases leading to lack of

penetration.[2,5] In certain investigations, intentional voltage varia-

tions have been made to produce diffused fusion boundaries.[14,15] The

current influence on BMD is negligible at medium currents.

From the foregoing, it is clear that the current and voltage para-

meters require very critical selection. Theoretical calculations sug-

gest possibilities for welding at low power levels. But, it is not

possible in practice due to the rapid conduction of the heat into the

base plates. Frost et al.[11] have considered these current and voltage

effects and have suggested an operable range to produce successful welds,

as shown in Figure 4. The lowest possible voltage is governed by a

threshold level for achieving complete penetration. The second boundary

is established by a critical energy input below which hot cracking may

occur at the weld center. The third boundary is set by the power supply

limitation and the final limit is established by the minimum electrode

velocity capable of producing defect-free welds.

The final electrical variable, namely the resistance, is a slag

property. The slag must be sufficiently conductive to carry the welding

current from the electrode to the weld pool and the edges of the plates

without arcing.[16] The electrical resistance of the molten slag controls
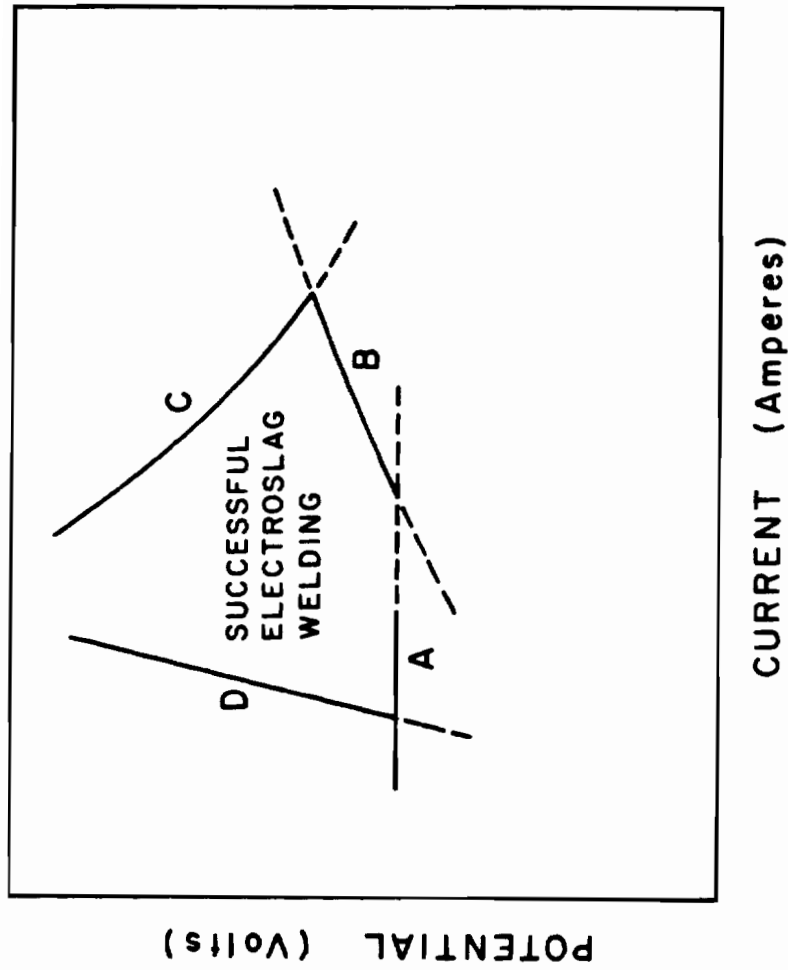
Figure 4. SCHEMATIC REPRESENTATION OF ESW PROCESS BOUNDARIES FOR SUCCESSFUL OPERATION:

A--THRESHOLD POTENTIAL, B--CRITICAL ENERGY INPUT, C--POWER SUPPLY LIMIT, D--MINIMUM ELECTRODE VELOCITY (FROST et al.[13]).

the current distribution in the slag pool and governs the weld pool shape. A high slag resistance will draw too little current, allowing the slag to cool. On the other hand, a low resistance slag will draw excessive current, raising the slag temperature. This temperature increase may increase the slag resistance in turn. For a stable process operation, the slag resistance should not change appreciably with temperature, and slag viscosity must be in the range between a "sluggishness" which would prevent settling of small metal droplets and fluidity which would leak through small crevices between the shoes and the work.[16] Calcium fluoride additions have been shown to increase the fluidity of the slag and allow lower voltages and increased welding speed, thus reducing HAZ size.[17,18]

1.1.1.b. Electrode. The electrode geometry and size play an important role in controlling the heat distribution in the slag and the weld pools. Dilawari et al.[19] have suggested two forces which cause fluid motion, namely, buoyancy forces caused by density differences and Lorentz forces caused by the interaction between a spatially non-uniform current distribution and the magnetic field. As indicated by several investigators, a bend or a "cast" in the electrode may affect these Lorentz forces, hence, changing the heat distribution in the weld pool.[19-21] Thus, electrode straightening is essential to maintain symmetrical weld penetration about the weld axis. Jones et al.[13] have shown a drastic anisotropy of heat affected zone width and penetration occurring in misaligned vertical electroslag welds in which the weld axis

is inclined only slightly from vertical. The intensity of heat genera-
tion near the electrode can be up to an order of magnitude greater than
the heat generated near the slag/plate interface and the variation is
significantly larger in the direction of the cooling shoe. By displacing
the electrode by about 10% from the central planes of symmetry, Deb Roy
et al.[20] has shown using theoretical calculations that irrespective of
the heat transport in the slag through conduction and convection, signi-
ficant asymmetry occurs in the heat generation. This causes an excessive
dilution in one plate while producing lack of fusion in the second plate.

Both cylindrical as well as strip (rectangular) electrodes have been
used in the past.[22] Dilawari et al.[19] have indicated a more efficient
electrode melting with the use of strip electrodes.

1.1.1.c. Slag Depth. In ESWs, the slag pool temperatures are
non uniform and are several hundred degrees higher than the molten metal
pool temperatures.[19] This leads to a higher heat flux occurring from
the slag to the base metal than from the weld to the base metal and a
majority of the heat transferred from the slag to the base metal is used
to heat and melt the base metal. The heat flux from the slag to the base
metal is governed by the metal and slag depth.[5] Hence, knowing and
monitoring the proper slag depth during welding is mandatory.

Variations in slag depth affect the shape and the size of the weld
pool due to the redistribution of the heat input in the slag pool. At a
constant energy input as the slag depth increases, a majority of the heat
is dissipated into the base metal and the weld pool is deeper but narrower.

This can adversely affect the weld metal grain orientation and cause weld center hot cracking.[5] The decrease in weld width can also be attributed to the increased slag volume to be heated.[2]

On the other hand, a shallow slag pool results in large fluctuations in current and voltage and enhance the probability of microcrack formation along the proeutectoid ferrite boundaries in the weld center.[23] In addition, hydrogen, when present, reportedly diffuses easily across the shallow slag pool into the weld metal and causes microcracking.[24] Hence, the weld shape can be controlled and microcracking eliminated by using a medium slag depth (1-1/2 to 2 inches).

A thin layer of slag freezes between the cooling shoe and the weld metal and leads to continuous slag loss during welding. Continuous slag level monitoring and replenishment is thus necessary. Probing the molten pool with a wire has been practiced to measure the slag depth intermittently.[3] Mitchell et al.[25] have used acoustic emission monitoring for the slag level detection.

1.1.1.d. Guide Tube Geometry. The standard consumable guide ESW utilizes a cylindrical guide tube to direct the welding electrode into the slag pool. In such cases, the guide tube and the welding gap cross sections are circular and rectangular, respectively. This combination leads to lack of penetration near plate edges when welding at low voltages and/or narrow gaps. Welding at high currents can also lead to resistance heating and warping of the guide tube. Evstratov[26] has proposed using a larger guide tube cross sectional area to solve this

problem, but a large guide tube cross section can also lead to some loss in current control because of the large currents required.[27] Hence, a guide tube design with an optimum cross sectional area and geometry is necessary. A wing guide tube design in which rectangular fins are welded onto a cylindrical tube, used by several investigators in the past, meets most of these requirements.[3,15,28-30] Provision of a higher ratio of the guide to gap cross sectional area also helps to increase the welding speed.[27,31,32] The wing guide tube eliminates the necessity for electrode oscillation while welding thicker section materials.[3] Narrow gap welds can be made using the wing guide tube without edge penetration difficulties.[30] The wing guide tube can also be used for welding plates with varying thickness.[29,33] Finally, the guide tube chemistry should be carefully manipulated to achieve required weld properties since it constitutes a finite fraction of the weld metal.

1.1.1.e. Welding Speed. It has been shown by earlier investigators that the temperature field, heat input, and, consequently, the depth to which plate edges are penetrated and overheated (HAZ) depends on the specific energy used for the welding process and the thermal and physical properties of the metal welded.[27,32,34] The specific energy, in turn, depends mainly on the voltage, welding current, and welding speed. Two methods of reducing the specific energy are lowering the welding voltage, which leads to lack of penetration, and increasing the welding rate, which can result in centerline cracking. The latter

requires increasing the electrode feed rate and/or reducing the gap to a minimum such that arcing between the guide tube and plate edges does not occur.

Since the rise in the current is slower than the rise in the electrode feed rate, higher welding current will reduce the specific energy input and decrease the weld penetration.[35] But decreasing the specific heat input through welding at higher currents may lead to the formation of hot cracks at the weld center since in ESWs the weld surface is in compression while the weld center experiences triaxial tension as it solidifies last.[36] Narrow gap procedures can offset this by establishing a smaller weld pool which leads to less shrinkage stresses and lower hot cracking susceptibility.[14]

Thus, a combination of narrow gap, high welding current, and optimum guide tube geometries may improve the mechanical properties and refine the weld microstructure.[14,22] The specific heat input can be reduced by adapting this technique which will help in controlling the size and properties of the HAZ. These HAZ characteristics are controlled by the peak temperature experienced and the dwell time above the AC_3 transformation temperature.[37,38] Eichhorn et al.[41,42] have suggested that by decreasing the specific heat input, the beginning of coarse grain formation in the HAZ can be shifted to a higher peak temperature due to a shortened dwell time in the critical temperature range.

An increase in welding speed has also been achieved by several investigators through external metal powder additions to the slag pool.[39-42]

The metal powder additions increase the metal deposition rate, thereby increasing the welding speed. The powder additions also quench the slag pool as it melts. Both of these effects lower the specific energy input for the weld.

1.1.1.f. Weld Pool Agitation.

Vibration has been reported in the literature to produce grain refinement in solidifying castings.[43-51] Various types of vibrations including electromagnetic, mechanical, ultrasonic and impact have been used in those works. Campbell[52] has extensively reviewed the effects of vibration during solidification and a reported technique induced vibration within the solidifying liquid by using a probe inserted into the liquid metal.

Sytyrin[49] and Garlic et al.[43] have suggested that the vibration during solidification causes favorable nucleation at higher temperatures and increases the number of crystallite nuclei to provide a fine grain size. However, Coward[45] has shown these effects of vibration to depend on process conditions and the material being welded.

There are two generally accepted hypotheses available to explain the grain refinement achieved in castings through vibration. Garlic et al.[43] have proposed the "pressure wave theory" in which the pressure wave of vibration decreases the size of the critical nucleus during solidification. The rate of nucleation, as a result, increases to provide grain refinement. The other hypothesis proposed by Brown et al[54] has attributed the grain refinement to the shear forces originating from the relative flow motion between the solid/liquid metal interface. The shear dependent

mechanisms are the fragmentation of dendrites to increase number of nuclei, the viscous shear growth of embryos, and the mixing of the higher melting composition into the lower temperature layers enhancing the nucleation.

1.1.2. Alloy Additions. Culp[4] has suggested that the proeutectoid ferrite phase bordering the columnar grains provides the least resistance to propagating cracks and several investigators have found defects (microcracks, grain boundary separations, and hydrogen induced cracking) in the proeutectoid ferrite phase.[6,23,53] Apps et al.[54] have found an improvement in the Charpy impact toughness of the weld metal with a reduction in the amount of the proeutectoid ferrite phase. Elimination of proeutectoid ferrite by alloy design consideration should improve the weld toughness.

Several investigators have controlled the amount of proeutectoid ferrite by adding alloying elements such as molybdenum, manganese, chromium, etc., to the weld metal.[41,55,56] Alloy additions also result in refined microstructures and improved mechanical properties.[31,54,56,57]

Kawaguchi et al.[58] have shown that reducing the silicon content promotes polygonal ferrite formation in certain welds, and improves weld toughness. Meanwhile, Medovar et al.[59] reported that silicon, phosphorus and sulfur reductions improved the hot cracking resistance.

These microstructure and mechanical property improvements can also be achieved in low alloy-structural steel weldments through selective weld metal alloy additions, which can be made through flux, guide tube,

and electrode modifications. The level of additions must be chosen
carefully to accommodate the base metal dilution in the weld metal and
the slag/metal reaction.

Alloy additions cannot be made through fused fluxes as they react
during the fusion processing of the flux.[60] Unfused fluxes must be
used for such additions. Suzuki[61] has used an insulated consumable
guide tube containing Ferro-Molybdenum as an alloying agent to strengthen
the weld. Alloy additions through the welding electrode is the most
effective method as more volume of wire is melted during welding than
either the flux or the guide tube. Both solid and flux cored-type wires
have been used in the past for this purpose.[19,65]

1.1.3. Mechanical Properties. Mechanical properties criteria for
non-conventional welding techniques, such as ESW, are usually taken from
recommendations valid for conventional welding processes. This often
creates rather conservative estimations.[63] The requirement to reach the
values of the weld joint notch toughness analogous to those of manual or
submerged arc weld joints, or to achieve the weld joint toughness equi-
valent to that of the base metal may not, however, express the true re-
sistance of the whole welded joint towards brittle failure under real
loading conditions. Several investigators believe that Charpy toughness
evaluations do not rate welds in their true order.[14,36,64-66] Since full
thickness testing of the weldments is expensive and difficult, Charpy
impact toughness evaluation serves as an initial qualification test for
ES welds. The use of other testing methods, like Pellini drop weight

test or the full thickness fatigue precracked-COD general yielding fracture mechanics test, has been recommended when ES welds fail to meet Charpy toughness requirements before requiring heat treatment procedures.[14,66]

Charpy impact toughness evaluations of electroslag weldments have revealed low toughness values in both the WCL and the coarse grained HAZ.[4,18,19] The CCG zone is tougher than the WCL zone made up of TCGs.[2] This fact challenges the majority opinion that the coarse grain structure found in electroslag welds is indicative of a high susceptibility to brittle fracture. Tuliani et al.[65] and Jackson[67] have reported scatter in the Charpy impact toughness along the weld length. This factor, as well as the small size of the Charpy specimens, lead to conflicting toughness results in certain weld evaluations.[65,68,69]

1.1.4. Post Weld Heat Treatment. When the electroslag welded joint toughness properties in the as-welded condition are inadequate, post weld heat treatments have been employed. Pense et al[70] have shown this to reduce mechanical property variations across the joint. There are basically three types of postweld heat treatment applied to electroslag weld joints. First, a normalizing treatment has been performed above AC_3 (approximately 900°C) transformation temperature.[27,71] But, distortion problems have been frequently encountered. Second, an inner critical anneal at 780°C to partially recrystallize the welded joint has been reported by Patchett[27] to reduce distortion. Finally, a stress relief treatment has been carried out at about 650°C.[36,55,57] Additionally,

local normalizing of electroslag welds has also been studied by Soroka.[72] The response to these different heat treatment techniques depends mainly on the base and weld metal chemistry and adequate as-welded properties eliminate the need and expenses of post weld heat treatment.

1.2. Scope of Investigation

ESW usually involves welds several feet in length and consistent weld quality is essential. Since process variables strongly influence weld characteristics, the first stage of this investigation involved establishing the effects of electrode grounding and centering, slag level, welding current and voltage, guide tube geometry, joint gap, etc., on the weld consistency and quality. Based on these results, the proper process variables were selected. New techniques were developed to minimize the operator control and further improve the weld consistency. The second stage of the investigation involved using various vibrational techniques to induce a stirring motion in the weld pool and achieve grain refinement in the as-welded condition. The final stage, an alloy design study, utilized weld metal alloy additions to control the microstructure and mechanical properties. Throughout this investigation, these process and alloy variables were related to their associated influence on microstructure and mechanical properties of ES welds.

2. EXPERIMENTAL PROCEDURE

2.1 Material

ANSI/ASTM A588-77A Grade B structural steel was used as the base material for welding in this investigation. Hot rolled steel plates, 2 x 49 x 260 inches, were supplied by the Oregon Steel Mill Division of Gilmore Steel Corporation. The chemical composition and mechanical properties are given in Table I. The microstructure of the as-received material is shown in Figure 5. The plates were cut into sections measuring 2 x 18 x 24 inches (Figure 6) with the 18 inch side parallel to the rolling direction. This orientation allowed the faying edge (24 inch side) to be perpendicular to the rolling direction, in accordance with the AWS Structural Welding Code D1.1, and prevent lamellar tearing adjacent to the weld fusion line.

Wire A (Hobart 25P--AWS E70S-3) was used as a filler material for the welding process. Hobart type PF-201 running flux (fused and ground) constituted the welding slag. The filler wire and weld metal analyses are given in Table II. Chemistry and basicity of the slag are shown in Table III.

2.2 Electroslag Welding

2.2.1. Plate Fixturing. Two plates initially 2 x 18 x 24 inches were placed on a 2 inch thick bottom plate with the 24 inch edge held vertical. The plates were tack welded to the bottom plate with a 3/4 to 1-1/4 inch gap between the vertical faying edge. Six 1/2 inch thick strong backs,three on each side, were welded to the plates (Figure 7).

Table I.

BASE METAL ANALYSIS

Supplier: Oregon Steel Mills
Material: ANSI/ASTM A588-77A, Grade B, Structural Steel

Chemical Analysis

Element	Amount in wt.%
C	0.182
Mn	1.074
Si	0.247
Cr	0.506
Ni	0.052
Cu	0.308
S	0.021
P	0.007
Al	0.033
V	0.081

Mechanical Properties

Charpy V notch Impact Toughness at 0°F = 37.45 ft.lbs.
Yield Strength   = 62.5 KSi
Tensile Strength   = 81.5 KSi
Percent elongation in 8 inches   = 20%
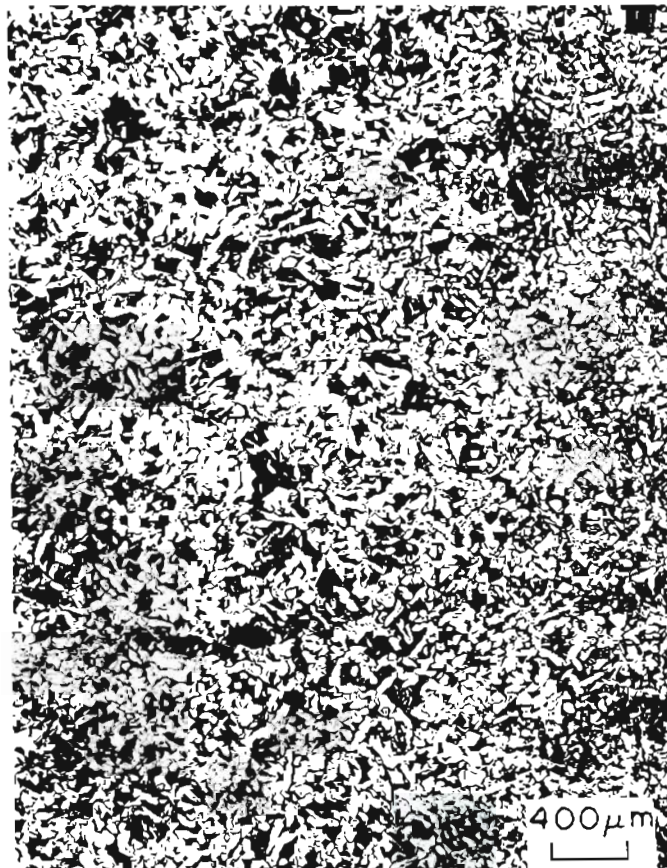
Figure 5.   A588 BASE METAL MICROSTRUCTURE (AS RECEIVED).
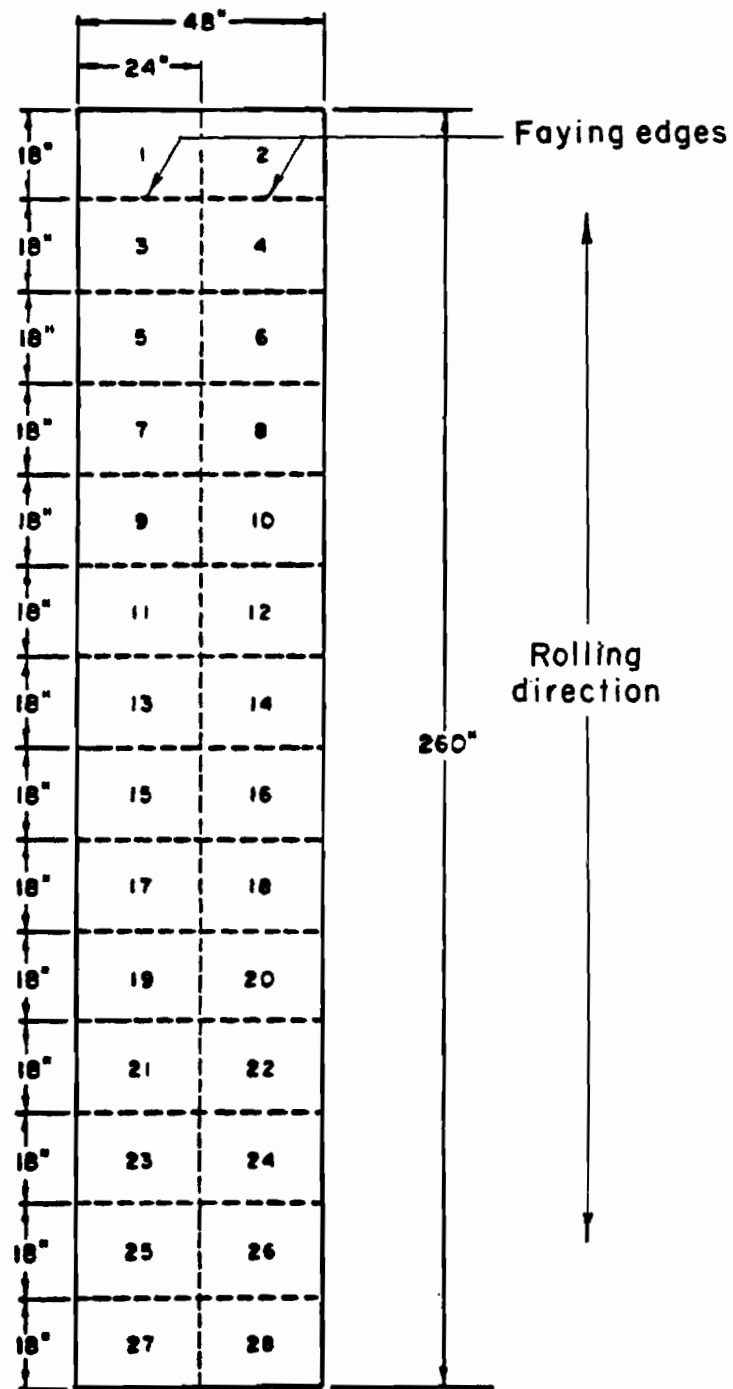
Figure 6. SCHEMATIC REPRESENTATION OF BASE PLATE LOCATIONS AND ORIENTATION.

Table II.

FILLER METAL ANALYSIS

Supplier: Hobert Brothers Company
Type: Hobart 25P--(AWS E70S-3)*--3/32" diameter solid wire

Chemical Analysis

Element	Wire	With PF 201 flux (undiluted)
C	0.11	0.14
Mn	1.12	1.11
Si	0.50	0.45
P	0.020	0.008
S	0.019	0.019

Mechanical Properties

Charpy V notch Impact Toughness at 0°F	= 30 ft.lbs.
Yield Strength	= 45.75 KSi
Tensile Strength	= 73.325 KSi
Percent elongation in 2 inches	= 26.5%

*Referred to as wire A in this text.

Table III.

ESW FLUX CHEMISTRY AND BASICITY

Supplier: Hobart Brothers Company
Type: Hobart PF 201 Running Flux

Flux Chemistry

Compound	Amount in wt.%
CaO	12.20
MgO	2.34
MnO	22.46
CaF_2	8.62
SiO_2	32.95
Al_2O_3	8.32
TiO_2	8.02
K_2O	0.88
Na_2O	0.57
FeO	1.81
P_2O_5	< 0.05

Basicity[*] = 0.9

[*]Basicity is determined using the relation

$$Basicity = \frac{CaO + MgO + CaF_2 + Na_2O + K_2O + 0.5\ (MnO + FeO)}{SiO_2 + 0.5\ (Al_2O_3 + TiO_2)}$$

using mole fractions of each compound.
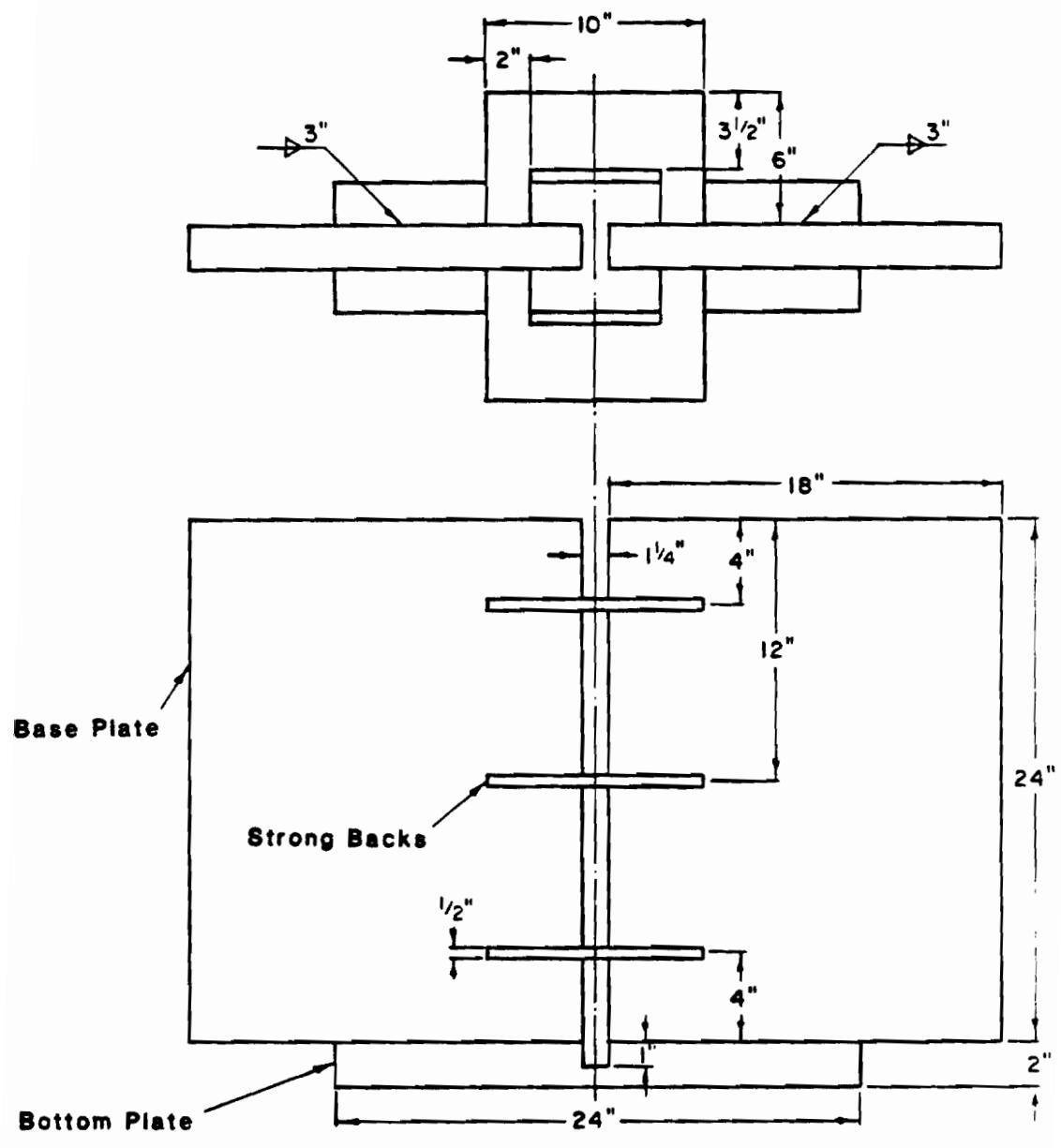
Figure 7.   SCHEMATIC REPRESENTATION OF ELECTROSLAG WELD
             PLATE FIXTURE.

2.2.2. Consumable Guide Tube Preparation. Various guide tube con-
figurations were used in this investigation to achieve complete edge
fusion during controlled base metal dilution and grain refinement. The
tube interior was cleaned using an air jet and acetone. The standard
procedure utilized a 1/2 inch diameter mild steel guide tube (Hobart
type 48) with 3 ceramic consumable insulators placed at regular intervals.
The insulators prevented the guide tube from being drawn to the plate
edge and short circuiting.

A minimum of 7/8 inch joint spacing was required with the use of
such insulators (outer diameter of the insulator = 7/8 inch). Hence, for
narrow gap welds made using a 3/4 inch joint spacing, a 1/16 inch thick
flux coating was used. The composition of the flux coating was similar
to that of the slag.

For grain refinement purposes, mullite (3/16 and 1/16 inch wall
thicknesses), quartz (0.04 inch wall thickness), plasma-sprayed zirconia
and alumina were used as guide tube shielding materials. Such shielding
was necessary to extend the guide tube into the slag. Water-based alumina
paste was used as a binder between the metallic guide tube and mullite
shroud. A binder was not used with quartz shroud. A flare formed on the
top edge of the quartz shroud facilitated securing the quartz to the guide
tube, Figure 8.

Even distribution of heat across the thickness is necessary in order
to achieve complete edge fusion at low welding voltages. This was achieved
by widening the effective guide tube towards the edges of the plate by
gas tungsten arc welding a 1/4 x 5/8 x 24 inch wing on both sides of the

½" D

Ceramic
Insulators

Flux
Coating

2-4

¼"

5/8" ¼" 5/8"

**Standard bare
guide tube**

**Flux coated
guide tube**

**Wing
guide tube**

Binder

Clamp

2-4

Mullite
Shroud

Quartz
Shroud

Alloy
Wire

**Mullite shrouded
guide tube**

**Quartz shrouded
guide tube**

**Alloy
guide tube**
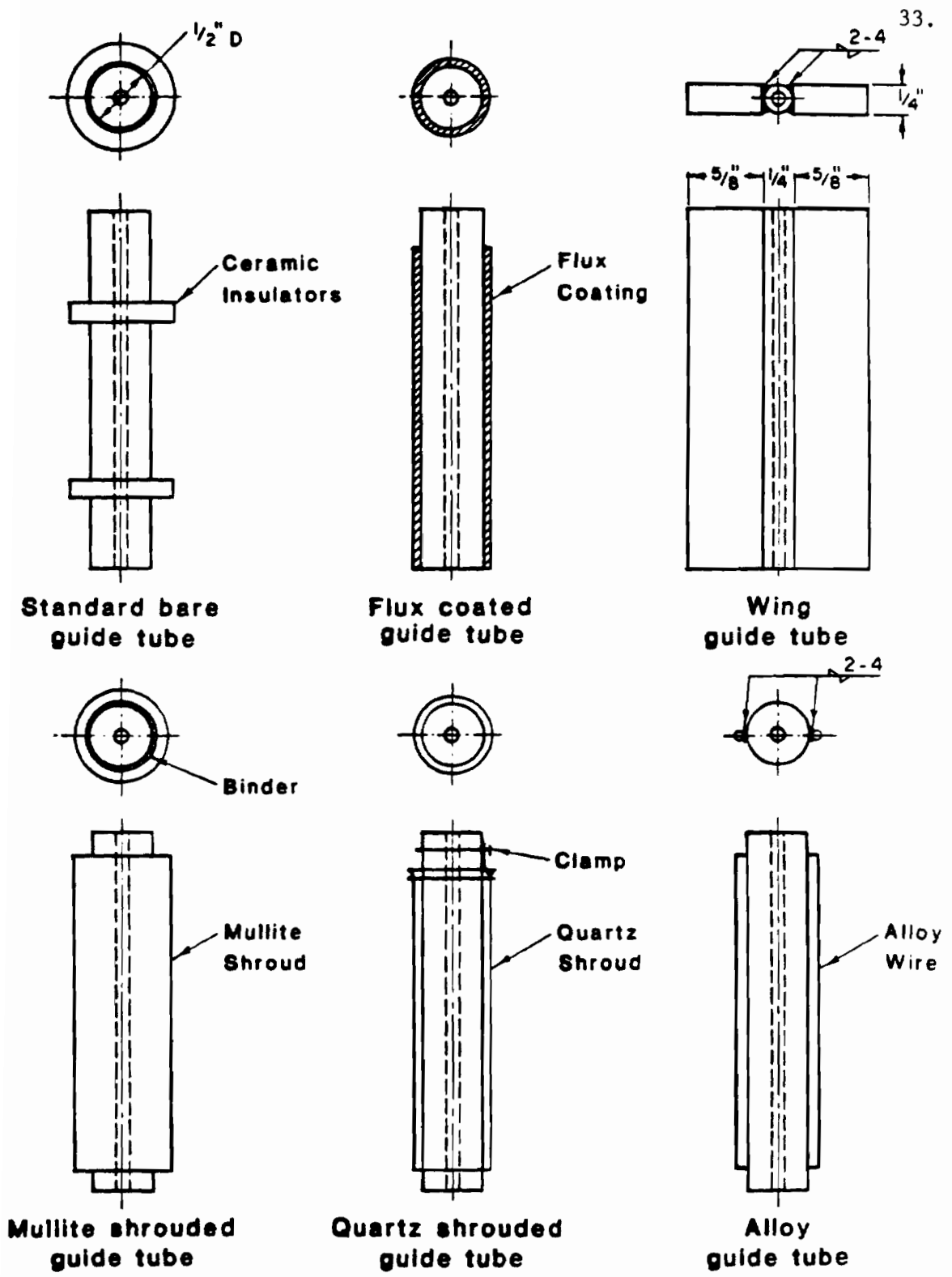
Figure 8.   SCHEMATIC REPRESENTATION OF VARIOUS CONSUMABLE
GUIDE TUBE DESIGNS USED IN THE INVESTIGATION.

cylindrical guide tube. A 1/4 inch diameter guide tube was used in the center instead of the normal 1/2 inch diameter guide (Figure 8). In the case of the 3/4 inch gap, ceramic insulators were sandwiched between the guide and the faying edges.

2.2.3. Cooling Shoe Design. Water cooled copper shoes were used to dam the weld and slag pools and extract the heat. Two shoe designs were used, one a 24 inch long fixed shoe assembly, and the other a 12 inch long sliding shoe assembly.

The permenent shoe consisted of an Aluminum box with water circulation, sandwiched between a copper and an Aluminum backing plate. A weld reinforcement depression was machined into the copper face. Its dimensions varied for different joint spacing as shown in Figure 9. The shoe was wedged in place between the plates and the strong backs during welding.

The sliding shoe consisted of a copper channel with weld reinforcement on one side machined into it with water passage behind it. The shoe was held against the plates under spring tension and raised during welding by a jack assembly. This allowed detailed observation of the slag bath and guide tube.

2.2.4. Flux Addition. During the electroslag welding process, slag freezes between the cooling shoe and the weld metal. As a result, slag depletion occurs as the weld progresses. This slag loss was compensated for by continuous flux addition using a precision metal powder feeder system manufactured by TAPCO International.
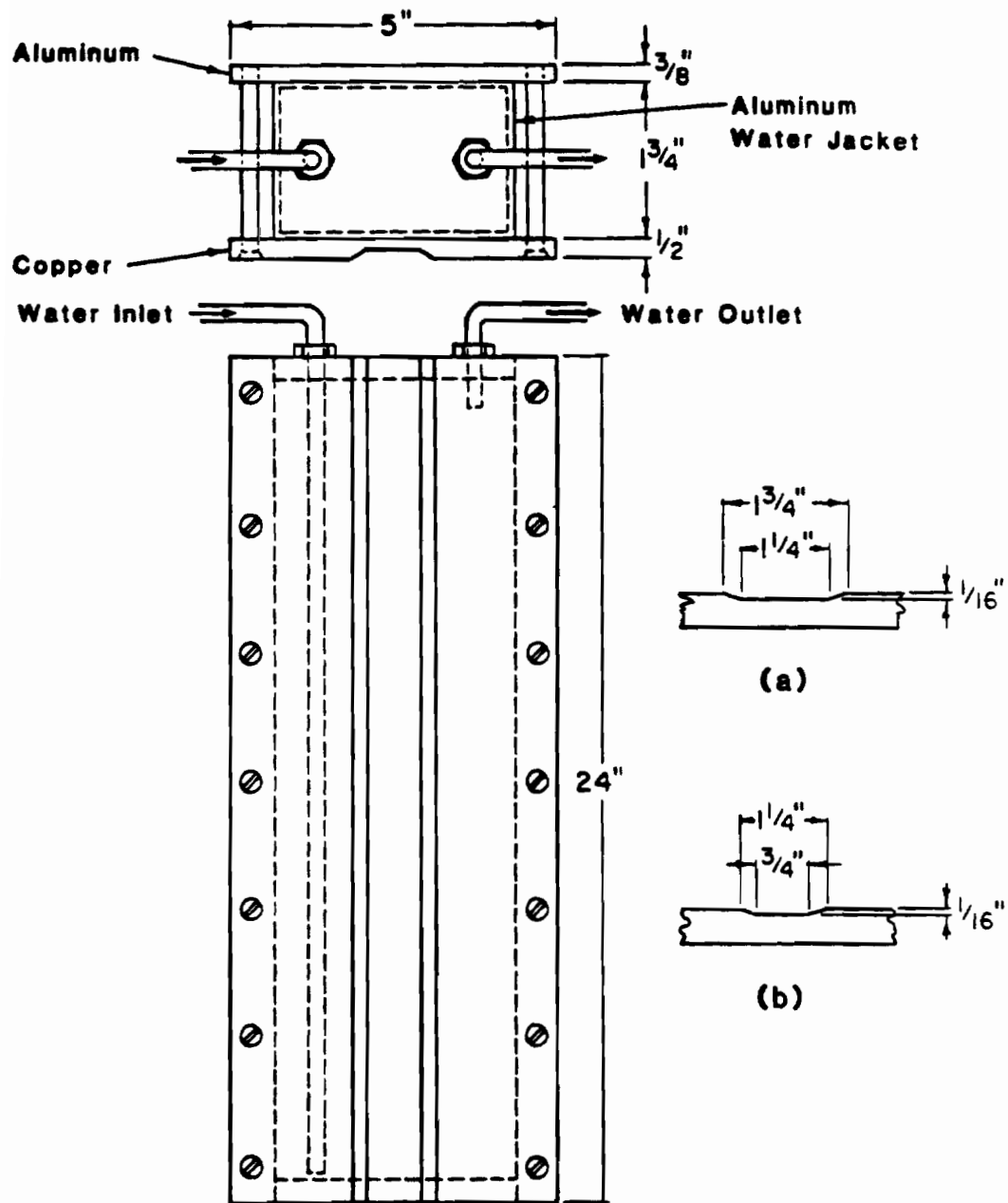
Figure 9. SCHEMATIC REPRESENTATION OF WATER COOLED-
RETAINING SHOE, WELD REINFORCEMENT DIMENSIONS
FOR (a) 1-1/4" ROOT GAP, AND (b) 3/4" ROOT GAP.

In this system, flux stored in a hopper flows through a tube into a cylindrical reservoir. A paddle wheel rotated by an electrically driven variable speed D.C. motor scoops the flux from the reservoir and transfers it down a tube into the slag pool. The rate of flux addition can be controlled by both motor speed and paddle wheel size. In this investigation, the flux was added at a rate of approximately 4 grams/minute in order to balance the slag losses.

The flux hopper was mounted above the welding head and the powder metering device was located just above the guide tube mount; Figure 10.

2.2.5. Current, Voltage and Wire Feed Analysis. Current and voltage fluctuations were monitored during the welding process to detect and analyze slag depletion, weld wire arcing, intermittent contact between the slag pool and consumable guide, etc., A record of these variations was made using a GULTON strip chart recorder. A storage oscilloscope was also used to monitor and record the current and voltage fluctuations. Records of both current and voltage operating levels were made for each weld with both strip chart recorder and oscilloscope. The wire feed rate was measured using a JET-LINE wire feed measuring device,

2.2.6. Weld Pool Vibration. Vibratory forces were transferred to the weld pool in three modes, namely, through vibration of plates being welded, an external stirrer inserted into the slag bath, and the consumable guide tube.

The first case utilized a vibration table consisting of a 48 x 72 x 1 inch aluminum top mounted on air cushions. An eccentrically loaded
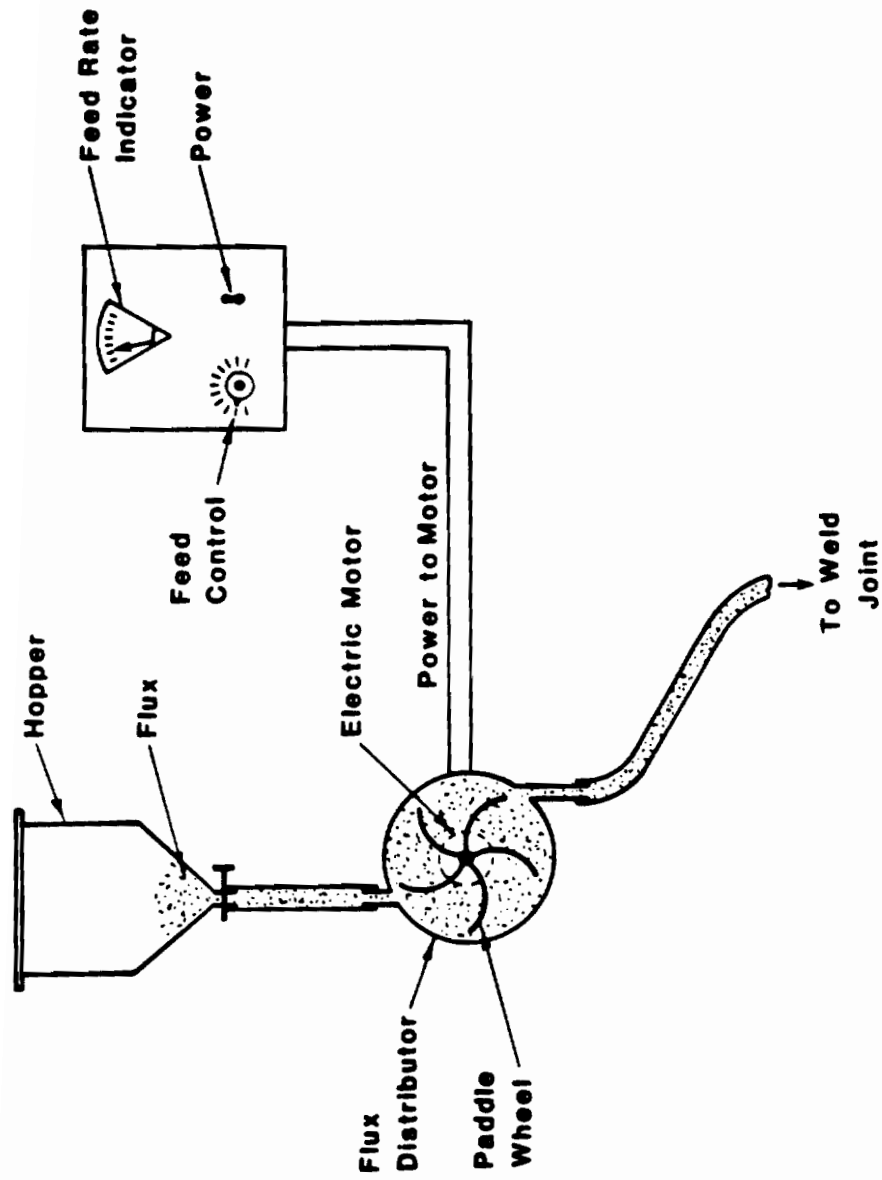
Figure 10. SCHEMATIC ILLUSTRATION OF THE CONTINUOUS-METERED FLUX FEED SYSTEM.

vibration motor (METALAX-BONAL CORPORATION) and the plate to be welded were mounted on the aluminum plate (Figure 11). A magnetic transducer for vibration analysis was mounted as shown in Figure 11. The control panel for the system consisted of a rheostat to vary the vibration motor speed, a frequency indicator, and a peak amplitude meter to indicate the resonance frequencies. By gradually increasing the speed of the motor, various resonance frequencies were identified. Two resonance frequencies, one a low and the other a high amplitude, were selected for use during electroslag welding.

The second vibration method involved the vibration of a 1/2 inch diameter quartz rod which served as an external stirrer. Part of the quartz was consumed by the slag during the process. Both pneumatic and ultrasonic vibrations were performed in this case.

The third approach consisted of vibrating the consumable guide tube to achieve weld pool agitation. A BONAL vibration motor was bolted to the guide tube with the motor axis parallel to the guide tube axis (Figures 12 a & b). Resonant vibration was performed in a manner similar to the plate vibration. The vibratory motion was transferred from the shielded guide tube to the slag pool and the weld metal. The specific conditions for each experimental weld are shown in Table IV.

2.2.7. Weld Metal Alloy Additions. Alloy additions were made to the electroslag weld metal by both alloyed weld wire and pure metal wires welded to the guide tube. Low alloy filler wires used included Wire B (A588), Wire C (Mn-Si), Wire D (Mn-Mo) and Wire E (Cr-Mo). The composi-
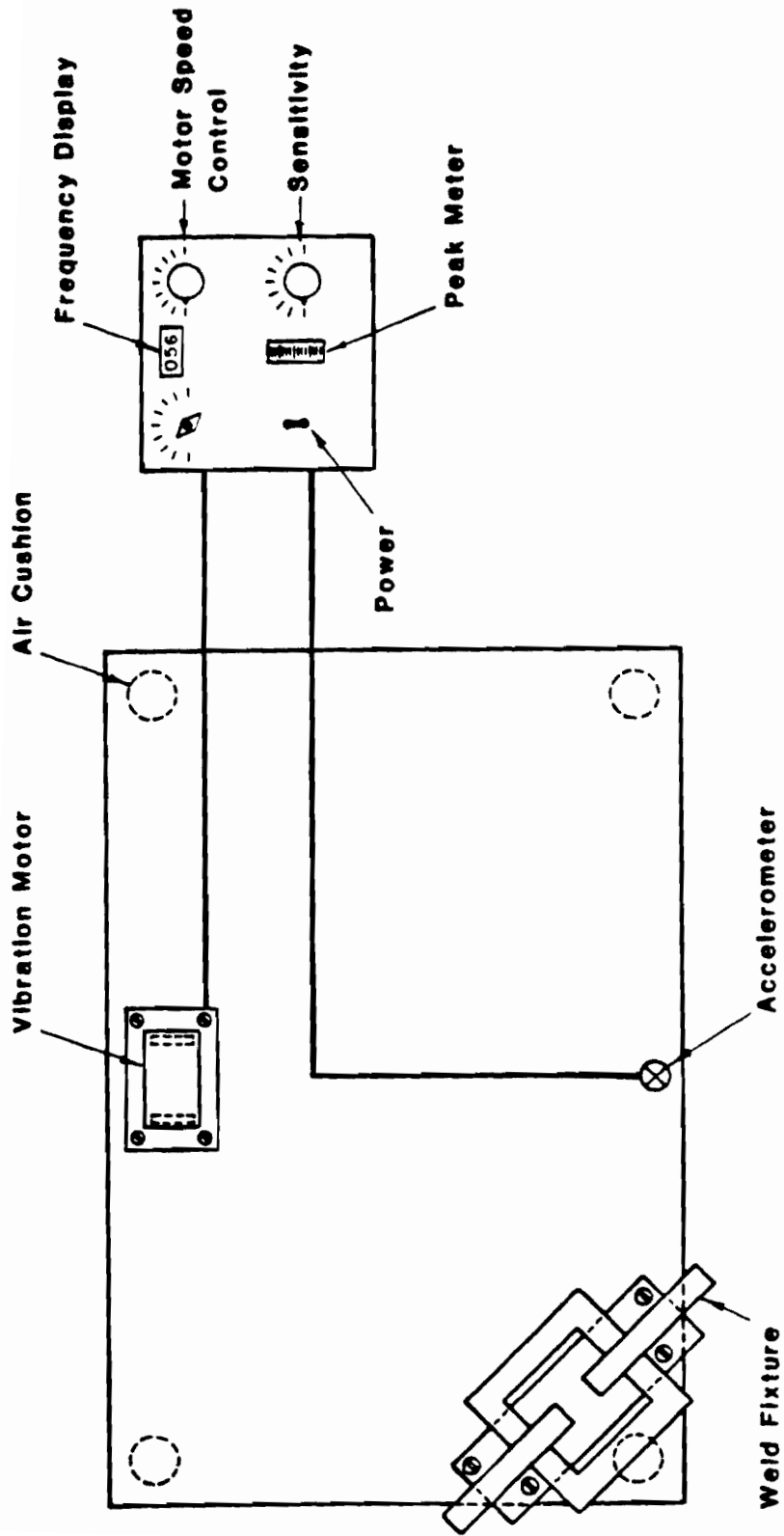
Figure 11. SCHEMATIC REPRESENTATION OF TABLE TOP-ELECTROSLAG PLATE FIXTURE VIBRATION SETUP.
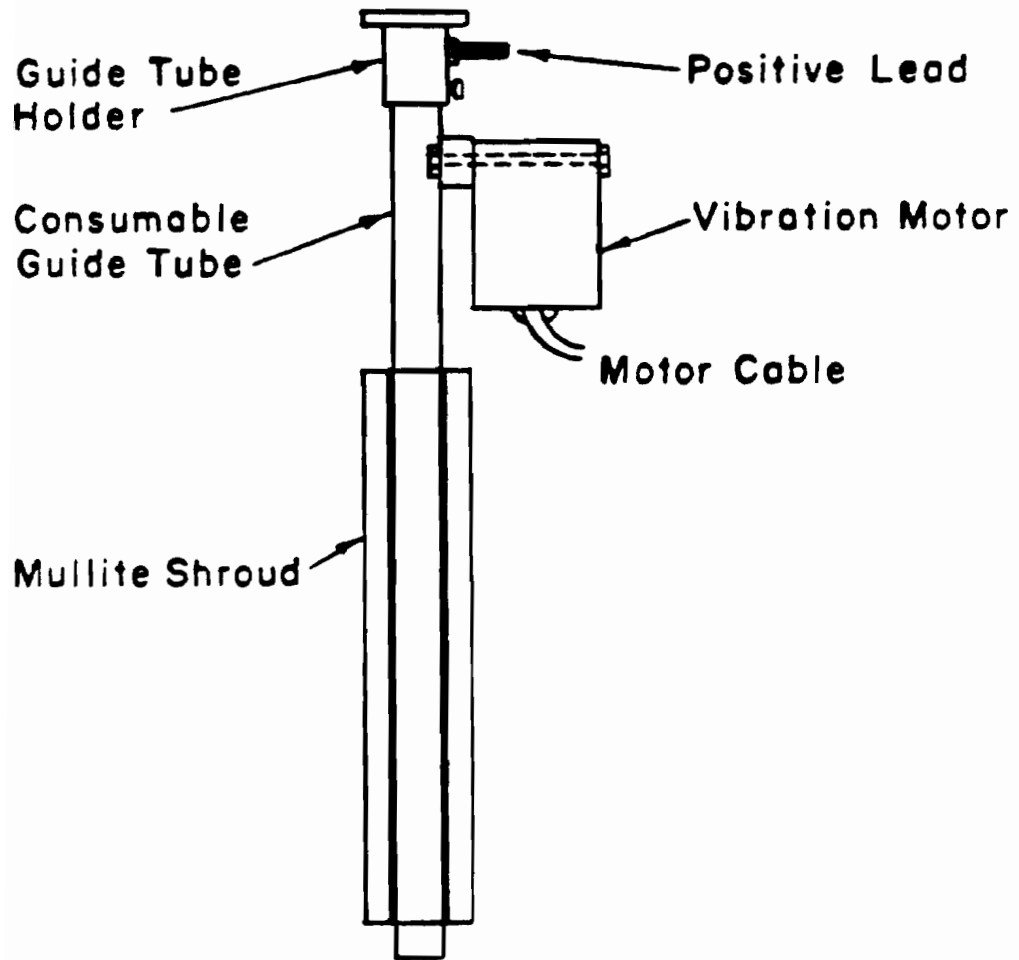
Figure 12a.   SCHEMATIC ILLUSTRATION OF SHIELDED CONSUMABLE
GUIDE TUBE VIBRATION SETUP.
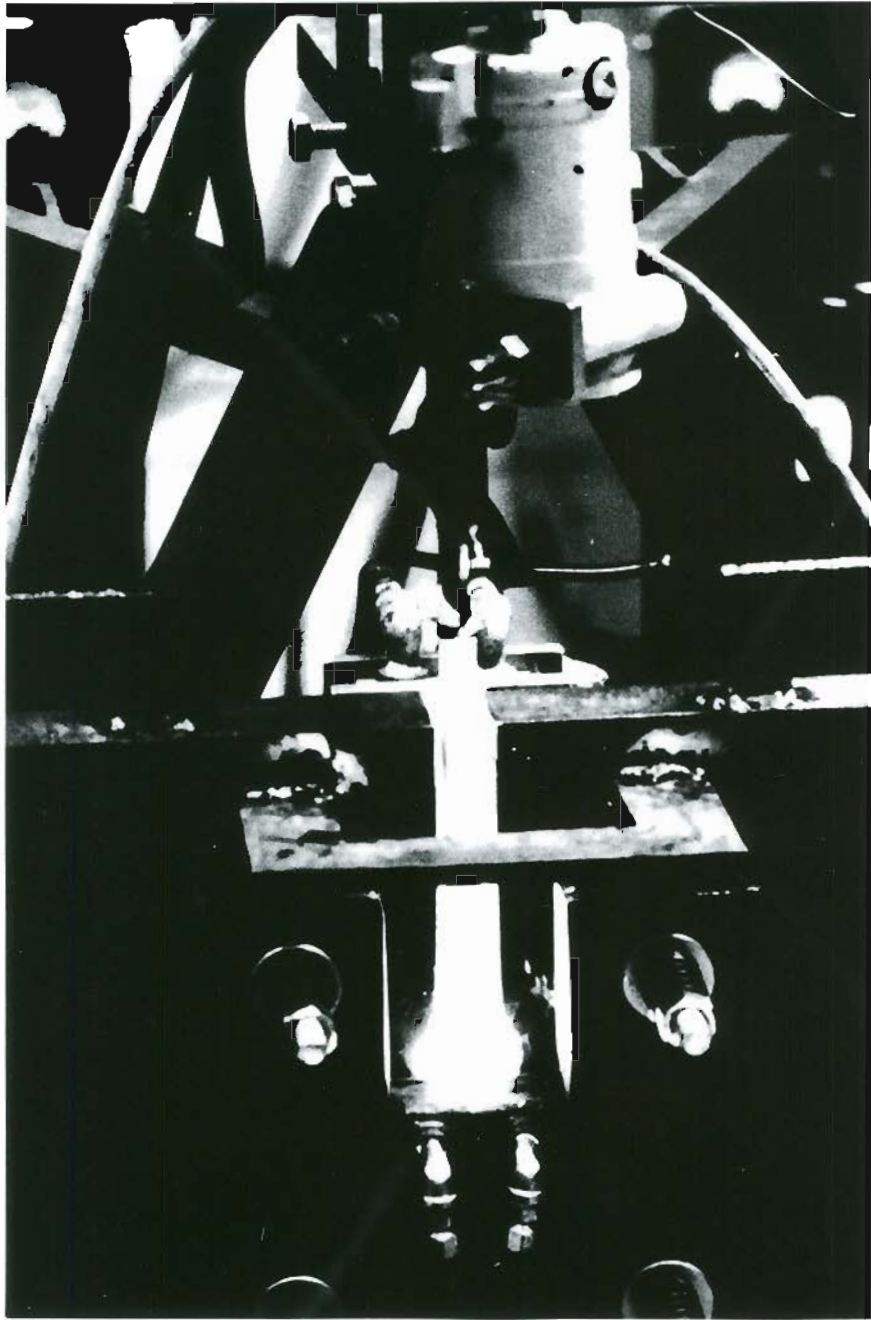
Figure 12b.   SHIELDED CONSUMABLE GUIDE TUBE VIBRATION SETUP.

Table IV.

WELDING PARAMETERS

#	Type	Root Gap mm	Current Amps	Voltage volts	Vibration
1	Standard	32	600	42	None
2	Solid Quartz Probe Stirring	32	600	40	Pneumatic Vibration 217 Hz
3	Mullite Shielded Guide Tube	32	500	45	None
4	Mullite Shielded Guide Tube	32	500	45	Eccentric Loaded Motor Vibration 35 Hz
5	Quartz Shielded Guide Tube	32	600	48	None
6	Tube Weld, First Half Standard, Second Half Quartz-Shielded Guide Tube	32	500	42	None

tions of these wires are shown in Table V. The welding conditions for selected welds are given in Table VI.

2.2.8. Thermal Distribution Analysis. Electroslag weld HAZ thermal cycles were recorded using Chromel-Alumel thermocouples (22 gage) located at various distances from the faying edge. These thermocouples were sandwiched between two 1 inch thick plates. Three sets of 5 thermocouples were placed at bottom, middle and top sections of the 24 inch long plate (Figure 13). Thermocouple millivolts output were recorded by a 16 channel multiplexed Motorola microprocessor. The thermocouple outputs were scanned successively at a rate of 10 channels every 3 seconds. Scanned data were then amplified to a 0-10 volts scale (60 mv equals 10v), digitized and recorded on a 9 track magnetic tape. The recorded temperature data for selected welds were analyzed using a Prime computer and complete time-temperature relationships for each thermocouple were plotted.

2.2.9. Weld Setup/Procedure. The welding head consisting of the flux feeding system, oscillation mechanism and a guide tube holder was mounted on one of the plates being welded. The consumable guide was centered in the joint gap within a limit of 1/16 inch. All welds were made with a Hobart model RC 750, DC constant voltage power source using reversed polarity. Both plates to be welded were grounded. The consumable guide tube was connected to the positive terminal of the power supply using two 4.0 copper cables. The weld setup schematic is shown in Figures 14 a & b.

Table V.

ESW ALLOY FILLER CHEMISTRY

| Wire ID | Manufacturer ID | Element in wt.% | | | | | | | | |
		C	Mn	Si	Cr	Ni	Mo	Cu	S	P
Wire A*	Hobart 25P	0.11	1.12	0.50	–	–	–	–	0.02	0.019
Wire B[c]	Linde WS	0.09	0.50	0.30	0.55	0.50	–	0.30	0.025	0.02
Wire C	Airco Metal core 6	0.05	1.60	0.80	–	–	–	–	0.02	0.01
Wire D[c]	Linde 40B	0.10	1.15	0.03	–	–	0.53	–	0.024	0.017
Wire E[c]	Page AS521	0.07/ 0.12	0.4/ 0.7	.45/ .60	2.25/ 2.75	–	0.9/ 1.1	–	0.025	0.025

*Used in standard welds

[c]Copper coated wire

Table VI.

WELDING PARAMETERS USED IN ALLOY ADDITION METHODS (SELECTED)

#	Type	Root Gap mm	Current Amps	Voltage Volts	Comment
1	Elemental Mo Addition	32	600	42	Three levels of addition, 0.53, 0.66 and 1.07 wt.%
2	Cr, Mo addition through filler wire--standard guide tube	32	600	42	Wire E*
3	Cr, Mo addition through filler wire--winged guide tube	19	1000	40	Wire E*

*see Table V for wire description.
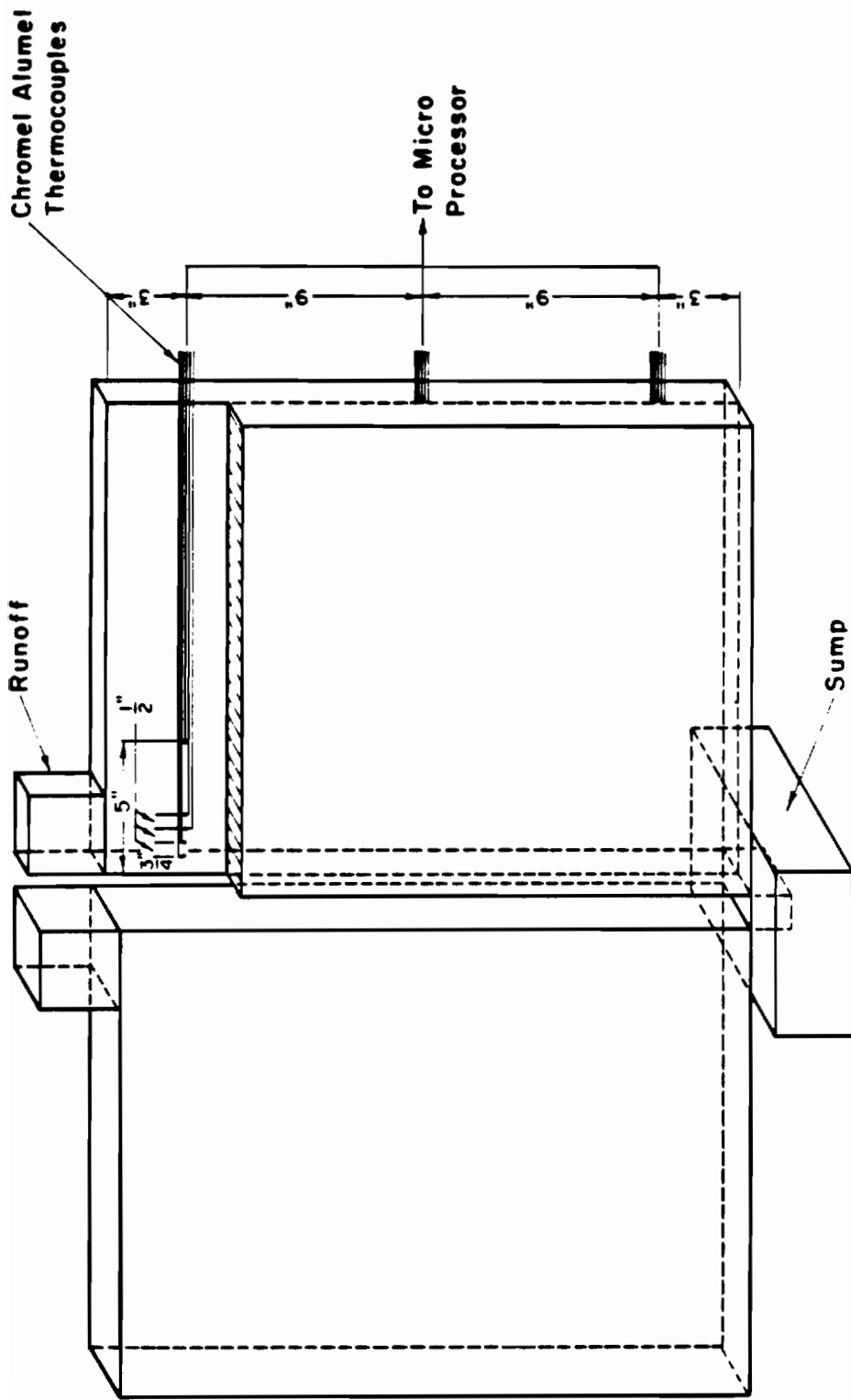
Figure 13. SCHEMATIC REPRESENTATION OF ELECTROSLAG WELD PLATE FIXTURE SHOWING THERMOCOUPLE LOCATIONS.
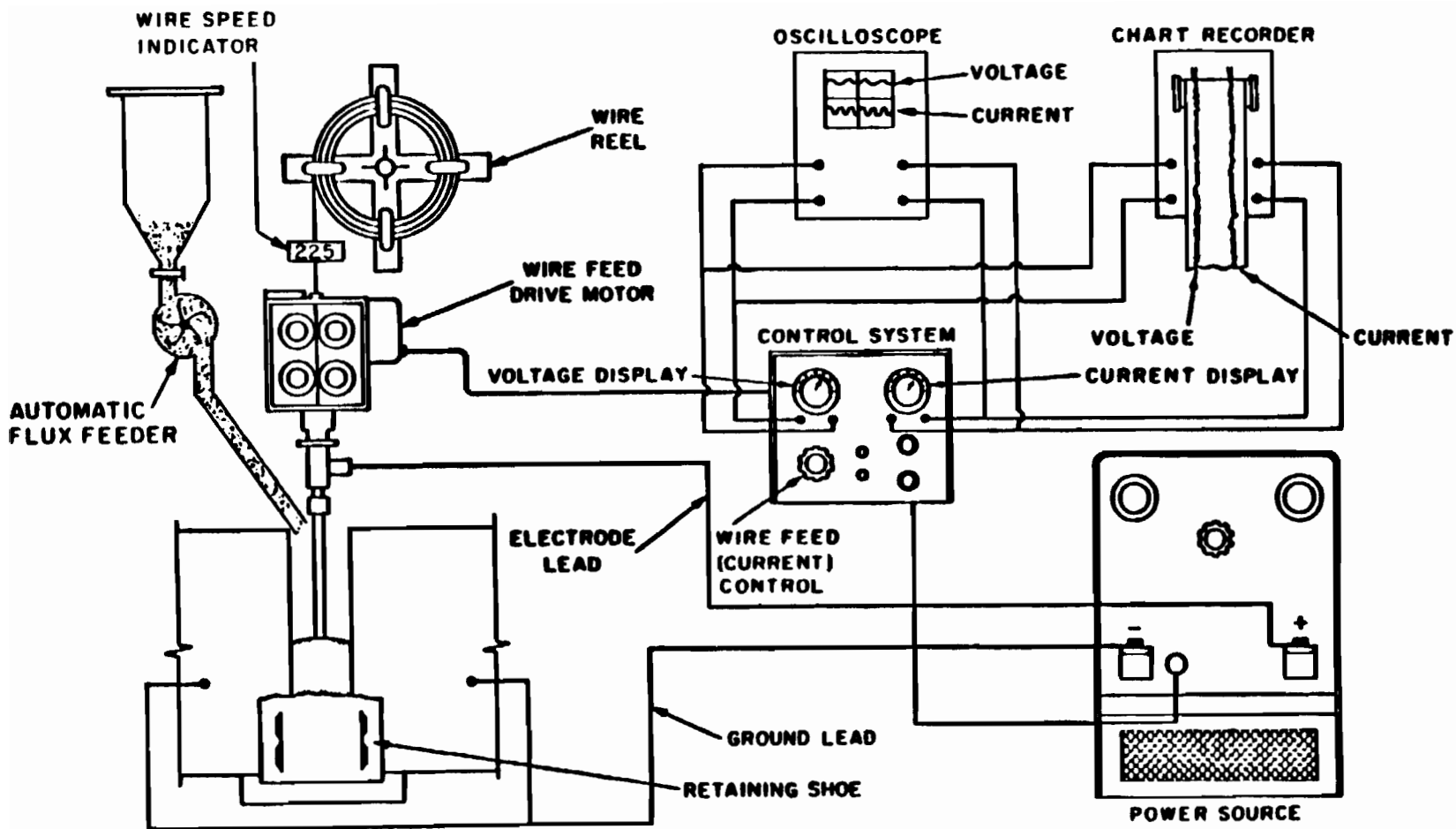
Figure 14a. SCHEMATIC ILLUSTRATION OF CONSUMABLE GUIDE ELECTROSLAG WELD SYSTEM USED IN THE INVESTIGATION.
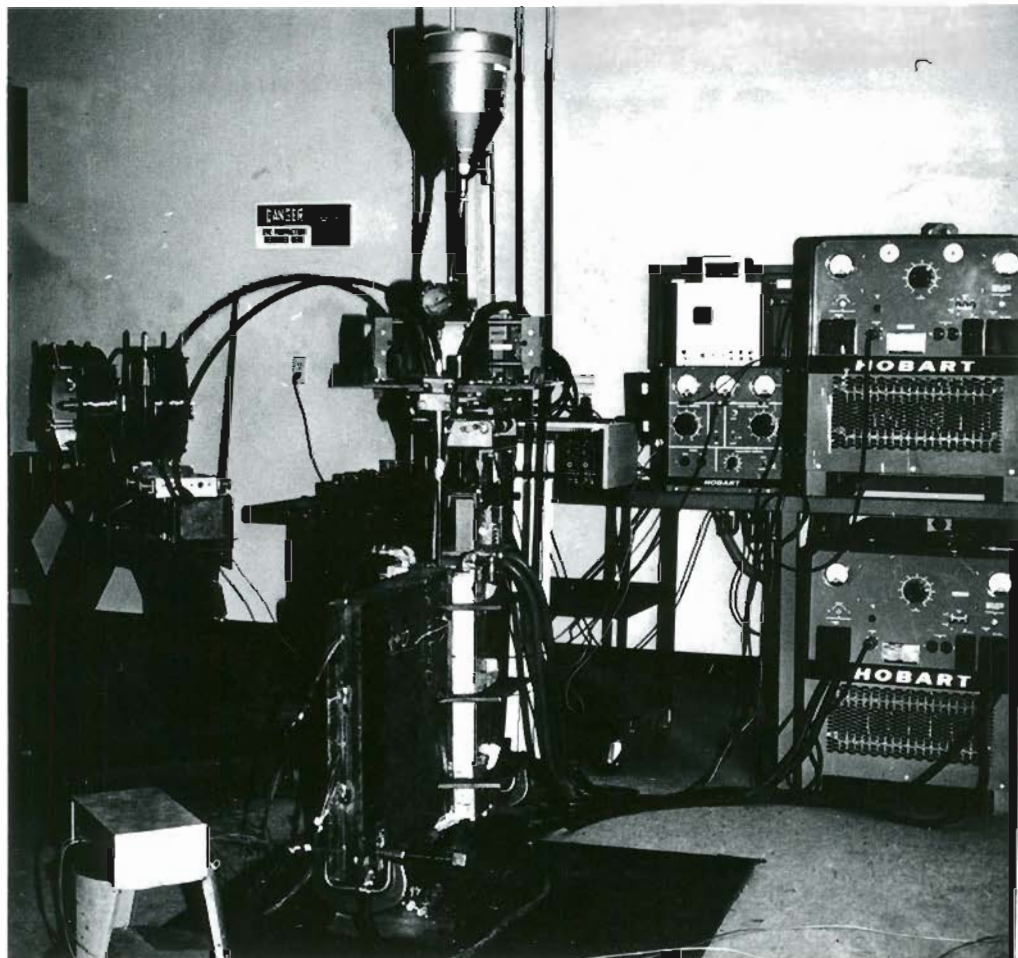
Figure 14b. CONSUMABLE GUIDE ELECTROSLAG WELD SYSTEM USED IN
THE INVESTIGATION.

Prior to starting the weld, the strip chart recorder, oscilloscope and wire feed rate measuring device were actuated and water circulation in the cooling shoes started. Welding was initiated with an open arc and a premeasured amount of flux (75 grams/cubic inch of slag) was slowly added to provide sufficient time for complete melting of the flux as it was added. A dynamic equilibrium was achieved after the proper slag level was obtained. The desired current and voltage were then set and the automatic flux feed system activated at a preset feed rate.

2.3. Weldment Evaluation

2.3.1. Macrostructural Examination. A 6 inch wide section was removed from the weldment by oxy-acetylene cutting with a Victor VU 150 cutting machine (Figure 15). The section was then saw cut at mid-thickness and the reinforcement removed from one side. The mid-thickness surface was ground using the 86 grit wheel in a Thompson surface grinder and then macroetched with a 10% Nitric acid solution in anhydrous ethyl alcohol mixture for 5 to 10 minutes. The etched surface was cleaned under running water, rinsed in anhydrous alcohol and immediately dried.

Macrostructures of specimens prepared from various welds were studied with respect to base metal dilution, weld metal grain size and orientation, HAZ size, presence of weld defects, weld metal segregation, solute banding, etc.

2.3.2. Microstructural Examination.

Figure 15. SCHEMATIC ILLUSTRATION OF SECTIONS MADE ON ELECTROSLAG WELDS FOR WELD EVALUATION.

2.3.2.a. Optical Metallography. One inch wide sections were

removed from the macroetched specimens and coupons cut from key regions.

The macroetched surface was ground on 120, 240, 400 and 600 grit grinding

papers successively. Polishing was carried out first on a 6 micron dia-

mond lap wheel followed by 0.3 and 0.05 micron alumina compound. The

surface was then etched in 2% Nital solution for a few seconds. This

etching technique was repeated several times with intermediate polishing

on 0.3 and 0.05 micron alumina lap wheels to remove deformed surface

layers and surface artifacts. A 2% Picral etch was also used in certain

cases. Specimens were then studied with a Zeiss optical microscope at

magnifications from 25 to 1000x.

2.3.2.b. Scanning Electron Microscopy. Weld specimens were

polished in the same manner used for optical metallography. The polished

surface was first etched using a saturated picric acid solution in ethyl

alcohol for a period between 20 and 30 seconds. The surface was then

etched in a 2% nital solution for about 5 seconds. Etched specimens

were then studied using a JEOL (JSM-35) scanning electron microscope at

25 KV secondary operating voltage and a 39 mm working distance. The in-

verse image contrast mode was used to achieve a contrast similar to that

of optical micrographs.

2.3.2.c. Transmission Electron Microscopy. Thin foils for

transmission electron microscopy were taken from the macroetched speci-

mens in the longitudinal direction. About 0.05 inch thick sections were

removed using an abrasive slicing wheel. Cut sections were then

mechanically polished to about 0.005 inch in thickness. 3 mm diameter discs were punched from these slices and electropolished using a "Fishione" double jet polishing unit. The polishing electrolyte was made up of a solution of 100 grams of chromium trixoide, 540 cc of glacial acetic acid and 28 cc of distilled water. Power settings were 55V and 40 mA/3 mm disc. The temperature of the electrolyte was maintained between 5 and 10°C. Thin foils were then studied using a Hitachi HU 11B electron microscope at 100KV operating voltage.

2.3.3. Hardness Analysis. A one inch wide strip was removed from the macro-etched specimen for hardness analysis. The side opposite to the etched surface was ground flat and parallel. The hardness was measured across the weld fusion zone, heat affected zones and base metal using a Rockwell hardness tester. B scale (1/16 inch diameter spherical steel indentor under a 100 Kilograms major load) was employed. C scale (Brale indentor under a 150 Kilograms major load) measurement was made whenever the hardness value exceeded R_b 100. Three measurements were made at each region of interest and an average was determined.

2.3.4. Charpy Impact Testing. Both standard and precrack Charpy impact specimens were tested in this study. Standard ASTM Charpy impact specimens (Figure 16) were machined from two thickness locations as shown in Figure 17. The V notch was ground perpendicular to the welding direction (Figure 17). Notches were located in four regions, namely base metal, HAZ, CCG and weld center line (WCL). Samples were coded with
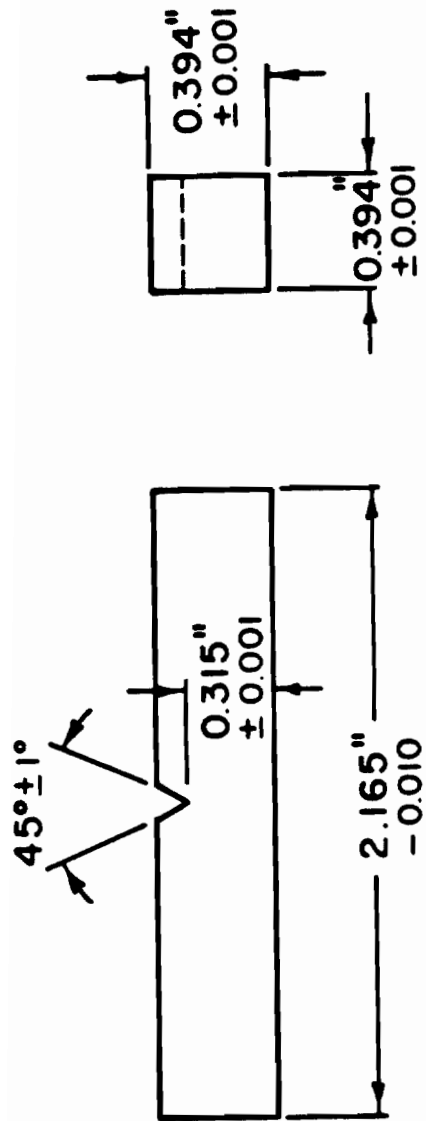
Figure 16. ASTM STANDARD CHARPY V-NOTCH IMPACT TEST SPECIMEN.
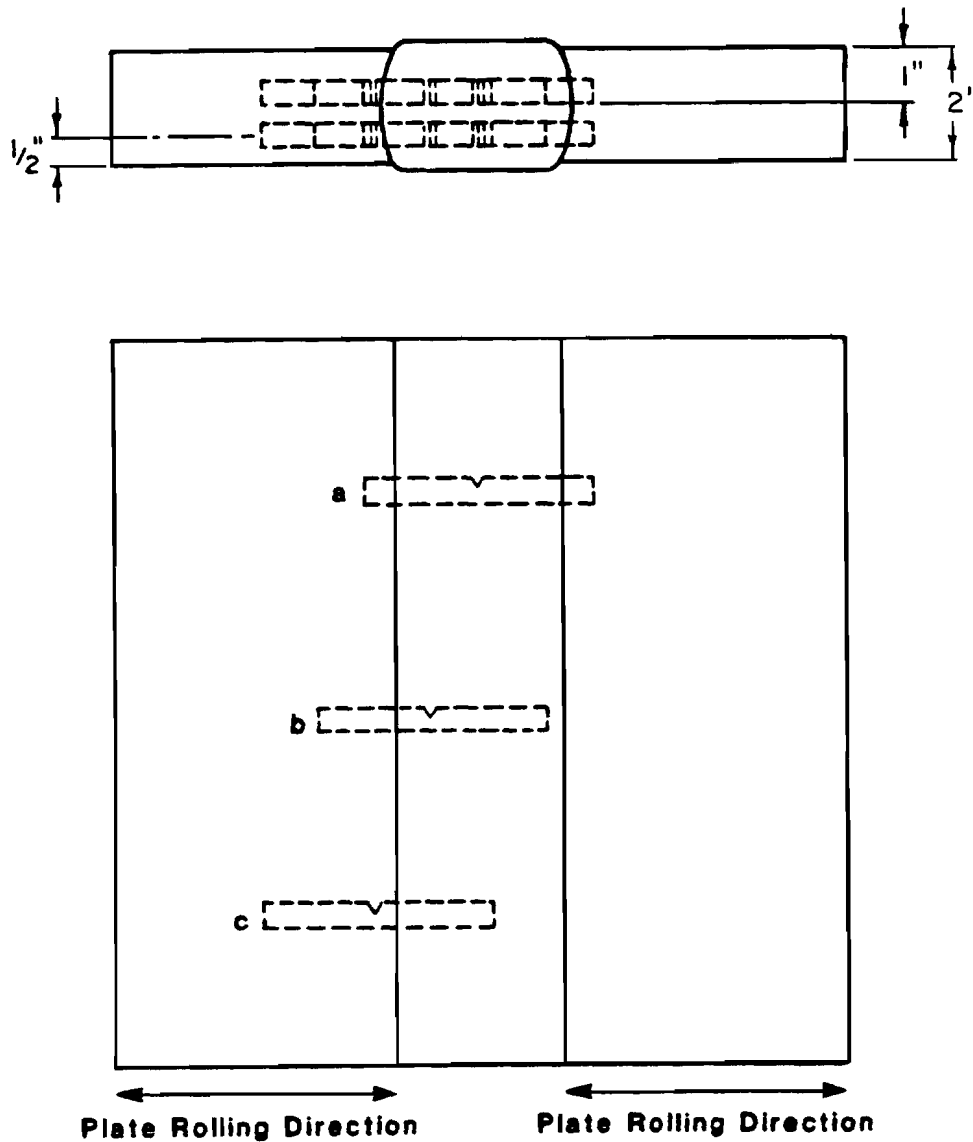
Figure 17.   SCHEMATIC ILLUSTRATION OF CHARPY V-NOTCH IMPACT
             SPECIMEN LOCATIONS. (a) WELD CENTERLINE,
             (b) COARSE COLUMNAR GRAIN ZONE, AND (c) HEAT
             AFFECTED ZONE 1.

respect to their notch location, weld number, material, etc., The

Charpy specimens for the ductile-brittle transition characteristics

determination were precracked by fatigue cycling to a total depth (in-

cluding the V notch) of 0.12-0.01 inch, using tension-zero loading with

cantilever beam loading.

Charpy specimens were then equilibrated in a liquid bath maintained

at the testing temperature (-100°F to 150°F). Specimens were then tested

individually in a 264 ft.lb. Tinius Olsen pendulum type instrumented

impact testing machine. This system is located at Battelle Northwest

Laboratories.

The automated instrumented impact system consisted of an instrumented

tup (strain gaged striker), velocity measuring/trigger unit, microproc-

essor, printer/plotter and a floppy disk drive. The load sensing gages

forming a wheatstone bridge circuit were cemented to the striker to sense

the compressive force interaction between the impact machine and specimen.

A photo-electric device was used to measure the hammer velocity and to

coordinate the data collection with the actual time of test. The device

employed a flag to interrupt a high intensity light immediately prior to

the instrumented tup impacting the test specimen. The signals generated

by the instrumented tup during the test were processed in a signal con-

ditioning module for signal amplification and selective filtering. This

data was then stored by a transient signal recorder and written on a

floppy disk. The stored data was then processed in a MOTOROLA micro-

processor unit to obtain the total energy absorbed (Charpy V-notch

impact toughness) by the specimen. The operational sequence of the testing procedure is shown in Figure 18.

The fracture surfaces were dried and coated with Tru-test Hi Q spray coating for protection.

2.3.5. Fracture Morphology. The fractured surfaces of selected Charpy specimens were cleaned ultrasonically in acetone and their fracture morphology studied using a JEOL (JSM-35) scanning electron microscope at 25 KV secondary operating voltage and a 39 mm working distance.

2.3.6. Crack Propagation Path. It was necessary to section the fracture surface perpendicular to the notch line (Figure 19) to study the relationship between the microstructure and the fracture path. The fracture surface was Nickel plated using a Watt's Nickel bath. Bath chemistry and plating conditions are given in Table VII. The plated specimen was sectioned in the orientation shown in Figure 19 using an abrasive cutoff wheel, and the microstructure was examined as described earlier.

2.3.7. Weldment Chemistry. Chemical analyses of the base metal and selected welds were carried out using a spectrographic analyser located at ESCO Corporation.
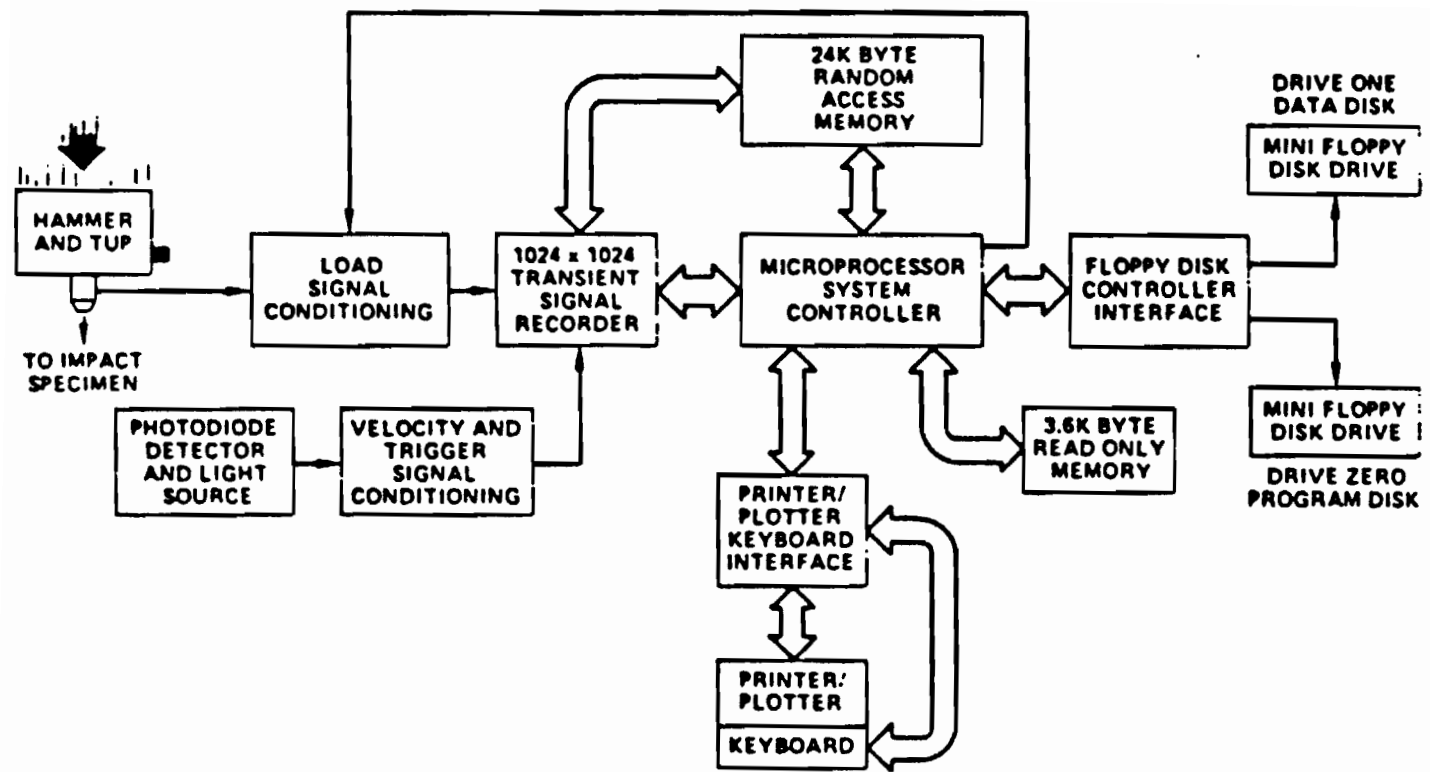
Figure 18. BLOCK DIAGRAM ILLUSTRATING AUTOMATED INSTRUMENTED IMPACT TESTING SYSTEM.

A

A

Crack Propagation Direction

V Notch

Fracture Surface

Sectioned Surface
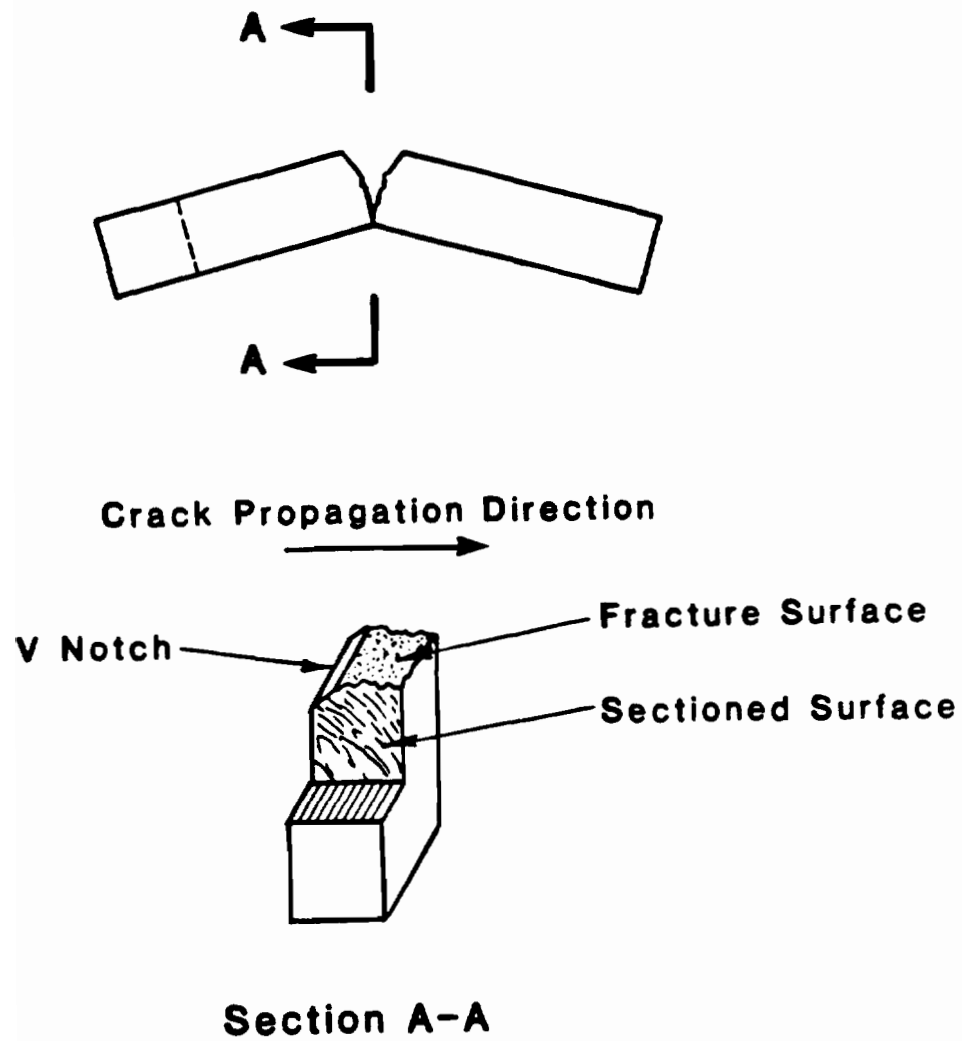
Section A-A

Figure 19.   SCHEMATIC ILLUSTRATION SHOWING SECTIONS MADE
ON FRACTURED CHARPY V-NOTCH IMPACT SPECIMEN
FOR CRACK PROPAGATION PATH ANALYSIS.

Table VII.

NICKEL PLATING SOLUTION CHEMISTRY AND PLATING CONDITIONS

Solution: Watt's Nickel Plating Solution
Anode: Graphite

Solution Chemistry

Compound	Amount
Nickel Sulphate	300 gms/liter
Nickel Chloride	45 gms/liter
Boric Acid	35 gms/liter
Hydrogen Peroxide	5 drops/gallon

Operational Conditions

pH range	$= 2$ to 4
Temperature	$= 50°C$
Current Density	$= 0.05$ Amps/sq.cm.
Voltage	$= 6$ to 12 volts

3. RESULTS

3.1. Process Variables

3.1.1. <u>Plate Grounding and Electrode Centering</u>. The location of the ground leads and the electrode plays an important role in controlling the weld penetration and providing a consistent weld width along the entire weld length. Four combinations of these two variables were studied in this investigation. They were off-centered and centered electrode positions with single and double ground connections. Results are shown in Figures 20-24. The grounding of both plates being welded and a centered electrode position (1/16 inch) resulted in uniform weld penetration and consistent weld width along the entire weld length.

3.1.2. <u>Slag Level</u>. Fluctuations in the current and the voltage were utilized to study the slag depletion during ESW. Photographs of the voltage-current display taken at three distinctive slag level situations are shown in Figure 25. Current fluctuations were minimal when an 1-1/2 inch deep slag was maintained (Case a). Intermittent spikes of medium amplitude were observed when the level was less than an inch (Case b). Finally, severe arcing and more frequent large amplitude current spikes occurred when the slag level was less than 1/2 inch. Oscilloscope analysis of the current and the voltage allowed the proper slag level to be maintained during welding.

3.1.3. <u>Current and Voltage Fluctuations</u>. Since the current and voltage provide the welding heat input and, hence, control the weld
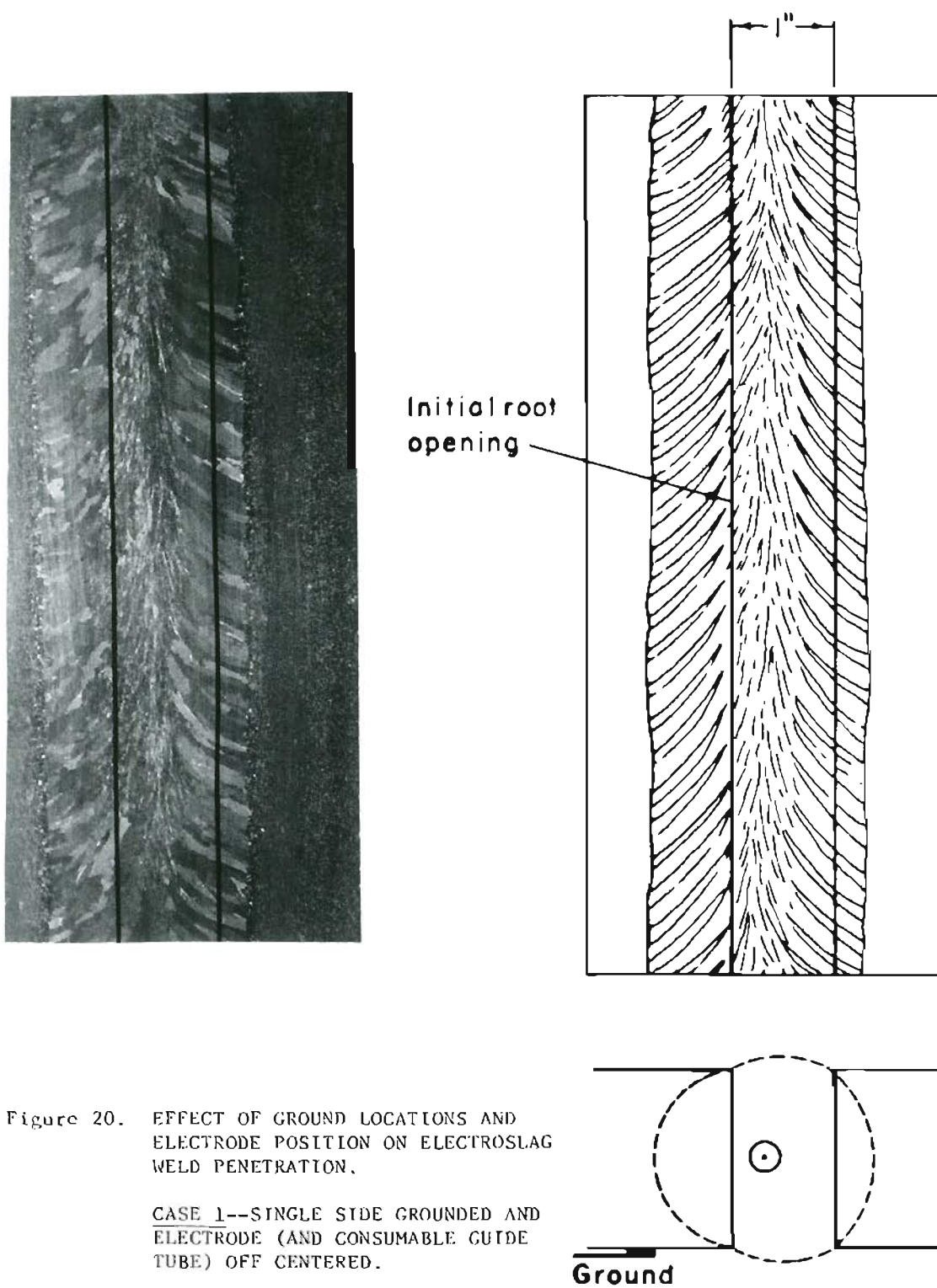
Figure 20. EFFECT OF GROUND LOCATIONS AND ELECTRODE POSITION ON ELECTROSLAG WELD PENETRATION.

CASE 1--SINGLE SIDE GROUNDED AND ELECTRODE (AND CONSUMABLE GUIDE TUBE) OFF CENTERED.

Initial root opening
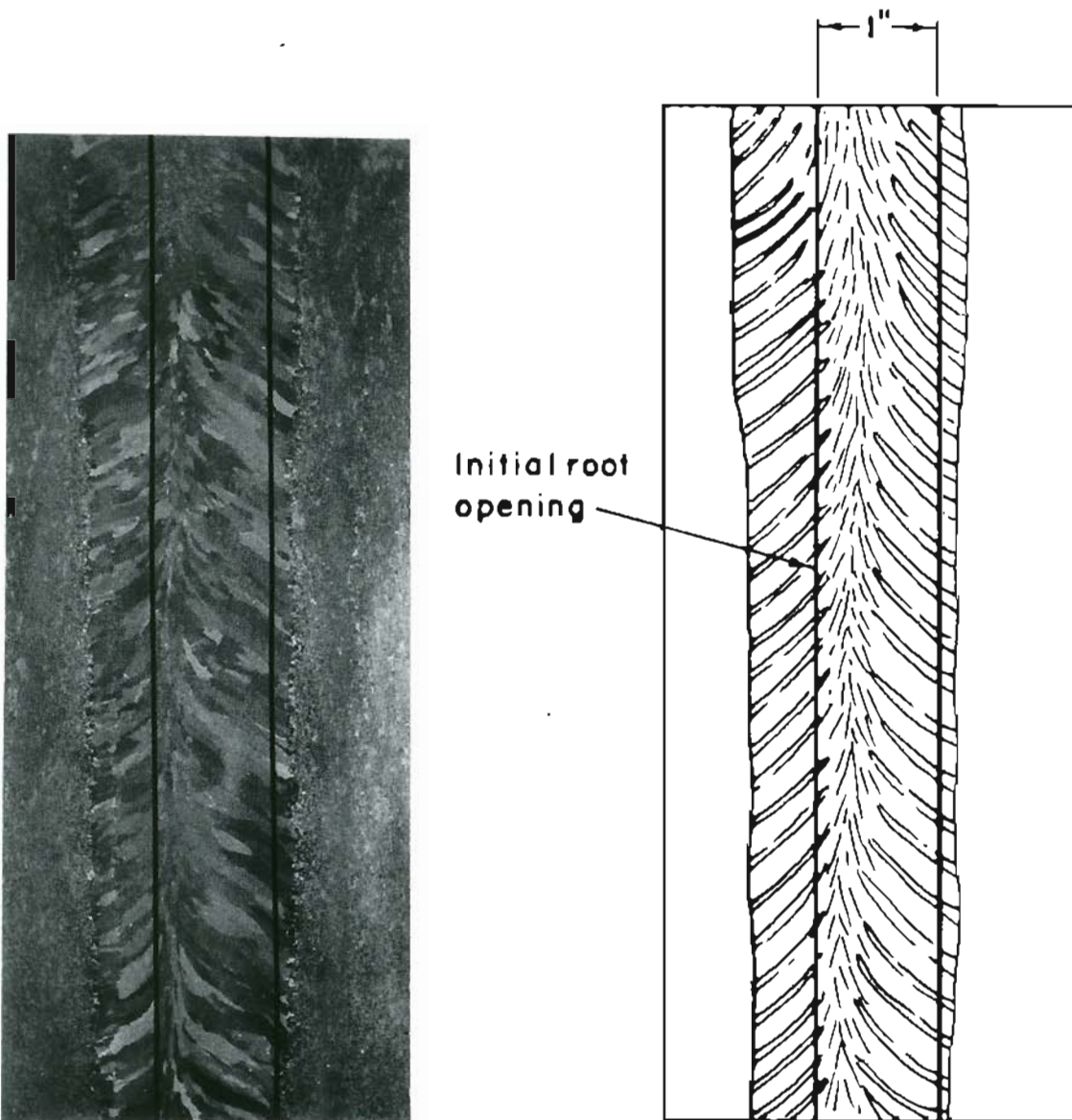
Figure 21. EFFECT OF GROUND LOCATION
AND ELECTRODE POSITION ON
ELECTROSLAG WELD PENETRATION.

CASE 2--BOTH PLATES GROUNDED
AND ELECTRODE (AND CONSUMABLE
GUIDE TUBE) OFF CENTERED.

Ground   Ground

Initial root opening
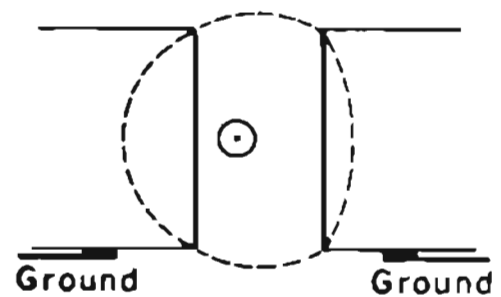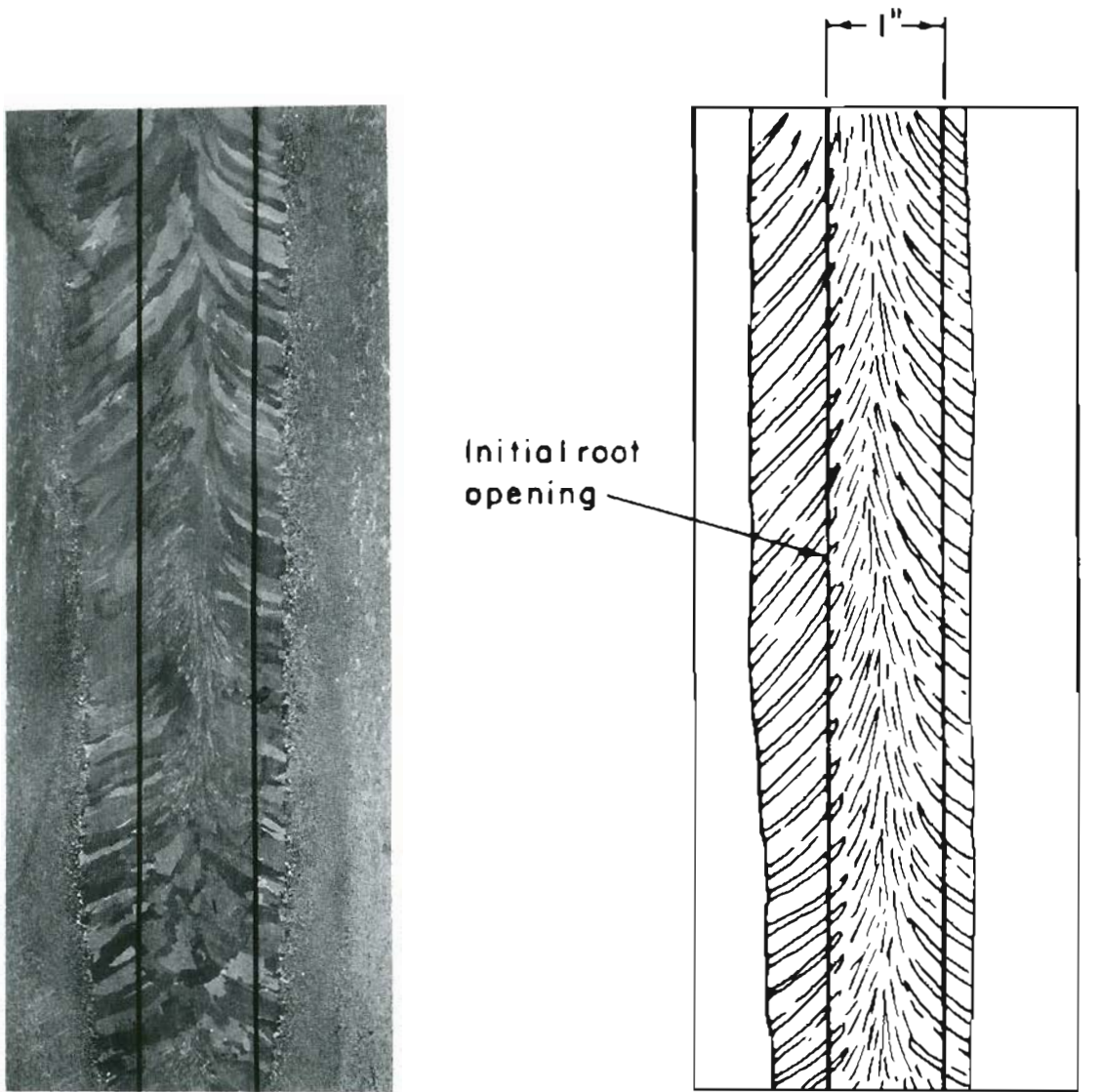
Figure 22. EFFECT OF GROUND LOCATION AND
ELECTRODE POSITION ON ELECTRO-
SLAG WELD PENETRATION.

CASE 3--SINGLE SIDE GROUNDED AND
ELECTRODE (AND CONSUMABLE GUIDE
TUBE) CENTERED.

Ground

Figure 23. EFFECT OF GROUND LOCATION AND ELECTRODE POSITION ON ELECTRO-SLAG WELD PENETRATION.

CASE 4--BOTH PLATES GROUNDED AND ELECTRODE (AND CONSUMABLE GUIDE TUBE) CENTERED.
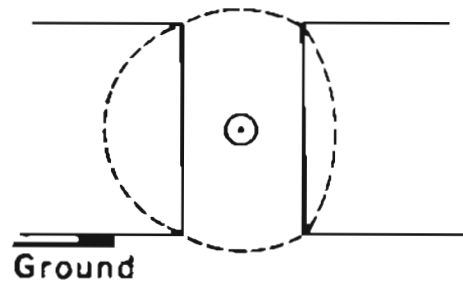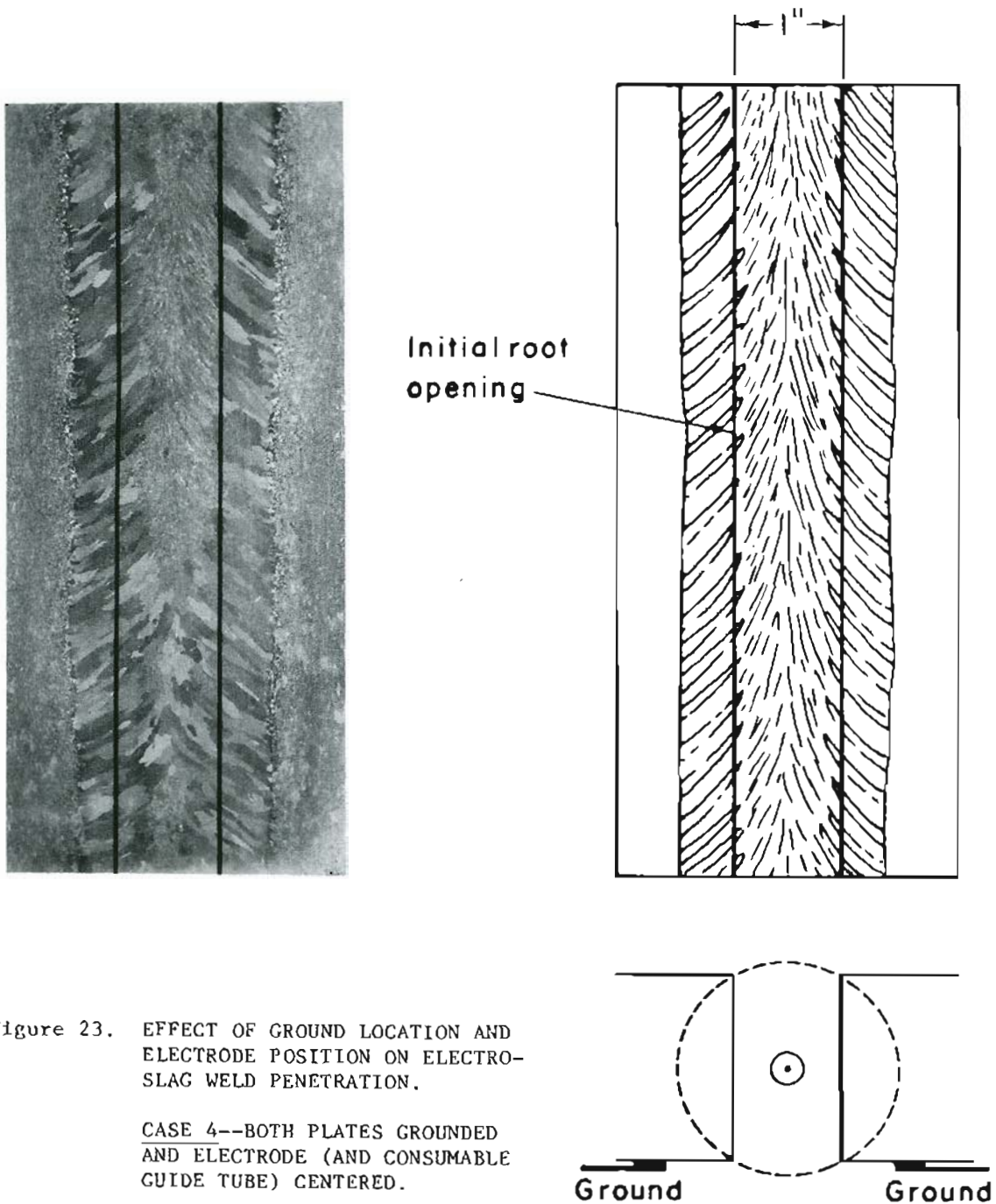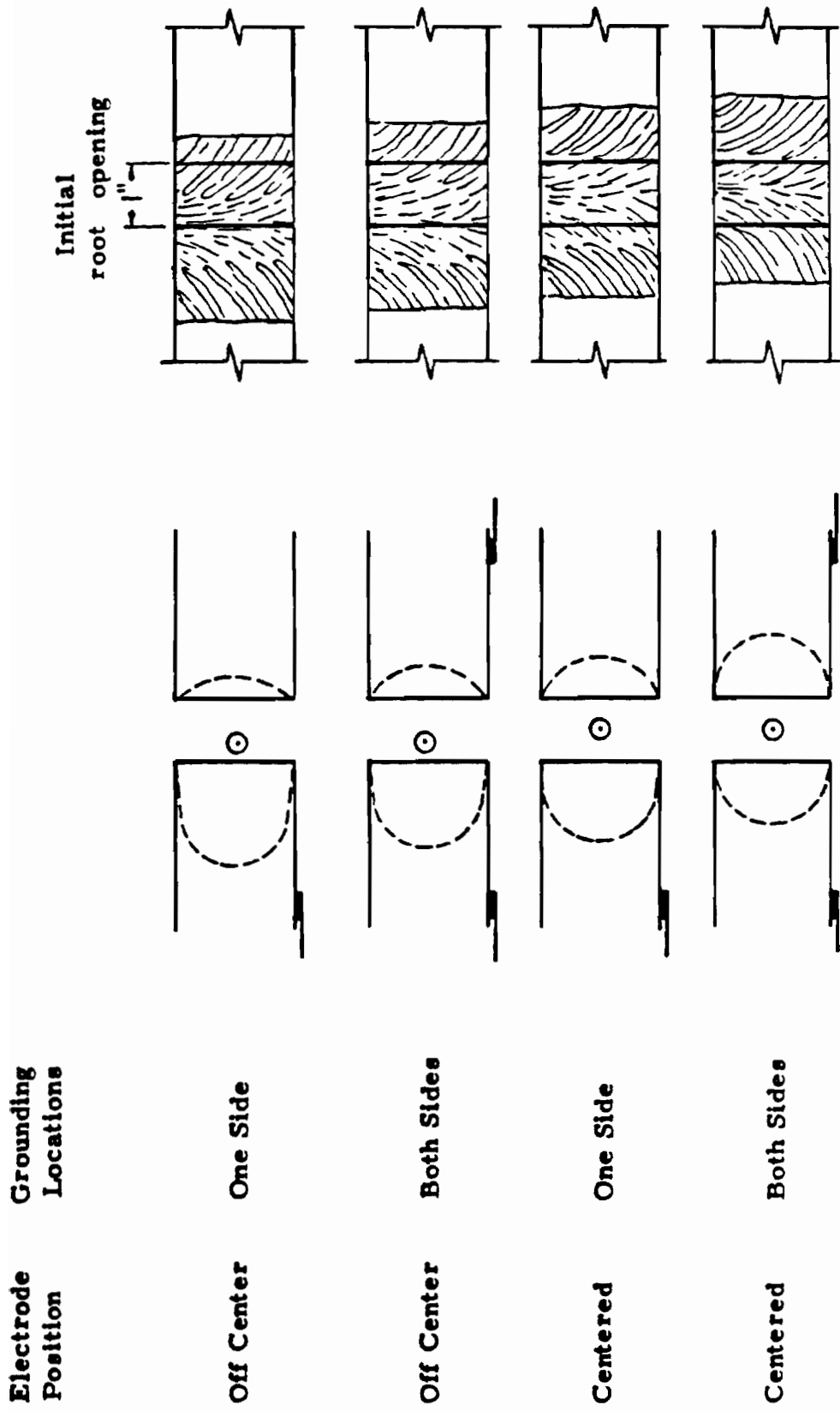
Figure 24. SUMMARY OF EFFECTS OF GROUND LOCATION AND ELECTRODE POSITION ON ELECTROSLAG WELD PENETRATION.
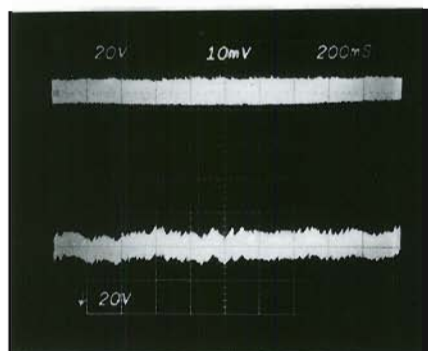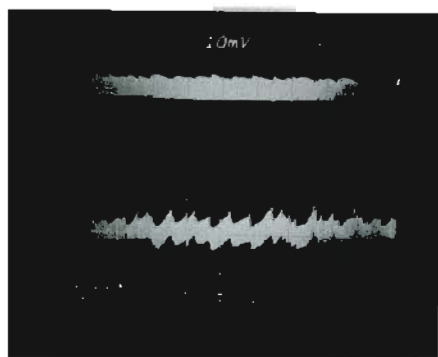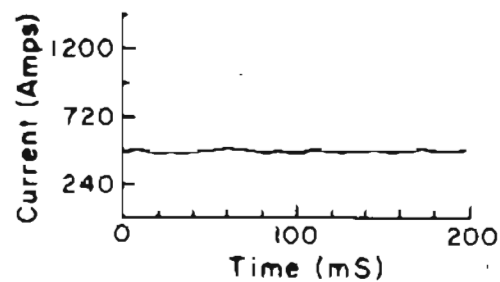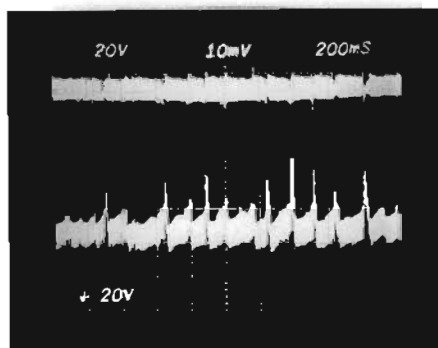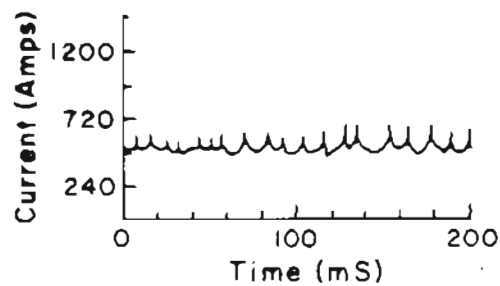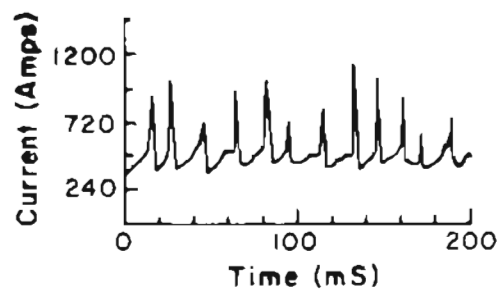
Figure 25. OSCILLOGRAPHS ILLUSTRATING THE SEQUENCE OF SLAG DEPLETION
DURING THE WELDING PROCESS

(a) Smooth running with proper slag depth
(b) Minor slag depletion
(c) Very shallow slag pool.

penetration/base metal dilution, weld chemistry, etc., their optimization and control is essential.

Periodic current fluctuations due to the guide tube melt off were observed in standard welds made with the bare metal consumable guide tube. Macrostructural analysis of those welds revealed a relation between such fluctuations and solute banding in welds. The relationship is illustrated in Figure 26.

Voltage fluctuations also affected the weld penetration. In extreme cases, slag entrapment occurred, Figure 27.

3.1.4. Current, Voltage, Guide Tube Geometry and Joint Gap.

Influence of process variables such as current, voltage, guide tube geometry, and joint gap on weld characteristics were studied. The voltage was selected as the first variable to assess its effect on the base metal dilution. Weld fixtures with two joint spacings, 1-1/4 and 3/4 inches, were used with bare metal and flux coated guide tubes, respectively. The current was held constant at 500 amperes while the voltage was varied from 30 to 45 volts at regular intervals. The relation between the voltage and the base metal dilution obtained is shown in Figure 28. A minimum of 42 volts was required in both cases to achieve complete edge fusion. Then, two additional welds with similar fixturing were made at that potential, varying the current from 500 to 800 amperes at set time intervals. Figure 29 illustrates the current vs. base metal dilution relationship. Current had a minor influence on dilution compared to voltage.
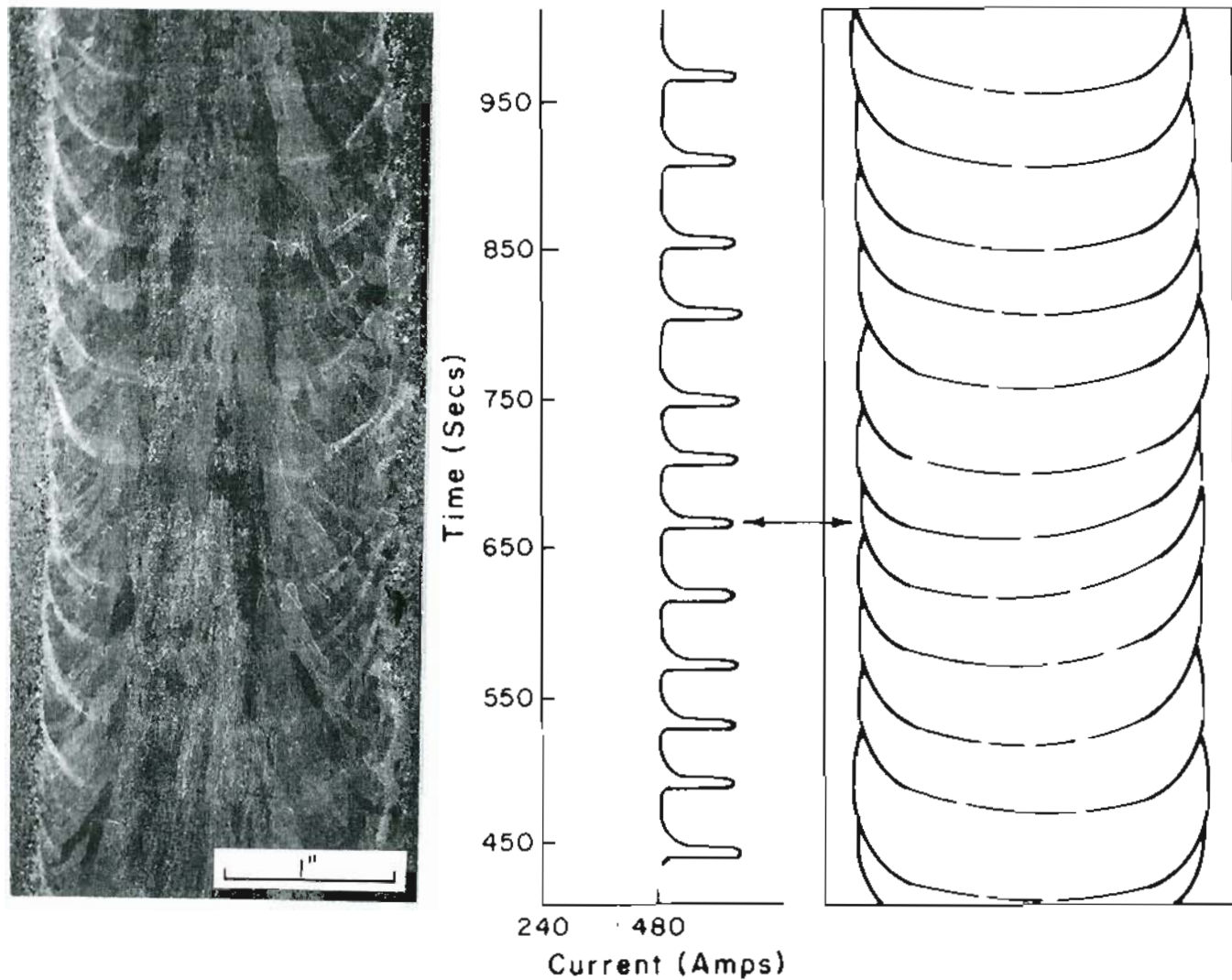
Figure 26. EFFECT OF MACROSCOPIC CURRENT FLUCTUATIONS ON THE ELECTROSLAG WELD MACROSTRUCTURE; SOLUTE BAND FORMATION.

68.

Figure 27. ES WELD MACROSTRUCTURE SHOWING SLAG ENTRAPMENT
RESULTING FROM A SEVERE FLUCTUATION IN VOLTAGE
(45 to 32 VOLTS).
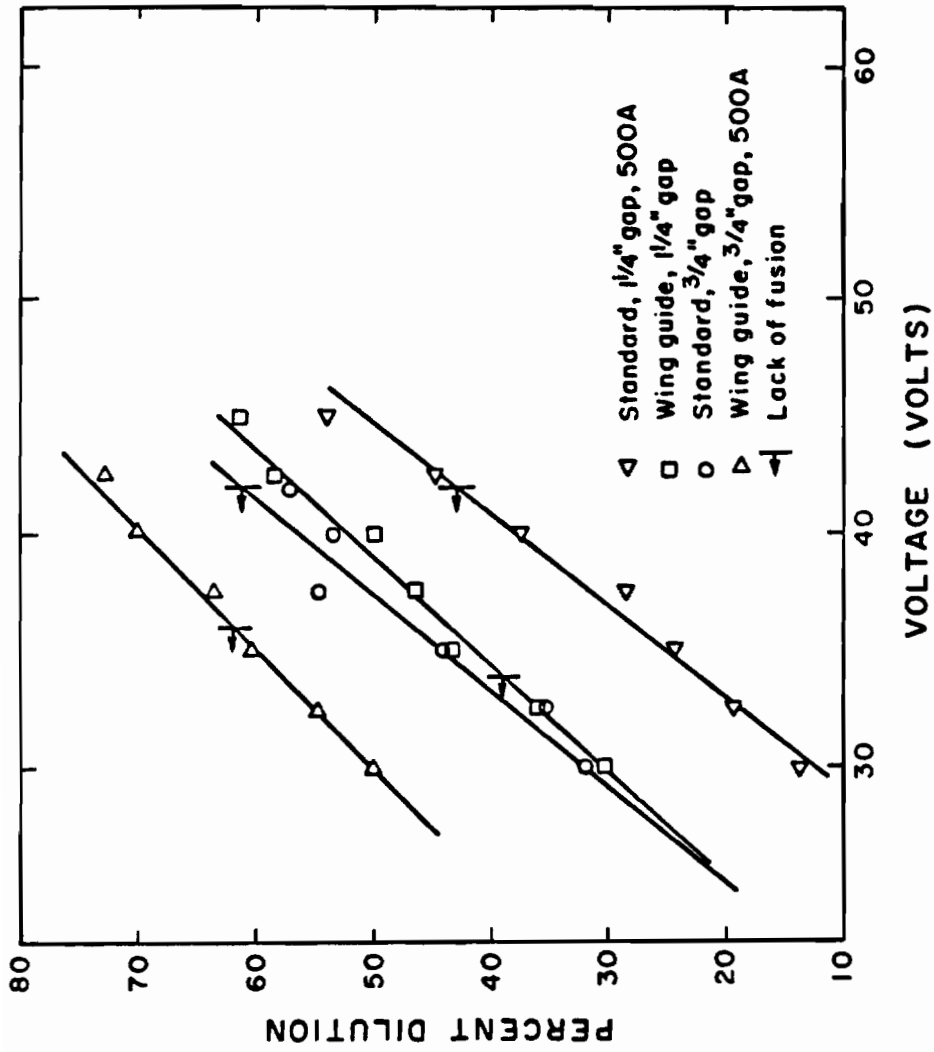
Figure 28. EFFECT OF WELDING VOLTAGE ON BASE METAL DILUTION FOR VARIOUS GUIDE TUBE GEOMETRIES AND JOINT SPACINGS IN ESW.
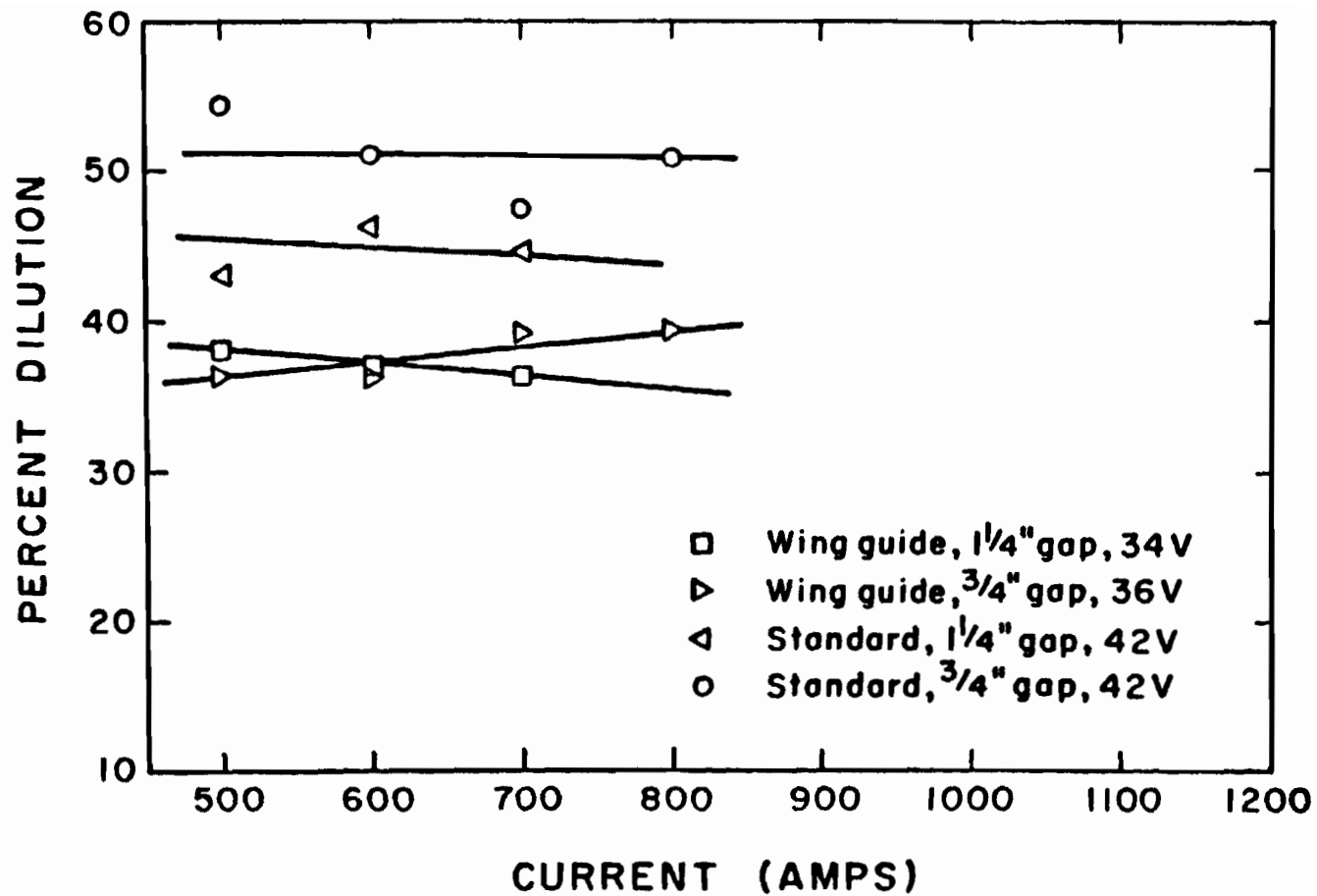
Figure 29. EFFECT OF WELDING CURRENT ON BASE METAL DILUTION FOR VARIOUS GUIDE TUBE GEOMETRIES AND JOINT SPACINGS IN ESW.

An even distribution of heat towards the plate edge was necessary
in order to achieve complete edge penetration in welds made below 42
volts. Hence, a wing guide tube was used and four welds were made under
the conditions described above. Complete weld penetration was achieved
at 34 volts in the case of 1-1/4 inch root gap, while 36 volts were
necessary for a 3/4 inch joint spacing. Base metal dilution vs. voltage
and current relationships are presented in Figures 28 and 29, respec-
tively.

Current and wire feed rate were interdependent since a constant
voltage power source was used for the electroslag welding process. The
feed rate increased with an increase in current. The wing guide tube
configuration used in this investigation had 50 percent more cross sec-
tional area that the standard cylindrical guide tube (0.3493 compared to
0.2344 sq. inch) and, hence, a higher current carrying capacity. As a
result, at a particular current setting, the wire feed rate was signifi-
cantly reduced for the wing guide tube compared to the standard one. The
current vs. wire feed rate relations for two guide tube geometries (wing
and standard guides) at different joint spacings (1-1/4 and 3/4 inches)
are presented in Figure 30.

The wing guide tube used with a 3/4 inch joint spacing carried the
maximum current at a given wire feed rate. This feature was utilized to
prepare a high current/narrow gap weld using a 1000 amperes current at
40 volts. The wire feed rate was 325 inches per minute (ipm), and the
weld was completed in 12 minutes. Whereas a standard weld made with 600
amperes current at 42 volts with the wire feed rate of 225 ipm using an

73.
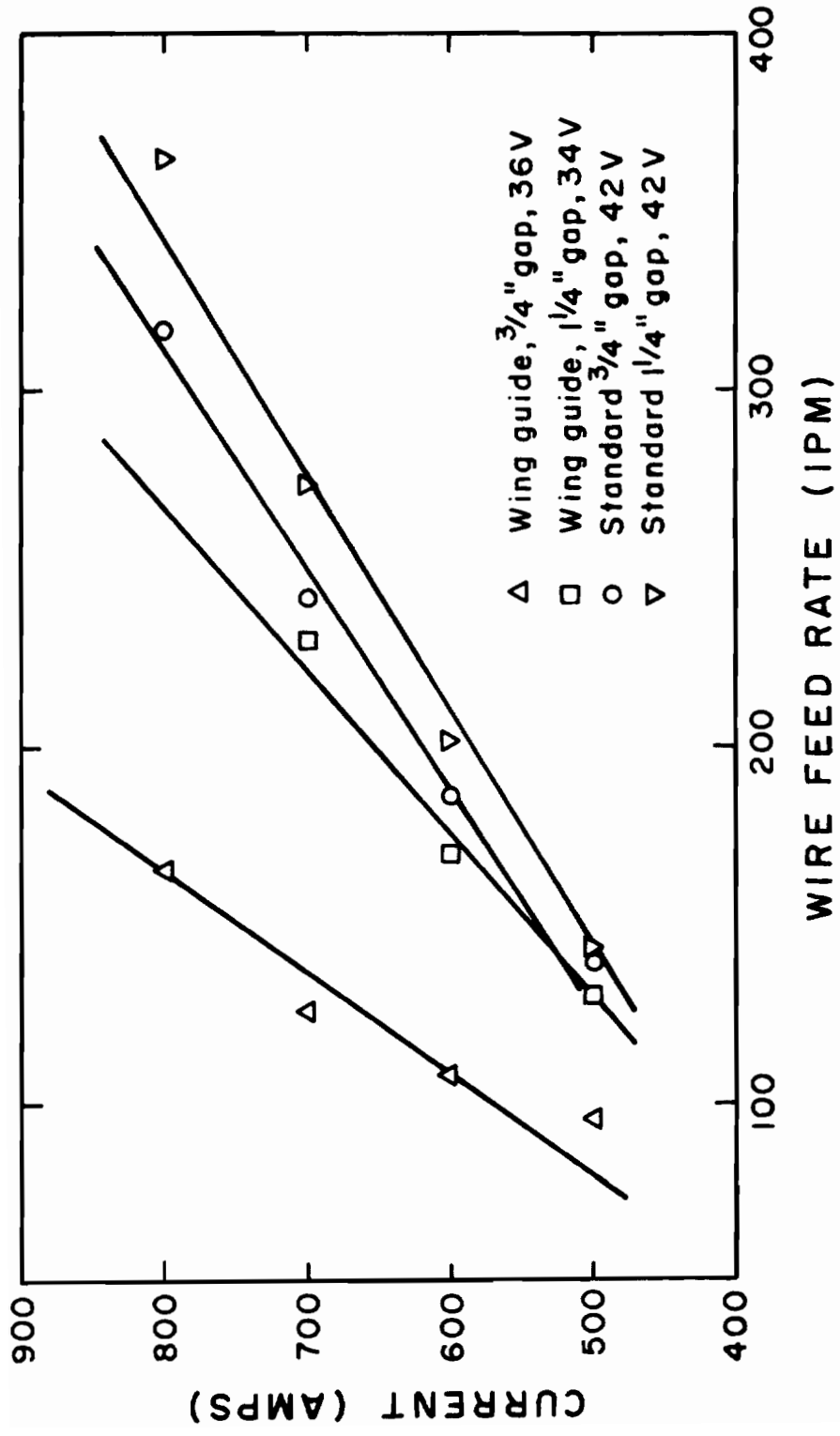
Figure 30. RELATIONSHIP BETWEEN WELDING CURRENT AND WIRE FEED RATE FOR VARIOUS GUIDE
TUBE GEOMETRIES AND JOINT SPACINGS IN ESW.

1-1/4 inch joint spacing required about 36 minutes. The reduced weld time resulted in about 50% reduction in heat input per inch of the weldment (see Appendix A for the heat input calculations). The percent base metal dilution for the high current/narrow gap and the standard welds were 58 and 41 percent, respectively. From analysis of the macrostructures of these two welds, Figure 31, it is evident that angle of inclination of the CCG's in the narrow gap weld was less than that in the standard weld.

The weld centerline microstructures of both welds are given in Figures 32a through c. The narrow gap weld grain structure was slightly refined and the proeutectoid ferrite dispersed. Whereas in the standard weld, the proeutectoid ferrite was present in the form of continuous films along the grain boundaries parallel to the welding direction. A microstructural comparison between the heat affected zones of the standard and the high current/narrow gap welds, Figure 33, revealed a 50 percent reduction in width of the coarse grained HAZ size for the high current/narrow gap weld. Yet, the HAZ grain size immediately adjacent to the fusion line did not change.

3.2. As-Welded Grain Refinement

Typical microstructures of weldments made using the mullite-shielded consumable guide tube assembly are shown in Figure 34. The mullite shielding, per se, did not result in any grain refinement. However, when mechanical vibration was coupled to the mullite shrouded guide tube, significant grain refinement occurred. This grain refinement,
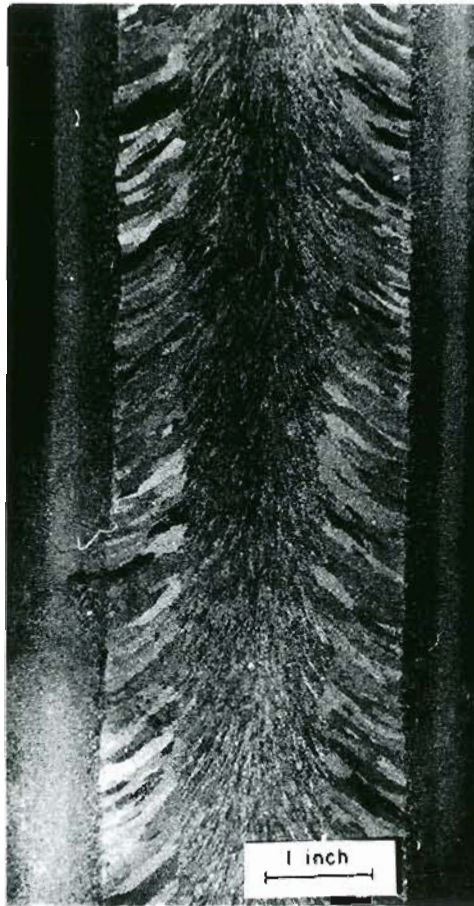
Standard
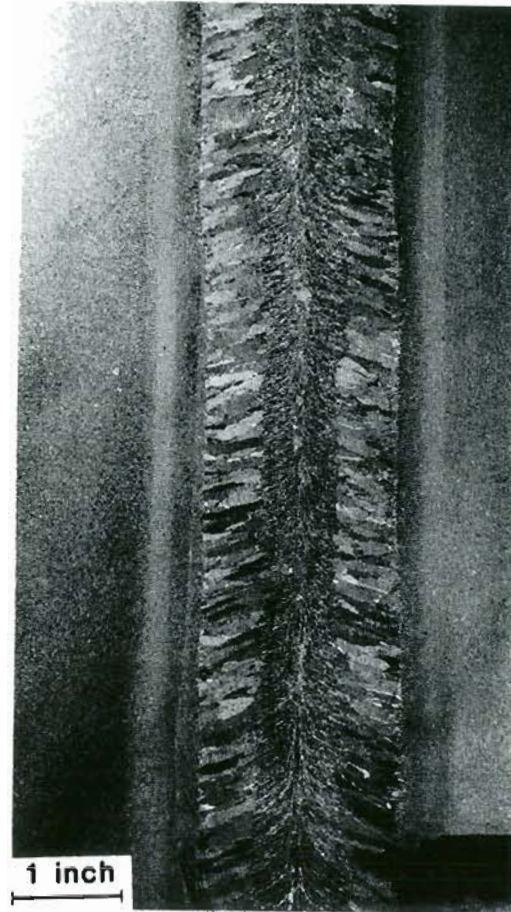
Narrow Gap-High Current

Figure 31. COMPARISON OF STANDARD (CYLINDRICAL GUIDE, 1-1/4" GAP, 600 AMPS, 42 VOLTS) AND HIGH CURRENT/NARROW GAP/WINGED GUIDE (1000 AMPS, 3/4" GAP, 40 VOLTS) I.S WELD MACROSTRUCTURES (FILLER WIRE A). ETCHANT--10% NITAL.
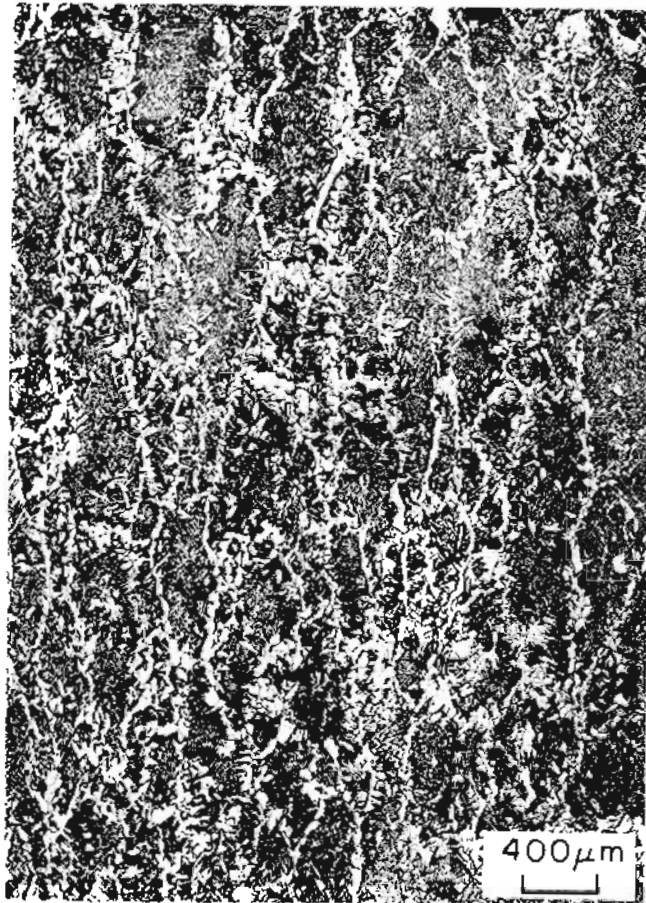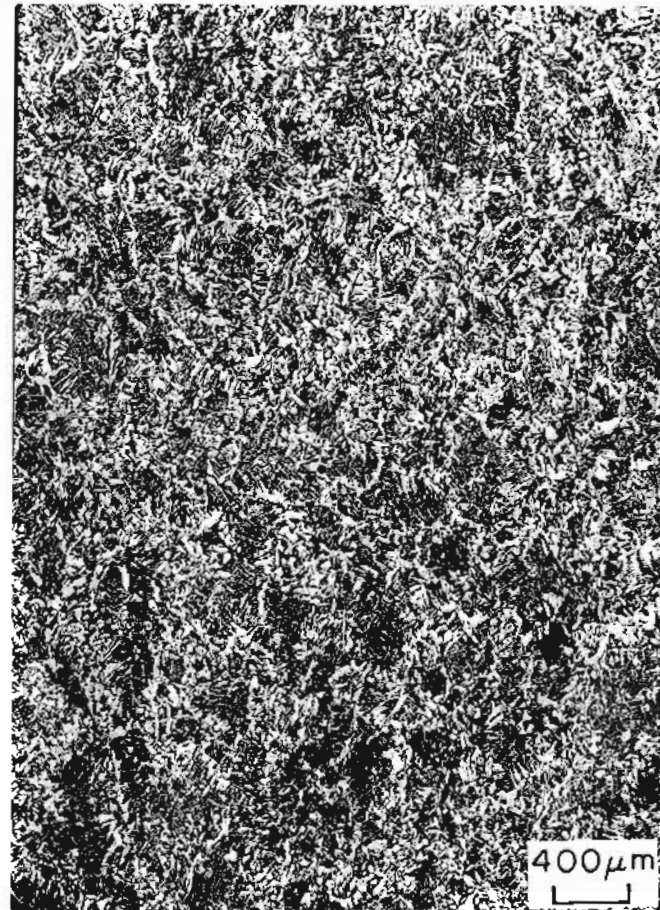
Standard   High Current/Narrow gap/Winged guide

Figure 32a.   COMPARISON OF STANDARD (CYLINDRICAL GUIDE, 1-1/4" GAP, 600 AMPS, 42 VOLTS) AND
               HIGH CURRENT/NARROW GAP/WINGED GUIDE (1000 AMPS, 3/4" GAP, 40 VOLTS) ES WELD
               MICROSTRUCTURES AT WELD CENTERLINE LOCATION (FILLER WIRE A). ETCHANT--2% NITAL.
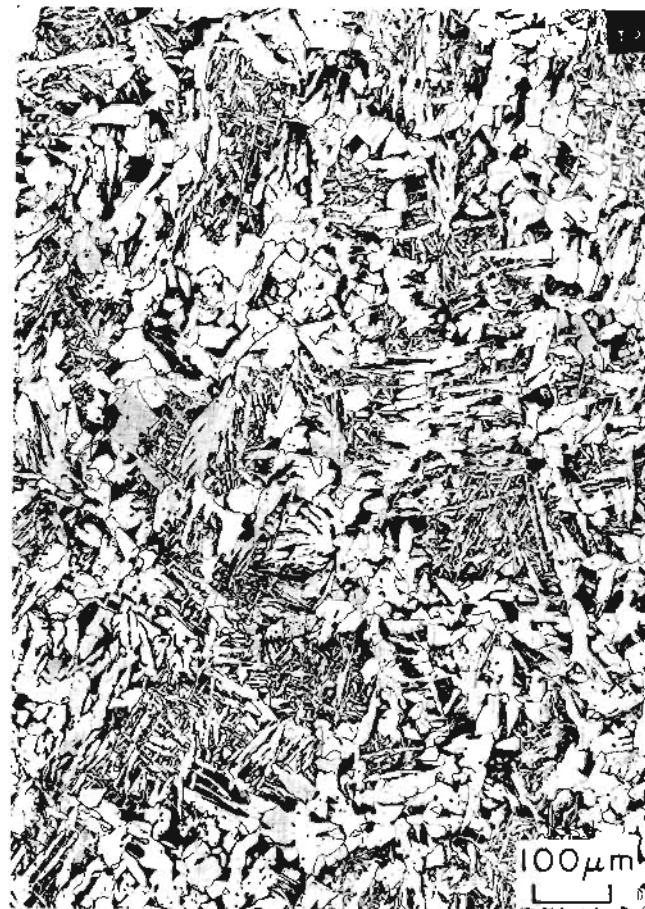
Standard   High Current/Narrow gap/Winged guide

Figure 32b.   COMPARISON OF STANDARD (CYLINDRICAL GUIDE, 1-1/4" GAP, 600 AMPS, 42 VOLTS) AND
HIGH CURRENT/NARROW GAP/WINGED GUIDE (1000 AMPS, 3/4" GAP, 40 VOLTS) ES WELD
MICROSTRUCTURES AT WELD CENTERLINE LOCATION (FILLER WIRE A). ETCHANT--2% NITAL.

Standard   High Current/Narrow gap/Winged guide

Figure 32c.   COMPARISON OF STANDARD (CYLINDRICAL GUIDE, 1-1/4" GAP, 600 AMPS, 42 VOLTS) AND
              HIGH CURRENT/NARROW GAP/WINGED GUIDE (1000 AMPS, 3/4" GAP, 40 VOLTS) ES WELD
              MICROSTRUCTURES AT WELD CENTERLINE LOCATION (FILLER WIRE A).   ETCHANT--PICRAL.

Fusion line
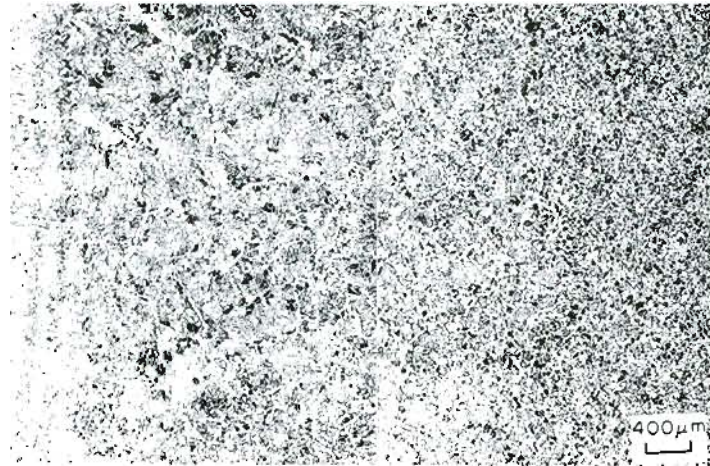
High current/narrow gap/winged
guide weld HAZ

Figure 33. COMPARISON BETWEEN HEAT AFFECTED ZONES
OF STANDARD (CYLINDRICAL GUIDE, 42 VOLTS,
600 AMPS, AND 1-1/4" GAP) AND HIGH
CURRENT/NARROW GAP/WINGED GUIDE (40 VOLTS,
1000 AMPS, AND 3/4" GAP) ES WELDS. A
50% REDUCTION IN HAZ 1 WIDTH WAS
OBSERVED.

400µm

Fusion line

Standard weld HAZ

400µm

MULLITE SHROUD--VIBRATION

BARE GUIDE TUBE

a. Non Vibrated   b. Vibrated
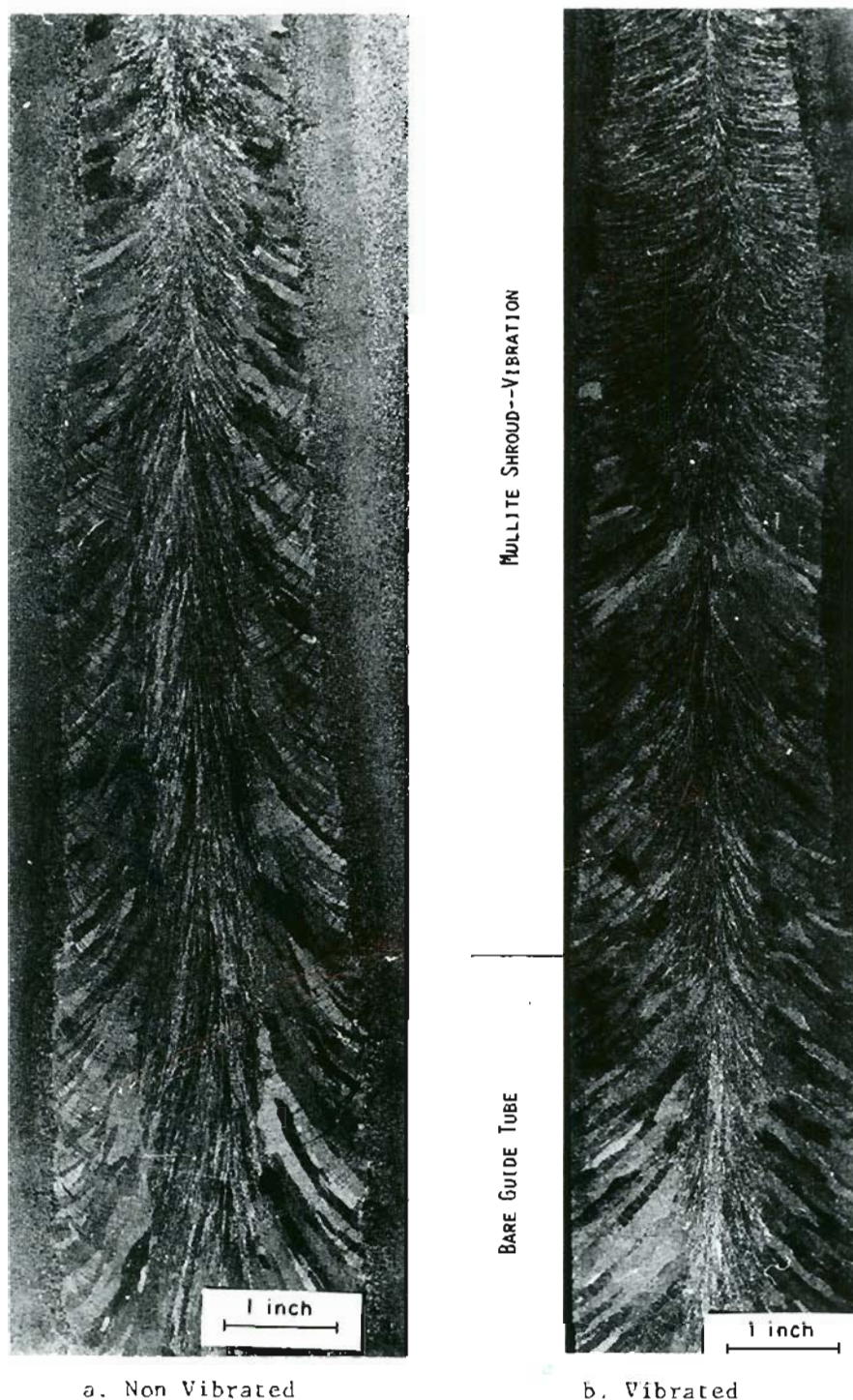
Figure 34. MACROSTRUCTURES OF ES WELDS MADE WITH MULLITE (3/16 INCH SHROUDED CONSUMABLE GUIDE (ETCHANT--10% NITAL)

a. NON VIBRATED GUIDE
b. VIBRATED CONSUMABLE GUIDE (35 HZ RESONANCE VIBRA-TION).

however, occurred only after 5 inches of the weld had been completed. During this initial 5 inch section, mullite was consumed into the slag pool which resulted in a highly viscous and cooler slag. Furthermore, the mullite shrouding was fragile and easily chipped during welding resulting in entrapped mullite in the weld. Thus, in order to induce grain refinement with mullite shielding, supplemental vibration was necessary as well as a change in slag bath chemistry and characteristics.

On the other hand, the use of fused quartz shrouding around the consumable guide tube produced a substantial grain refinement in all cases, as shown in Figure 35. The quartz sleeve effectively shielded the guide tube and resulted in deep extension of the quartz and guide tube into the slag (Figure 36). Significantly, grain refinement was achieved without supplemental mechanical vibration unlike the case of mullite. Furthermore, grain refinement was achieved immediately upon contact of the quartz sleeve with the slag bath and the resulting weld structure was uniform across the entire weld. Slag contamination was reduced since the quartz sleeve was only 0.04 inch thick versus 3/16 inch thick for the mullite and macroscopic solute banding normally present in conventional welds was not observed. Throughout the electroslag weld process in which the quartz was inserted, persistent arcing occurred as shown by voltage and current trace analysis, Figure 37. Furthermore, an intense stirring action was observed even without supplemental mechanical vibration. Due to the thermal shielding behavior of the quartz shroud, a high voltage (48 volts) was required in order to achieve com-

82.

QUARTZ SHROUD

BARE
METAL
GUIDE
TUBE

1 inch

1inch

a. Non Vibrated
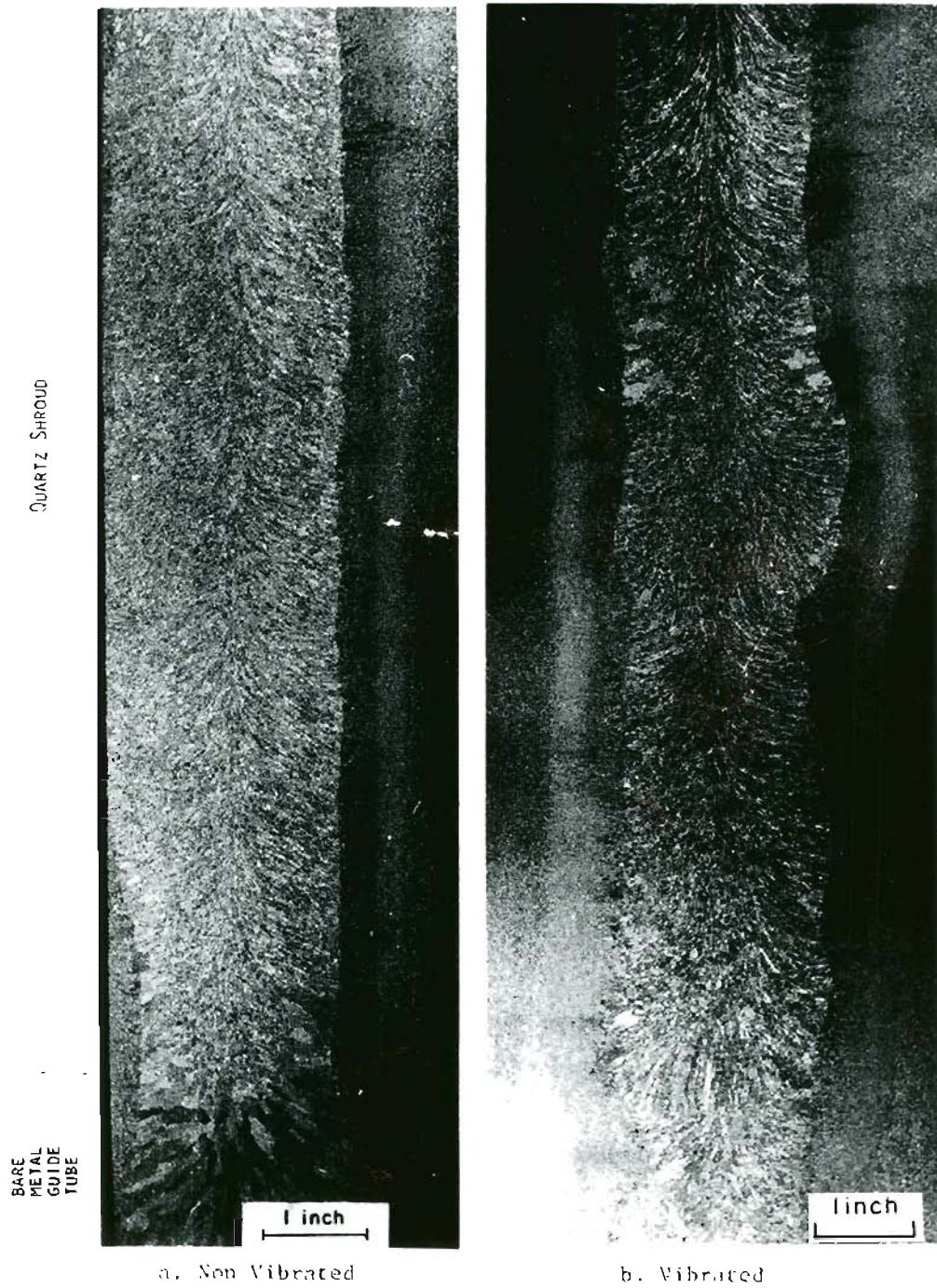
b. Vibrated

Figure 35. MACROSTRUCTURES OF ES WELDS MADE WITH QUARTZ (1 mm
THICK SHROUDED CONSUMABLE GUIDE (ETCHANT--10% NITAL)

a. NON VIBRATED GUIDE
b. VIBRATED CONSUMABLE GUIDE (35 HZ RESONANCE VIBRA-
TION).
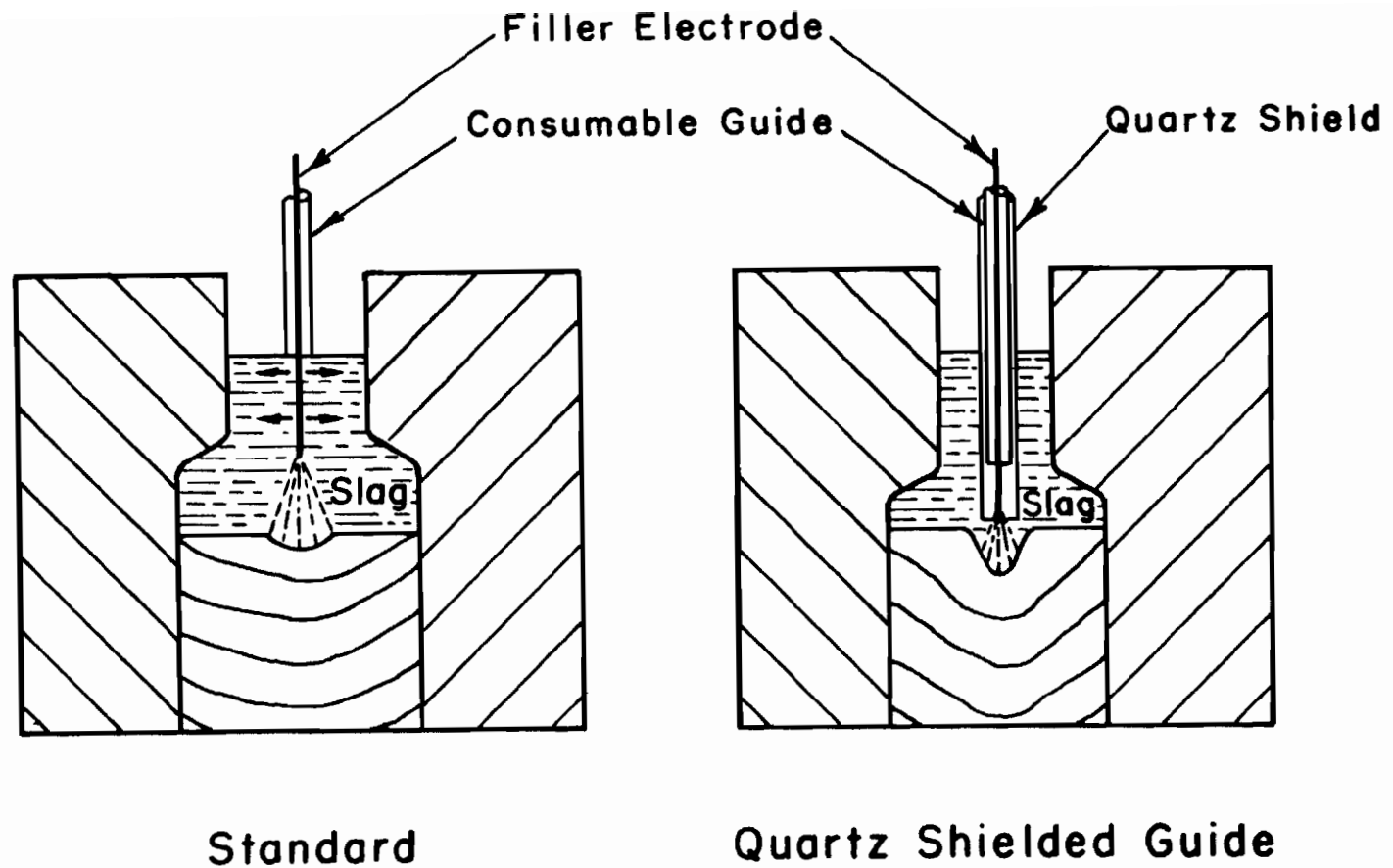
Figure 36. SCHEMATIC REPRESENTATION OF GUIDE TUBE POSITION IN THE SLAG POOL DURING STANDARD AND QUARTZ SHIELDED GUIDE TUBE ELECTROSLAG WELDING.
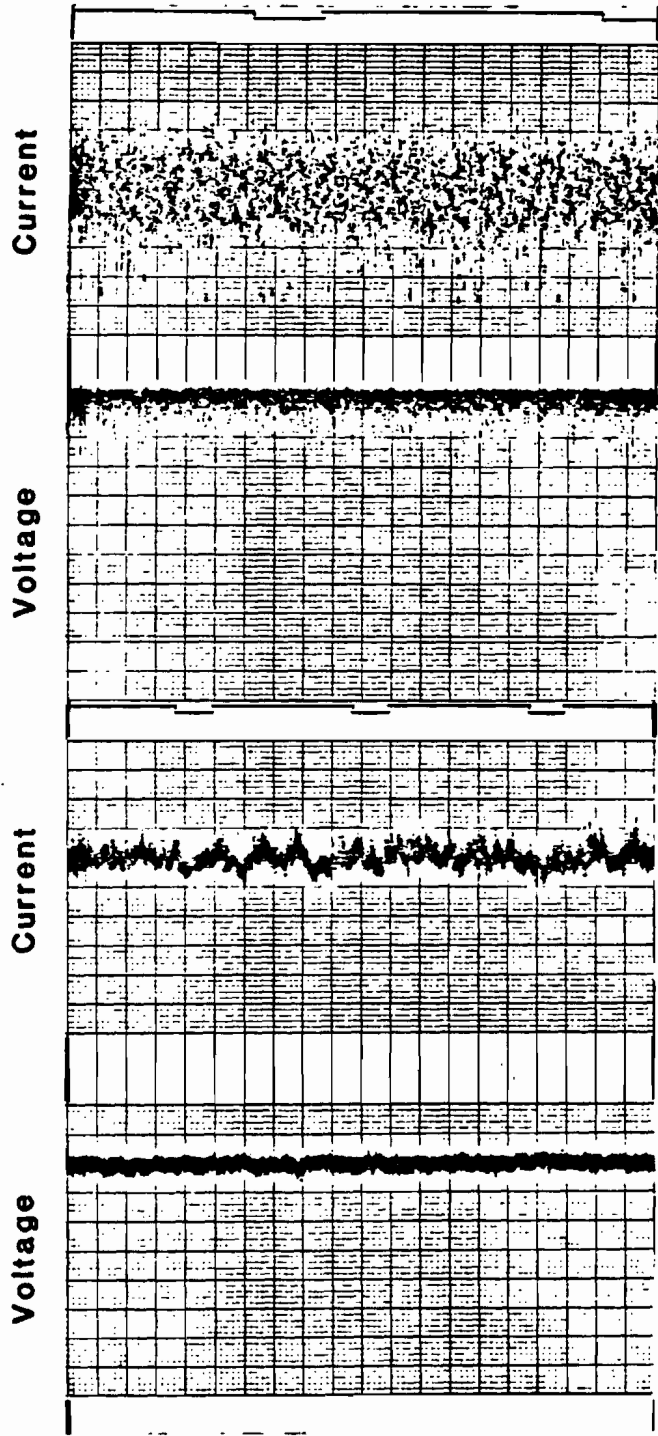
Figure 37. CURRENT AND VOLTAGE RECORD MADE DURING STANDARD AND QUARTZ SHIELDED GUIDE
TUBE ELECTROSLAG WELDING.

plete edge fusion. The guide tube/weld pool interactions are shown schematically in Figure 38 for both standard as well as grain-refined welds.

ES welds made with either an independently vibrated quartz probe inserted into the slag bath or vibration of the entire plate fixture (table top) failed to exhibit any grain refinement. Macro and microstructures of the table top vibrated weld are shown in Figures 39-40. Insulating materials other than the 3/16 inch thick mullite shroud and 0.04 inch thick quartz shroud used in this investigation, were ineffective in shielding the consumable guide tube.

Microstructural analysis of the standard and the quartz shielded grain refined welds presented in Figure 41a-f revealed that despite a uniform grain size across the quartz-refined weld, the grains were still elongated. Welds exhibiting refined grains also exhibited increased amounts of proeutectoid ferrite. Weld centerline structures remained identical for both standard and refined weldments, but the quartz shielding effectively eliminated the entire coarse columnar zone.

3.3 Weld Metal Alloy Additions

The macrostructure of the ES weld made using alloyed filler wire E (Cr-Mo) is shown in Figure 42. The weld metal consisted of a bainitic microstructure, Figures 43a and b. The transmission electron microscopy showed a heavily dislocated, lath type ferrite structure, Figure 44, and identified cementite along the lath boundaries, Figure 45. Complete absence of proeutectoid films in the alloyed weld metal is shown in

a.

b.

c.

Figure 38.   GUIDE TUBE-SLAG POOL INTERACTION DURING ELECTROSLAG
             WELDING

             a. STANDARD CYLINDRICAL GUIDE--GUIDE TUBE MELT-OFF
             b. MULLITE SHIELDED GUIDE TUBE--GUIDE TUBE EXTENSION
                INTO THE SLAG POOL
             c. QUARTZ SHIELDED GUIDE TUBE--GUIDE TUBE EXTENSION
                INTO THE SLAG POOL WITH VIGOROUS STIRRING ACTION.

1 inch
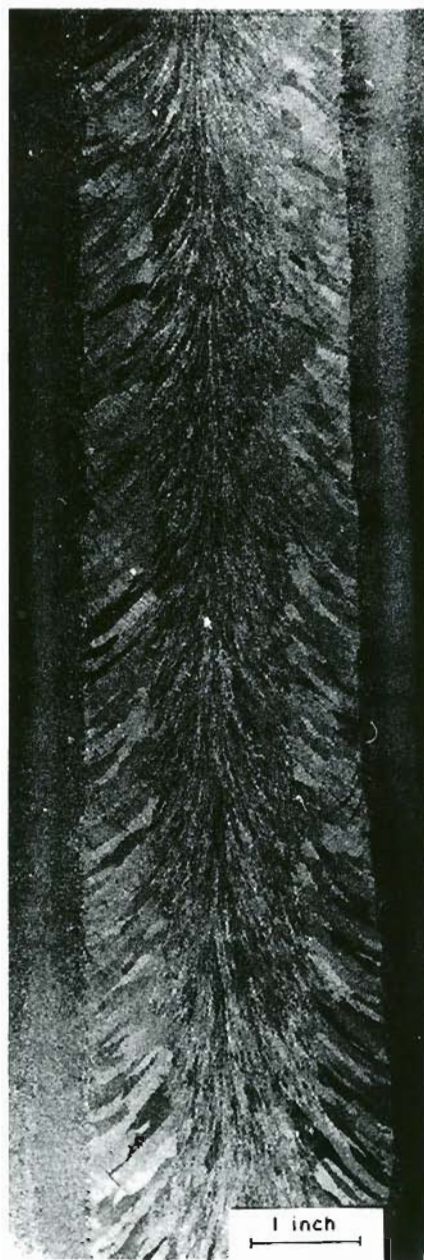
Figure 39.   TABLE TOP (PLATE FIXTURE) VIBRATED ES WELD MACRO-
STRUCTURE (WIRE A).   ETCHANT--10% NITAL.
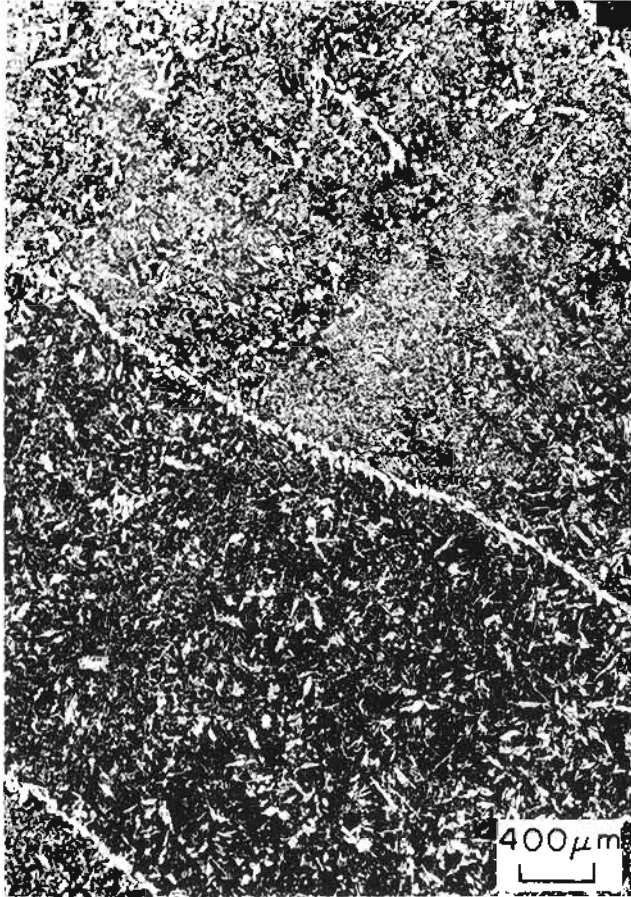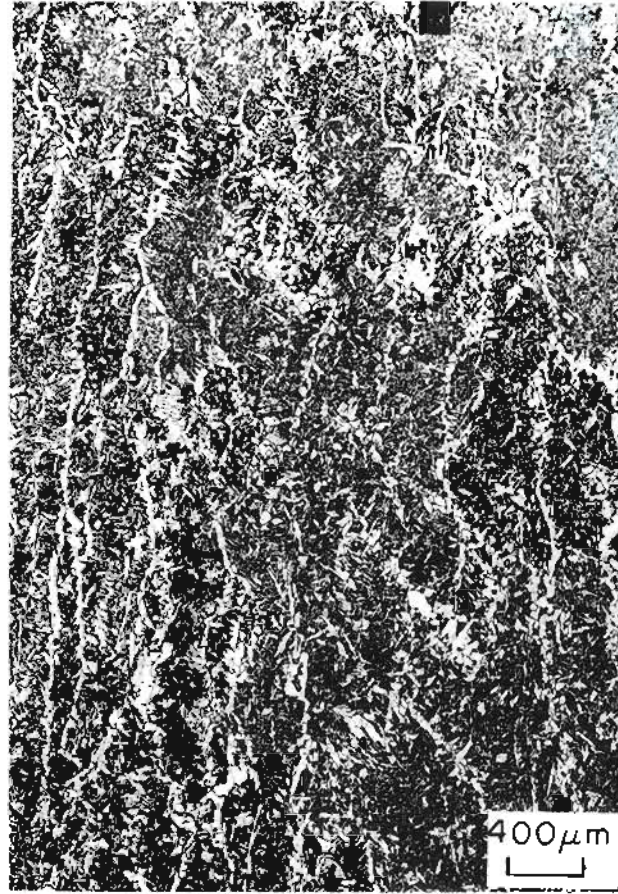
Coarse Columnar Grain Zone   Weld Center Line

Figure 40.   TABLE TOP (PLATE FIXTURE) VIBRATED ES WELD MICROSTRUCTURES (WIRE A).
             ETCHANT--2% NITAL.
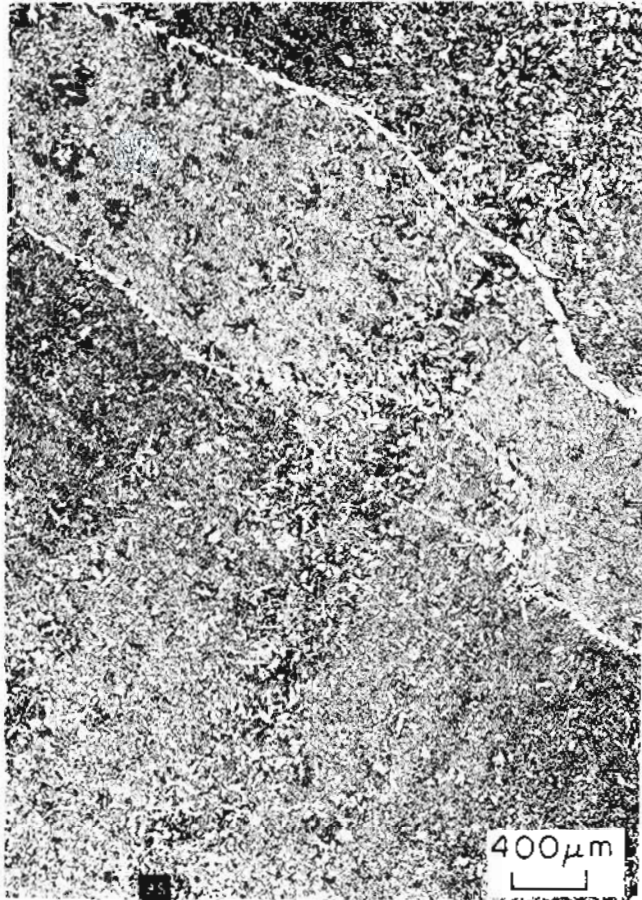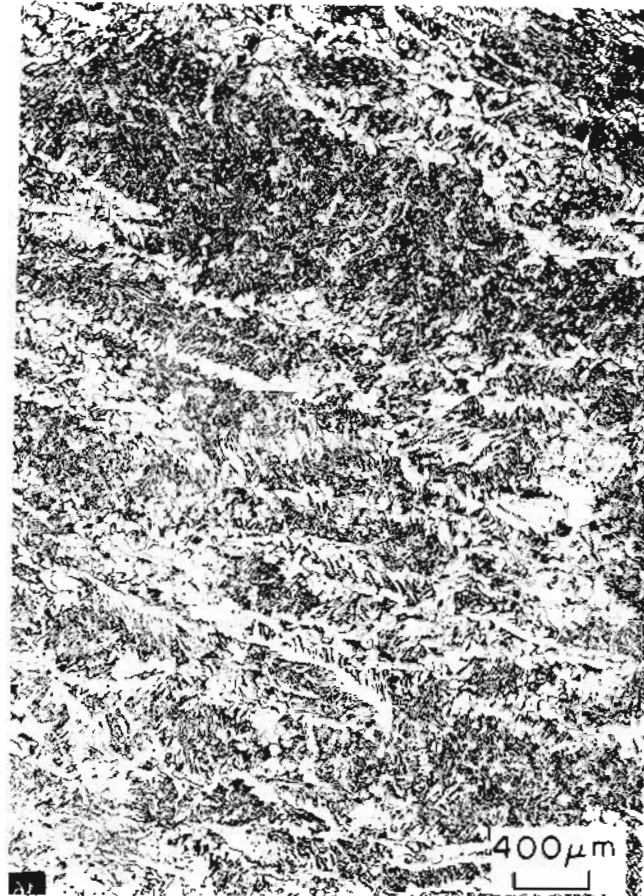
Standard   Grain Refined (Quartz Shielded)

Figure 41a.   COMPARISON OF STANDARD (CYLINDRICAL GUIDE, 1-1/4" GAP, 42 VOLTS, 600 AMPS)
              AND GRAIN REFINED (QUARTZ SHIELDED GUIDE, 1-1/4" GAP, 48 VOLTS, 600 AMPS)
              ES WELD MICROSTRUCTURES ADJACENT TO FUSION LINE (WIRE A).   ETCHANT--2% NITAL.

89.

Standard   Grain Refined (Quartz Shielded)

Figure 41b.   COMPARISON OF STANDARD (CYLINDRICAL GUIDE, 1-1/4" GAP, 42 VOLTS, 600 AMPS)
               AND GRAIN REFINED (QUARTZ SHIELDED GUIDE, 1-1/4" GAP, 48 VOLTS, 600 AMPS)
               ES WELD MICROSTRUCTURES ADJACENT TO FUSION LINE (WIRE A).   ETCHANT--2% NITAL.

Standard   Grain Refined (Quartz Shielded)

Figure 41c.   COMPARISON OF STANDARD (CYLINDRICAL GUIDE, 1-1/4" GAP, 42 VOLTS, 600 AMPS)
AND GRAIN REFINED (QUARTZ SHIELDED GUIDE, 1-1/4" GAP, 48 VOLTS, 600 AMPS)
ES WELD MICROSTRUCTURES ADJACENT TO FUSION LINE (WIRE A).   ETCHANT--PICRAL.
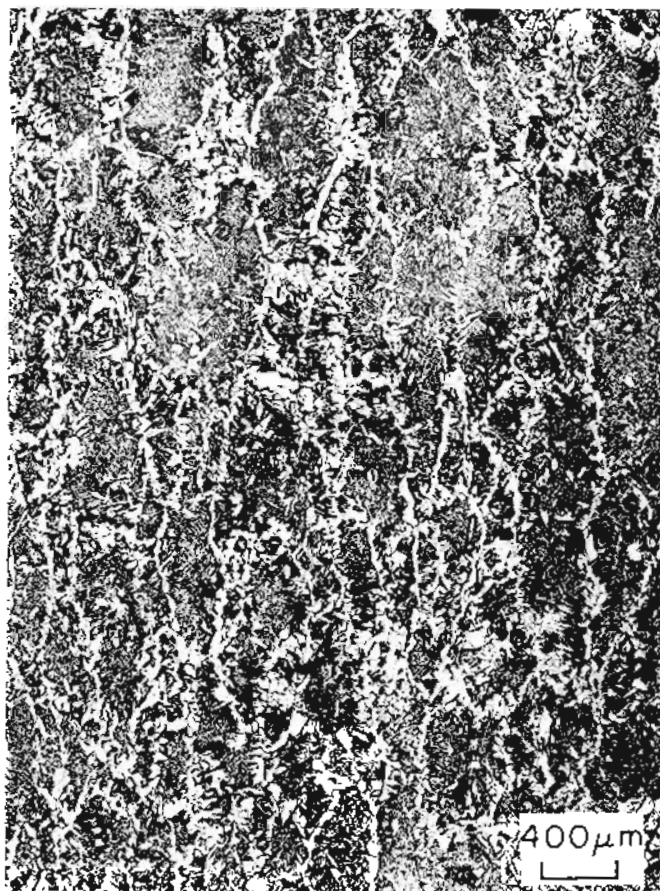
Standard   Grain Refined (Quartz Shielded)
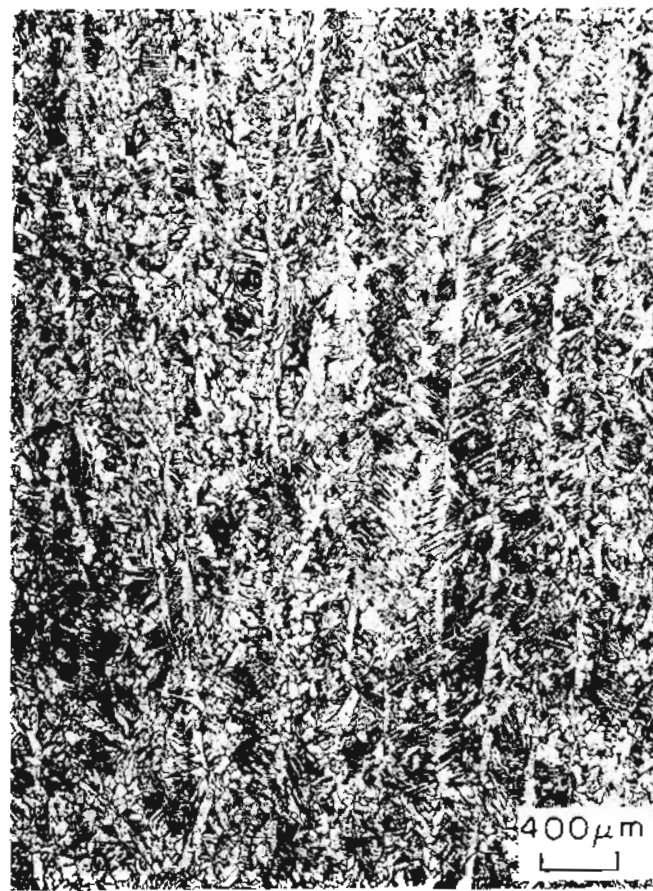
Figure 41d.   COMPARISON OF STANDARD (CYLINDRICAL GUIDE, 1-1/4" GAP, 42 VOLTS, 600 AMPS)
              AND GRAIN REFINED (QUARTZ SHIELDED GUIDE, 1-1/4" GAP, 48 VOLTS, 600 AMPS)
              ES WELD MICROSTRUCTURES AT WELD CENTERLINE LOCATION (WIRE A).   ETCHANT--
              2% NITAL.

Standard   Grain Refined (Quartz Shielded)

Figure 41e.   COMPARISON OF STANDARD (CYLINDRICAL GUIDE, 1-1/4" GAP, 42 VOLTS, 600 AMPS)
               AND GRAIN REFINED (QUARTZ SHIELDED GUIDE, 1-1/4" GAP, 48 VOLTS, 600 AMPS)
               ES WELD MICROSTRUCTURES AT WELD CENTERLINE LOCATION (WIRE A).   ETCHANT--
               2% NITAL.
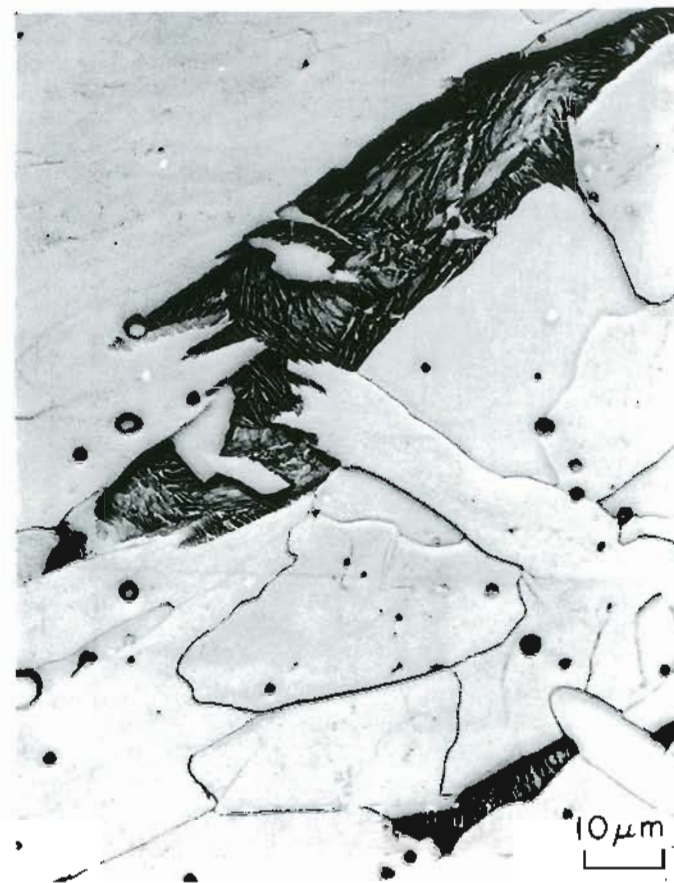
Standard   Grain Refined (Quartz Shielded)

Figure 41f.   COMPARISON OF STANDARD (CYLINDRICAL GUIDE, 1-1/4" GAP, 42 VOLTS, 600 AMPS)
               AND GRAIN REFINED (QUARTZ SHIELDED GUIDE, 1-1/4" GAP, 48 VOLTS, 600 AMPS)
               ES WELD MICROSTRUCTURES AT WELD CENTERLINE LOCATION (WIRE A).   ETCHANT--
               PICRAL.

1 inch
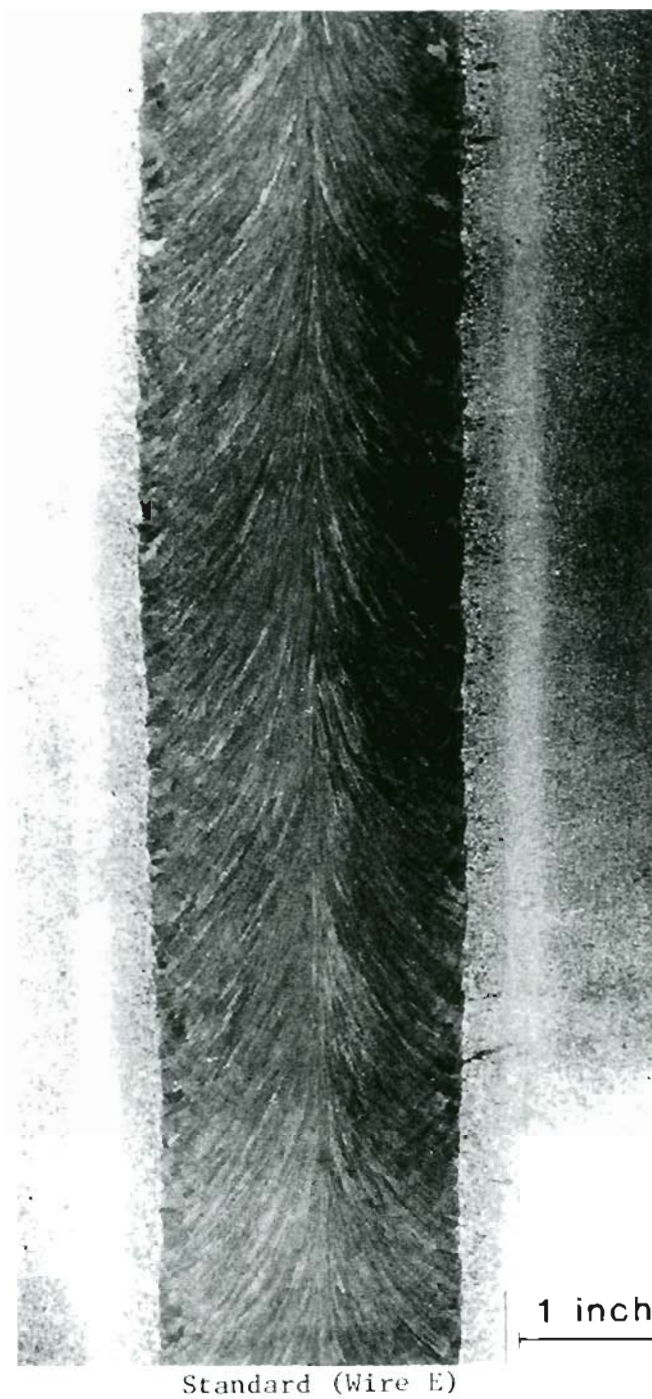
Standard (Wire E)

Figure 42. MACROSTRUCTURE OF STANDARD (CYLINDRICAL GUIDE, 1-1/4"
GAP, 42 VOLTS, 600 AMPS) ES WELD MADE USING FILLER
WIRE E. ETCHANT--10% NITAL.

Fusion line

HAZ ←——┃——→ WM
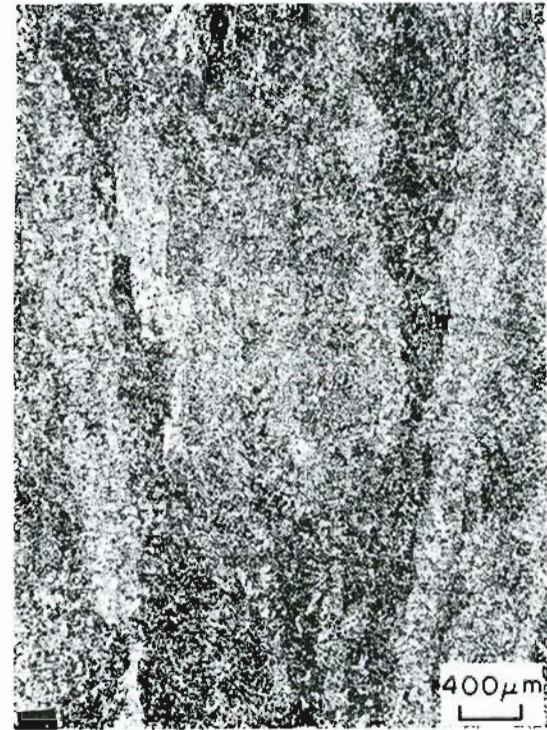
Fusion Line   Coarse Columnar Zone   Weld Center Line

Figure 43a. MICROSTRUCTURES OF STANDARD (CYLINDRICAL GUIDE, 1-1/4" GAP, 42 VOLTS, 600 AMPS) ES WELD MADE USING ALLOYED FILLER
           WIRE E. ETCHANT--2% NITAL.
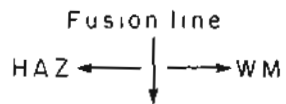
Fusion line
HAZ ←— | —→ WM

Fusion Line

Coarse Columnar Zone
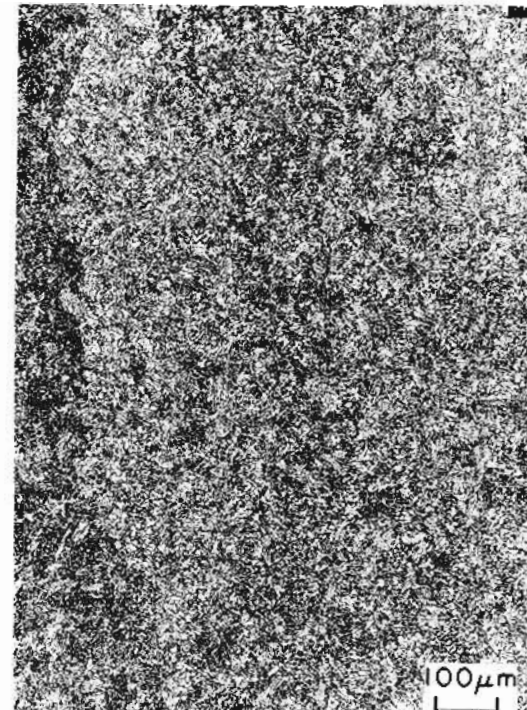
Weld Center Line

Figure 43b. MICROSTRUCTURES OF STANDARD (CYLINDRICAL GUIDE, 1-1/4" GAP, 42 VOLTS, 600 AMPS) ES WELD MADE USING ALLOYED FILLER WIRE E. ETCHANT--2% NITAL.
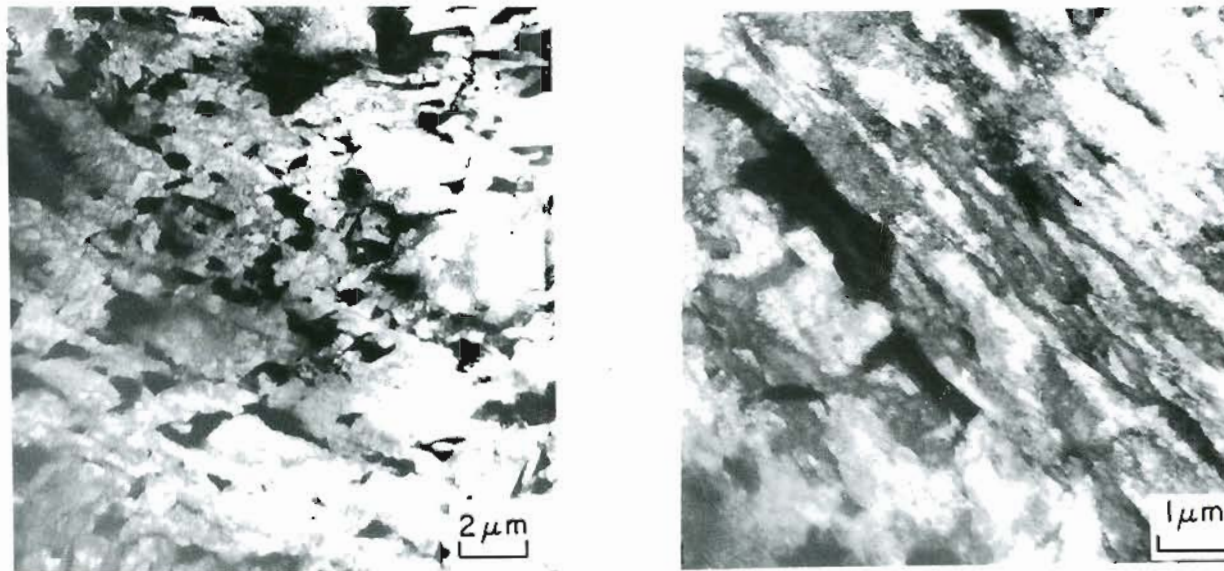
Figure 44. MICROSTRUCTURES OF STANDARD (CYLINDRICAL GUIDE, 1-1/4" GAP, 42 VOLTS, 600 AMPS) ES WELD MADE USING FILLER WIRE E SHOWING FERRITE MORPHOLOGY (TEM MICROGRAPHS).

SAD Pattern

$(\bar{1}\bar{2})_a$

$(002)_a$

$(020)_c$

$(020)_c$

$(112)_c$

(000)

$(\bar{1}\bar{1}\bar{2})_c$

$(0\bar{2}0)_c$

$(0\bar{2}0)_c$

$(00\bar{2})_a$

$(\bar{1}\bar{1}\bar{2})_a$

◻ – [110] Ferrite pattern

⊙ – [$\bar{2}$01] Cementite pattern

△ – (020) Spot from another orientation

Bright Field

Dark Field

Figure 45. SELECTED AREA DIFFRACTION ANALYSIS OF THE STANDARD
(CYLINDRICAL GUIDE, 42 VOLTS, 600 AMPS, AND 1-1/4" GAP)
ES WELD MADE USING ALLOY WIRE E. HEAVILY DISLOCATED,
LATH TYPE FERRITE STRUCTURE WAS OBSERVED WITH CEMENTITE
PRESENT ALONG LATH BOUNDARIES.

Figure 46. The uniform distribution of fine carbides in a bainitic

matrix structure in the alloyed weld is in contrast to the Widmanstatten

ferrite matrix structure with carbide aggregates along ferrite boundaries

and isolated pearlite colonies present in standard welds (Figures 47a-d,

and 48).

Typical macro and microstructures of high current/narrow gap (winged

guide tube) ES welds made using alloy wire E are shown in Figures 49 and

50a-d. The extent of the CCG zone in the weld was reduced. Again, weld

microstructures confirmed the absence of proeutectoid films and the pres-

ence of a bainitic ferrite structure with fine dispersion of carbides.

Meanwhile, macro analysis of ES welds made using alloyed filler

wires B (A588), C (Si-Mn), and D (Mn-Mo), Figure 51, confirmed that all

consisted of CCG and TCG structures. Weld microstructures, presented in

Figures 52 through 54, indicated the presence of proeutectoid ferrite

films along grain boundaries and Widmanstatten ferrite matrix structures.

Macrostructural analyses of ES welds made with varying amounts of

elemental molybdenum additions welded to the guide tube indicated severe

alloy segregations at weld center regions (Figure 55).

3.4. Hardness Analysis

Rockwell hardness data for standard gap (1-1/4") and narrow gap

(3/4") welds made with wires A & E as well as the grain refined weld

(quartz shroud) are presented with reference to the test locations in

Figures 56 through 60. Base metal and coarse grained HAZ hardness values

were about R_B 88 and 98, respectively. Hardness values for welds made
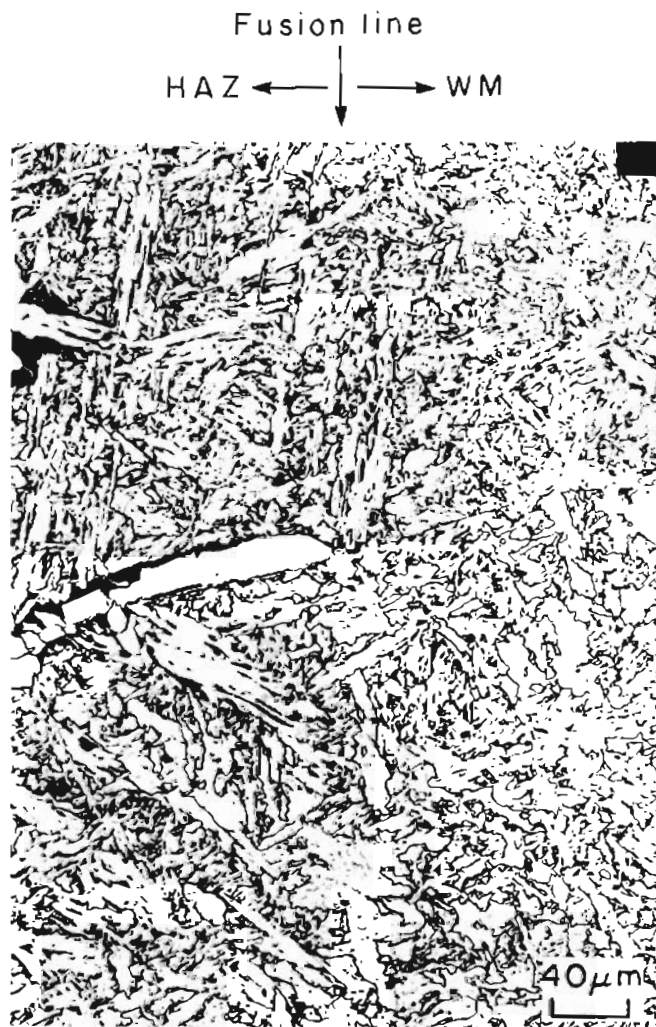
Figure 46.   FUSION LINE MICROSTRUCTURE OF STANDARD
             (CYLINDRICAL GUIDE, 1-1/4" GAP, 42 VOLTS,
             600 AMPS) ES WELD MADE USING ALLOYED FILLER
             WIRE E SHOWING ABSENCE OF PROEUTECTOID
             FERRITE IN THE WELD METAL.   THE PROEUTECTOID
             FERRITE PHASE PRESENT IN HAZ TERMINATES AT
             THE FUSION LINE.
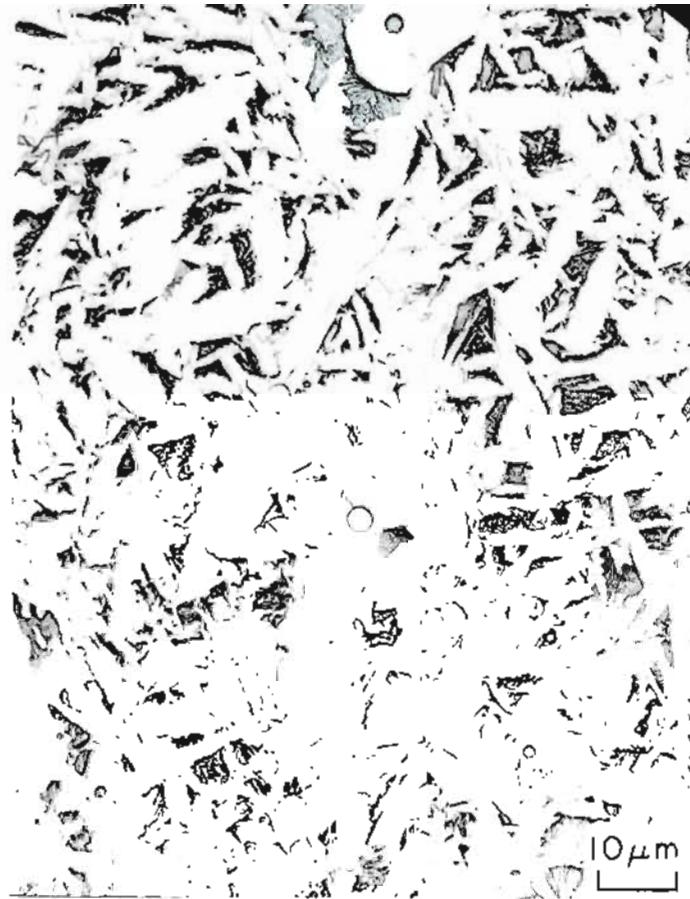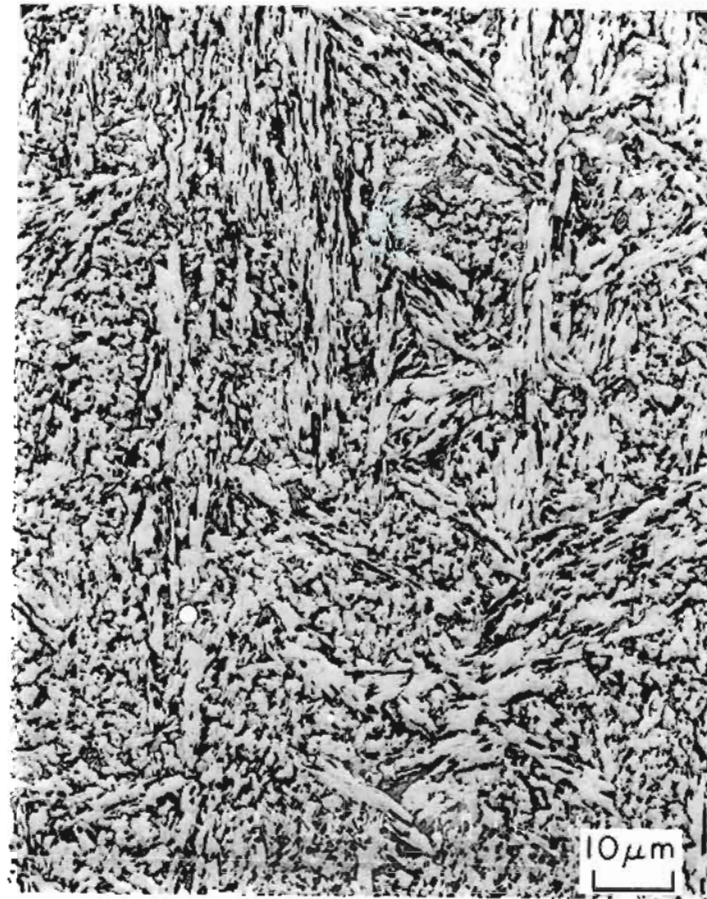
Standard (wire A)   Standard (wire E)

Figure 47a. COMPARISON OF MICROSTRUCTURES OF STANDARD (CYLINDRICAL GUIDE, 1-1/4" GAP,
             42 VOLTS, 600 AMPS) ES WELDS, ADJACENT TO FUSION LINE, MADE USING FILLER
             WIRES A AND E. ETCHANT--PICRAL

Standard (wire A)   Standard (wire E)

Figure 47b.   COMPARISON OF MICROSTRUCTURES OF STANDARD (CYLINDRICAL GUIDE, 1-1/4" GAP,
              42 VOLTS, 600 AMPS) ES WELDS, ADJACENT TO FUSION LINE, MADE USING FILLER
              WIRES A AND E.   ETCHANT--PICRAL.
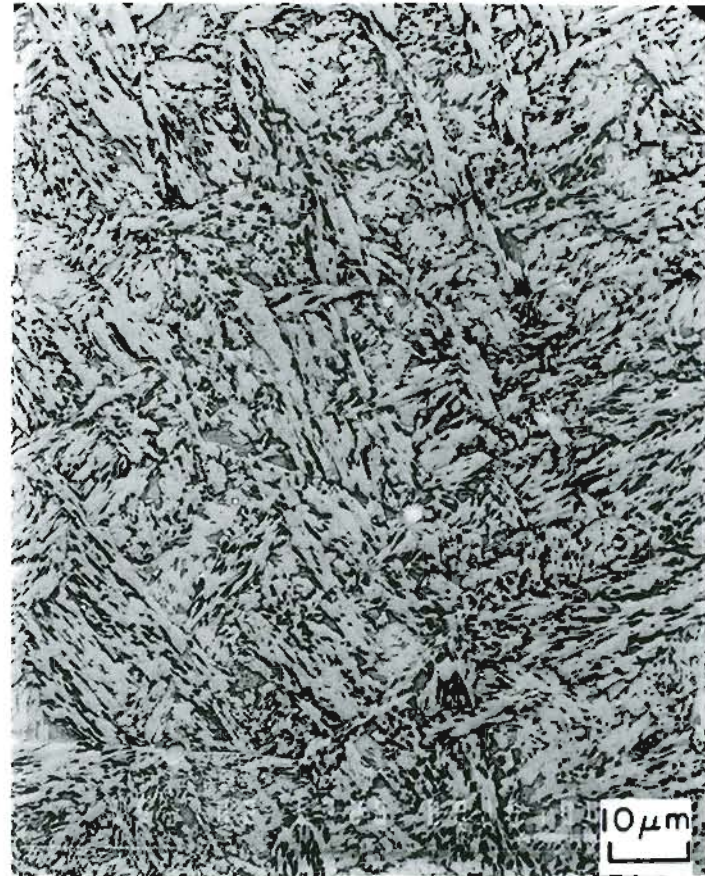
Standard (wire A)   Standard (wire E)

Figure 47c. COMPARISON OF MICROSTRUCTURES OF STANDARD (CYLINDRICAL GUIDE, 1-1/4" GAP,
            42 VOLTS, 600 AMPS) ES WELDS, AT WELD CENTERLINE LOCATION, MADE USING
            FILLER WIRES A AND E. ETCHANT--PICRAL.

Standard (wire A)   Standard (wire E)

Figure 47d. COMPARISON OF MICROSTRUCTURES OF STANDARD (CYLINDRICAL GUIDE, 1-1/4" GAP,
            42 VOLTS, 600 AMPS) ES WELDS, AT WELD CENTERLINE LOCATION, MADE USING
            FILLER WIRES A AND E. ETCHANT--PICRAL.
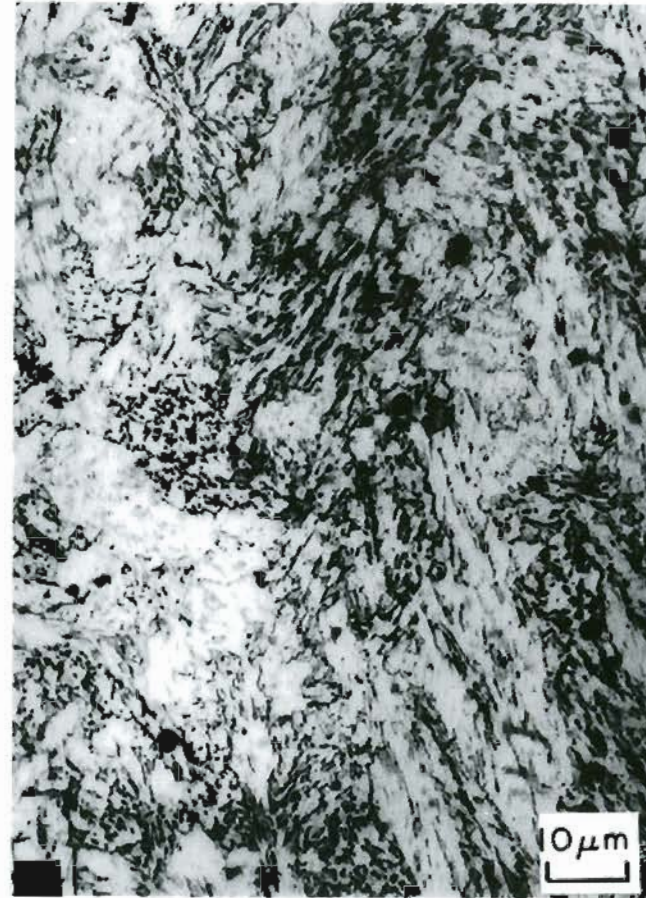
Standard (wire A)   Standard (wire E)

Figure 48.   COMPARISON OF MICROSTRUCTURES OF STANDARD (CYLINDRICAL GUIDE, 1-1/4" GAP, 42 VOLTS, 600 AMPS) ES WELDS, ADJACENT TO FUSION LINE, MADE USING FILLER WIRES A AND E.   ETCHANT--PICRAL + 2% NITAL.
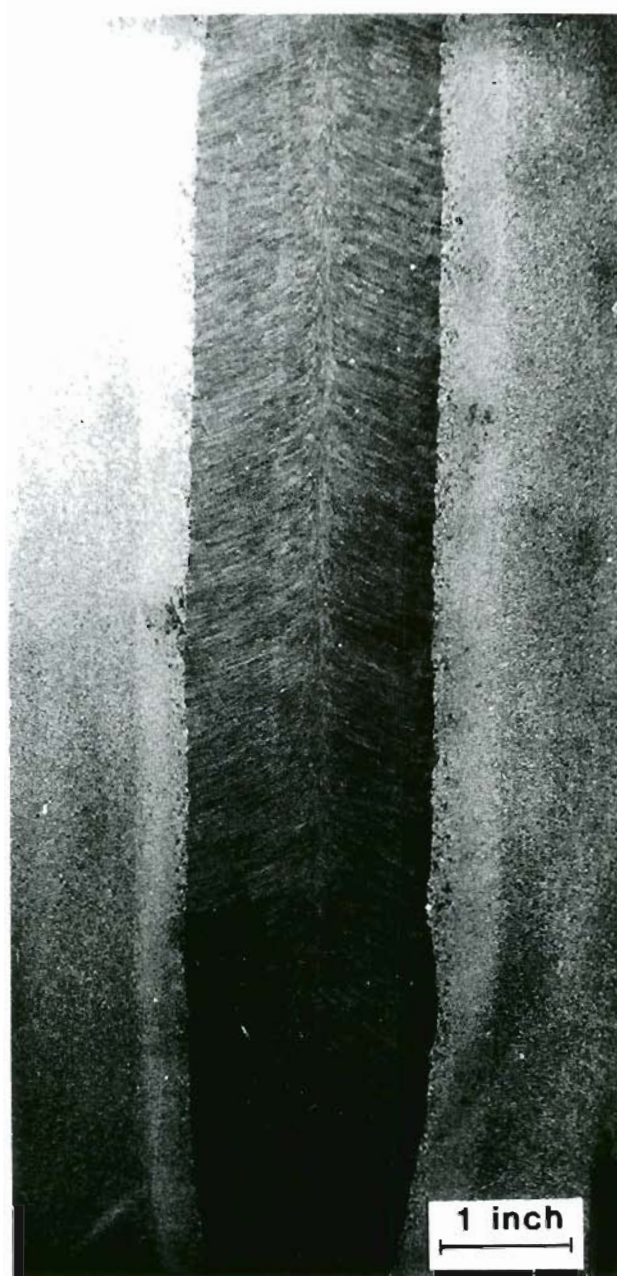
Figure 49. MACROSTRUCTURE OF HIGH CURRENT/NARROW GAP/WINGED GUIDE (3/4" GAP, 40 VOLTS, 1000 AMPS) ES WELD MADE USING ALLOYED FILLER WIRE E. ETCHANT--10% NITAL.

Fusion line

HAZ ← | → WM
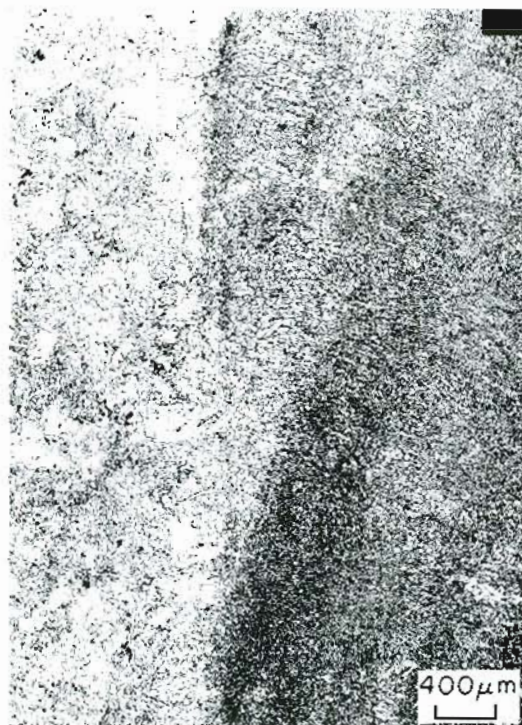
| Fusion Line | Coarse Columnar Zone | Weld Center Line |

Figure 50a. MICROSTRUCTURES OF HIGH CURRENT/NARROW GAP/WINGED GUIDE (3/4" GAP, 40 VOLTS, 1000 AMPS) ES WELD MADE USING ALLOYED FILLER WIRE E. ETCHANT--2% NITAL.

Fusion line

HAZ ←——— | ———→ WM
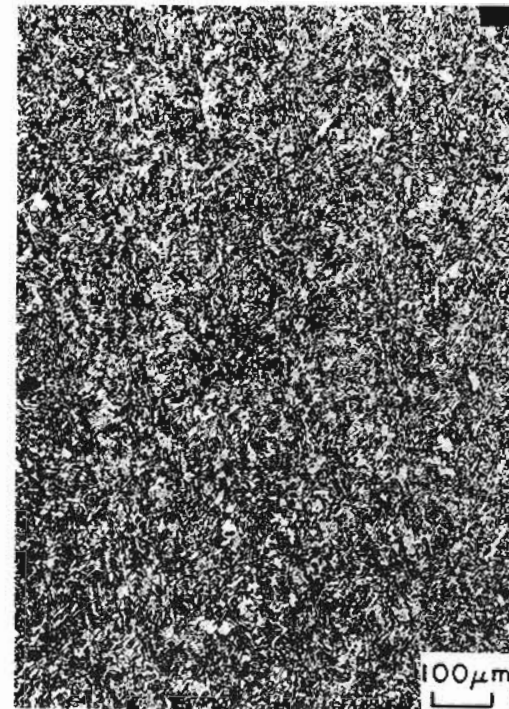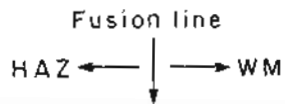
Fusion Line   Coarse Columnar Zone   Weld Center Line

Figure 50b. MICROSTRUCTURES OF HIGH CURRENT/NARROW GAP/WINGED GUIDE (3/4" GAP, 40 VOLTS, 1000 AMPS) ES WELD MADE USING ALLOYED
            FILLER WIRE E. ETCHANT--2% NITAL.
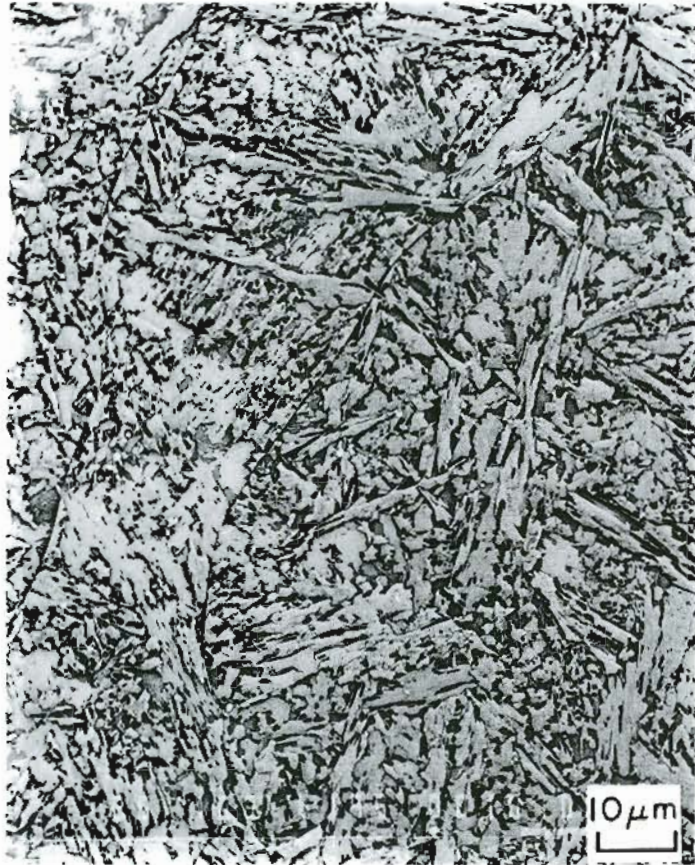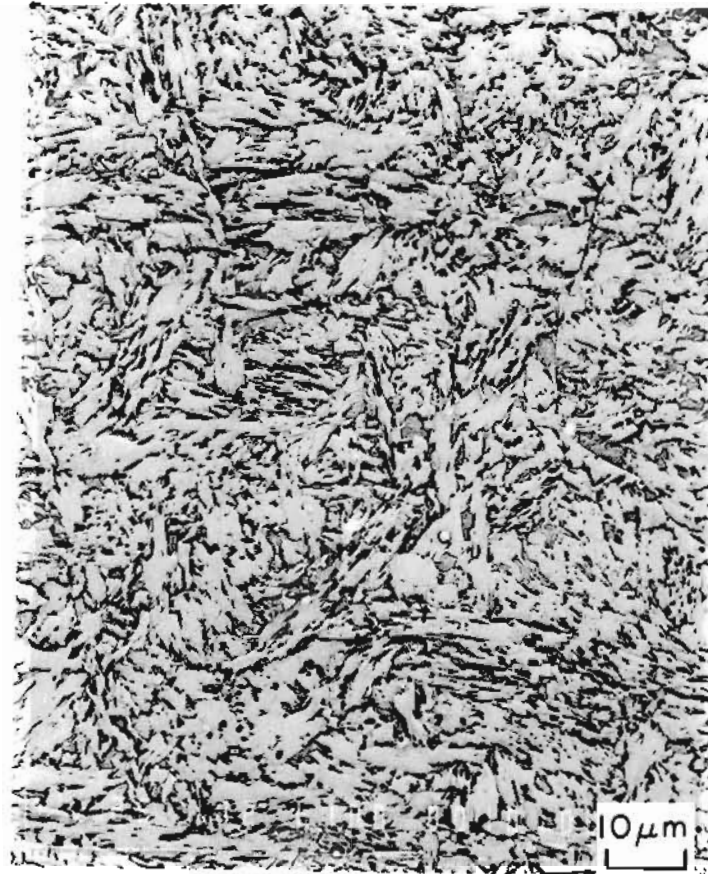
Coarse Columnar Zone   Weld Center Line

Figure 50c. MICROSTRUCTURES OF HIGH CURRENT/NARROW GAP/WINGED GUIDE (3/4" GAP, 40 VOLTS, 1000 AMPS) ES WELD MADE USING ALLOYED FILLER WIRE E. ETCHANT--PICRAL.

Coarse Columnar Zone   Weld Center Line

Figure 50d. MICROSTRUCTURES OF HIGH CURRENT/NARROW GAP/WINGED GUIDE (3/4" GAP, 40 VOLTS,
            1000 AMPS) ES WELD MADE USING ALLOYED FILLER WIRE E. ETCHANT--PICRAL.

Standard (Wire B)   Standard (Wire C)   Standard (Wire D)
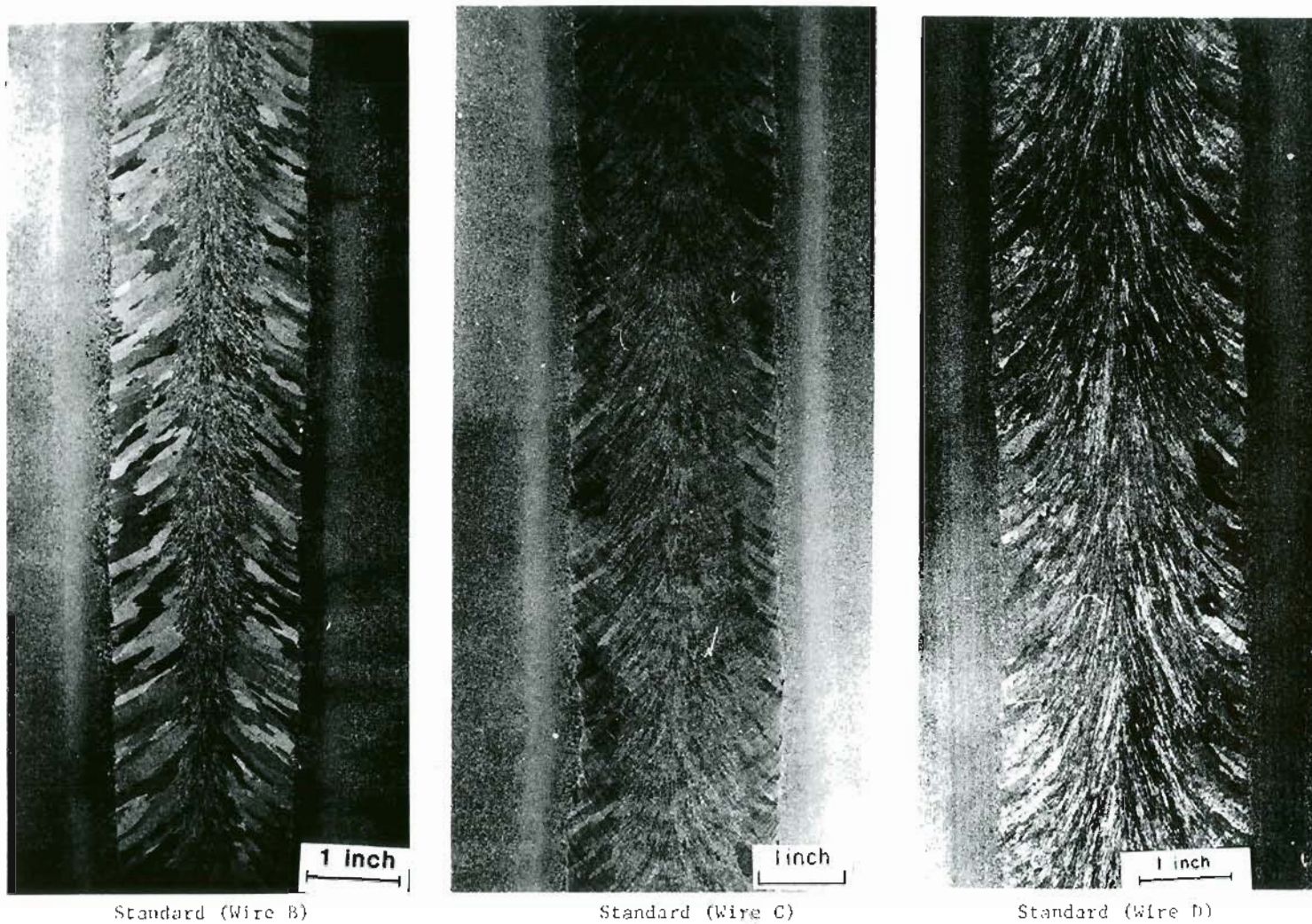
Figure 51.   MACROSTRUCTURES OF STANDARD (CYLINDRICAL GUIDE, 1-1/4" GAP, 42 VOLTS, 600
             AMPS) ES WELDS MADE USING FILLER WIRES B, C, AND D.   ETCHANT--10% NITAL.
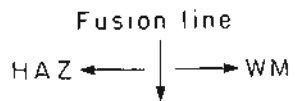
Fusion line
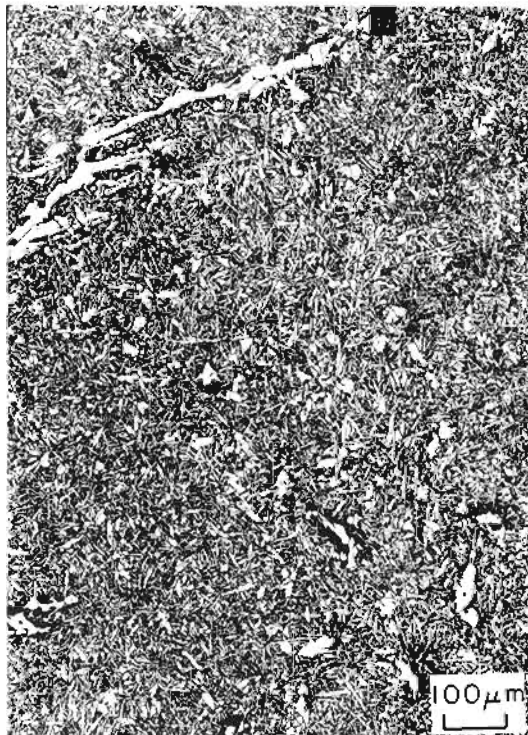
HAZ ←——— | ———→ WM

Fusion Line

Coarse Columnar Zone

Weld Center Line

Figure 52.   MICROSTRUCTURES OF STANDARD (CYLINDRICAL GUIDE, 1-1/4" GAP, 42 VOLTS, 600 AMPS) FS WELD MADE USING ALLOYED FILLER WIRE B.   ETCHANT--2% NITAL.

Fusion line
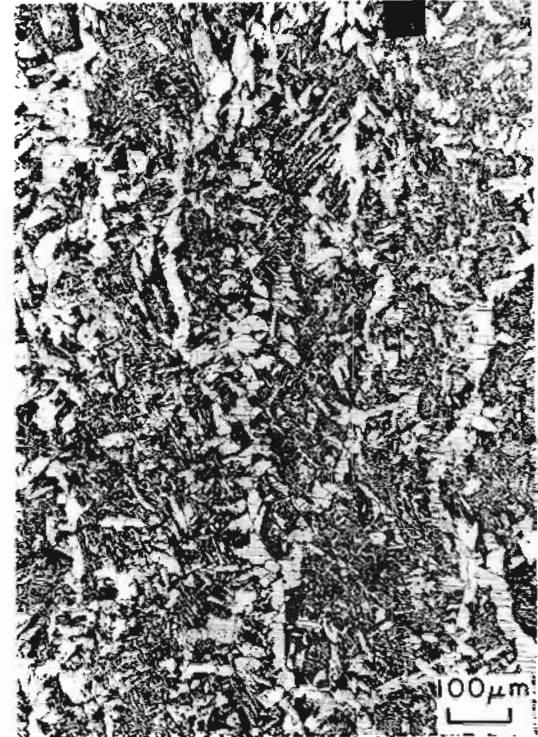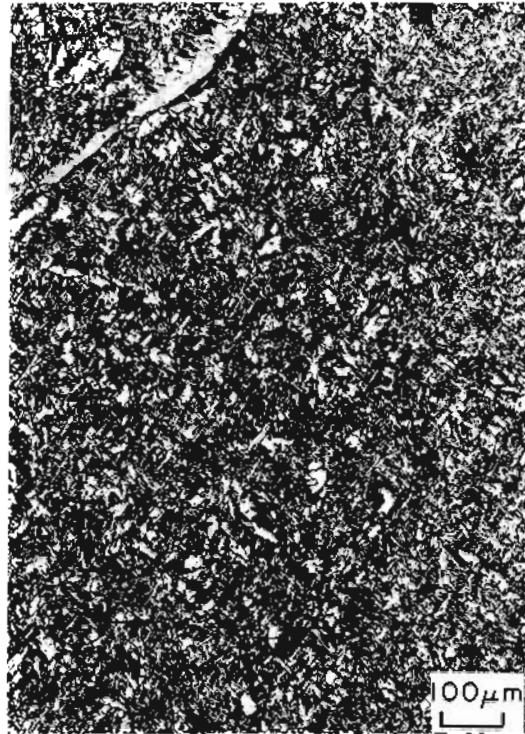
HAZ ◄──── | ────► WM

Fusion Line   Coarse Columnar Zone   Weld Center Line

Figure 53.   MICROSTRUCTURES OF STANDARD (CYLINDRICAL GUIDE, 1-1/4" GAP, 42 VOLTS, 600 AMPS) ES WELD MADE USING ALLOYED FILLER
              WIRE C. ETCHANT--2% NITAL.

Fusion line

HAZ ←——— | ———→ WM

Fusion Line   Coarse Columnar Zone   Weld Center line

Figure 54. MICROSTRUCTURES OF STANDARD (CYLINDRICAL GUIDE, 1-1/4" GAP, 42 VOLTS, 600 AMPS) ES WELD MADE USING ALLOYED FILLER
WIRE D. ETCHANT--2% NITAL.

Severe
Weld Center
Segregation

1inch
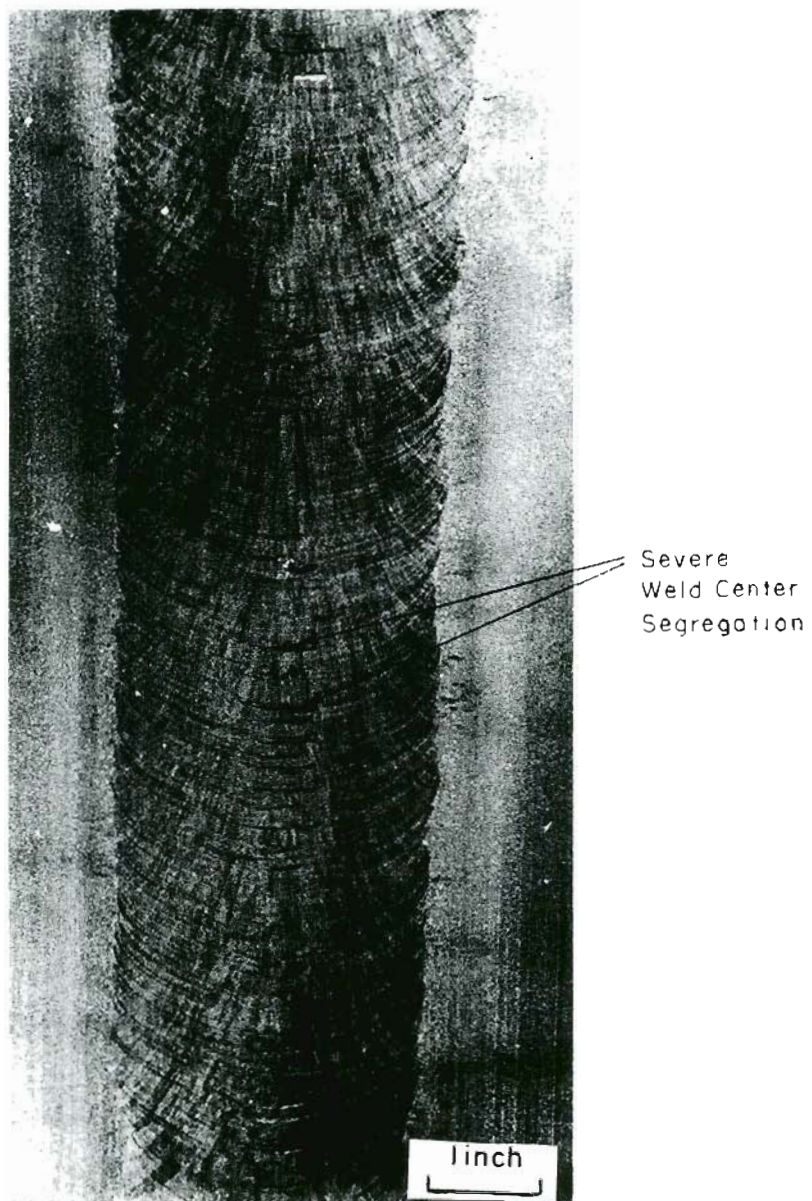
Figure 55.   MACROSTRUCTURE OF ES WELD (1-1/4" GAP, 42 VOLTS, 600
             AMPS, CYLINDRICAL GUIDE WITH ALLOY ADDITION--REFER
             FIGURE 8) MADE WITH ELEMENTAL MOLYBDENUM ADDITIONS.
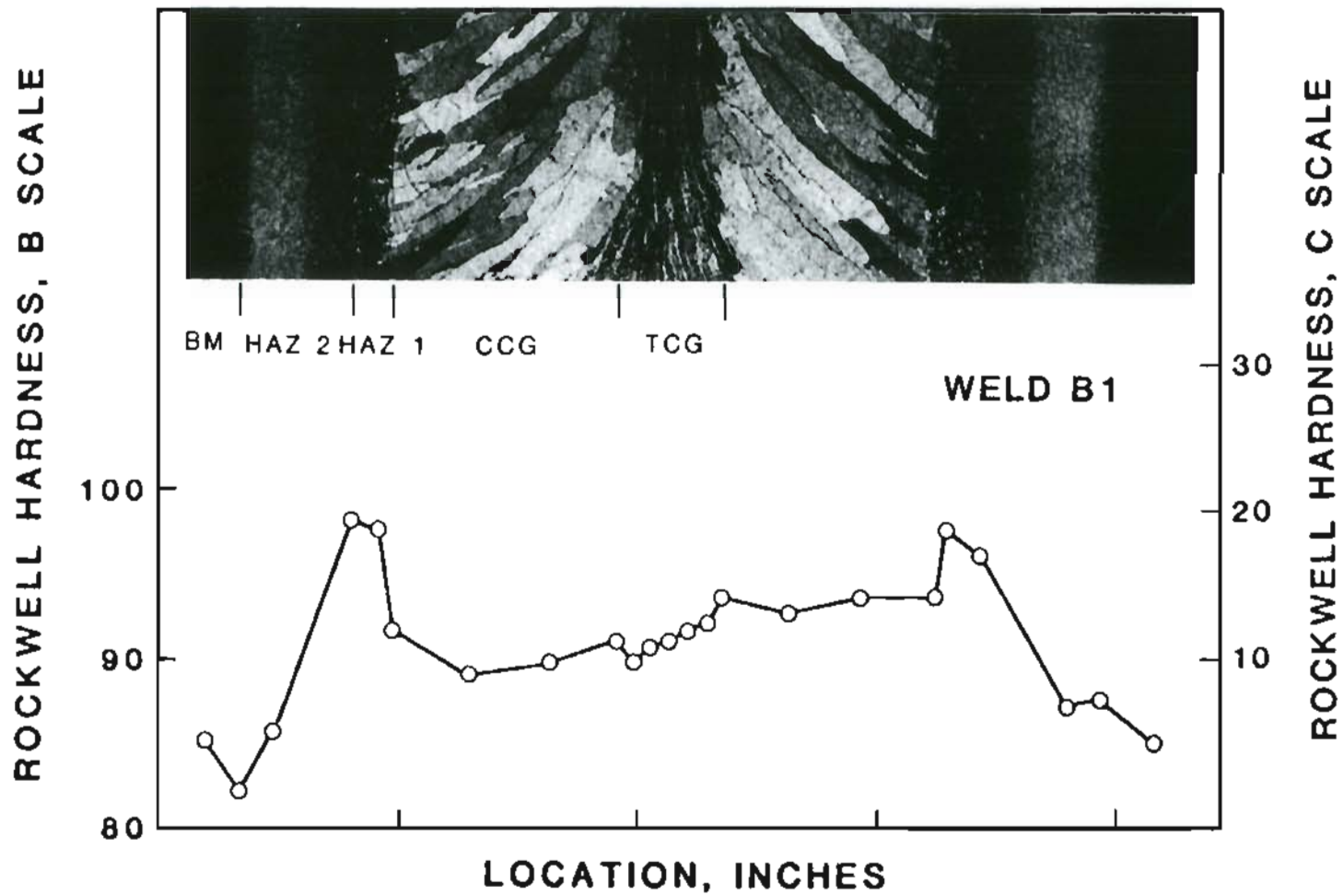
Figure 56. HARDNESS TRAVERSE OF STANDARD (CYLINDRICAL GUIDE, 1-1/4" JOINT GAP) ES WELD MADE USING FILLER WIRE A. MACROSTRUCTURE INDICATES LOCATIONS OF HARDNESS MEASUREMENTS.
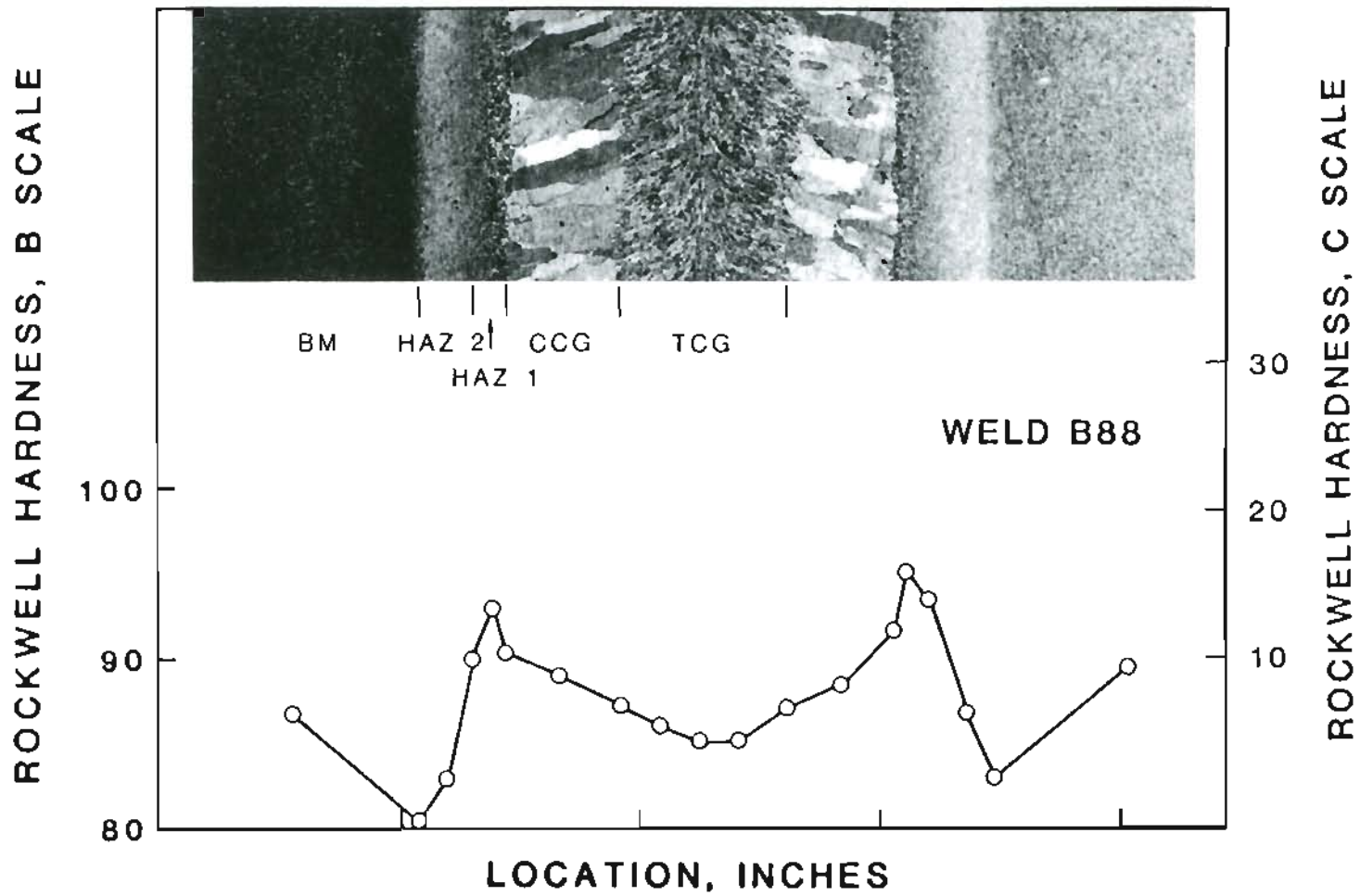
Figure 57. HARDNESS TRAVERSE OF THE HIGH CURRENT (1000A) NARROW GAP (3/4") WINGED GUIDE TUBE ES WELD MADE USING FILLER WIRE A. MACROSTRUCTURE INDICATES LOCATIONS OF HARDNESS MEASUREMENTS.
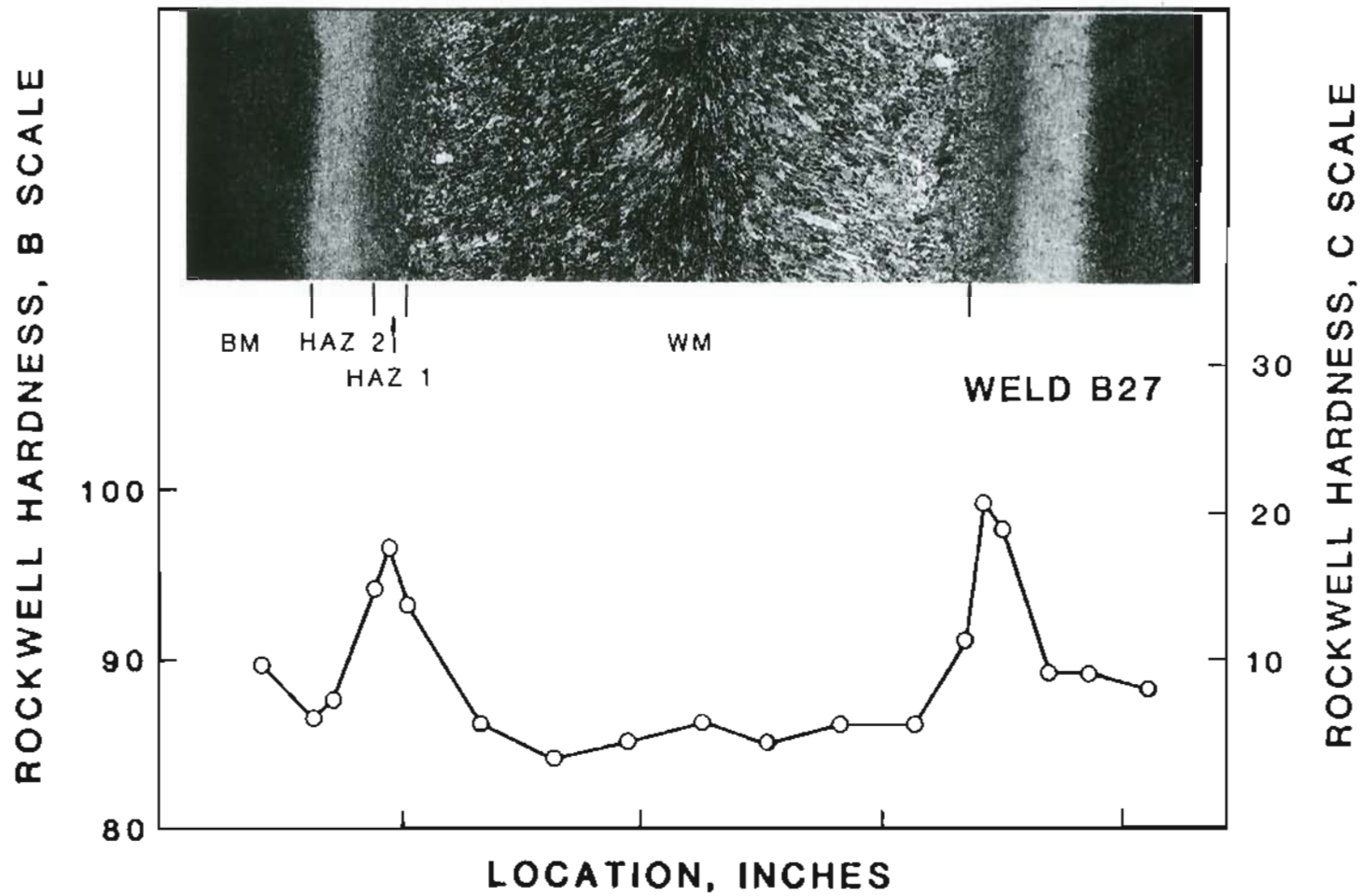
Figure 58. HARDNESS TRAVERSE OF QUARTZ SHIELDED GUIDE-GRAIN REFINED WELD MADE USING FILLER WIRE A. MACROSTRUCTURE INDICATES LOCATIONS OF HARDNESS MEASUREMENTS.
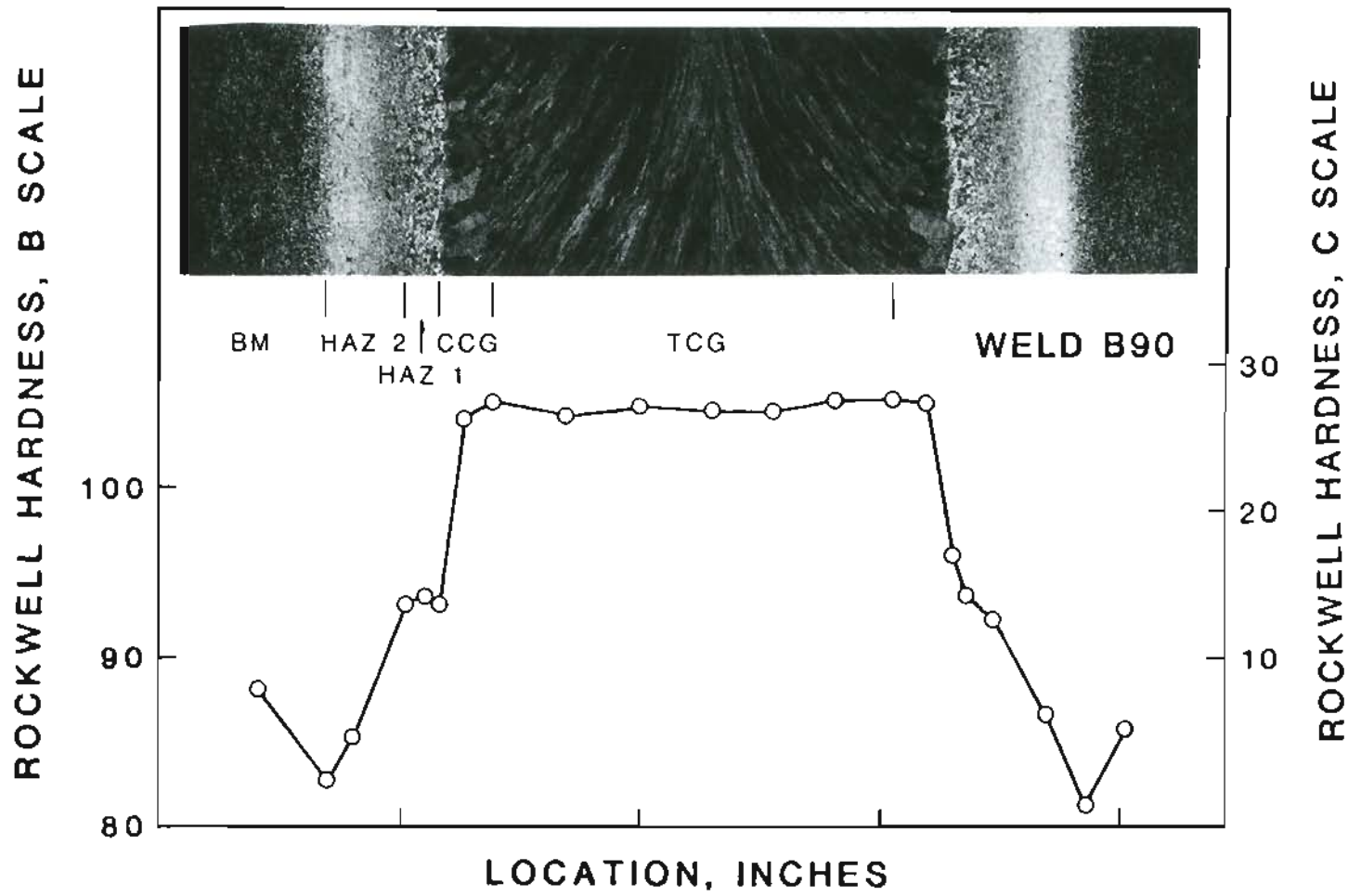
Figure 59. HARDNESS TRAVERSE OF STANDARD (CYLINDRICAL GUIDE, 1-1/4" JOINT GAP) ES WELD MADE USING ALLOYED FILLER WIRE E. MACROSTRUCTURE INDICATES LOCATIONS OF HARDNESS MEASUREMENTS.

Figure 60. HARDNESS TRAVERSE OF HIGH CURRENT (1,000A) NARROW GAP (3/4") WINGED GUIDE TUBE ES WELD MADE USING ALLOYED FILLER WIRE E. MACROSTRUCTURE INDICATES LOCATIONS OF HARDNESS MEASUREMENTS.
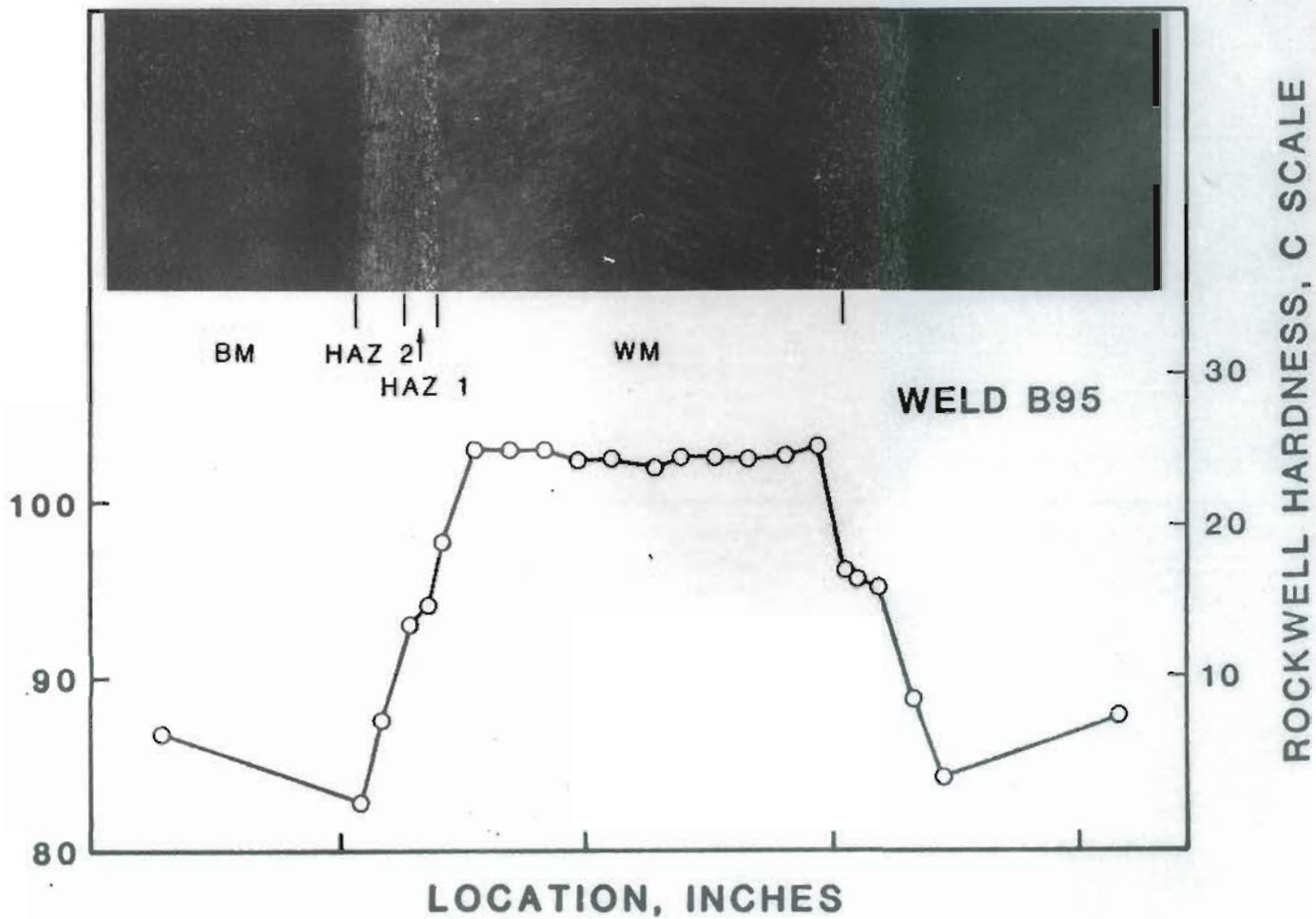
with wire A were in the range, R_B 88 to 93, while grain refined welds were between R_B 83 and 85. Both welds made with wire E were much harder than the base metal and HAZs. Their hardness values were between R_C 26 and 28. Narrow gap welds, in general, were slightly softer than standard gap welds.

3.5. Charpy Impact Toughness

Charpy V notch (CVN) impact toughness values tested at 0°F for various structural zones of several electroslag weldments and base metal are presented in Table VIII. Averages calculated by omitting the highest and the lowest values are shown in Table IX.

The average base metal CVN impact toughness was 37 ft.lbs. Welds made with filler wires A and B possessed low toughness properties in the weld center region at mid-thickness locations. In all welds, with the exception of the grain refined (quartz) weld, the average toughness value of the CCG zone was much higher than that of the WCL zone at the mid-thickness region. The average impact toughness of the CCG zone was in the range of 27 to 61 ft.lbs., while that of the WCL was between 4 and 11 ft.lbs.

CVN toughness at the WCL-quarter thickness locations of the standard ES weld was 19 ft.lbs. compared to 4 ft.lbs. at the WCL mid thickness location. The CCG region toughness remained the same for both thickness locations.

A 100% increase in toughness was observed in the WCL region of the grain refined weld when compared to the standard one (from 4 to 8 ft.lbs.).

Table VIII.

ESW CHARPY V NOTCH IMPACT TOUGHNESS AT 0°F

Specimen ID	Impact Toughness in Ft.lbs.	Zone (see note)
Base Metal (A588)		
B01	27.9	BM
B02	36.2	BM
B03	48.5	BM
B04	32.4	BM
B05	48.1	BM
B06	34.2	BM
B07	34.2	BM
B08	39.6	BM

Weld B36: Standard guide tube, voltage = 40 volts, current = 600 amperes, gap = 1-1/4", wire A.

36B01F	2.71	WCL
36B01B	6.16	WCL
36B02F	5.16	WCL
36B02B	3.53	WCL
36B03F	3.21	WCL
36B03B	3.39	WCL
36B04B	4.73	WCL
36B05F	33.50	WCL
36B13F	36.90	CCG
36B13B	40.50	CCG
36B14F	33.50	CCG
36B14B	45.40	CCG
36B15F	20.70	CCG
36B32F	17.70	HAZ

Table VIII.
(Cont.)

Specimen ID	Impact Toughness in Ft.1bs.	Zone (see Note)
Weld B36 (cont.)		
36B32B	30.20	HAZ
36B33F	17.90	HAZ
36B33B	25.00	HAZ
36B34F	8.42	HAZ

Weld B97: Standard guide tube, voltage = 42 volts, current = 600 amperes, gap = 1-1/4", wire A (Quarter-thickness) samples.

97B01	45.30	CCG*
97B02	24.90	CCG*
97B03	35.20	CCG*
97B04	36.10	CCG*
97B05	7.50	WCL*
97B06	29.90	WCL*
97B07	11.30	WCL*
97B08	25.80	WCL*
97B09	28.00	WCL*
97B10	8.90	WCL*

Weld B47: Quartz shielded guide tube (grain refined), voltage = 48 volts, current = 600 amperes, gap = 1-1/4", wire A.

47B01F	7.51	WCL
47B01B	7.44	WCL
47B02F	5.30	WCL
47B02B	24.00	WCL

Table VIII.
(Cont.)

Specimen ID	Impact Toughness in Ft.lbs.	Zone (see Note)
Weld B47 (cont.)		
47B03B	8.29	WCL
47B04B	8.34	WCL
47B05F	8.10	WCL
47B08F	8.70	WCL
47B13F	6.19	WM
47B13B	11.80	WM
47B14F	6.53	WM
47B14B	39.50	WM
47B16F	9.46	WM
47B32F	7.90	HAZ
47B32B	17.60	HAZ
47B33F	8.81	HAZ
47B33B	12.20	HAZ
47B34F	11.30	HAZ

Weld B51: Winged guide tube, voltage = 36 volts, current = 700 amperes, gap = 1-1/4", wire A.

51B01F	5.48	WCL
51B01B	5.80	WCL
51B02F	12.60	WCL
51B02B	38.30	WCL
51B03F	5.06	WCL
51B03B	36.60	WCL
51B04F	3.04	WCL
51B04B	10.10	WCL
51B13F	30.60	CCG

Table VIII.
(Cont.)

Specimen ID	Impact Toughness in Ft.lbs.	Zone (see Note)
Weld B51 (cont.)		
51B13B	15.80	CCG
51B14F	36.20	CCG
51B14B	35.30	CCG
51B15F	6.69	CCG
51B32B	21.90	HAZ
51B33F	14.30	HAZ
51B33B	12.10	HAZ
51B34F	6.30	HAZ
51B34B	18.20	HAZ

Weld B52: Winged guide tube, voltage = 40 volts, current = 600 amperes, gap = 3/4", wire A.

Specimen ID	Impact Toughness in Ft.lbs.	Zone
52B01F	5.80	WCL
52B01B	7.60	WCL
52B02F	9.10	WCL
52B02B	6.00	WCL
52B03F	5.00	WCL
52B03B	7.00	WCL
52B04F	5.00	WCL
52B04B	6.00	WCL
52B13F	30.60	CCG
52B13B	31.20	CCG
52B14F	32.80	CCG
52B14B	34.60	CCG
52B15F	47.10	CCG
52B32F	19.30	HAZ

Table VIII.
(Cont.)

Specimen ID	Impact Toughness in Ft.lbs.	Zone (see Note)
Weld B52 (cont.)		
52B32B	9.10	HAZ
52B33F	15.40	HAZ
52B33B	20.30	HAZ
52B34F	13.30	HAZ

Weld B88: Winged guide tube, voltage = 40 volts, current = 1,000 amperes, gap = 3/4", wire A.

Specimen ID	Impact Toughness in Ft.lbs.	Zone (see Note)
88B01	56.60	CCG
88B02	56.60	CCG
88B03	76.30	CCG
88B04	70.10	CCG
88B05	25.20	WCL
88B06	8.10	WCL
88B07	18.20	WCL
88B08	12.00	WCL
88B09	4.00	WCL
88B10	6.10	WCL
88B11	20.10	HAZ
88B12	13.10	HAZ
88B13	9.30	HAZ
88B14	10.80	HAZ
88B15	7.10	HAZ
88B16	9.40	HAZ
88B17	6.90	HAZ
88B18	8.40	HAZ

Table VIII.
(Cont.)

Specimen ID	Impact Toughness in Ft.lbs.	Zone (see Note)

<u>Weld B69B:</u> Standard guide tube, voltage = 42 volts, current = 600 amperes, gap = 1-1/4", filler = wire A, Mo addition = 0.53 wt.%.

69BB01	14.10	WCL
69BB02	13.40	WCL
69BB03	22.60	WCL
69BB04	17.60	WCL
69BB05	8.40	WCL
69BB06	10.90	WCL
69BB07	17.60	WCL
69BB08	9.90	WCL
69BB09	15.70	CCG
69BB10	16.60	CCG
69BB11	21.30	CCG
69BB12	19.50	CCG
69BB13	20.40	CCG

<u>Weld B70T:</u> Standard guide tube, voltage = 42 volts, current = 600 amperes, gap = 1-1/4", filler = wire A, Mo addition = 0.66 wt.%.

70TB01	13.80	WCL
70TB02	11.30	WCL
70TB03	5.00	WCL
70TB04	6.40	WCL
70TB05	7.90	WCL
70TB06	4.00	WCL
70TB07	13.70	WCL
70TB08	8.40	WCL

Table VIII.
(Cont.)

Specimen ID	Impact Toughness in Ft.lbs.	Zone (see Note)
Weld B70T (cont.)		
70TB09	14.70	CCG
70TB10	10.80	CCG
70TB11	21.60	CCG
70TB12	6.90	CCG
70TB13	19.90	CCG

Weld B69T: Standard guide tube, voltage = 42 volts, current = 600 amperes, gap = 1-1/4", filler = wire A, Mo addition = 1.07 wt.%.

69TB01	20.10	WCL
69TB02	19.10	WCL
69TB03	16.00	WCL
69TB04	8.90	WCL
69TB05	3.10	WCL
69TB06	3.30	WCL
69TB07	3.50	WCL
69TB08	4.50	WCL
69TB09	18.80	CCG
69TB10	14.00	CCG
69TB11	13.20	CCG
69TB12	15.60	CCG
69TB13	12.10	CCG

Weld B64: Standard guide tube, voltage = 42 volts, current = 600 amperes, gap = 1-1/4", wire D.

64B01	8.30	CCG
64B02	6.50	CCG

Table VIII.
(Cont.)

Specimen ID	Impact Toughness in Ft.lbs.	Zone (see Note)
Weld B64 (cont.)		
64B03	6.20	CCG
64B04	8.80	CCG
64B06	4.30	WCL
64B07	3.30	WCL
64B08	3.20	WCL
64B09	2.90	WCL
64B10	2.00	WCL

Weld B89: Standard guide tube, voltage = 42 volts, current = 600 amperes, gap = 1-1/4", wire B.

89B01	70.10	CCG
89B02	39.20	CCG
89B03	44.60	CCG
89B04	31.50	CCG
89B05	3.00	WCL
89B06	5.10	WCL
89B07	5.00	WCL
89B08	5.00	WCL
89B09	5.00	WCL
89B10	5.50	WCL

Weld B90: Standard guide tube, voltage = 42 volts, current = 600 amperes, gap = 1-1/4", wire E.

90B01	13.80	CCG
90B02	17.60	CCG
90B03	9.90	CCG

Table VIII.
(Cont.)

Specimen ID	Impact Toughness in Ft.lbs.	Zone (see Note)
Weld B90 (cont.)		
90B04	17.60	CCG
90B05	9.90	WCL
90B06	19.50	WCL
90B07	7.90	WCL
90B08	12.90	WCL
90B09	13.80	WCL
90B10	10.80	WCL

Weld B95: Winged guide tube, voltage = 40 volts, current = 1,000 amperes, gap = 3/4", wire E.

Specimen ID	Impact Toughness	Zone
95B01	19.30	CCG
95B02	24.40	CCG
95B03	13.60	CCG
95B04	14.80	CCG
95B05	10.90	WCL
95B06	17.70	WCL
95B07	21.40	WCL
95B08	15.80	WCL
95B09	24.10	WCL
95B10	22.00	WCL

Note: BM Base metal at mid-thickness location
WCL Weld centerline at mid-thickness location
CCG Coarse columnar grain at mid-thickness location
HAZ Heat affected zone at mid-thickness location
CCG* Coarse columnar grain at quarter-thickness location
WCL* Weld centerline at quarter-thickness location
WM Weld metal adjacent to fusion line at mid-thickness location.

Table IX.

AVERAGE CHARPY V NOTCH IMPACT TOUGHNESS OF ES WELDS AT 0°F

#	Weld ID	Voltage in Volts	Current in Amps.	Gap in inches	Guide Tube	Filler Wire	Average* Charpy V notch Impact Toughness in ft.lbs.			Comment
							WCL	CCG	HAZ	
1	Base metal	--	--	--	--	--		37.45		As received
2	B36	40	600	1-1/4	cylindrical	A	4.36	36.96	20.20	Half thickness location
3	B97	40	600	1-1/4	cylindrical	A	18.50	35.65	11.36	Quarter thickness location
4	B51	36	700	1-1/4	winged	A	12.60	27.23	14.86	Half thickness location
5	B52	40	600	3/4	winged	A	6.48	32.87	16.00	Half thickness location
6	B88	40	1000	3/4	winged	A	11.10	61.10	9.68	Half thickness location
7	B47	48	600	1-1/4	Quartz shrouded cylindrical	A	8.06	9.26**	10.77	Half thickness grain refined weld
8	B69B	42	600	1-1/4	cylindrical	A	13.92	18.83	-	Half thickness 0.53 wt% Mo addition
9	B70T	42	600	1-1/4	cylindrical	A	8.78	15.13	-	Half thickness 0.66 wt% Mo addition
10	B69T	42	600	1-1/4	cylindrical	A	9.15	14.26	-	Half thickness 1.07 wt% Mo addition
11	B89	42	600	1-1/4	cylindrical	B	5.02	41.90	-	Half thickness location
12	B64	42	600	1-1/4	cylindrical	D	3.17	7.40	-	Half thickness location
13	B90	42	600	1-1/4	cylindrical	E	11.85	14.73	-	Half thickness location
14	B95	40	1000	3/4	winged	E	17.05	19.23	-	Half thickness location

Notes: * Average was calculated omitting the high and low values

** Weld zone adjacent to fusion line

*Weld zone adjacent to fusion line

Meanwhile, the toughness of the zone representative of the CCG zone of standard welds dropped from 37 to 9 ft.lbs. However, the toughness was uniform throughout the entire fusion zone.

A general increase in the toughness of the mid thickness-CCG and mid thickness-WCL (TCGs) regions were observed in the high current/narrow gap (winged guide tube) weld made with wire A. The WCL toughness was 11 ft.lbs., while the CCG toughness increased to 61 ft.lbs.

Additions of molybdenum to the weld metal increased the WCL toughness with an accompanied reduction in the CCG zone toughness when compared to the standard weld. Elemental alloy additions resulted in extensive scatter in the WCL toughness. The average CVN toughness of the CCG zone for welds made with three levels of Mo additions was between 14 and 19 ft.lbs., while that of the WCL region was between 9 and 14 ft. lbs. However, a general trend of increasing WCL toughness was observed with molybdenum additions.

The weld made with standard conditions but with alloy wire E resulted in average CVN toughness properties of 12 and 15 ft.lbs. for the WCL and CCG zones, respectively. The scatter in toughness values of this weld was reduced when compared to those made with elemental alloy additions. But a similar weld made with wire D exhibited very poor toughness properties, 3 and 7 ft.lbs. in the WCL and CCG zones, respectively.

Finally, the high current/narrow gap weld made with wire E possessed toughness values of 17 and 19 ft.lbs. at the mid thickness locations of the WCL and CCG regions, respectively. Cr and Mo additions and reduced specific heat input resulted in the most improved weld metal CVN impact toughness.

The impact toughness of the coarse grained HAZ was in the range of 10 to 20 ft.lbs. for welds tested as shown in Table IX. Despite the reduction in the HAZ width in the high current/narrow gap weld, the average toughness dropped to 10 ft.lbs. The grain refined weld HAZ possessed an 11 ft.lbs. impact toughness. Schematic representations of average CVN toughness values for various zones of selected ES welds are presented in Figures 61-63.

Pre-cracked Charpy V notch (PCVN) toughness values of several ES weldments and base metal tested at various temperatures are given in Table X. Plots of PCVN toughness vs. temperature shown in Figures 64-68 indicated a brittle fracture behavior at 0°F for all test welds as well as the base metal.

3.6. Fracture Surface Morphology

Scanning electron micrographs of Charpy specimen fracture surfaces taken from CCG, WCL and HAZ regions of standard, grain refined and high current/narrow gap/Cr & Mo alloyed welds are shown in Figures 69-71. In all cases, at 0°F, the fracture surface morphology was quasi-cleavage. Several small cracks about 10 to 20 microns in size intersected the fracture surface in the alloyed weld.

3.7. Crack Propagation Paths

Cross sectional microstructures of the fractured Charpy specimens taken at the CCG, WCL and HAZ regions of the standard, the grain refined and the high current/narrow gap/alloy welds are shown in Figures 72-74.
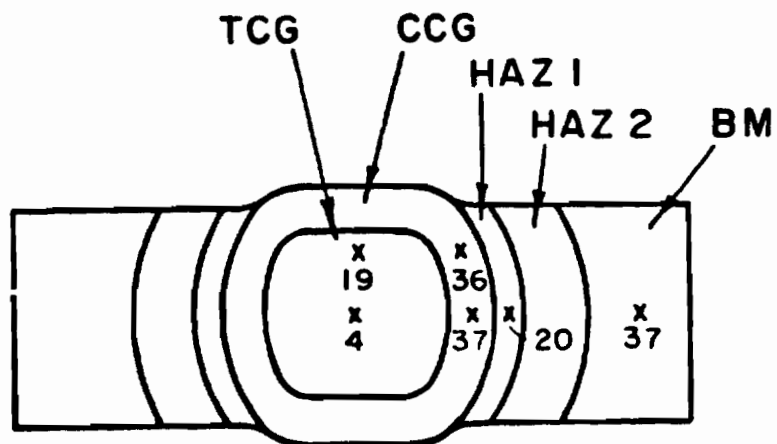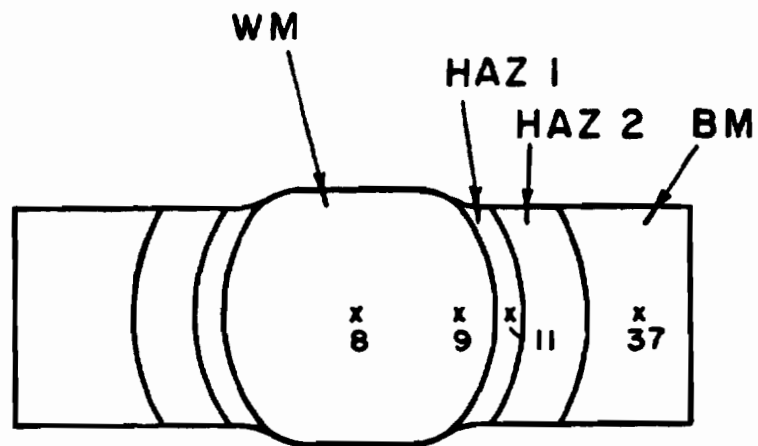
Figure 61. SCHEMATIC REPRESENTATION OF CHARPY V NOTCH IMPACT TOUGH-
NESS RESULTS FOR (a) STANDARD (CYLINDRICAL GUIDE; 1-1/4"
GAP) AND (b) GRAIN REFINED (QUARTZ SHROUDED GUIDE) ES
WELDS MADE USING FILLER WIRE A.
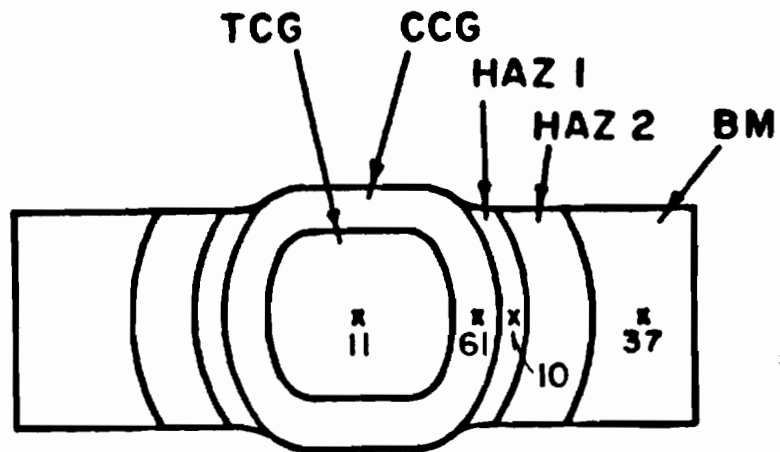
Figure 62. SCHEMATIC REPRESENTATION OF CHARPY V NOTCH IMPACT TOUGH-
NESS RESULTS FOR HIGH CURRENT (1000A) NARROW GAP (3/4")
WINGED GUIDE TUBE ES WELD MADE USING FILLER WIRE A.
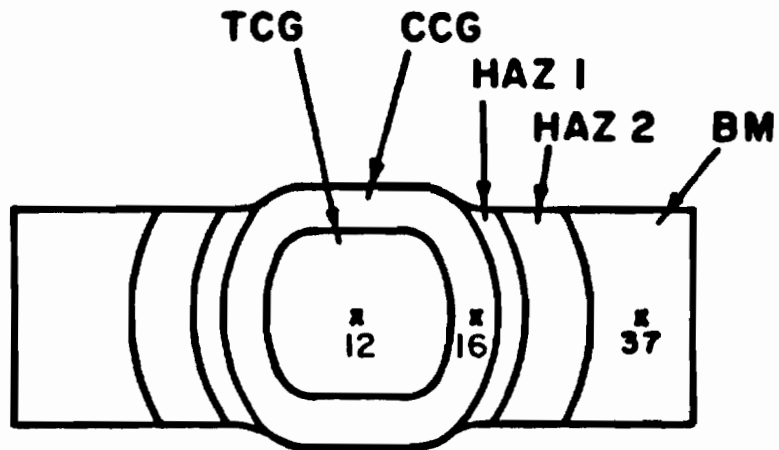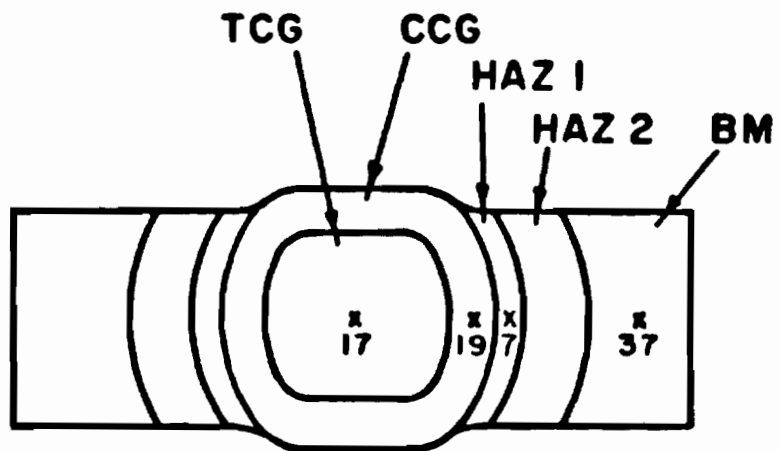
Figure 63. SCHEMATIC REPRESENTATION OF CHARPY V NOTCH IMPACT TOUGH-
NESS RESULTS FOR (a) STANDARD (CYLINDRICAL GUIDE; 1-1/4"
GAP) AND (b) HIGH CURRENT (1000A) NARROW GAP (3/4") WINGED
GUIDE TUBE ES WELDS MADE USING WIRE E.

Table X.

ESW PRECRACKED CHARPY V NOTCH IMPACT TOUGHNESS

Specimen ID	Zone	Testing Temperature in °F	Impact toughness in ft. lbs/sq.in.
Base Metal			
B 29	BM*	−100	6.0
B 30	"	−100	6.3
B 27	"	− 50	8.5
B 28	"	− 50	9.2
B 25	"	0	19.6
B 26	"	0	25.0
B 33	"	25	52.7
B 34	"	25	29.9
B 31	"	50	71.5
B 32	"	50	66.7
B 35	"	70	110.4
B 36	"	70	124.4
B 37	"	100	193.8
B 38	"	100	203.8
B 39	"	150	374.0
B 40	"	150	355.0

Weld B36: Standard guide tube, voltage = 40 volts, current = 600 amps, gap = 1-1/4", wire A.

36B07F	WCL**	−100	9.0
36B07B	"	−100	7.6
36B06F	"	− 50	13.2
36B06B	"	− 50	15.6
36B04F	"	0	42.5

Table X.
(cont.)

Specimen ID	Zone	Testing Temperature in °F	Impact toughness in ft. lbs/sq.in.
Weld B36 (cont.)			
36B05B	WCL**	0	25.4
36B09F	"	25	71.5
36B09B	"	25	58.0
36B08F	"	50	95.2
36B08B	"	50	77.2
36B10F	"	70	142.0
36B10B	"	70	151.0
36B11F	"	100	199.0
36B11B	"	100	172.0
36B12F	"	150	277.0
36B12B	"	150	245.0
36B18F	CCG#	−100	14.0
36B18B	"	−100	13.9
36B17F	"	− 50	42.6
36B17B	"	− 50	39.3
36B16F	"	0	116.1
36B16B	"	0	146.3
36B20F	"	25	198.7
36B20B	"	25	184.5
36B19F	"	50	225.6
36B19B	"	50	237.8
36B21F	"	70	238.0
36B21B	"	70	209.0
36B22F	"	100	405.0
36B22B	"	100	406.0

Table X.
(cont.)

Specimen ID	Zone	Testing Temperature in °F	Impact toughness in ft.lbs/sq.in.
Weld B36 (cont.)			
36B23F	CCG$^{\#}$	150	389.0
36B23B	"	150	436.0
36B26F	HAZ$^{\#\#}$	-100	8.4
36B26B	"	-100	6.3
36B25F	"	- 50	12.2
36B25B	"	- 50	11.3
36B24F	"	0	34.1
36B24B	"	0	43.1
36B28F	"	25	45.6
36B28B	"	25	59.5
36B27F	"	50	88.3
36B27B	"	50	88.8
36B29F	"	70	111.0
36B29B	"	70	97.0
36B30F	"	100	142.0
36B30B	"	100	145.0
36B31F	"	150	224.0
36B31B	"	150	276.0
Weld B47:	Quartz shielded guide tube (grain refined), voltage = 48 volts, current = 600 amps, gap = 1-1/4", wire A.		
47B06F	WCL**	-100	8.3
47B07B	"	-100	10.0
47B04F	"	- 50	14.7
47B06B	"	- 50	26.1

Table X.
(cont.)

Specimen ID	Zone	Testing Temperature in °F	Impact toughness in ft.lbs/sq.in.
Weld B47 (cont.)			
47B03F	WCL**	0	31.8
47B05B	"	0	51.1
47B09F	"	25	56.9
47B09B	"	25	56.7
47B07F	"	50	95.5
47B08B	"	50	117.9
47B10F	"	70	98.0
47B10B	"	70	139.0
47B11F	"	100	159.0
47B11B	"	100	152.0
47B12F	"	150	197.0
47B12B	"	150	231.0
47B18F	WM+	−100	17.7
47B18B	"	−100	11.8
47B16B	"	− 50	22.7
47B17B	"	− 50	30.8
47B15F	"	0	66.6
47B15B	"	0	56.6
47B20F	"	25	63.1
47B20B	"	25	74.3
47B19F	"	50	117.3
47B19B	"	50	107.9
47B21F	"	70	161.0
47B21B	"	70	195.0
47B22F	"	100	269.0

Table X.
(cont.)

Specimen ID	Zone	Testing Temperature in °F	Impact toughness in ft.lbs/sq.in.
Weld B47 (cont.)			
47B22B	WM$^+$	100	221.0
47B23F	"	150	267.0
47B23B	"	150	292.0
47B26F	HAZ$^{\#\#}$	-100	11.7
47B26B	"	-100	7.7
47B25F	"	- 50	17.6
47B25B	"	- 50	14.9
47B24F	"	0	43.2
47B24B	"	0	23.5
47B28F	"	25	61.2
47B28B	"	25	39.7
47B27F	"	50	135.9
47B27B	"	50	62.0
47B29F	"	70	123.0
47B29B	"	70	93.0
47B30F	"	100	206.0
47B30B	"	100	107.0
47B31F	"	150	254.0
47B31B	"	150	186.0

Weld B51: Winged guide tube, voltage = 36 volts, current = 700 amps, gap = 1-1/4", wire A.

51B07F	WCL**	-100	8.2
51B07B	"	-100	9.3
51B06F	"	- 50	12.5

Table X.
(cont.)

Specimen ID	Zone	Testing Temperature in °F	Impact toughness in ft.lbs/sq.in.
Weld B51 (cont.)			
51B06B	WCL**	− 50	17.5
51B05F	"	0	29.3
51B05B	"	0	49.1
51B09F	"	25	47.2
51B09B	"	25	67.0
51B08F	"	50	99.3
51B08B	"	50	97.1
51B10F	"	70	122.0
51B10B	"	70	138.0
51B11F	"	100	200.0
51B11B	"	100	281.0
51B12F	"	150	203.0
51B12B	"	150	345.0
51B18F	CCG#	−100	16.4
51B18B	"	−100	17.7
51B17F	"	− 50	33.0
51B17B	"	− 50	45.0
51B16F	"	0	137.4
51B16B	"	0	113.0
51B20F	"	25	191.4
51B20B	"	25	108.0
51B19F	"	50	213.4
51B19B	"	50	233.7
51B21F	"	70	334.0
51B21B	"	70	346.0

Table X.
(cont.)

Specimen ID	Zone	Testing Temperature in °F	Impact toughness in ft.lbs/sq.in.
Weld B51 (cont.)			
51B22F	CCG$^{\#}$	100	388.0
51B22B	"	100	350.0
51B26B	HAZ$^{\#\#}$	-100	7.9
51B27F	"	-100	6.8
51B25F	"	- 50	9.8
51B25B	"	- 50	11.9
51B24F	"	0	22.4
51B24B	"	0	23.5
51B28B	"	25	44.0
51B29F	"	25	33.9
51B27B	"	50	59.5
51B28F	"	50	64.4
51B29B	"	70	92.0
51B30F	"	70	133.0
51B30B	"	100	190.0
51B31F	"	100	131.0
51B31B	"	150	219.0
51B32F	"	150	292.0

Weld B52: Winged guide tube, voltage = 40 volts, current = 600 amps, gap = 3/4", wire A.

52B06F	WCL**	-100	10.3
52B06B	"	-100	9.3
52B12F	"	- 50	21.6
52B12B	"	- 50	27.1

Table X.
(cont.)

Specimen ID	Zone	Testing Temperature in °F	Impact toughness in ft.lbs/sq.in.
Weld B52 (cont.)			
52B05F	WCL**	0	66.0
52B05B	"	0	60.1
52B08F	"	25	58.6
52B08B	"	25	72.8
52B07F	"	50	90.3
52B07B	"	50	89.8
52B09F	"	70	168.0
52B09B	"	70	120.0
52B10F	"	100	188.0
52B10B	"	100	191.0
52B11F	"	150	291.0
52B11B	"	150	241.0
52B17F	CCG#	-100	14.8
52B17B	"	-100	30.7
52B23F	"	- 50	37.8
52B23B	"	- 50	93.5
52B16F	"	0	189.0
52B16B	"	0	169.0
52B19F	"	25	184.0
52B19B	"	25	137.5
52B18F	"	50	214.0
52B18B	"	50	221.0
52B20F	"	70	331.0
52B20B	"	70	318.0
52B21F	"	100	364.0

Table X.
(cont.)

Specimen ID	Zone	Testing Temperature in °F	Impact toughness in ft.lbs/sq.in.
Weld B52 (cont.)			
52B21B	CCG$^\#$	100	362.0
52B24B	HAZ$^{\#\#}$	−100	16.5
52B25F	"	−100	17.8
52B31F	"	− 50	11.6
52B30B	"	− 50	10.3
52B24F	"	0	36.0
52B31B	"	0	22.8
52B27F	"	25	39.8
52B27B	"	25	49.2
52B26F	"	50	47.0
52B26B	"	50	67.6
52B28F	"	70	99.0
52B28B	"	70	108.0
52B29F	"	100	158.0
52B29B	"	100	233.0
52B25B	"	150	341.0
52B30F	"	150	214.0

Note: BM* Base Metal (as received)
WCL** Weld centerline--mid-thickness location
CCG$^\#$ Coarse columnar grain--mid-thickness location
HAZ$^{\#\#}$ Heat affected zone--mid-thickness location
WM$^+$ Weld metal adjacent to fusion line at mid-thickness location.
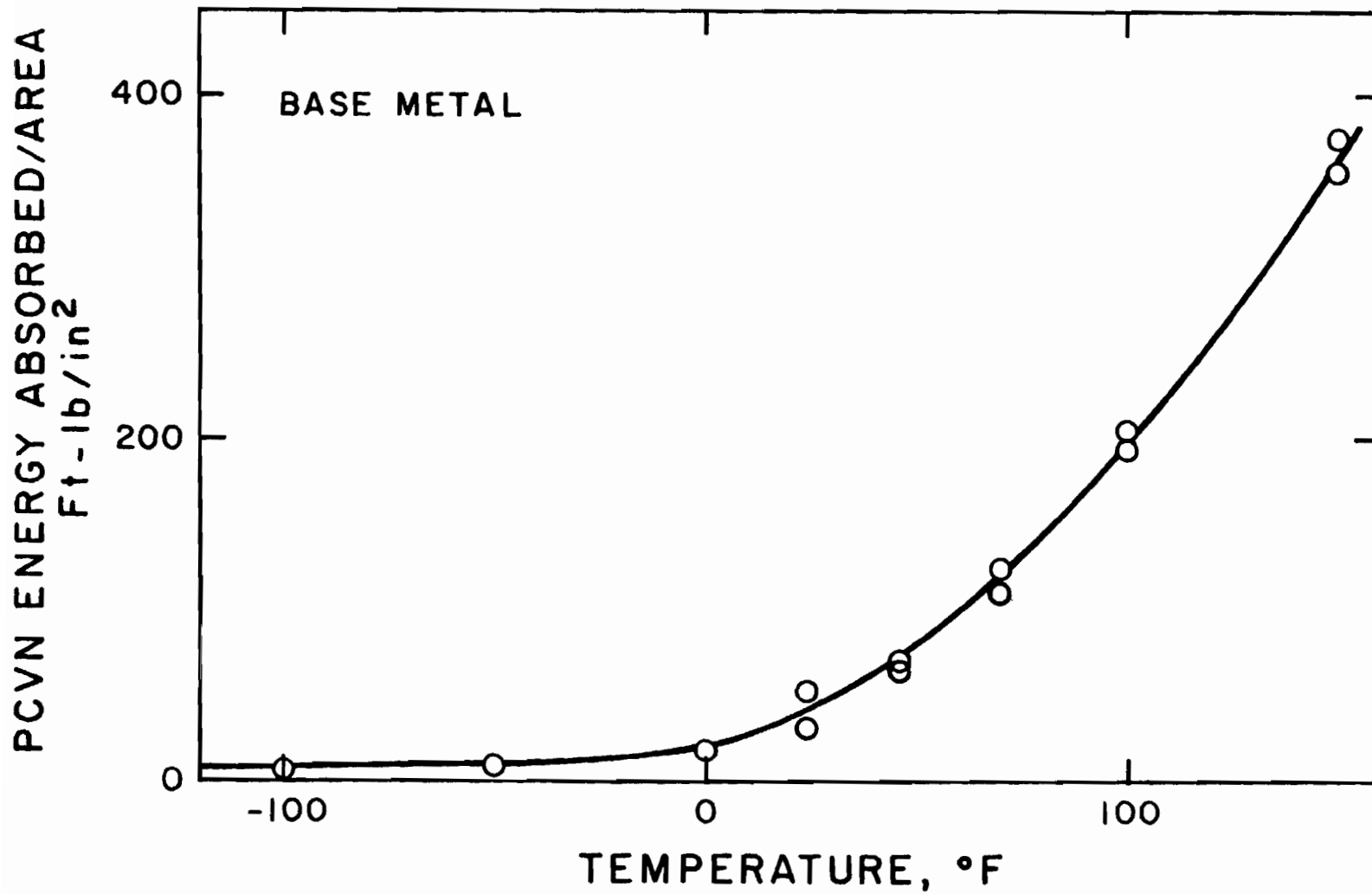
Figure 64. TEMPERATURE VS. FATIGUE PRECRACKED CHARPY V NOTCH IMPACT ENERGY/AREA
RELATIONSHIP FOR THE A588 BASE METAL.
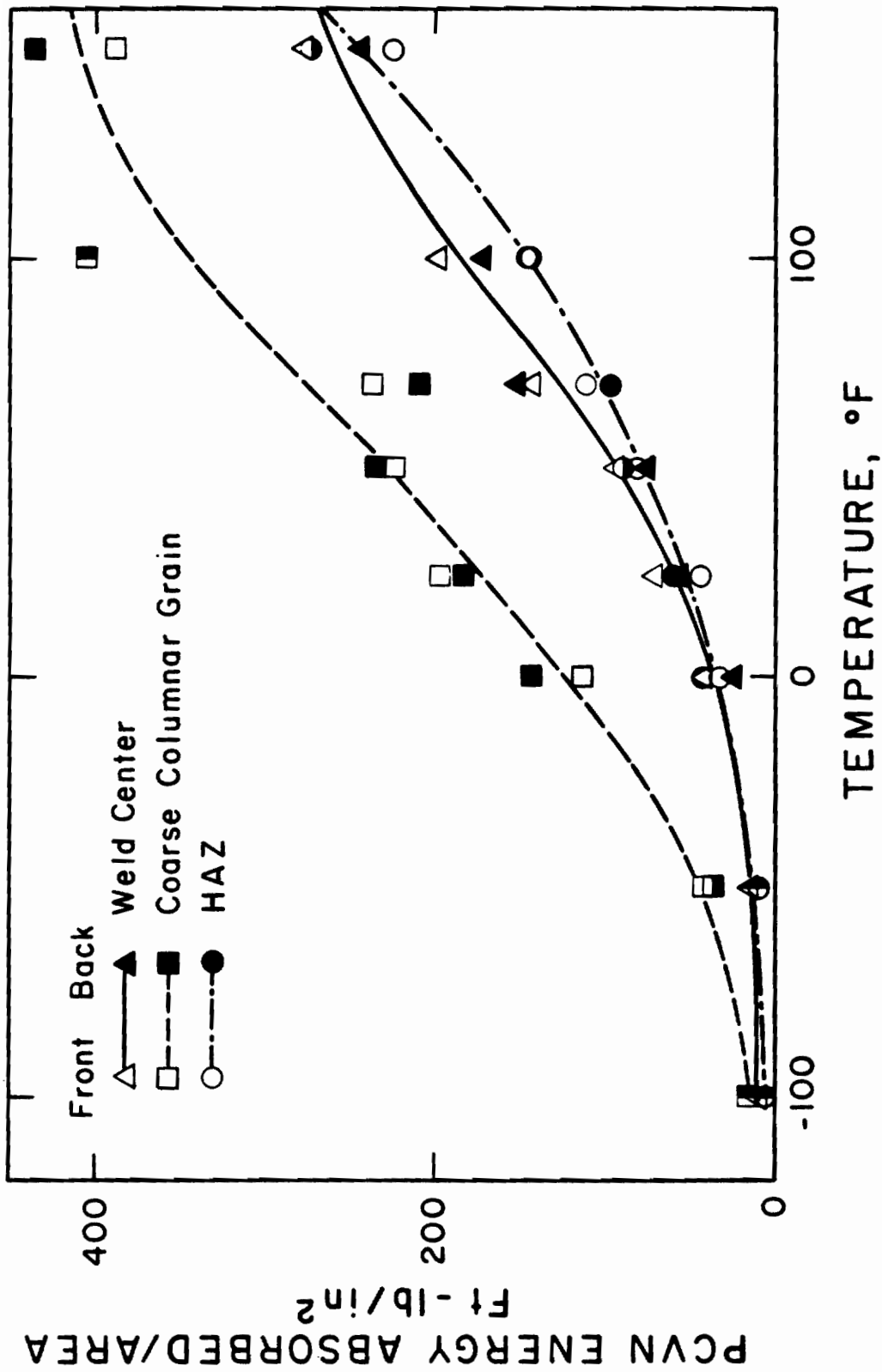
Figure 65. TEMPERATURE VS. FATIGUE PRECRACKED CHARPY V NOTCH IMPACT ENERGY/AREA RELATION-
SHIPS FOR STANDARD (CYLINDRICAL GUIDE; 1-1/4" GAP) ES WELD MADE USING WIRE A.
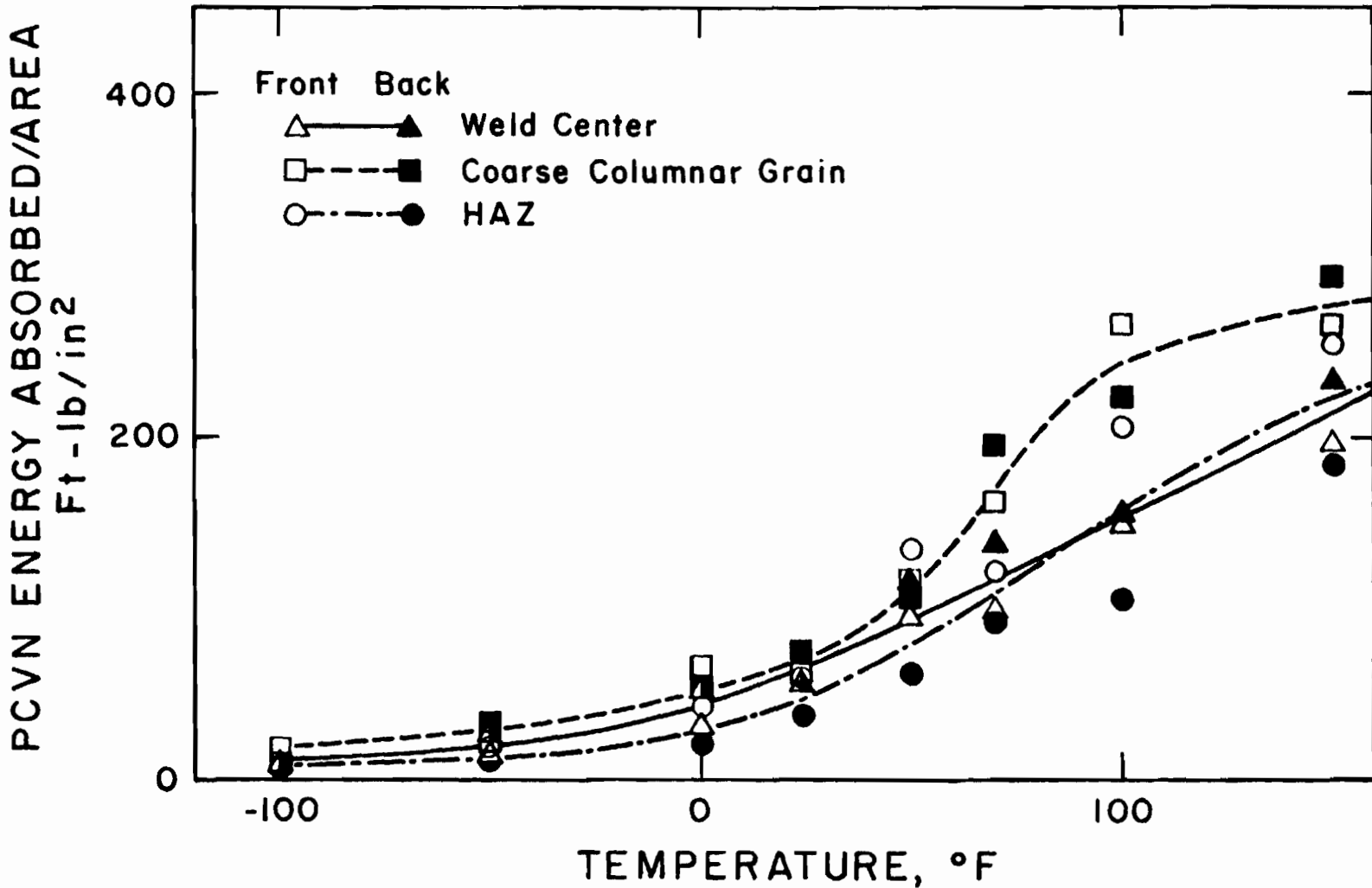
Figure 66. TEMPERATURE VS. FATIGUE PRECRACKED CHARPY V NOTCH IMPACT ENERGY/AREA RELATION-
SHIPS FOR GRAIN REFINED (QUARTZ SHIELDED GUIDE) ES WELD MADE USING WIRE A.
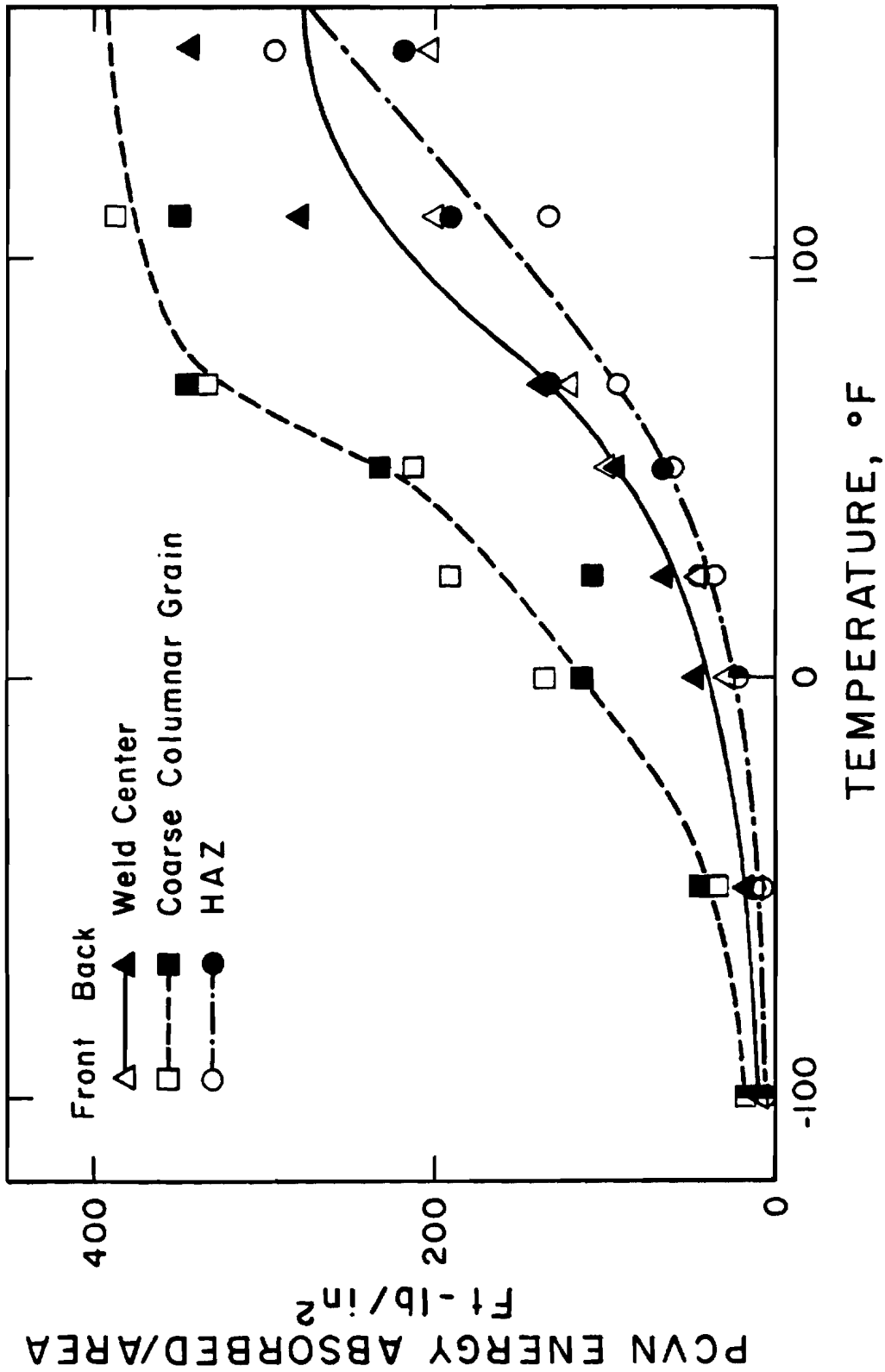
Figure 67. TEMPERATURE VS. FATIGUE PRECRACKED CHARPY V NOTCH IMPACT ENERGY/AREA RELATION-SHIPS FOR STANDARD GAP (1-1/4") WINGED GUIDE TUBE ES WELD MADE USING WIRE A.
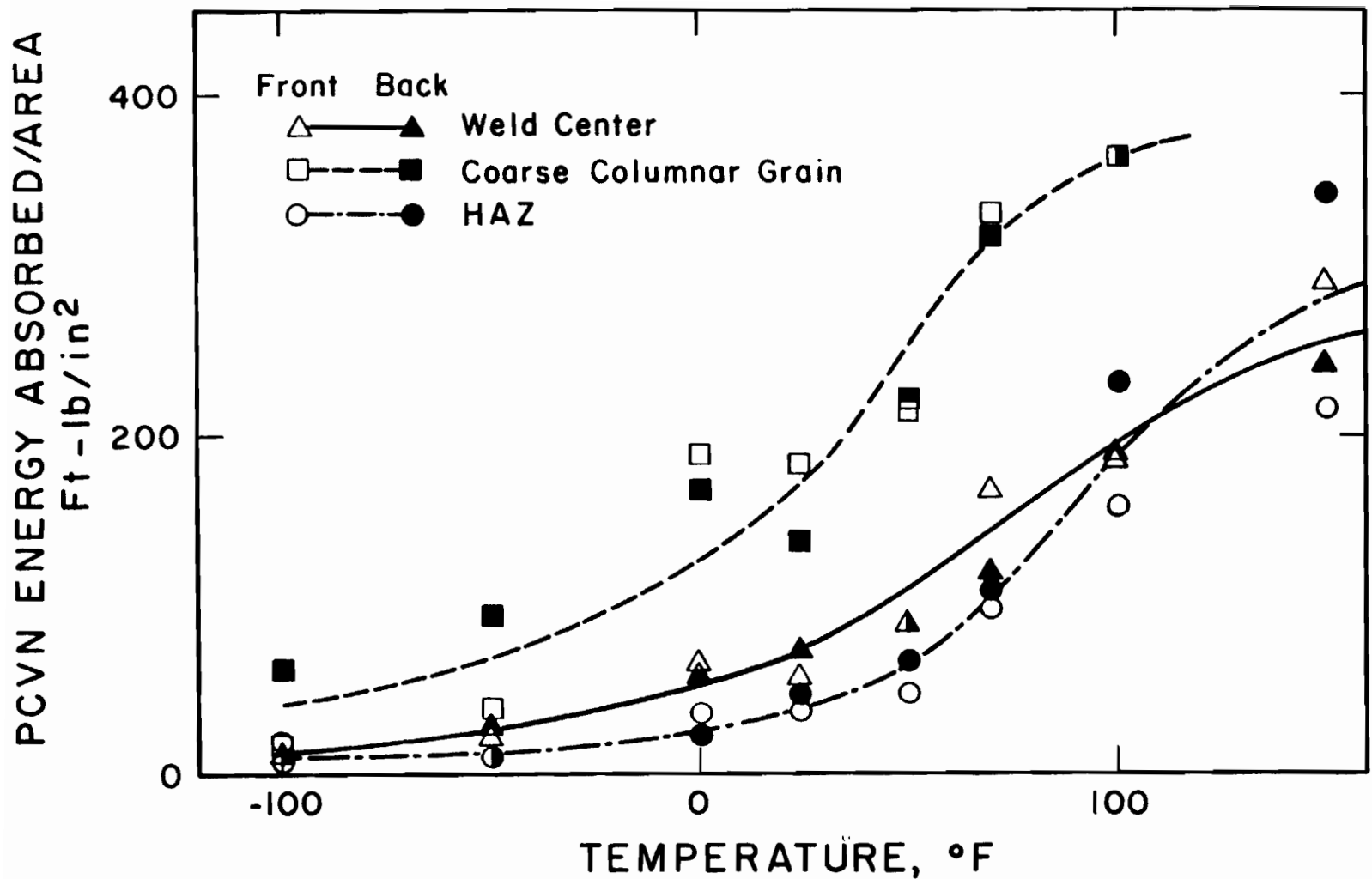
Figure 68. TEMPERATURE VS. FATIGUE PRECRACKED CHARPY V NOTCH IMPACT ENERGY/AREA RELATION-
SHIPS FOR NARROW GAP (3/4") WINGED GUIDE TUBE ES WELD MADE USING WIRE A.

Notch →   Notch →   Notch →

Standard (wire A)   Grain Refined (Quartz Shielded)   High Current/Narrow Gap/Winged Guide (Wire E)
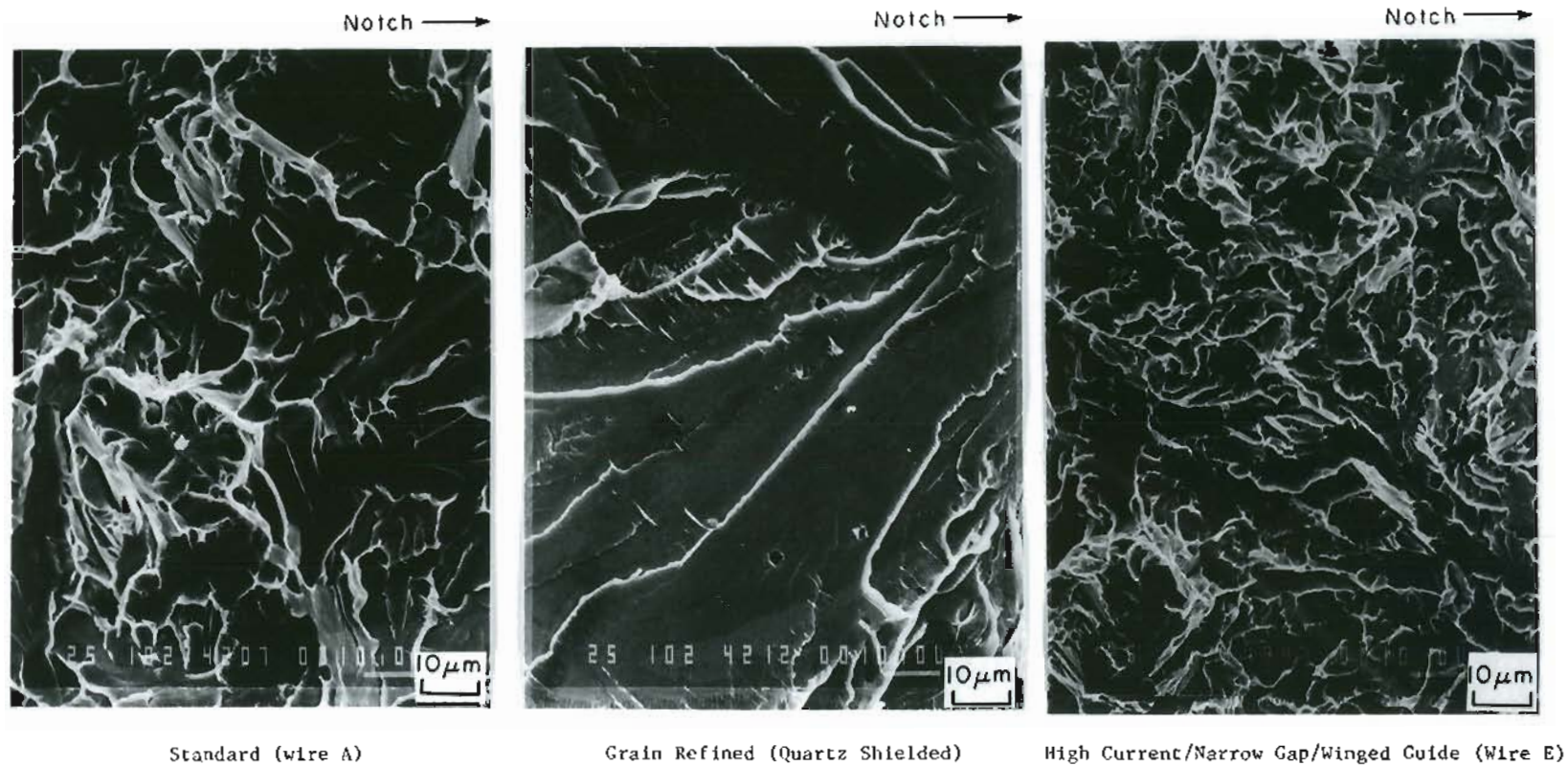
Figure 69. FRACTURE SURFACE APPEARANCE IN CVN SPECIMENS WITH THE NOTCH LOCATED AT CCG ZONE OF ESW.
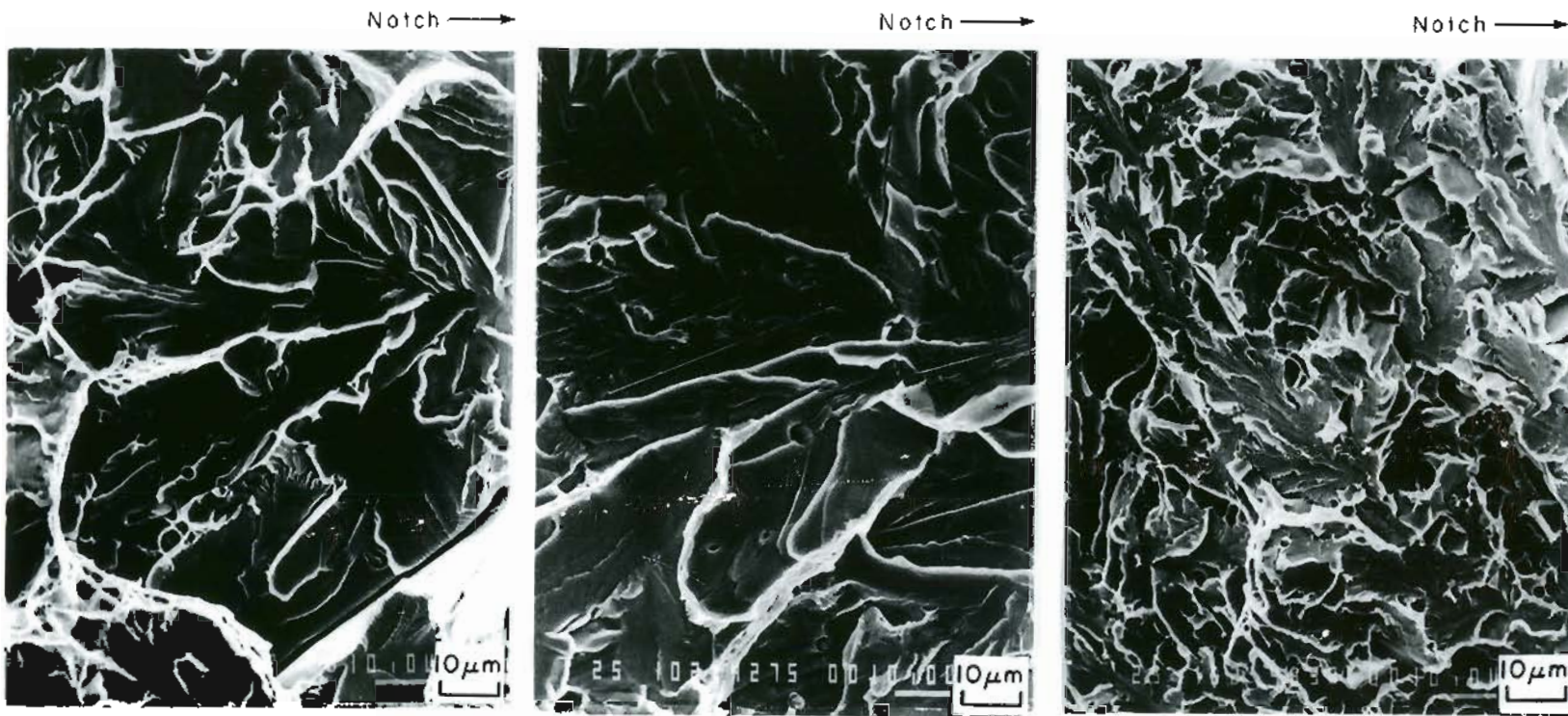
Notch ⟶   Notch ⟶   Notch ⟶

Standard (Wire A)   Grain Refined (Quartz Shielded)   High Current/Narrow Gap/Winged Guide (Wire E)

Figure 70.   FRACTURE SURFACE APPEARANCE IN CVN SPECIMENS WITH THE NOTCH LOCATED AT WCL ZONE OF ESW.
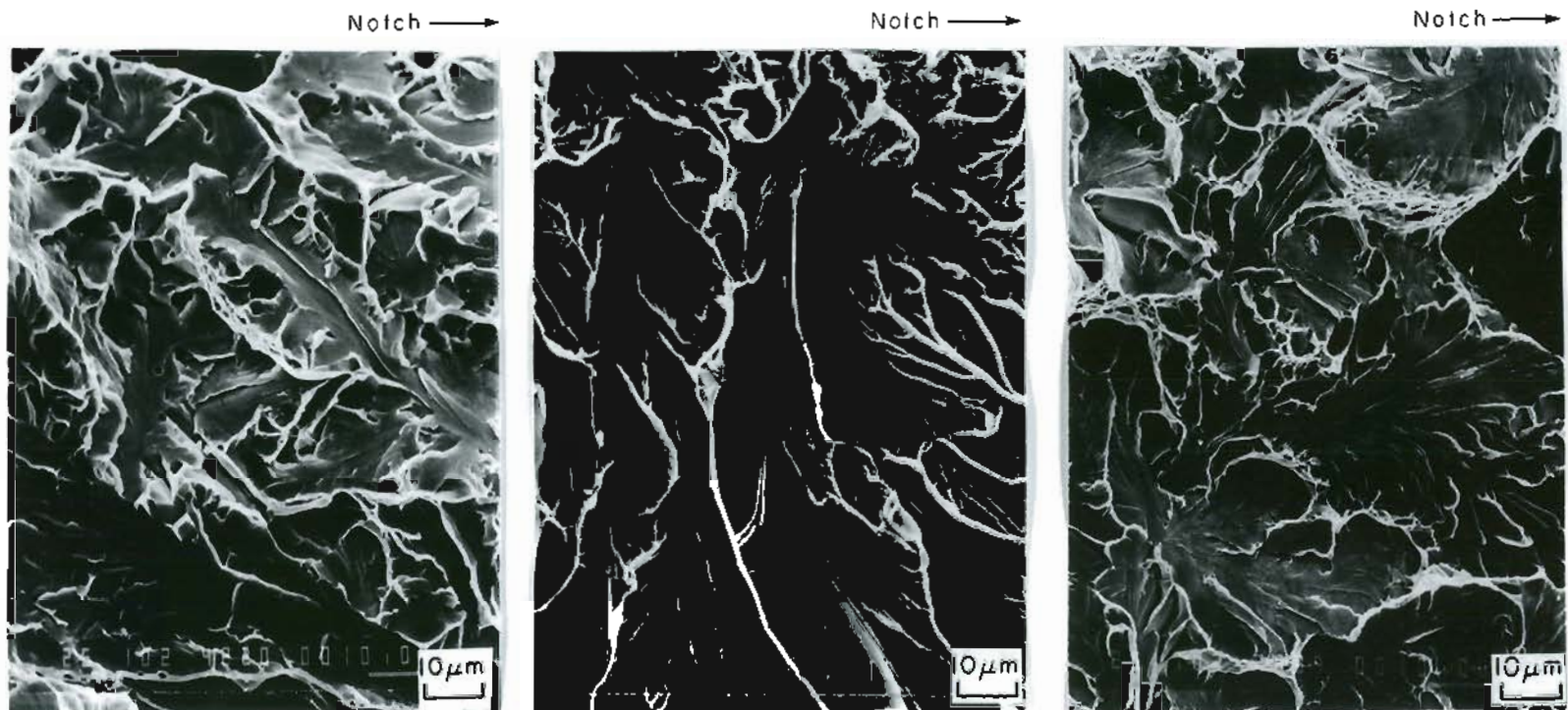
Notch ⟶   Notch ⟶   Notch ⟶

Standard (wire A)   Grain Refined (Quartz Shielded)   High Current/Narrow Gap/Winged Guide (Wire E)

Figure 71. FRACTURE SURFACE APPEARANCE IN CVN SPECIMENS WITH THE NOTCH LOCATED AT HAZ1 OF ESW.
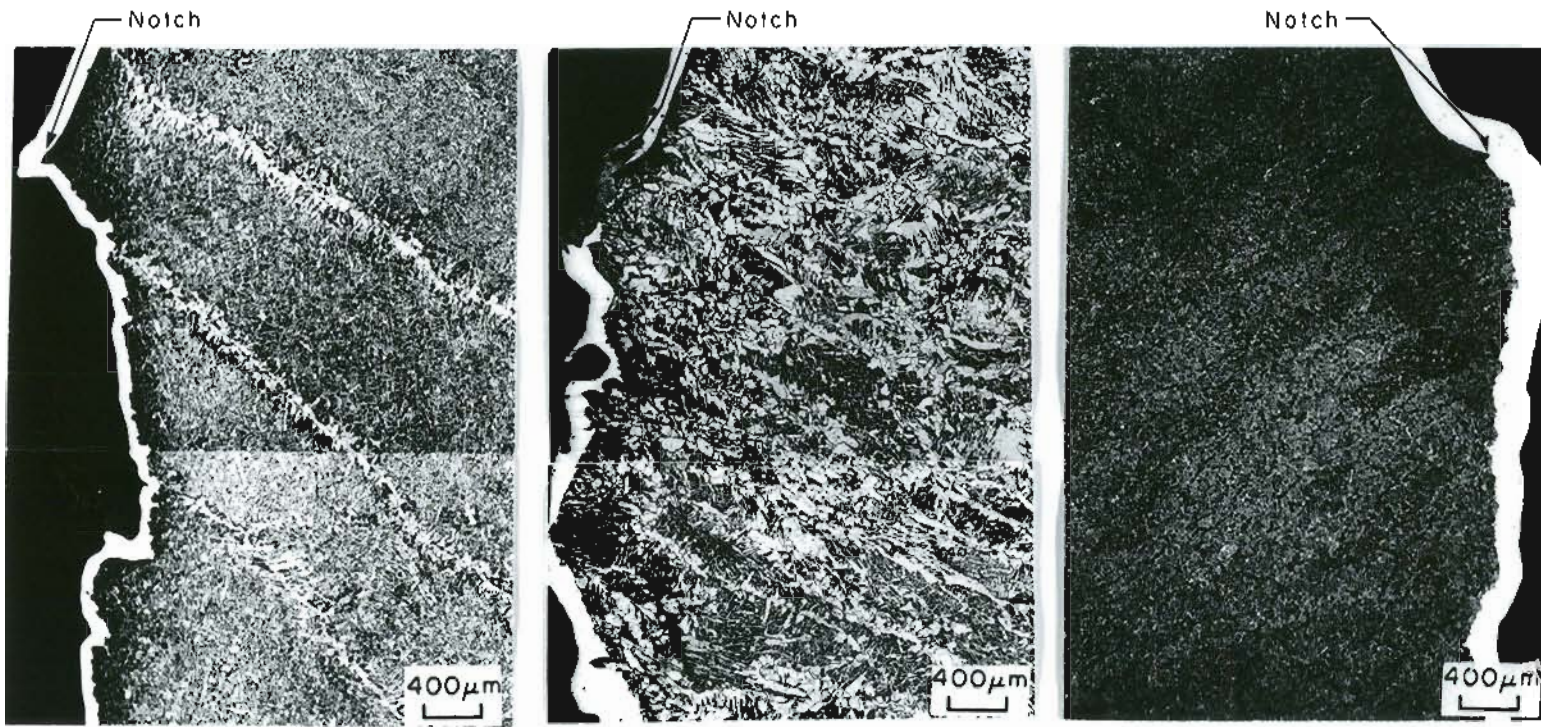
Standard (wire A)   Grain Refined (Quartz Shielded)   High Current/Narrow Gap/Winged Guide (Wire E)

Figure 72. CRACK PROPAGATION PATHS IN CVN SPECIMENS WITH THE NOTCH LOCATED AT CCG ZONE OF ESW.

Figure 73. CRACK PROPAGATION PATHS IN CVN SPECIMENS WITH THE NOTCH LOCATED AT WCL ZONE OF ESW.
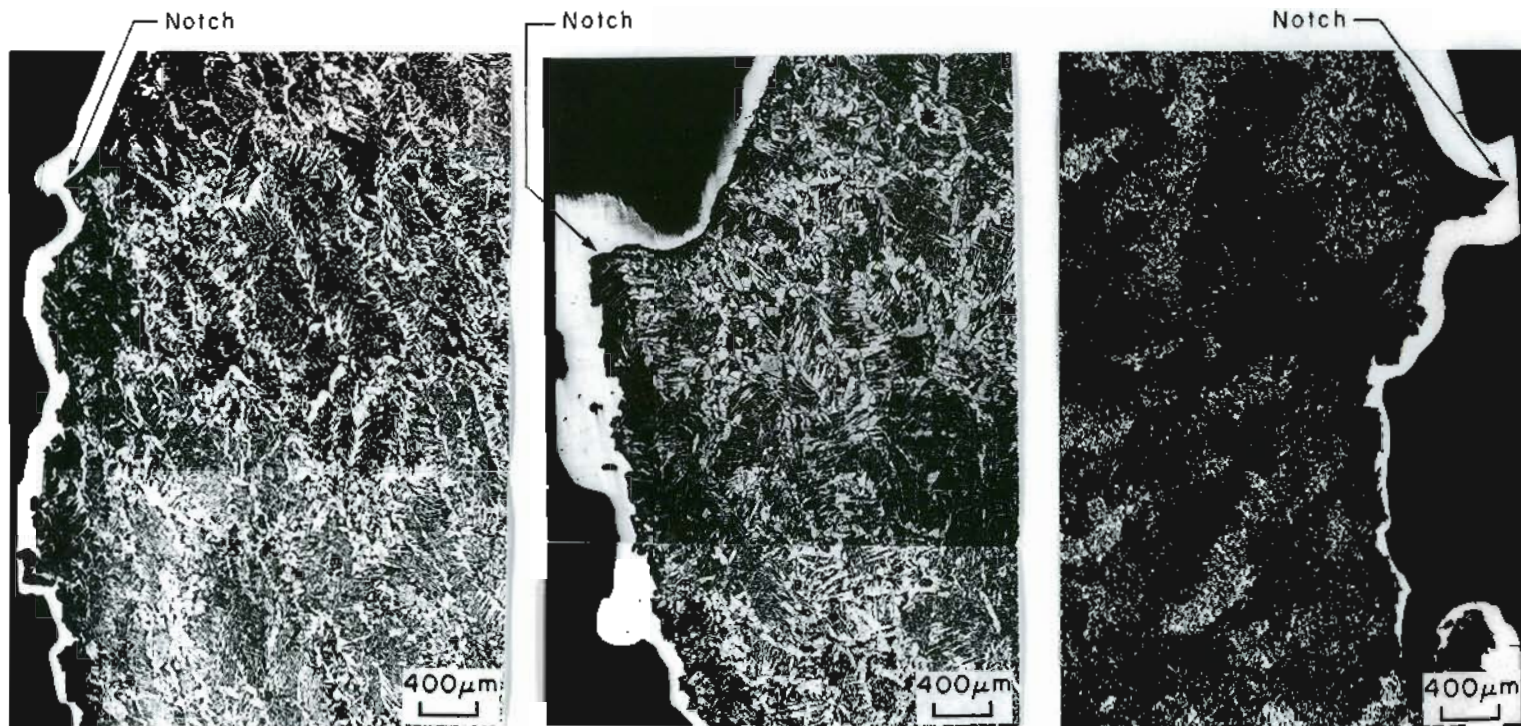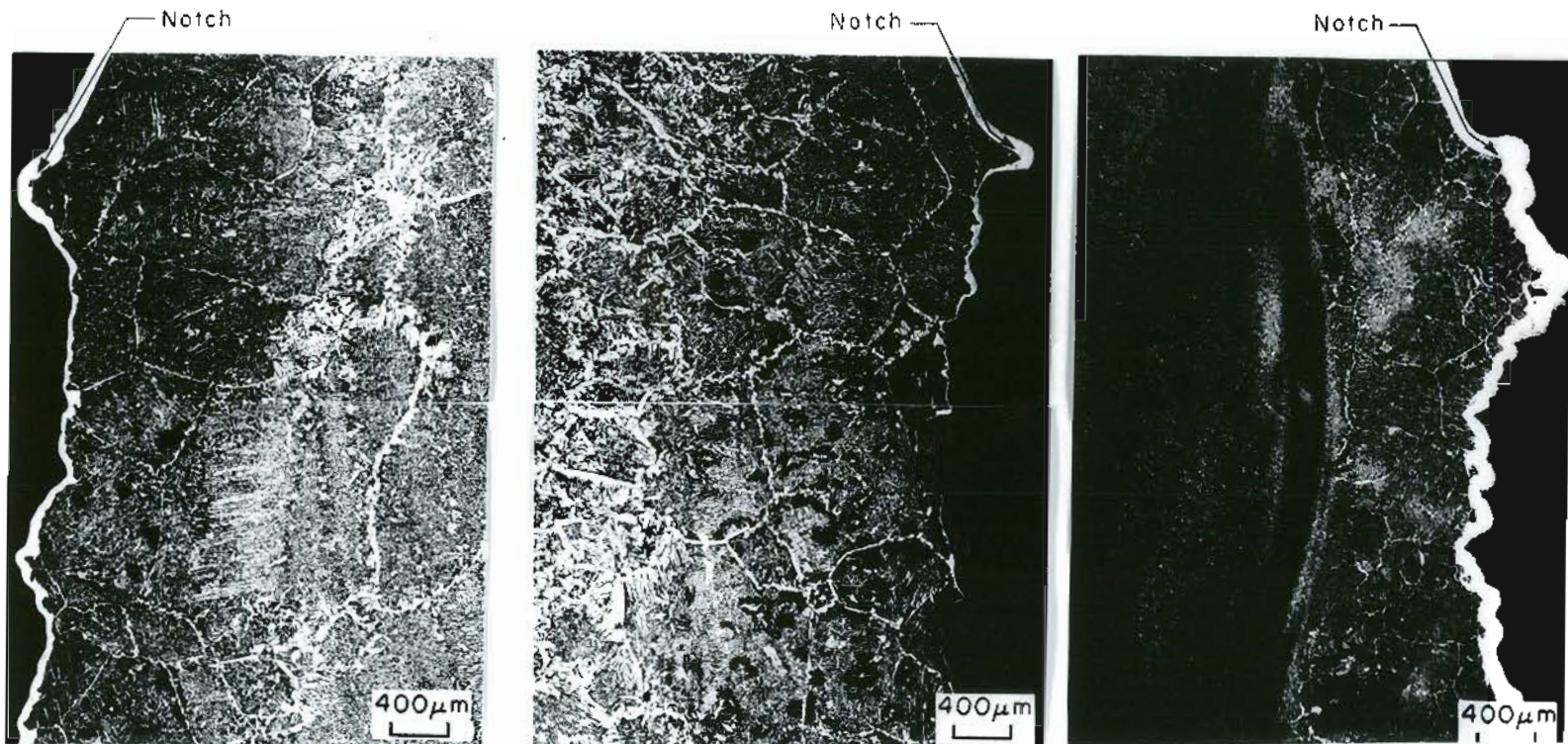
Standard (wire A) Grain Refined (Quartz Shielded) High Current/Narrow Cap/Winged Guide (Wire E)

Standard (wire A)   Grain Refined (Quartz Shielded)   High Current/Narrow Gap/Winged Guide (Wire E)

Figure 74. CRACK PROPAGATION PATHS IN CVN SPECIMENS WITH THE NOTCH LOCATED AT HAZ1 OF ESW.

In the CCG zone of standard welds, initial crack extension along proeutectoid grain boundaries was observed. The preferential crack propagation along ferrite boundaries was distinctive in the grain refined weld, Figure 75, while no preferential path was observed in high current/narrow gap welds made with wire E. No preferential CVN crack propagation paths were found in the HAZ region either, for all welds tested.

3.8. Chemical Analysis

Spectrographic chemical analyses of various welds are shown in Table XI. The carbon content of welds was in the range of 0.11 to 0.15 wt.%. Sulfur and phosphorus levels were 0.02 to 0.03 and 0.01 to 0.02, respectively. An increase in Cr and Cu was observed in the weld made using wire B when compared to the standard weld made using wire A. Use of a quartz shroud increased the Si content by 0.1 wt.% and reduced the Mn level by 0.17 wt.%, in the grain refined weld. Similar results were obtained in welds made using a mullite shroud. Both Mn and Si contents were increased in welds made with wire C.

Elemental Mo additions resulted in Mo levels ranging from 0.53 to 1.07 wt.%, depending on the input level, whereas in welds made using wire E, higher Cr and Mo contents were obtained (Cr--1.22 to 1.58 and Mo--0.35 to 0.50 wt.%). Alloy contents of the high current/narrow gap weld were slightly lower when compared to the standard gap weld due to increased base metal dilution.
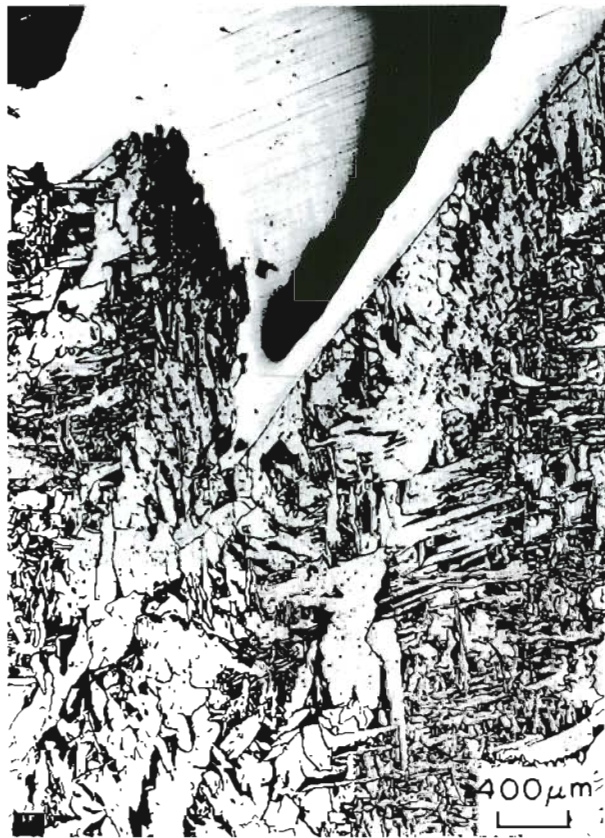
Grain Refined Weld (Quartz Shielded)

Figure 75. MICROSTRUCTURE ILLUSTRATING BRITTLE CRACK
PROPAGATION ALONG THE PROEUTECTOID FERRITE
FILM IN ES WELDS.

Table XI.

SPECTROGRAPHIC WELD METAL ANALYSIS

#	Weld ID	Weld Description	Composition wt.%										
			C	Mn	Si	Cr	Ni	Mo	Cu	S	P	Al	V
1	B23	Standard—wire A*	0.14	1.09	0.38	0.20	0.03	–	0.13	0.02	0.01	0.01	0.03
2	B6	Mullite shielded guide, 35Hz vibration, 45V, 500A, 1-1/4"gap, wire A	0.11	1.01	0.46	0.22	0.02	–	0.12	0.02	0.01	0.01	0.03
3	B27	Quartz shielded guide, no vibration, 48V, 600A 1-1/4" gap, wire A	0.11	0.92	0.48	0.23	0.03	–	0.14	0.03	0.01	0.01	0.04
4	B69B	Standard—0.53 wt.% Mo addition*	0.15	1.09	0.35	0.26	0.04	0.53	0.17	0.02	0.01	0.01	0.04
5	B70T	Standard—0.66 wt.% Mo addition*	0.15	1.06	0.34	0.28	0.04	0.66	0.18	0.02	0.01	0.01	0.05
6	B69T	Standard—1.07 wt.% Mo addition*	0.15	1.02	0.34	0.28	0.03	1.07	0.17	0.02	0.01	0.02	0.04
7	B89	Standard—wire B*	0.11	0.80	0.28	0.57	0.45	–	0.51	0.02	0.01	0.01	0.03
8	B74	Standard—wire C*	0.13	1.77	0.71	0.22	0.04	–	0.14	0.02	0.01	0.01	0.03
9	B64	Standard—wire D*	0.14	1.13	0.19	0.31	0.04	0.20	0.24	0.02	0.01	0.01	0.05
10	B90	Standard—wire E*	0.15	0.85	0.35	1.58	0.07	0.50	0.22	0.02	0.01	0.01	0.04
11	B95	Winged guide, 40V, 1000A, 3/4" gap, wire E	0.15	0.92	0.32	1.22	0.05	0.35	0.22	0.02	0.01	0.02	0.05

Note: *Standard procedure involves use of cylindrical guide, 42V, 600A, and 1-1/4" joint spacing.

3.9. Heat Flow Analysis

Temperature distributions in standard and high current/narrow gap electroslag welds, as a function of time, are presented in Figures 76a-c and 77a-c. The peak temperatures were attained much faster in high current/narrow gap welds than in standard welds. They were also higher compared to peak temperature attained in standard welds, with an exception of locations near the top of the weld. The holding period above the transformation temperature (approximately 1400°F) was considerably reduced for high current/narrow gap welds.
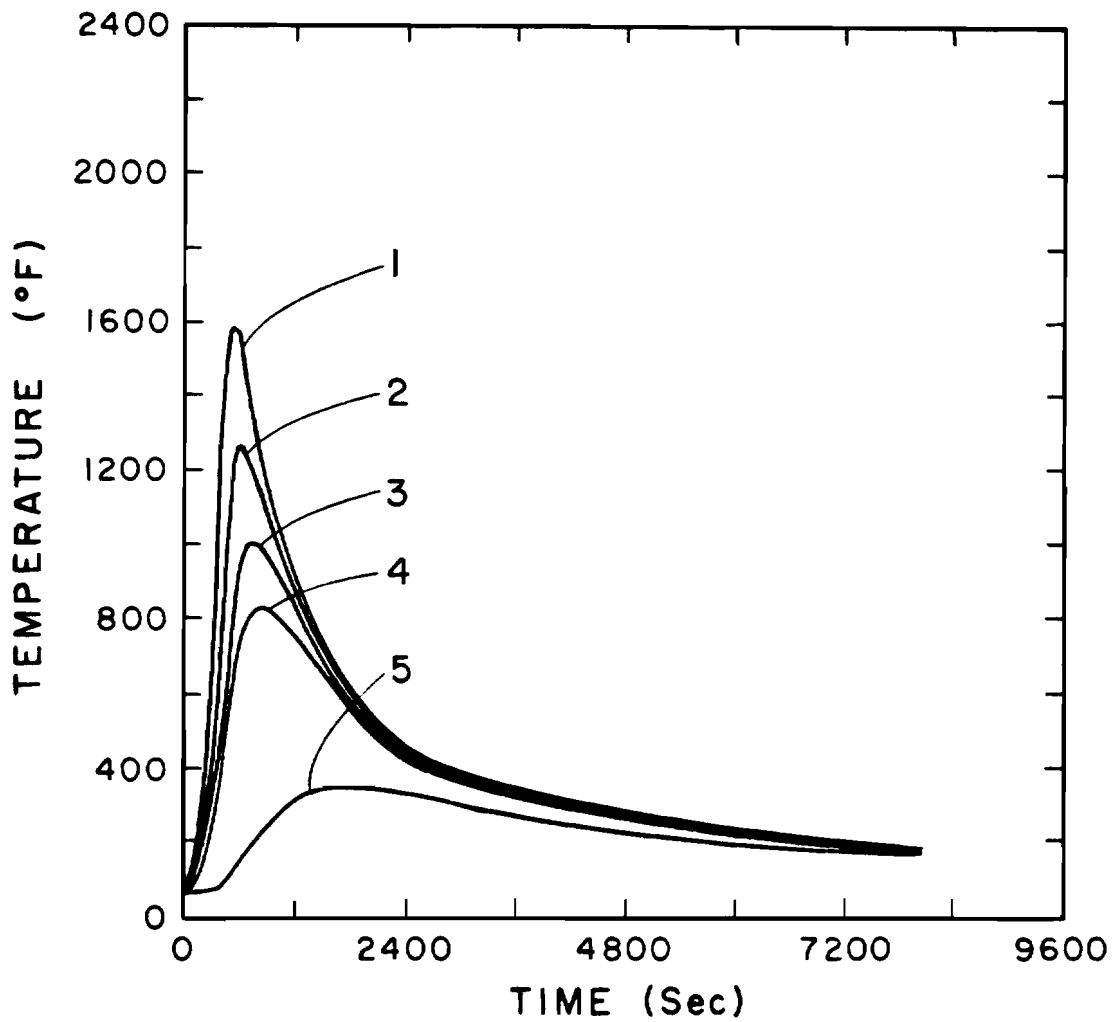
Figure 76a. TEMPERATURE DISTRIBUTION IN THE STANDARD (CYLINDRICAL
GUIDE TUBE, 1-1/4" GAP, 42 VOLTS AND 600 AMPS) ES WELD.
THERMOCOUPLES 1 THROUGH 5, THERMOCOUPLE LOCATION FROM
FUSION LINE (IN INCHES): 1--0.54, 2--0.92, 3--1.48,
4--1.96 and 5--6.0.
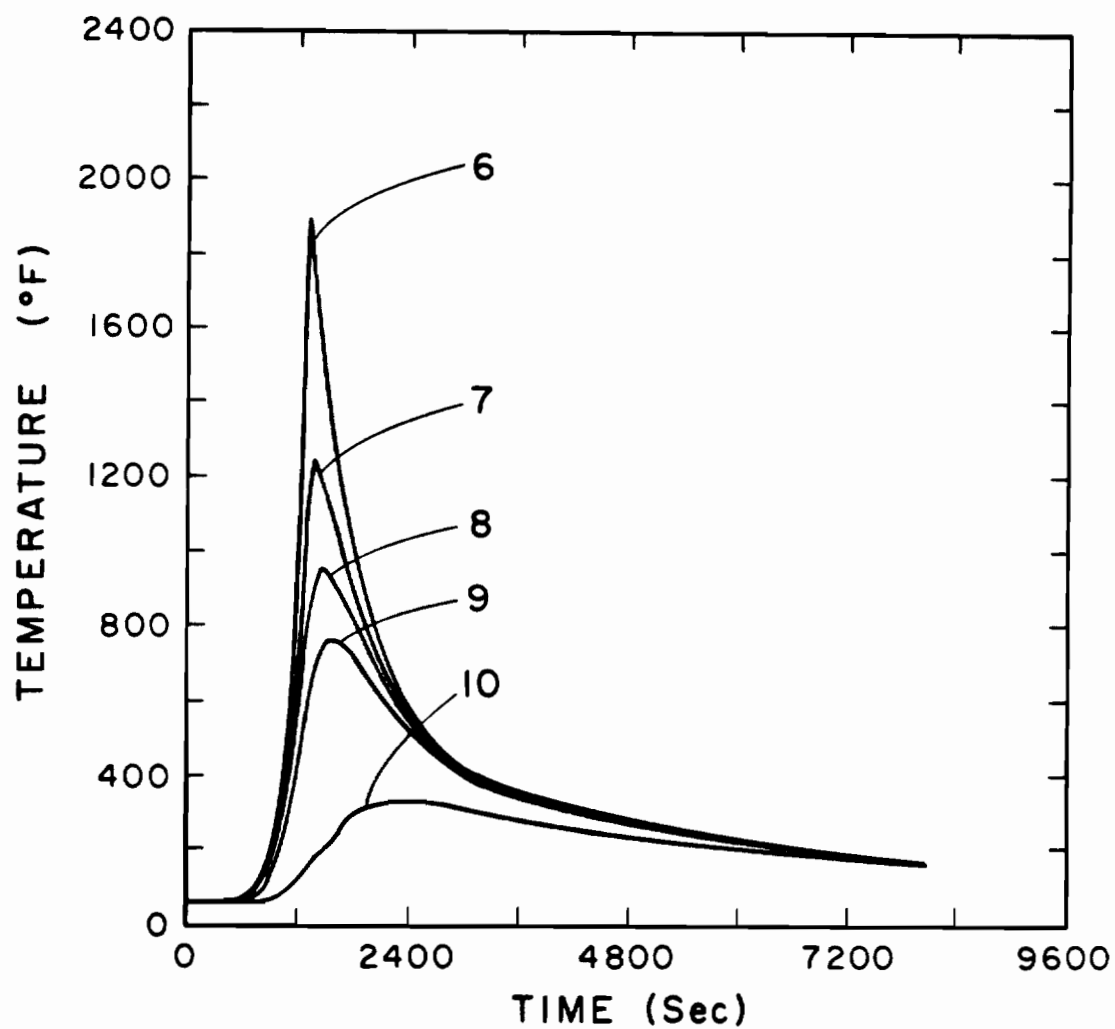
Figure 76b. TEMPERATURE DISTRIBUTION IN THE STANDARD (CYLINDRICAL
GUIDE TUBE, 1-1/4" GAP, 42 VOLTS, AND 600 AMPS) ES WELD.
THERMOCOUPLES 6 THROUGH 10, THERMOCOUPLE LOCATION FROM
FUSION LINE (IN INCHES): 6--0.32, 7--0.83, 8--1.32,
9--1.85, AND 10--5.84.
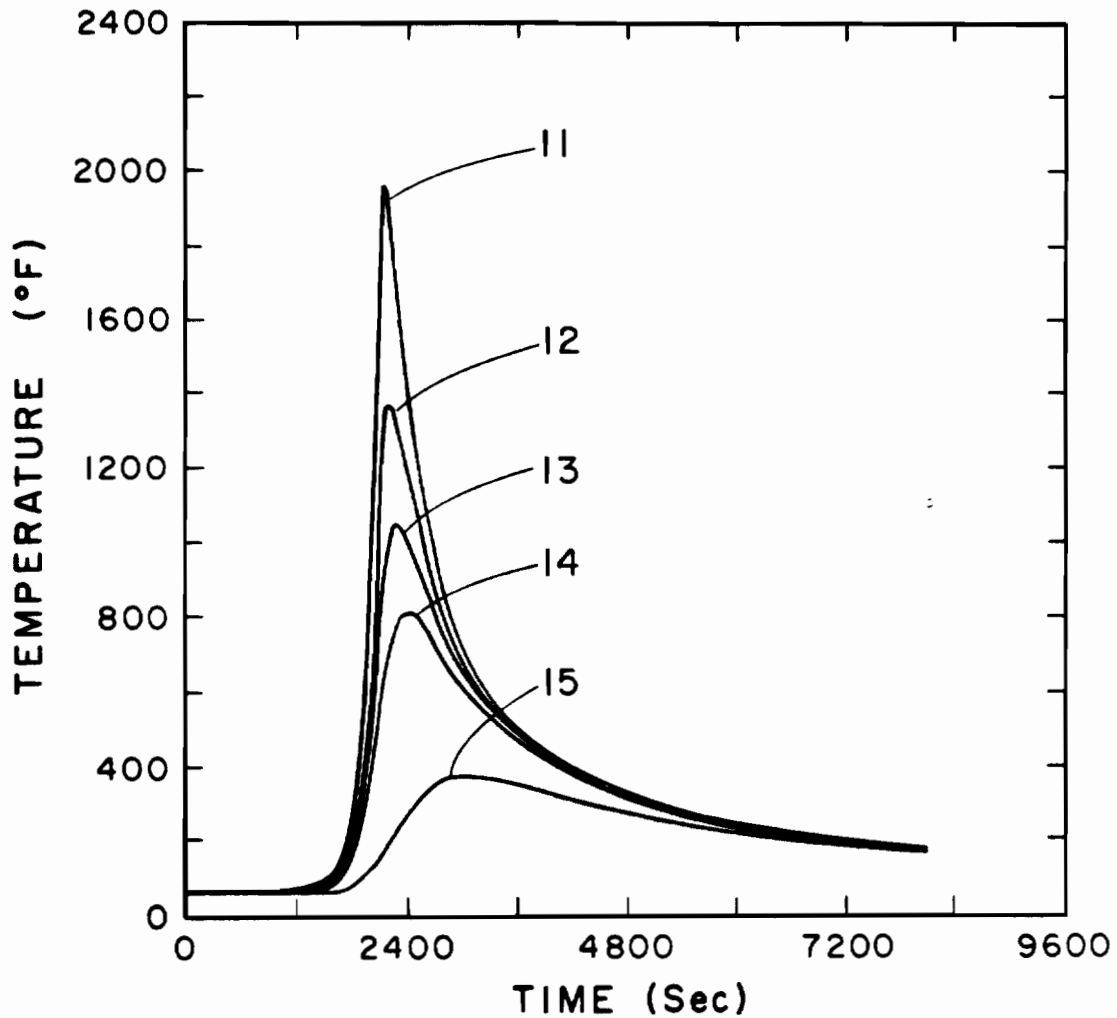
Figure 76c. TEMPERATURE DISTRIBUTION IN THE STANDARD (CYLINDRICAL
GUIDE TUBE, 1-1/4" GAP, 42 VOLTS, AND 600 AMPS) ES WELD.
THERMOCOUPLES 11 THROUGH 15, THERMOCOUPLE LOCATION FROM
FUSION LINE (IN INCHES): 11--0.30, 12--0.72, 13--1.3,
14--1.92 AND 15--5.76.
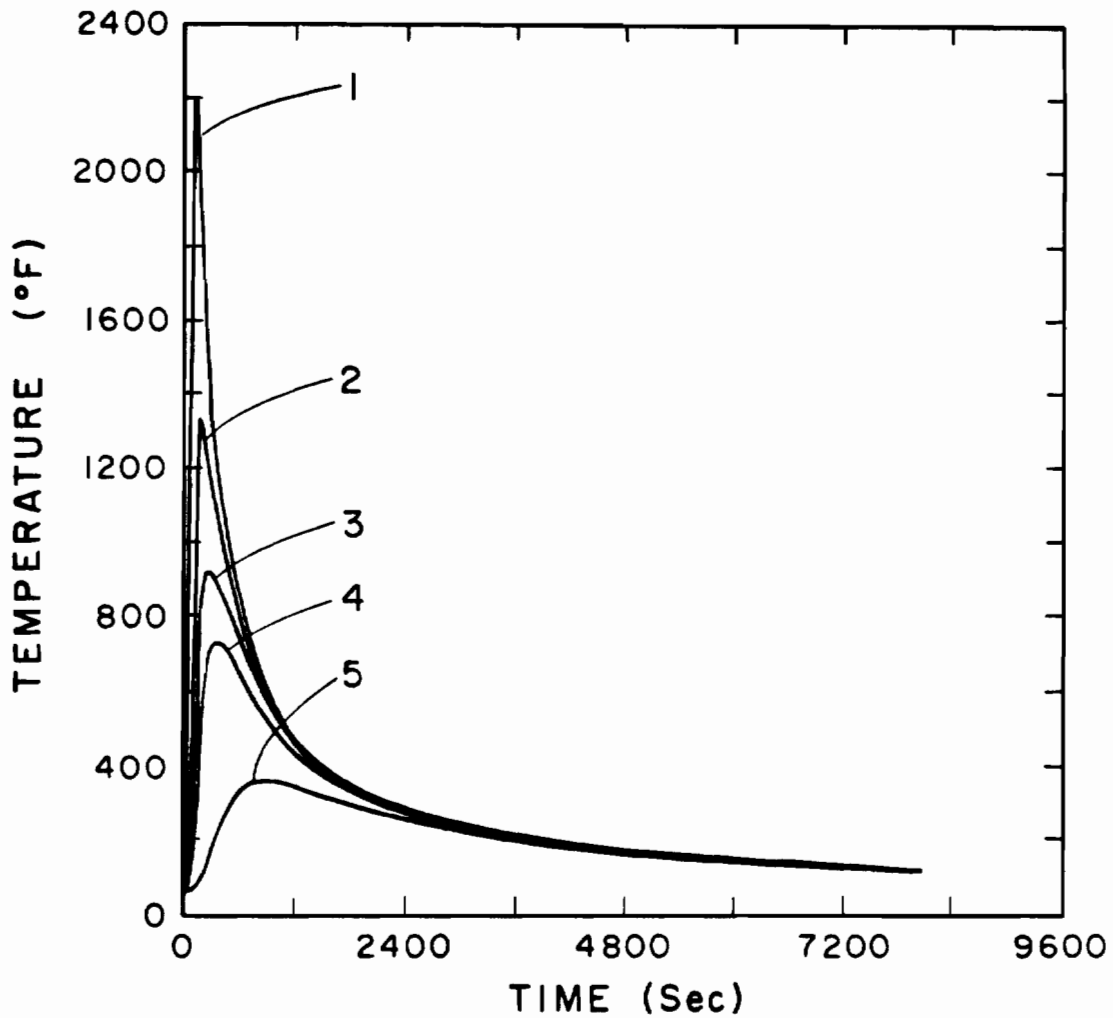
Figure 77a. TEMPERATURE DISTRIBUTION IN THE HIGH CURRENT (1000 AMPS, 40 VOLTS) NARROW GAP (3/4") WINGED GUIDE TUBE ES WELD. THERMOCOUPLES 1 THROUGH 5, THERMOCOUPLE LOCATION FROM FUSION LINE (IN INCHES): 1--0.17, 2--0.55, 3--1.13, 4--1.63, AND 5--4.42.
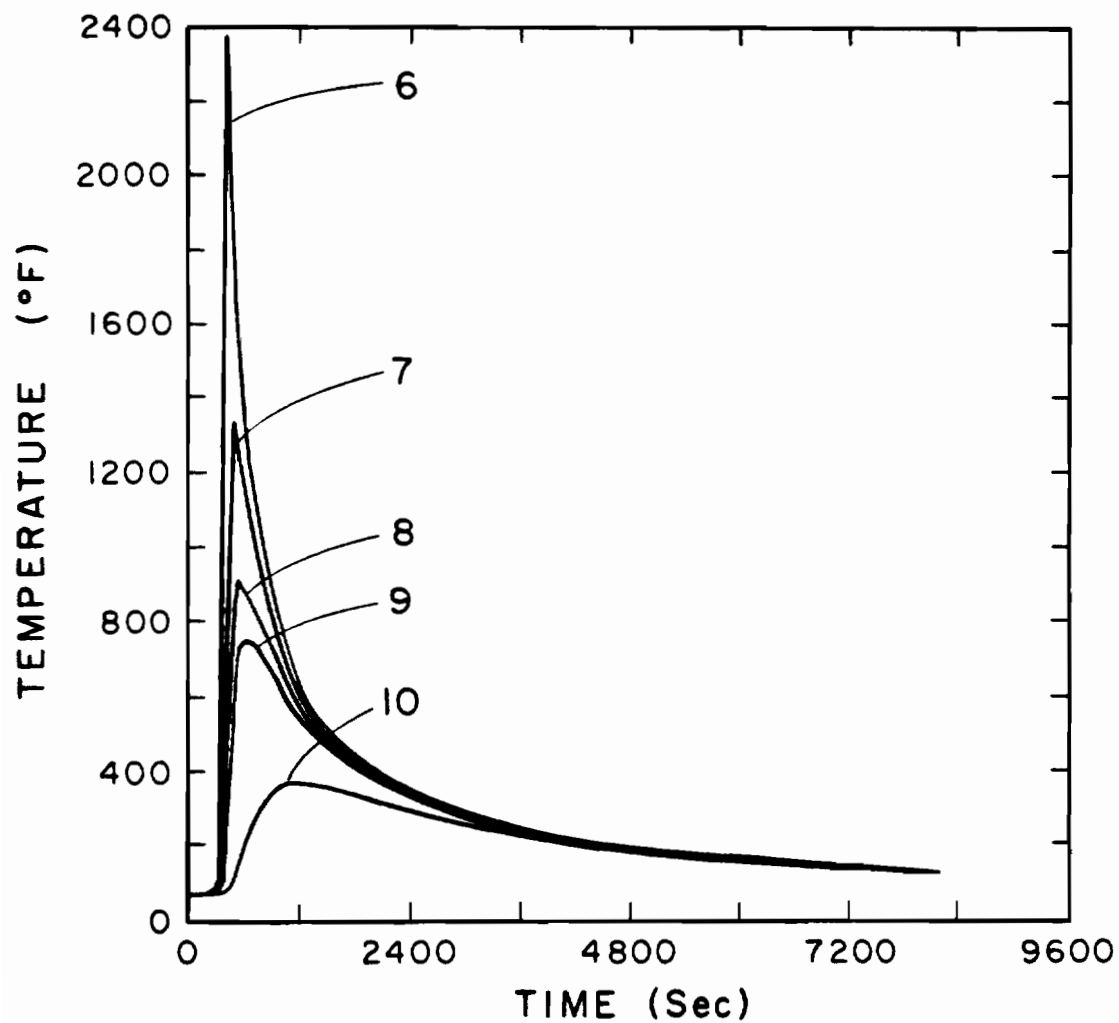
Figure 77b. TEMPERATURE DISTRIBUTION IN THE HIGH CURRENT (1000 AMPS, 40 VOLTS) NARROW GAP (3/4") WINGED GUIDE TUBE ES WELD. THERMOCOUPLES 6 THROUGH 10, THERMOCOUPLE LOCATION FROM FUSION LINE (IN INCHES): 6--0.13, 7--0.65, 8--1.23, 9--1.73 AND 10--4.38.
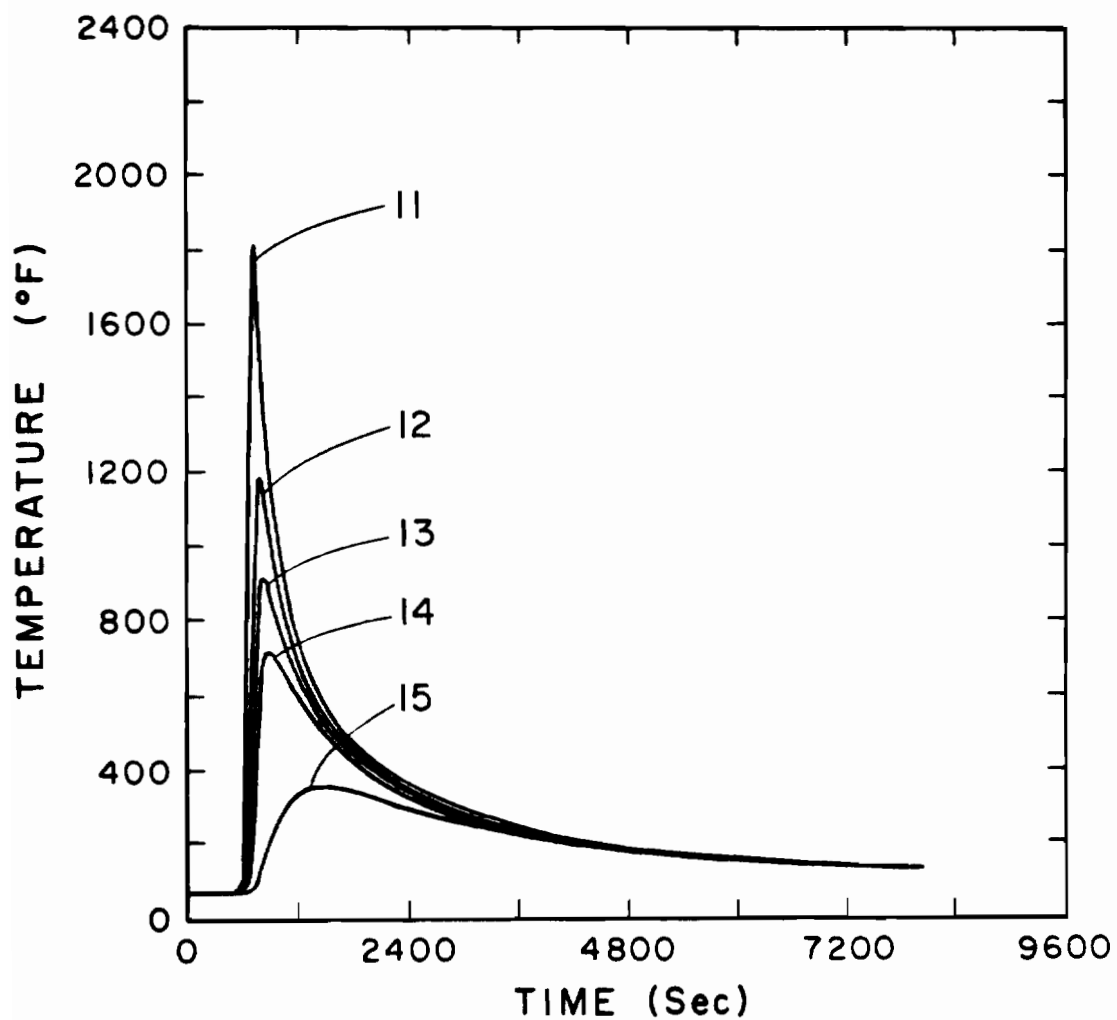
Figure 77c. TEMPERATURE DISTRIBUTION IN THE HIGH CURRENT (1000 AMPS, 40 VOLTS) NARROW GAP (3/4") WINGED GUIDE TUBE ES WELD. THERMOCOUPLES 11 THROUGH 15.

4. DISCUSSION

4.1. Process Optimization

Welding current and voltage, welding speed, guide tube geometry, joint spacing, etc., each exert a strong influence on the resulting electroslag weld. In addition, plate grounding and electrode position-ing affect both weld consistency and quality. The proper selection and control of these variables are necessary to produce reproducible optimum welds.

4.1.1. Plate Grounding and Electrode Centering. The ground loca-tion and the electrode (and consumable guide) position in the joint gap control both weld penetration uniformity into each plate being welded and weld symmetry with respect to faying edges. When a single ground was used, weld penetration into the grounded plate was enhanced (Figures 20 and 21). Similarly, in welds made with an off-centered electrode, more penetration occurred into the plate closer to the electrode (Figures 20 and 22). Grounding of both plates and positioning the electrode with-in 1/16 inch from the geometric center of the joint gap provided a sym-metrical weld with equal penetration into both of the plates (Figure 23). Hence, the plate grounding and the electrode centering are important in providing the weld consistency.

DebRoy et al.,[20] through a mathematical model, have shown that the intensity of heat generation near the electrode could be up to an order of magnitude greater than the heat generated near the slag/plate

interface. Thus, greater penetration should have occurred on the side closer to the electrode, due to a higher heat generation in its vicinity. The ground location may have an influence on the current distribution in the slag pool, thus affecting the weld penetration.

Since the heat generation is concentrated in the vicinity of the wire electrode, the resulting weld structure will depend on the electrode position. It will be symmetrical about the electrode instead of the geometrical center of the joint. The complex, directional microstructure of ES welds results in anisotropic weld mechanical properties. Thus, variations in the electrode position along the weld length will result in weld structure and mechanical properties variations along the length of the weld. A bend or "cast" in the wire electrode will also direct it towards one of the plate edges causing weld asymmetry. These factors are very critical because they could cause lack of penetration defects, variation in the HAZ size and structure, non-uniform weld penetration, slag entrapment and failure to achieve steady state process conditions.

These factors become more critical with increasing weld length. Longer guide tubes have less stiffness and, hence, are harder to position during welding. Temporary wooden wedges can be used in these cases to prevent guide tube movement during the process. A wing guide tube design can also be used to avoid this problem. Use of such a guide tube along with ceramic insulators in a narrow gap joint spacing (3/4") does not leave any room for the electrode misalignment, thus eliminating the error in electrode positioning. The bend or the "cast" in the wire can be

eliminated using a wire straightener at a location immediately ahead of the wire feed rollers.

4.1.2. Slag Level Maintenance. Heat generation during the ESW process occurs mainly in the slag pool. Hence, the slag level used during welding and its maintenance are critical in establishing the steady state welding condition. A certain slag level is necessary to maintain the resistance heat generation mode. A shallow slag pool leads to severe arcing, a deviation from resistance heating. In addition, heat is not generated uniformly in the entire slag pool. The bulk of the heat is generated in a limited slag pool region surrounding the electrode tip.

An excessive slag depth (3 inches and above) delays the process stabilization (achievement of an equilibrium weld width and consistent weld microstructure produced with minimum current and voltage fluctuations). A greater slag volume must be heated first. In addition, the primary heat generation site is moved away from the slag/molten pool interface leading to a greater heat loss through faying edges and effectively delaying the process stabilization. As a result, longer starting sumps would be required.

On the other hand, a shallow slag pool leads to severe arcing. The mode of heat generation changes from resistance to arc, which reduces the heat generation efficiency and alters the temperature distribution in the slag pool as well as the solidifying metal pool. Microstructural

variations resulted under such conditions. Very shallow slag levels resulted in regions of coarse grain structure as shown in Figure 78.

Although the slag level used and its maintenance during welding play a critical role, they have been taken very lightly in practice. The slag pool is not readily accessible when permanent cooling shoes are used. The technique used in practice for slag level measurement, that of probing the molten pool with a wire, requires a sliding shoe arrangement to provide continuous access to the pool. Further, the differentiation between the slag and the metal pool depth measured by this technique is ambiguous. Yet, currently, this is the most widely used technique. The current vs. slag level relationship established in this investigation provides a better and simpler technique for the slag level measurement.

The ammeter provided in the welding power supply indicates an average current reading. An oscilloscope, on the other hand, reveals the microscopic current fluctuations on a millisecond time scale.

In welds made with an optimum slag depth (1-1/2 to 2 inches) using a medium current and voltage, the electrode extended a moderate distance into the slag pool, with the heat generated primarily in the central region of the slag pool. Under these circumstances, fluctuations in the current and voltage were negligible (Figure 25a). With slag depletion, the electrode reached the proximity of the metal pool. As a result, occasional arcing occurred causing intermittent current spikes of medium amplitude (Figure 25b). When the slag level was too shallow, the

16" from start

Excessive arcing

Slag depletion

Flux addition

Excessive arcing

Slag depletion

3" from start
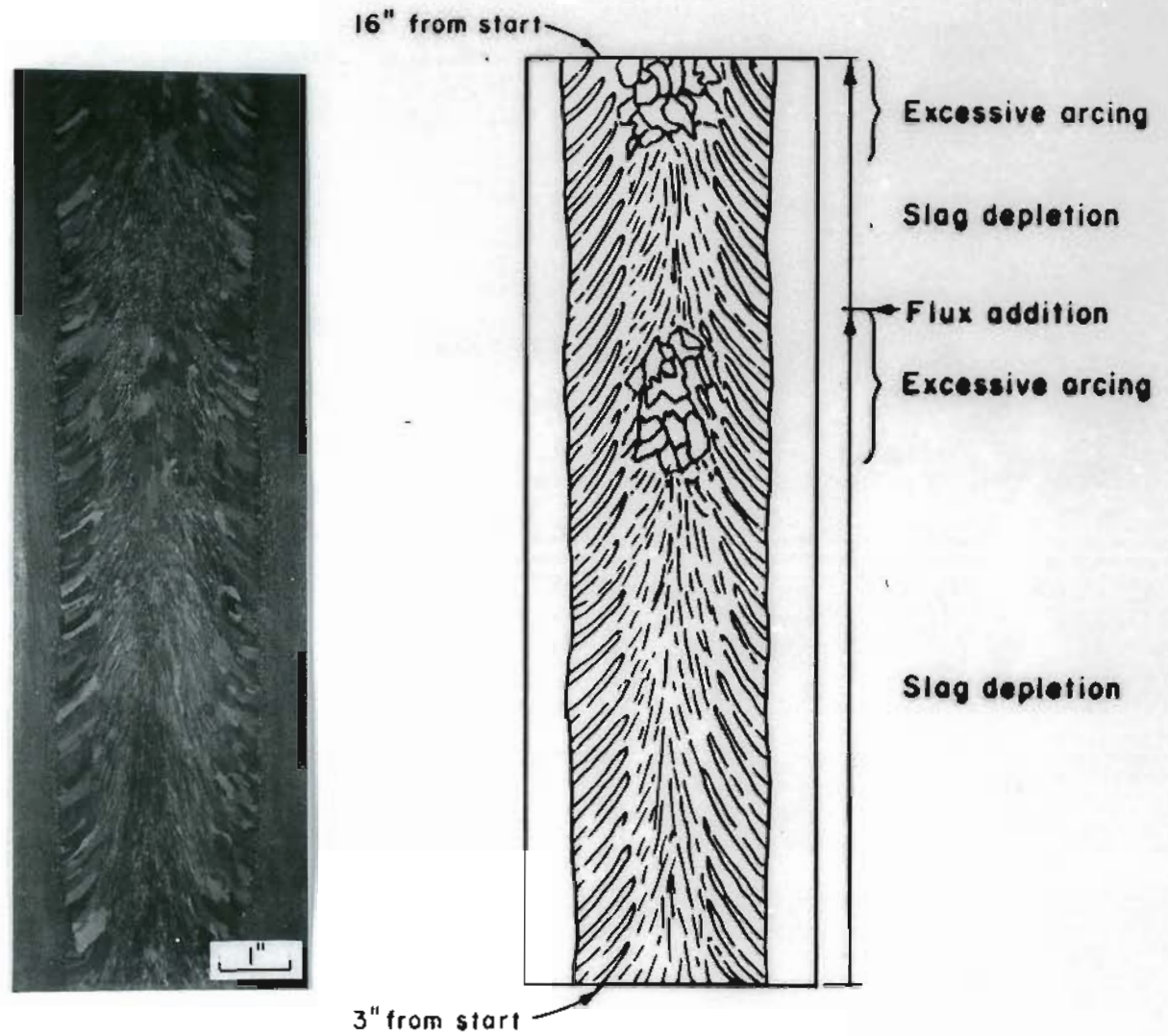
Figure 78. ES WELD MACROSTRUCTURE ILLUSTRATING THE EFFECT OF SLAG DEPLETION. VERY SHALLOW SLAG LEVELS CAUSED GRAIN COARSENING AT THE WCL.

resistance mode of heat generation changed to an arc mode. The welding process became erratic and the slag volume was insufficient to provide a dynamic thermal equilibrium. The electrode extended to the vicinity of the molten metal pool causing severe arcing and more frequent, large amplitude current spikes (Figure 25c).

The current vs. slag level relationship monitored using an oscilloscope provides an excellent tool for indirect slag level measurement. This is especially useful on occasions when extreme slag loss occurs from a misfit between cooling shoes and welding plates. Optimum slag level can be reestablished by adding powder flux till the current level reaches the stage shown in Figure 25a. But, this technique is applicable only for slag levels ranging from a very shallow to an optimum level (1-1/2 to 2 inches). The current distribution cannot differentiate between an optimum and an excessive slag depth.

The continuous loss of the slag freezing between the cooling shoes and the solidifying metal necessitates flux additions during welding. The quantity and the frequency of these additions are critical since they affect the thermal equilibrium established during the process and potentially influence weld characteristics. A marked variation in the current was observed immediately after a bulk flux addition (Figure 79). In present practice, the welder makes these additions manually using the arc noise as an indicator for slag depletion, This investigation clearly indicates the arcing stage to be an advanced case of slag depletion which would require an addition of a major quantity of powder flux to
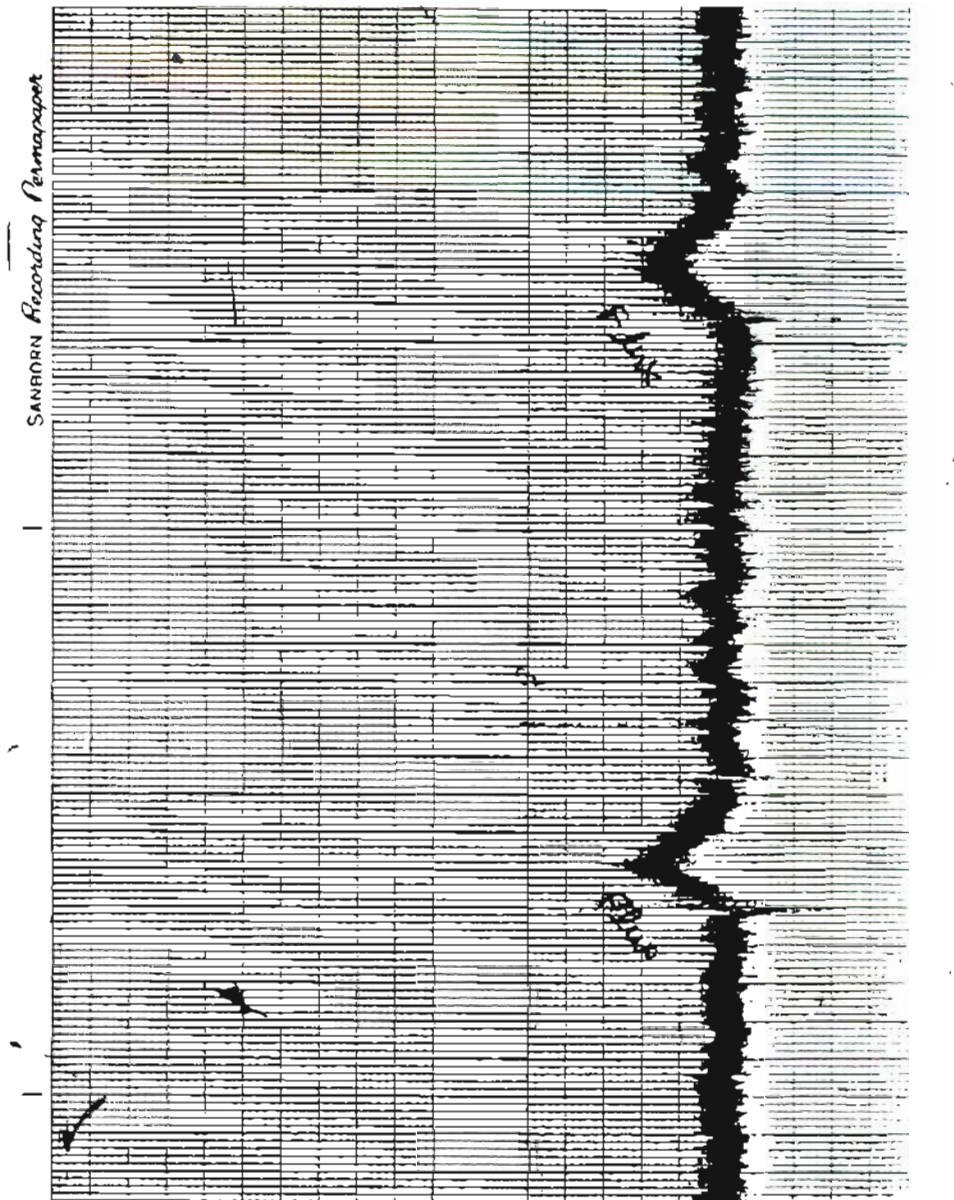
Figure 79.   EFFECT OF BULK FLUX ADDITION ON WELDING CURRENT.

re-establish the optimum slag depth (approximately 75 grams of flux for 2" thick plate weld with a 1-1/4" joint gap.) That would severely affect the dynamic thermal equilibrium established during the welding process. This problem can be avoided using a continuous flux feeding device. A TAPCO metal powder addition device was used in this investigation for that purpose. A continuous flux addition made at a rate of 4 grams/minute compensated for slag losses and helped maintain a constant slag level throughout the process without affecting its dynamic thermal equilibrium. The current and voltage fluctuations were minimal. Resultant welds were consistent in their width and microstructures. Furthermore, after initiation with a pre-measured amount of flux to achieve an optimum starting slag depth, the use of a continuous flux feeder largely eliminates the operator influence on weld characteristics.

4.1.3. Welding Speed (Energy Input, Guide Tube Geometry, and Joint Spacing. ES welding of a 2-inch thick plate under standard conditions uses a large specific heat input of 89.3 KJ/mm (Table XII) and this heat input combined with slow cooling results in a coarse grained weld metal and HAZ microstructures. Decreasing the specific heat input would be expected to improve the weldment microstructure and mechanical properties and can be achieved either by decreasing the welding voltage or by increasing the welding speed. The latter can be done either by increasing the electrode feed rate or by decreasing the joint spacing.

The welding voltage has a strong influence on weld penetration. At a relatively high voltage for a given current the electrode extends only

Table XII.

SPECIFIC HEAT INPUT FOR VARIOUS ES WELDS

#	Weld ID	Guide Type	Gap in.	Current A	Volts V	Weld Speed mm/sec.	Specific Weld Heat Input KJ/mm.
1	B23	Cylindrical	1-1/4	600	42	0.282	89.3
2	B21	Cylindrical	3/4	600	42	0.363	69.5
3	B50	Wing guide	1-1/4	600	36	0.236	91.4
4	B51	Wing guide	1-1/4	700	36	0.318	79.4
5	B52	Wing guide	3/4	600	40	0.339	70.9
6	B88	Wing guide	3/4	1000	40	0.847	47.2

a short distance into the slag pool causing a wide, shallow molten metal pool with a high form factor.[13] On the other hand, at a relatively low voltage for the same current the electrode extends nearly to the bottom of the slag pool resulting in a narrow, deep molten metal pool having a low form factor. According to Solari et al.,[9] in welds made with relatively high voltages, the slag pool penetrates deep into the base metal forming a pendulant overhang on which a layer of molten base metal adheres by surface tension (Figure 80). Increasing the pool depth by decreasing the voltage decreases the adhering base metal layer thickness due to more effective convective mixing and eliminates the pendulant overhang. As a result, when the voltage fluctuates from a high to a low value, the slag will be trapped in the region X shown in Figure 80 causing weld defects along fusion boundaries (Figure 27). The same is responsible for weld defects observed at restart locations of ES welds.

In addition to microscopic current fluctuations associated with slag level variations, periodic large scale current fluctuations were also observed in standard welds made with the cylindrical bare metal guide tube. These fluctuations arose from a periodic guide tube melt off that occurred during welding and resulted in changes in the temperature gradient in the solidifying metal pool and solidification rate leading to solute band formations.[7] But, those solute bands did not inhibit either the growth or the orientation of the CCG's (Figure 26). Yet, care must be exercised while welding with large weld metal alloy additions to prevent severe segregation and microcrack formation along solute bands.
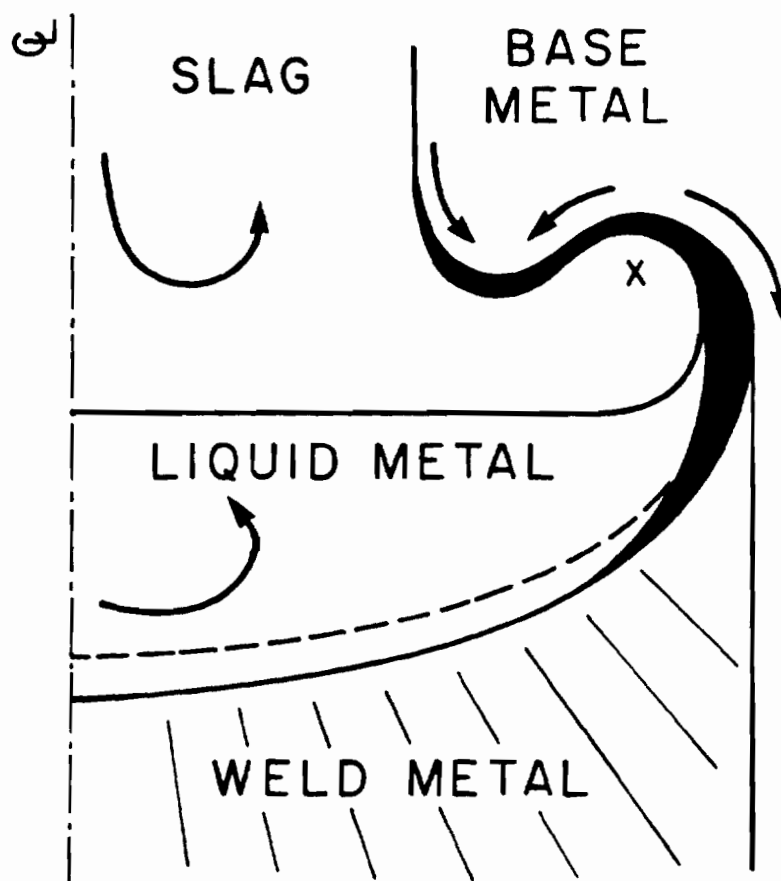
Figure 80. SCHEMATIC REPRESENTATION OF WELD PENETRATION PATTERN
IN ESW (SOLARI ET AL[9]).

When a constant potential dc power source is used in ES welding, the electrode feed rate and the welding current are interdependent. But the rise in the electrode feed rate is faster than the rise in the current. As a result, the welding current and the electrode feed rate should be considered individually when studying their effects on weld characteristics. The joint spacing and the guide tube design have also been shown in this investigation to influence the electrode feed rate. Hence, for the process optimization, a thorough knowledge of relationships between welding current, voltage, electrode feed rate, guide tube geometry, and joint spacing and the influence of these variables on weld characteristics is necessary.

As previously discussed, the voltage strongly influences the weld penetration. Welding at lower voltages (less than 42 volts) using a cylindrical guide tube in a rectangular joint gap is ruled out due to lack of penetration on plate edges. In addition, welding with higher electrode feed rates (and currents) is limited by the guide tube resistance heating. A winged guide tube with a rectangular cross section was used in this investigation and aids in solving these problems. The winged guide tube design provides a higher guide to gap cross sectional area ratio. The larger electrode cross section enables the guide to carry a larger proportion of current in comparison to the standard cylindrical guide tube. This feature along with the rectangular cross section of the winged guide tube provides an even distribution of the heat across the plate thickness enabling welding at lower voltages with complete edge fusion. The larger electrode cross sectional area also provides a higher current carrying

capacity and, hence, can be used to weld at high current levels. The winged guide tube appeared to be in continuous contact with the slag pool during welding. But direct measurement of its extension into the slag was not possible.

The current vs. wire feed rate relationships for various guide tube designs and joint spacings are shown in Figure 30. For any given current value, narrow gap (3/4") ES welds utilized lower wire feed rates compared to standard gap (1-1/4") ES welds, irrespective of the guide tube design. The shorter distance between the electrode and faying edges in narrow gap welds reduces the resistance for the current passage. As a result, at a given current, less resistance heat (I^2R) is available to melt the electrode causing reduction in the electrode (wire) feed rate.

In welds made with identical joint spacing, at any given current, the winged guide tube design used lower wire feed rates compared to cylindrical guide tube design. Winged guide tubes carry larger proportion of the current compared to cylindrical guide tubes. As a result, heat available to melt the electrode is reduced causing a reduction in electrode feed rate.

At any given voltage and current, narrow gap welds possessed a higher percent base metal dilution in comparison to standard gap welds irrespective of the guide tube design used (Figure 28). In narrow gap welds, faying edges are closer to the heat concentration region surrounding the electrode tip which results in melting of a higher volume of base metal. With all other parameters fixed, a linear inverse relationship

between base metal dilution and joint spacing was observed in this investigation (Figure 81), whereas the joint spacing had minimal influence on the weld form factor, Figure 82. Major variables controlling the welds form factor are welding current and voltage.

The standard cylindrical guide tube required a minimum voltage of 42 volts to achieve complete edge fusion, whereas the wing guide tube enabled welding successfully at voltages as low as 34 volts and 36 volts for joint spacings 1-1/4" and 3/4", respectively. These voltage limits were derived for welds made at 500 amperes welding current. An increase in the current value would raise these voltage limits due to an accompanying increase in the welding speed.

For a given joint spacing, current and voltage, winged guide tube ES welds possessed higher base metal dilution in comparison to standard cylindrical guide tube ES welds. Two major reasons for this feature are the decrease in electrode feed rate (Figure 30) and the even heat distribution in the slag pool while using winged guide tubes. The former factor leads to a reduction in welding speed and an increase in specific heat input for winged guide tube ES welds. Thus, at any given voltage and current, narrow gap/winged guide tube ES welds possessed maximum base metal dilution while standard gap/cylindrical guide tube ES welds possessed the minimum.

The welding current had a minimum influence on the base metal dilution as shown in Figure 29. An increase in the welding current is always associated with an increase in the electrode feed rate and the welding
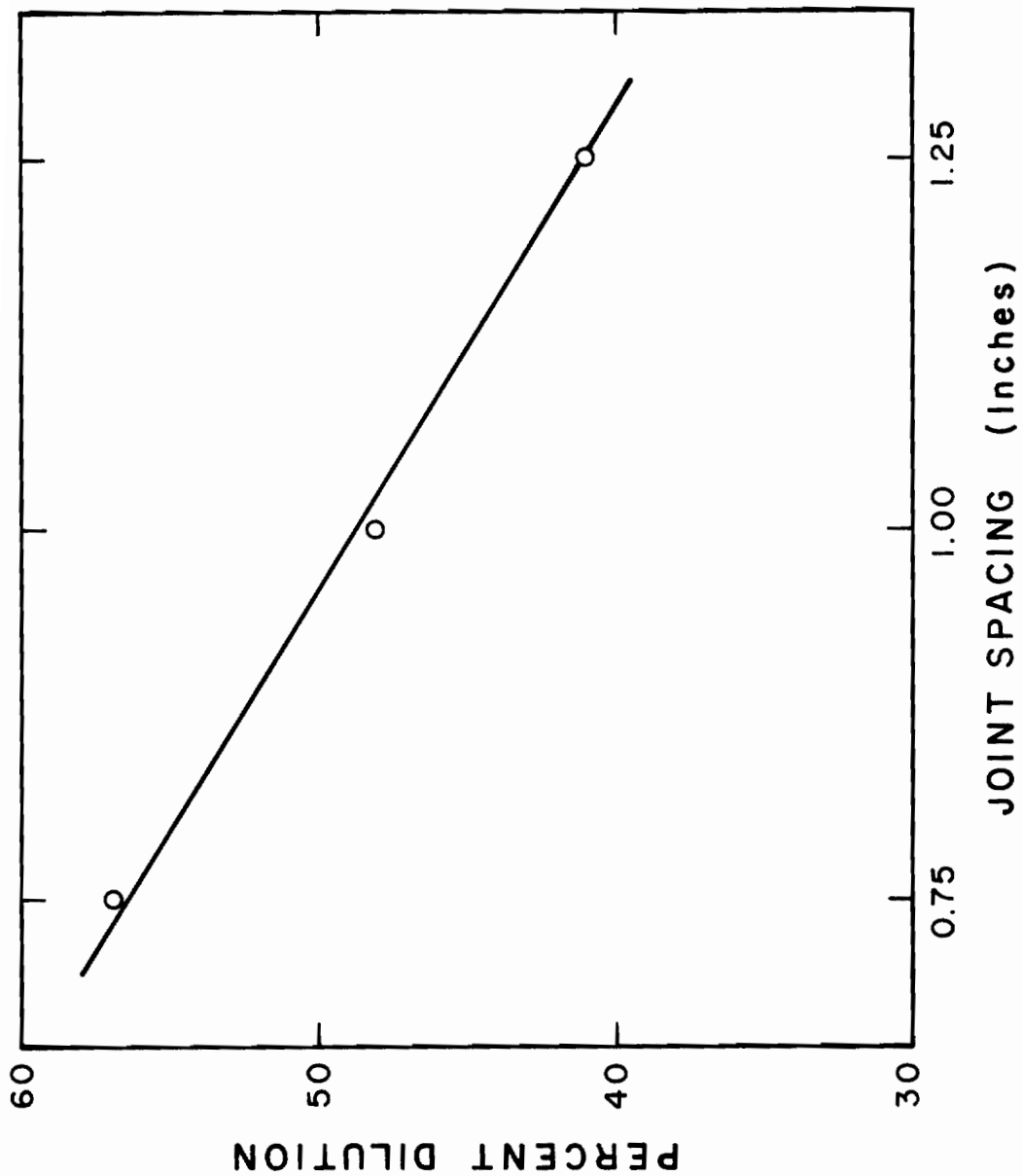
Figure 81. EFFECT OF JOINT SPACING ON BASE METAL DILUTION.
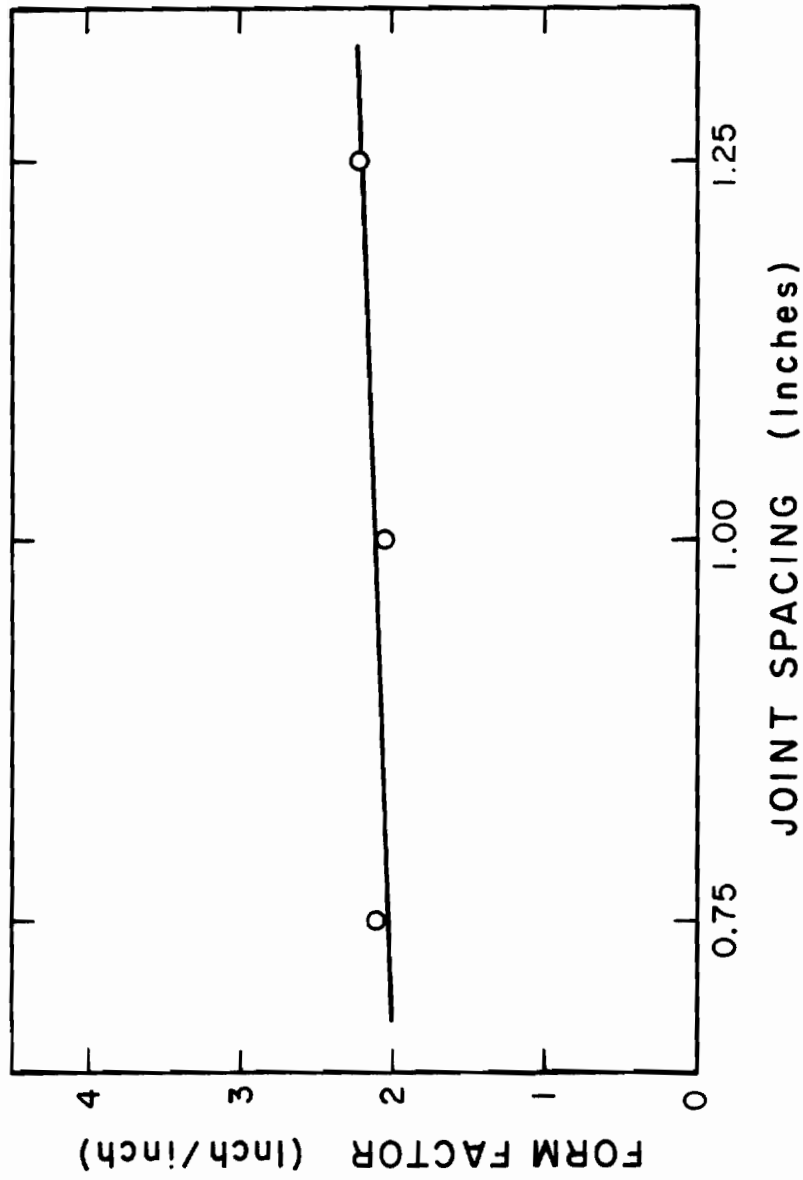
Figure 82. EFFECT OF JOINT SPACING ON WELD FORM FACTOR.

speed. As a result, variations in weld penetration is minimal in spite of changes in the form factor.

The current vs. electrode feed rate relationships determined in this investigation showed a decrease in the electrode feed rate with the use of narrow joint spacings as well as winged guide tubes for any given current setting. Filler melting efficiency in ESW can be defined as the volume of filler plus guide tube melted per minute. A thorough knowledge of relationships between filler melting efficiency and current (Figure 83) and welding speed and current (Figure 84) is necessary for selecting optimum operating conditions and improving weld properties and microstructures using narrow joint spacing and winged guide tube design. The decreased filler melting efficiency with decreased joint spacing was more pronounced in winged guide ES welds than in cylindrical guide ES welds (Figure 83). This is due to the relative drop in electrode feed rate in winged guide ES welds, Figure 30. However, welding speed vs. current relationships (Figure 84) indicates higher welding speeds at any given current for narrow gap welds made using either guide tube designs due to the reduced volume of filler metal required to fill the narrow joint gap.

For a given joint spacing and current setting, winged guide welds were made much slower than cylindrical guide welds due to reduction in electrode feed rate with winged guides. This led to increased specific heat input for winged guide welds compared to standard guide welds in spite of a considerable reduction in welding voltage, Table XII. To off-set these factors, higher currents must be used with the winged guide tube.
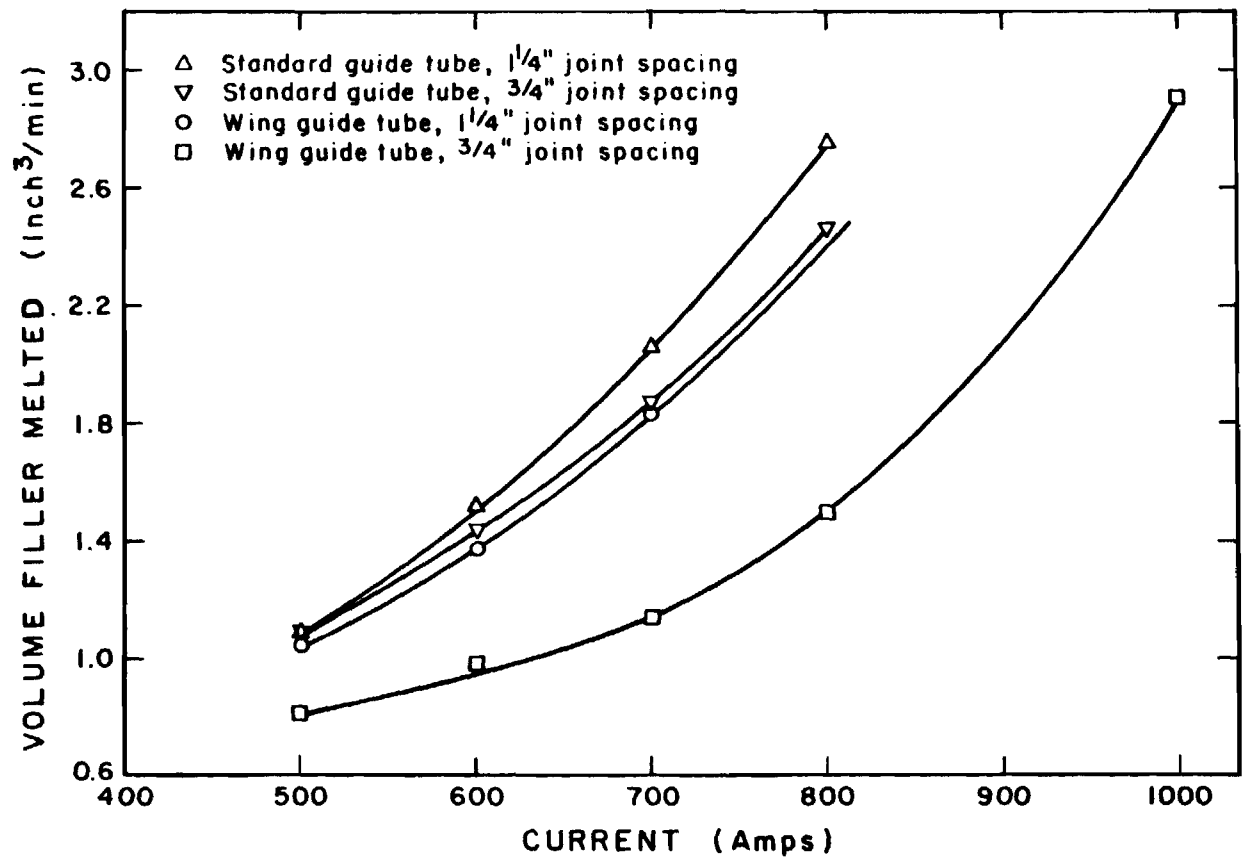
Figure 83. RELATIONSHIP BETWEEN WELDING CURRENT AND VOLUME FILLER MELTED/MINUTE, FOR VARIOUS GUIDE TUBE GEOMETRIES AND JOINT SPACINGS IN ESW.
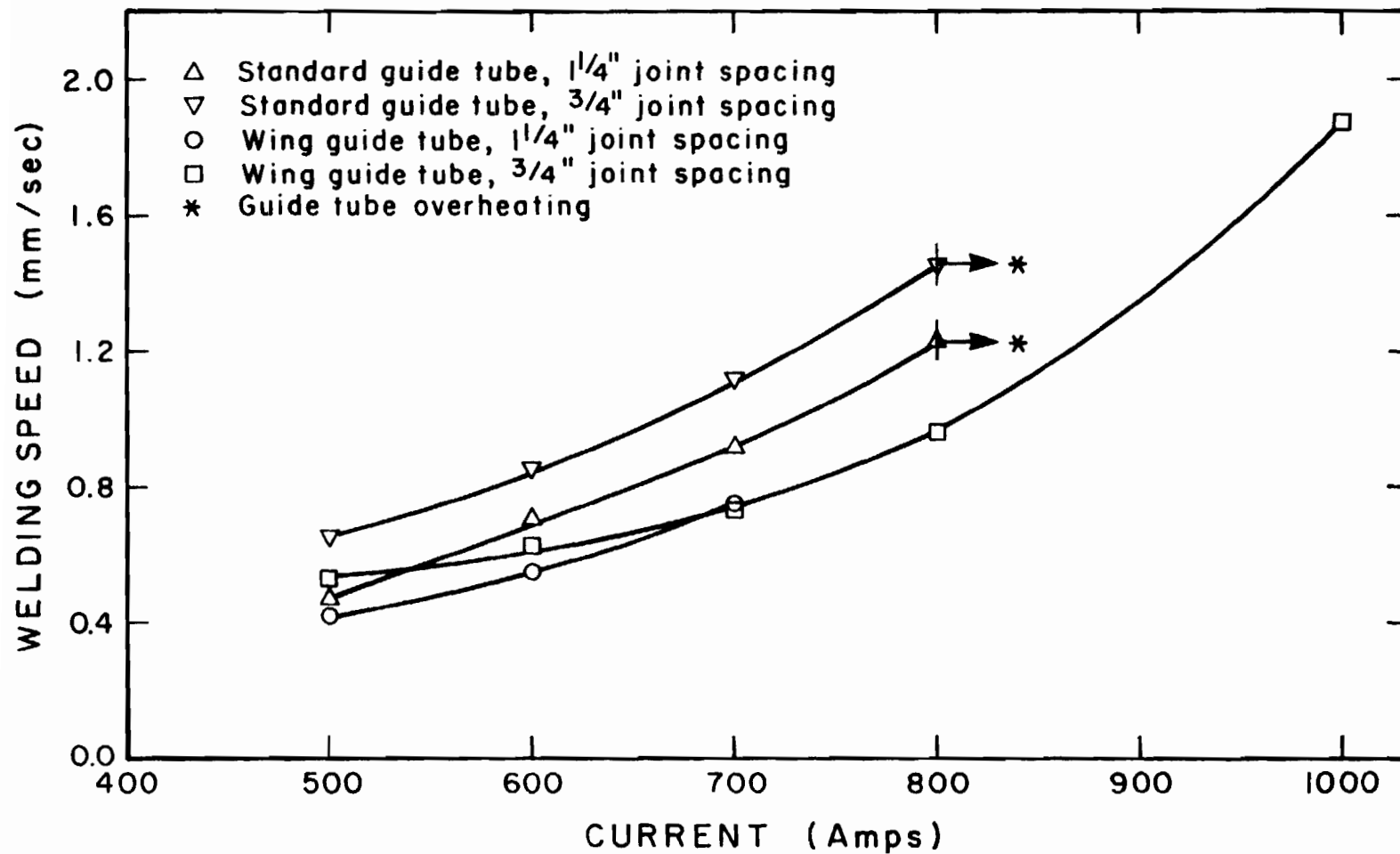
Figure 84. RELATIONSHIP BETWEEN WELDING CURRENT AND WELDING SPEED FOR VARIOUS GUIDE
TUBE GEOMETRIES AND JOINT SPACINGS IN ESW.

In fact, the larger cross section of the winged guide tube enables the use of high welding currents without the guide tube overheating. In addition, the even heat distribution across the plate thickness achieved with the winged guide design eliminates penetration difficulties normally associated with high speed welds.

The main concern in increasing welding current is the accompanying decrease in form factor since low form factor leads to grains meeting end on at weld centerline causing severe segregation and centerline solidification cracking. Figure 85 illustrates the relationships between the weld form factor and current. Nolan et al.[14] have found, under similar circumstances, the form factor to asymptotically approach a value of 1.2 at high currents rather than falling continuously. A similar trend was also observed in this investigation. The form factor for the winged guide weld made at 40 volts and 1000 amps in a 3/4 inch joint spacing was 1.3. No centerline cracking was observed in spite of the high current and welding speed used.

The high current/narrow gap/winged guide tube welds produced under conditions mentioned above utilized a specific heat input of 47.2 KJ/mm. This was about 50% of that required for standard welds (Table XII). The welding time was also reduced to 12 minutes which is 1/3 of that required for the standard procedure (1-1/4" joint gap, cylindrical guide tube, 42 volts and 600 Amps). The fusion zone width of the high current/narrow gap/winged guide ES weld was much smaller (1.85 inches) in comparison to that of the standard weld (2.81 inches). The reduction in specific heat
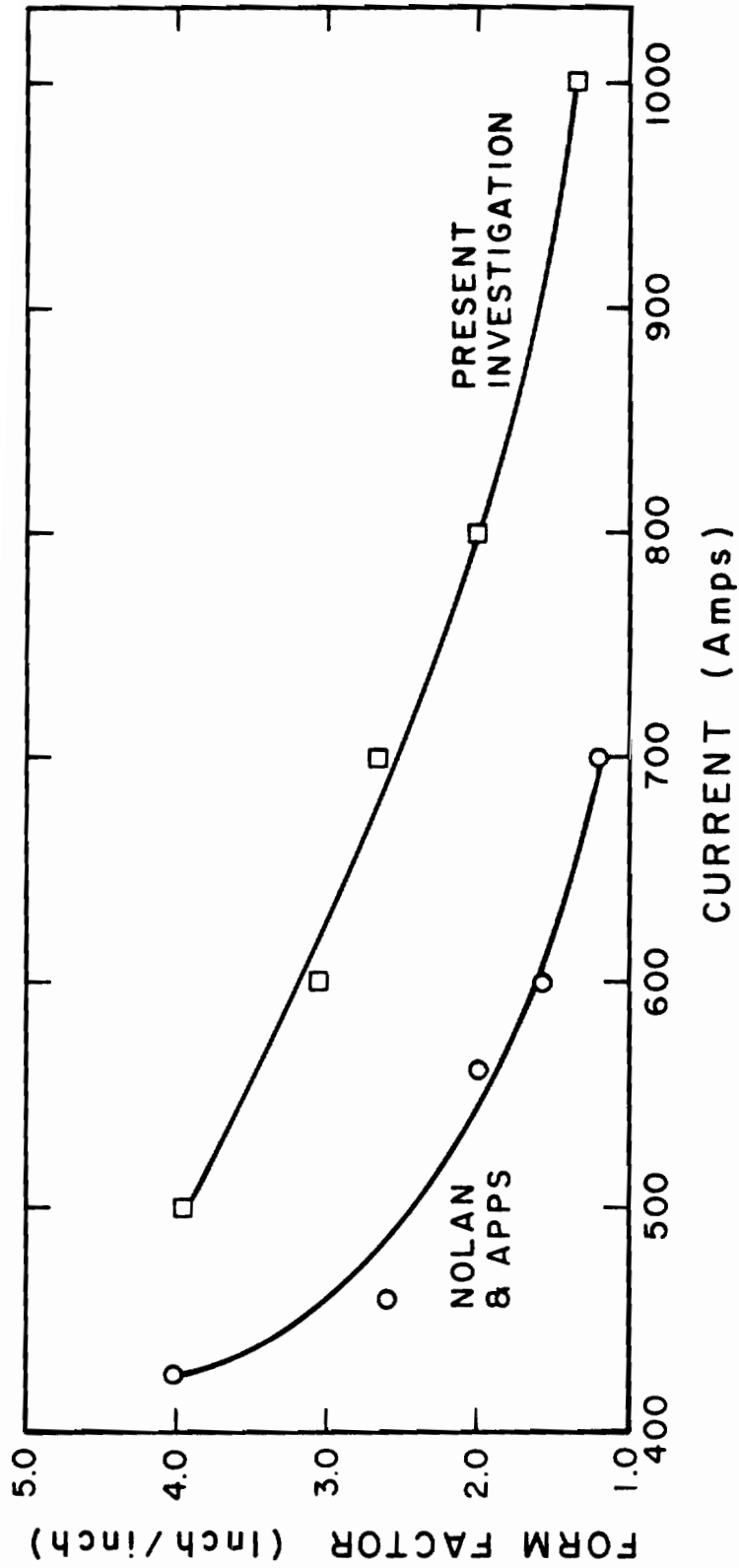
Figure 85. RELATIONSHIP BETWEEN WELDING CURRENT AND WELD FORM FACTOR IN ESW.

input and increase in welding speed in high current/narrow gap/winged guide welds provide an increase in weld cooling rate and improvements in weld microstructure and mechanical properties. These improvements will be discussed in a later section.

Dimensions of CCGs of high current/narrow gap/winged guide ES welds and standard ES welds were comparable but the inclination of these coarse grains to the weld axis was less acute in former welds than in latter welds due to change in the weld form factor, Figure 31. Weld center microstructures (Figures 32a-c) indicated significant refinement for high current/narrow gap/winged guide welds, and the proeutectoid ferrite films bordering grain boundaries in those welds were well dispersed as opposed to continuous films present in standard welds.

A marked reduction in the coarse grain HAZ width was achieved in high current/narrow gap/winged guide ES welds. The HAZ width was about half of that of standard welds, Figure 33, and can be explained by analyzing temperature profiles determined for these welds, Figures 76a through 77c. Those temperature profiles indicated peak temperatures and dwell times over the transformation temperature (approximately 1300°F) obtained at various locations in the base metal. Figure 86 illustrates peak temperature vs. the distance from the weld fusion line relationships obtained from the middle set of thermocouples for either welds. A general decrease in the peak temperature (about 100°F) experienced at any given location in the base metal adjacent to the fusion line was observed in high current/narrow gap/winged guide welds compared to standard welds.
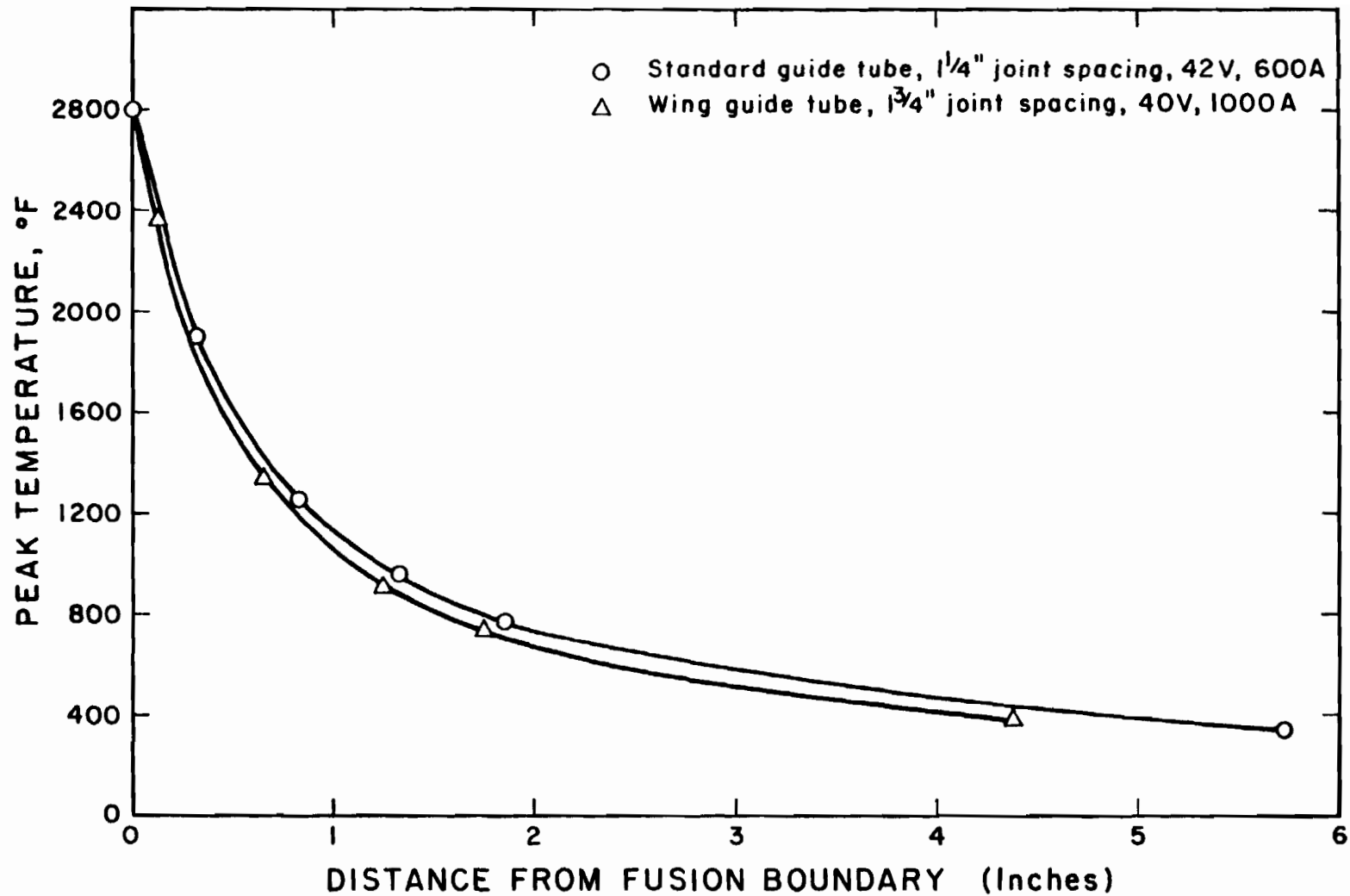
Figure 86. PEAK TEMPERATURE DISTRIBUTION IN BASE PLATE ADJACENT TO THE FUSION LINE OF STANDARD (CYLINDRICAL GUIDE, 1-1/4" GAP, 42 VOLTS) AND HIGH CURRENT/NARROW GAP/WINGED GUIDE (3/4" GAP, 40 VOLTS, 1000 AMPS) ES WELDS.

This decrease can be attributed to the reduction in specific heat input, higher welding speed and the reduction in the volume of the solidifying weld metal. The cooling rate measured at 1300°F at the location of thermocouple #6 in this set was 3.1°F/sec. for high current/narrow gap/ winged guide welds vs. 1.81°F/sec. for standard welds due to similar reasons. In addition, the base metal 0.13 inch away from fusion line in the high current/narrow gap/winged guide weld dwelled above the transformation temperature (1300°F) for about 200 seconds while that in the standard weld stayed above this temperature for about 370 seconds. The decrease in the peak temperature, increase in the weld cooling rate and reduction in dwell time above the transformation temperature led to the reduced HAZ width in high current/narrow gap/winged guide welds. However, the first few grains of the HAZ adjacent to the fusion line in those welds were still coarse causing poor HAZ properties. The peak temperatures experienced in that region were high enough to cause the undesirable grain growth and solid state transformation.

The winged guide tube design can be utilized for welding plates, several inches in thickness, with proper selection of the guide tube cross section area and the number of electrodes. Relationships between the filler melting efficiency and current, and welding speed and current should be established for the selected guide tube geometry and joint gap in order to select optimum welding conditions. Winged guide tubes also eliminated the need for electrode oscillation during welding and minimized the error in electrode positioning.

4.2. As Welded Grain Refinement

The results of this investigation have clearly shown that finer grains can be achieved in as-welded ES welds. Weld pool vibration was selected as a primary method to refine grains based upon prior studies in castings.[43-52] The grain refinement was achieved with or without vibration. However, both successful techniques required shielding of the consumable guide assembly with either mullite or quartz shroud. The guide tube shielding technique provided a continuous contact between the guide tube and slag pool by extending the guide deep into the slag and preventing the guide tube melt off phenomenon, which normally occurs with the use of a bare metal guide tube.[73]

It is proposed that the ceramic shroud resulted in grain refinement because the guide tube insulation provided a sharp thermal gradient between the weld centerline and the unmelted base plate (and shoes). In addition, the shroud extended the guide deeper into the slag while the growth rate remained essentially unchanged. The effects of electrode position on the temperature distribution in the slag pool have been verified by Deb Roy et al.[20] and Jones et al.[13] To maintain such an abnormally high gradient during welding, additional voltage (by about 15%) was required to preserve side wall fusion. Ultimately, the sharp thermal gradient provided an intense forced convective field capable of permitting extensive crystal multiplication by fragmentation or remelting of previously solidified material extending ahead of the solid/liquid interface. The quartz shrouded welds always resulted in dynamically stimulated grain

refinement. However, because the degree of convection produced by the mullite shrouding was insufficient, additional dynamic stimulation through vibration had to be provided to attain the grain refining mode.

In quartz shielded consumable guide tube welds, supplemental mechanical vibrations were not required to achieve as-welded grain refinement. Sufficiently intense convective fields were established by the quartz shroud as observed visually by the extremely turbulent activity of the slag pool.

Violent stirring action was not observed while using a mullite shrouded guide tube primarily due to the interaction between the mullite and the slag. A large volume of mullite was necessary to effectively insulate the guide tube in comparison to the quartz and the extensive contamination of the slag via mullite resulted in a highly viscous cooler slag than normal. Hence, supplemental mechanical vibration was necessary in order to achieve the stirring motion in the solidifying metal pool. Furthermore, the delayed effect of mullite upon weld grain size suggests that the lower slag temperatures due to the addition of mullite to the slag bath may play an integral role in the subsequent grain refinement mechanism.

ES welds made with either the vibration of the entire plate fixture (table top) or an independently vibrated quartz probe inserted into the slag pool exhibited no grain refinement. The plate fixture was vibrated at two natural resonance frequencies, 35 and 58 Hz, providing low and high amplitude vibration during welding. The quartz probe was vibrated

at 217 Hz using a pneumatic vibrator. The results of these two tech-
niques suggest that a simple agitation of slag and metal pools may not
be sufficient to bring forth as-welded grain refinement. A change in
the heat distribution achieved from the guide tube shielding is re-
quired, in addition to the stirring motion in the weld pool, to cause
grain refinement. Vibrational characteristics vary with the plate fix-
ture location on the vibration table,[74] in addition to amplitude varia-
tions along the plate length itself. Effects of these variables on weld
microstructures were not studied in this investigation, but are worth
exploring in the future.

The amount of the proeutectoid ferrite phase bordering grain boun-
daries was higher in quartz shrouded grain refined welds (Figure 41a-f).
This may be attributed to increased available nucleation sites along prior
austenite grain boundaries and the rise in the silicon content of the
weld metal. Generally, alloying with silicon is known to shift the criti-
cal transformation temperature (A_c) to higher values, and reduce the
austenite region at higher silicon concentrations.[75,76] Thus, the slight
increase in the silicon content of grain refined welds may have played
an integral role in increasing the proeutectoid ferrite phase.

Solute band formations found in standard welds were not observed in
grain refined welds. The intermittent contact between the slag bath and
the guide tube in standard welds leads to variations in solidification
rates, and solute concentrations ahead of the solid/liquid interface
causing solute band formation. The shrouded guide in the grain refined

weld is in continuous contact with the slag bath and the associated vigorous stirring motion in the slag and metal pools redistributes the segregating solute elements and prevents solute band formations.

ES welds made under severe restraint or with high weld pool velocity (low form factor) exhibit weld centerline cracking (Figure 87). The high impurity content of the weld metal solidifying last at the weld center and associated stresses are responsible for solidification hot cracking in the region. Again, the vigorous stirring action present in grain refined welds redistributes the segregating elements from the weld center, thus eliminating centerline cracking as shown in Figure 87.

4.3. Alloy Additions

Alloy additions to the ES weld fusion zone made either by welding alloy rods onto the consumable guide or by using alloyed filler wire provided excellent control of proeutectoid ferrite phase along grain boundaries as well as grain interior microstructure. The proeutectoid ferrite films normally present along grain boundaries were completely eliminated in the weld made with alloyed filler wire E (Cr-Mo additions). The weld HAZ consisted of a coarse, equiaxed grain structure with proeutectoid ferrite films along grain boundaries. The ferrite films terminated at the fusion boundary (Figure 46). The transmission electron microscopy of the fusion zone revealed a heavily dislocated, lath type ferrite structure with cementite present along the lath boundaries as well as lath interiors. Bee and Honeycombe[77,78] have classified a similar
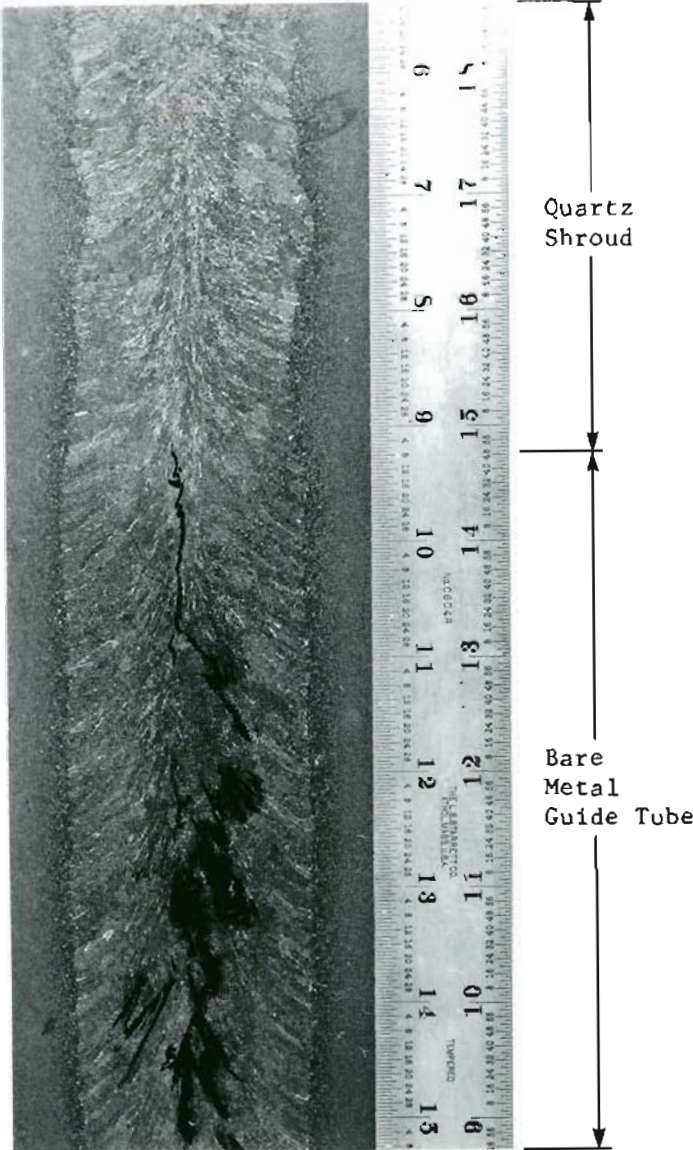
Figure 87.   TUBE WELD MACROSTRUCTURE ILLUSTRATING THE ABSENCE
OF CENTERLINE CRACKING WITH GRAIN REFINEMENT TECH-
NIQUE IN ES WELD MADE UNDER SEVERE RESTRAINT.

structure obtained in an Fe-10%Cr alloy transformed at 525°C as bainitic ferrite. The bainitic ferrite structure in alloyed ES welds is in contrast to the Widmanstatten-type acicular ferrite structure with carbide aggregates present in standard ES welds made using filler wire A. The extent of the coarse columnar zone in alloyed ES welds was reduced compared to standard ES welds. The presence of finely dispersed carbide precipitates in alloyed ES welds may have limited the extensive grain growth causing reduction in the CCG zone.

The higher weld metal alloy concentrations led to the increase in weld hardenability causing higher weld metal hardness and lower weld ductility. This effect was slightly reduced in high current/narrow gap/ winged guide ES welds made using filler wire E. Higher base metal dilution associated with these welds helped reducing the weld metal alloy concentrations. Yet, the bainitic ferrite structure and the proeutectoid ferrite control were maintained. Again, the extent of the CCG zone in these high current/narrow gap/winged guide ES welds were highly reduced. The finely dispersed carbides and the reduction in specific weld heat input may have played an integral role in controlling the grain growth.

On the other hand, ES welds made with alloyed filler wires B (A588), C (Si-Mn) and D (Mn-Mo) showed little improvement in microstructure. Their microstructures were comparable to that of a standard weld. The level of alloy addition accomplished using these wires were not sufficient to influence the solid state transformation during weld cool down.

The hardenability characteristics of molybdenum provided an excellent proeutectoid ferrite control in ES welds made using molybdenum rods welded

on to the consumable guide. This technique enabled the study of effects

of an individual alloy element upon fusion zone microstructures. In

addition, the minimum alloy concentration required for total proeutectoid

ferrite control can also be established by this method. For example,

in this investigation, about 1 wt.% Mo addition was determined to be

necessary for complete elimination of the proeutectoid ferrite phase in

the weld. However, this technique caused severe alloy segregation along

solute band formations. The intermittent contact between the guide tube

and the slag bath during welding causes discontinuous alloy additions to

the weld metal and severe solute segregation resulting in non-homogeneous

weld microstructures.

4.4. Charpy V Notch Impact Toughness

The anisotropic grain orientation and the complex microstructure of

ES welds render the geometric relationship between the specimen and the

microstructure very critical. For example, when the notch root was placed

close to the proeutectoid ferrite film, in the CCG zone of an ES weld,

the crack propagated along the film to a certain extent before failing

through the transgranular mode, Figure 72. This fracture behavior re-

sulted in lower impact toughness values for the zone. On the other hand,

when the notch root laid inside a CCG, the total failure was by the trans-

granular mode posting higher toughness values. This factor is responsible

for the wide scatter observed in CCG zone toughness properties of ES welds.

In addition, the ferrite morphology also played an important role in WCL

impact toughness properties. Extensive segregation occurred in this region since it was the last to solidify, especially in welds with high impurity contents where preferential segregation to the grain boundaries make them highly vulnerable to brittle crack propagation (Figure 75). Again, notch placement with reference to these axially-oriented continuous proeutectoid ferrite films caused wide scatter in WCL impact toughness values.

American Welding Society structural code D1.1[79] requires ES weld toughness evaluation at quarter-thickness locations for procedure qualification. Whereas, several investigators[4,6,36] have reported least WCL toughness values for samples taken at mid-thickness locations, Venkataramiah[36] has suggested that severe segregation at the weld center could induce the toughness variation with the plate thickness. Culp[4] has predicted the presence of either a CCG structure or a mixture of CCG and TCG structures in the fracture plane to be responsible for the increased weld toughness of quarter-thickness specimens. In spite of a complete TCG structure in the region of crack propagation of both mid-thickness and quarter-thickness specimens in this investigation, similar WCL toughness variations with the plate thickness were still observed. The TCG orientation with respect to the fracture plane can also significantly influence the weld center toughness. Mid-thickness specimens having these grains oriented parallel to the fracture plane caused an intergranular fracture mode. Quarter-thickness specimens having these TCGs inclined to the fracture plane caused a certain percentage of

transgranular fracture and an improvement in toughness. Hence, the grain orientation, impurity segregation and microstructural variations should be responsible for the variations in toughness with respect to the plate thickness. The standard weld prepared in this investigation using wire A would have met the code requirements in spite of poor toughness properties at mid-thickness locations. Therefore, in order to determine the least toughness achieved in ES welds, CVN specimens were taken from mid-thickness locations for all welds made in this investigation.

All ES welds made using wire A, with the exception of the grain refined weld, showed comparable scatter in the CCG zone toughness values, Figure 88. Reasons for the scatter have been discussed earlier. The increased scatter in grain refined weld toughness values could have been due to differences in microstructures. The grain refined weld had finer grain size and a larger amount of proeutectoid ferrite. On the other hand, WCL toughness data showed limited scatter for grain refined and narrow gap ES welds. The vigorous stirring action involved with the grain refinement technique reduced segregation at the WCL, and the refined WCL microstructure of high current/narrow gap/winged guide ES welds could have been responsible for the limited toughness scatter. Severe segregation found in alloy welds made using molybdenum rods welded onto the guide tube would be expected to cause wide variations in toughness. But, the scatter in toughness data was reduced considerably for both zones (Figure 89). This might have been due to the proeutectoid ferrite control and the improvement in microstructure (bainitic ferrite structure) achieved in
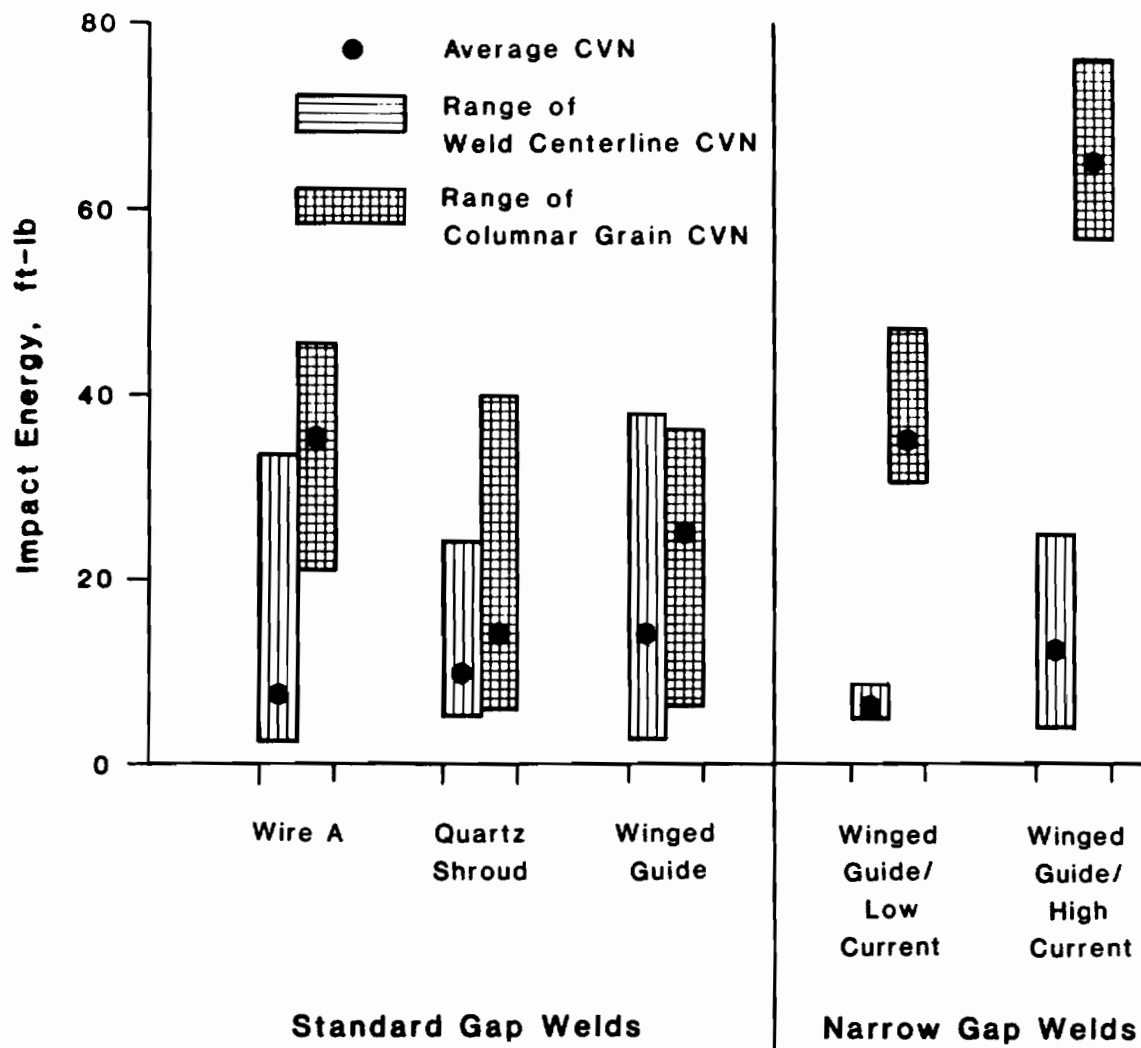
Figure 88. WCL AND CCG ZONE 0°F CVN TOUGHNESS DATA FOR ES WELDS MADE USING WIRE A.
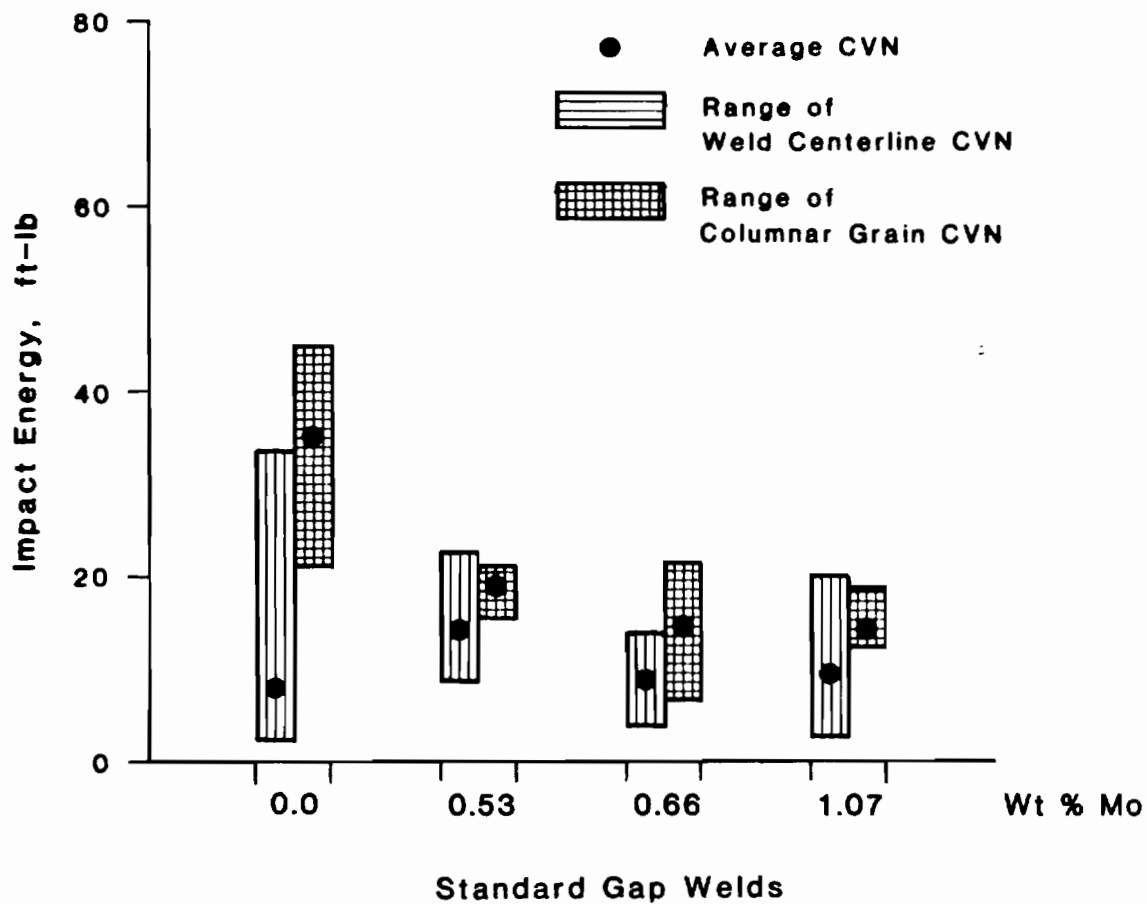
Figure 89. WCL AND CCG ZONE 0°F CVN TOUGHNESS DATA FOR ES WELDS
MADE WITH ELEMENTAL MOLYBDENUM ADDITIONS. MOLYBDENUM
RODS WERE WELDED ON TO THE CONSUMABLE GUIDE TUBE.

these welds. Similar results were also achieved in welds made using
alloyed filler wire D and E (Figure 90).

The HAZ toughness values for various welds made in this investiga-
tion ranged between 5 and 30 ft.lbs. (Figure 91). Process conditions,
such as welding speed, guide tube geometry and joint spacing, altered
the temperature distribution in the base plate, hence influencing the HAZ
size. Increasing welding speed decreased the HAZ width. Therefore,
location of the notch at a fixed distance from the fusion line for all
ES welds would not always place the notch in the coarse grained HAZ.
The narrow width of the HAZ makes the desired notch placement difficult.
Further, the curved nature of the HAZ makes it highly improbable, if not
impossible, to have the entire notch length in the zone. These factors
might have been responsible for the scatter in HAZ toughness properties.
Benter et al.[6] has suggested calculating the average toughness by omitting
high and low values to accommodate the general scatter in toughness prop-
erties. This method has been used in this investigation.

The average CVN toughness values for the CCG zone of ES welds made
with wire A were between 27 and 61 ft.lbs., depending on process condi-
tions. Variations in process conditions caused changes in the weld form
factor which in turn altered the CCG inclination with the weld axis. The
variation in grain inclination is mainly responsible for the wide range
of average CVN toughness values. A linear relationship was observed
between the angle of grain inclination and the average CVN toughness
values, Figure 92. Caution must be exercised in interpreting these tough-
ness values since Charpy specimens accommodate only two or three grains
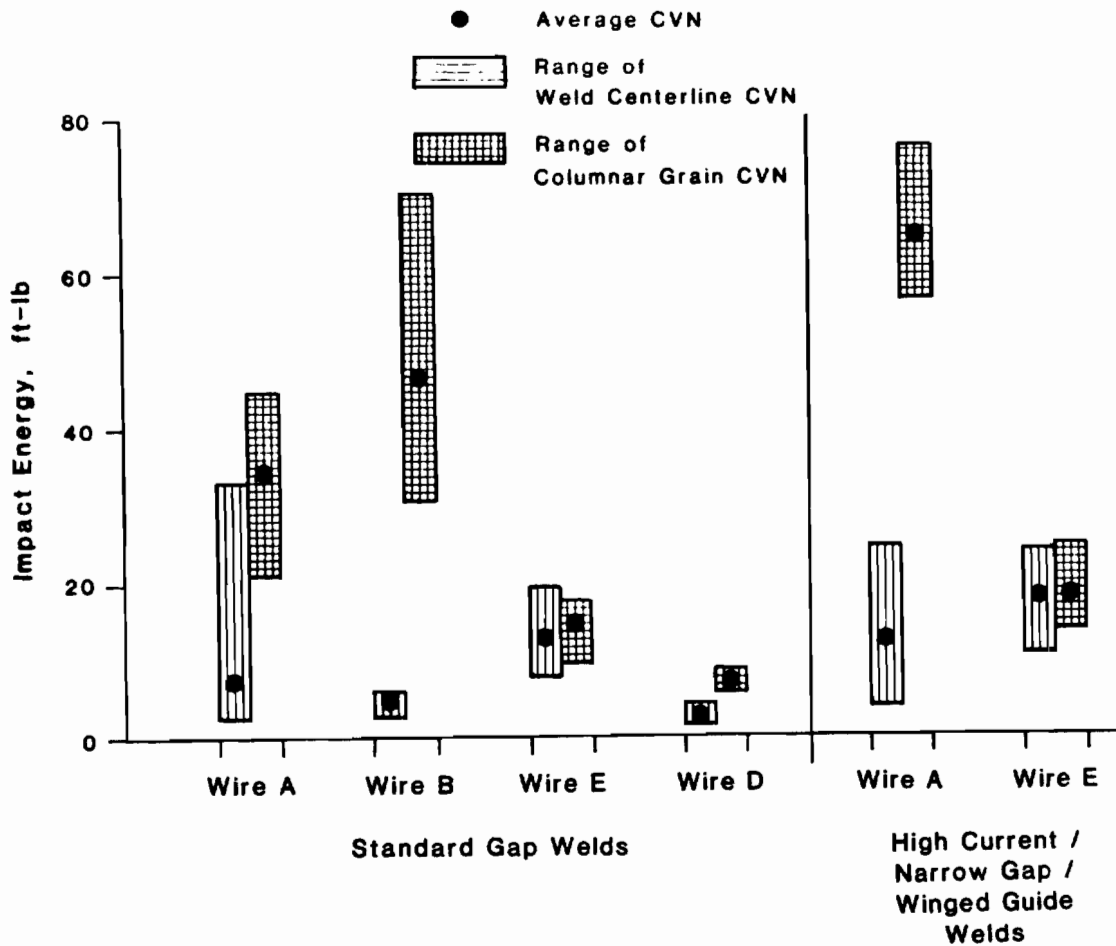
Figure 90. WCL AND CCG ZONE 0°F CVN TOUGHNESS DATA FOR ES WELDS
MADE USING VARIOUS FILLER WIRES. WIRE A—MILD STEEL,
WIRE B—A588, WIRE D—Mn,Mo, AND WIRE E—Cr,Mo.
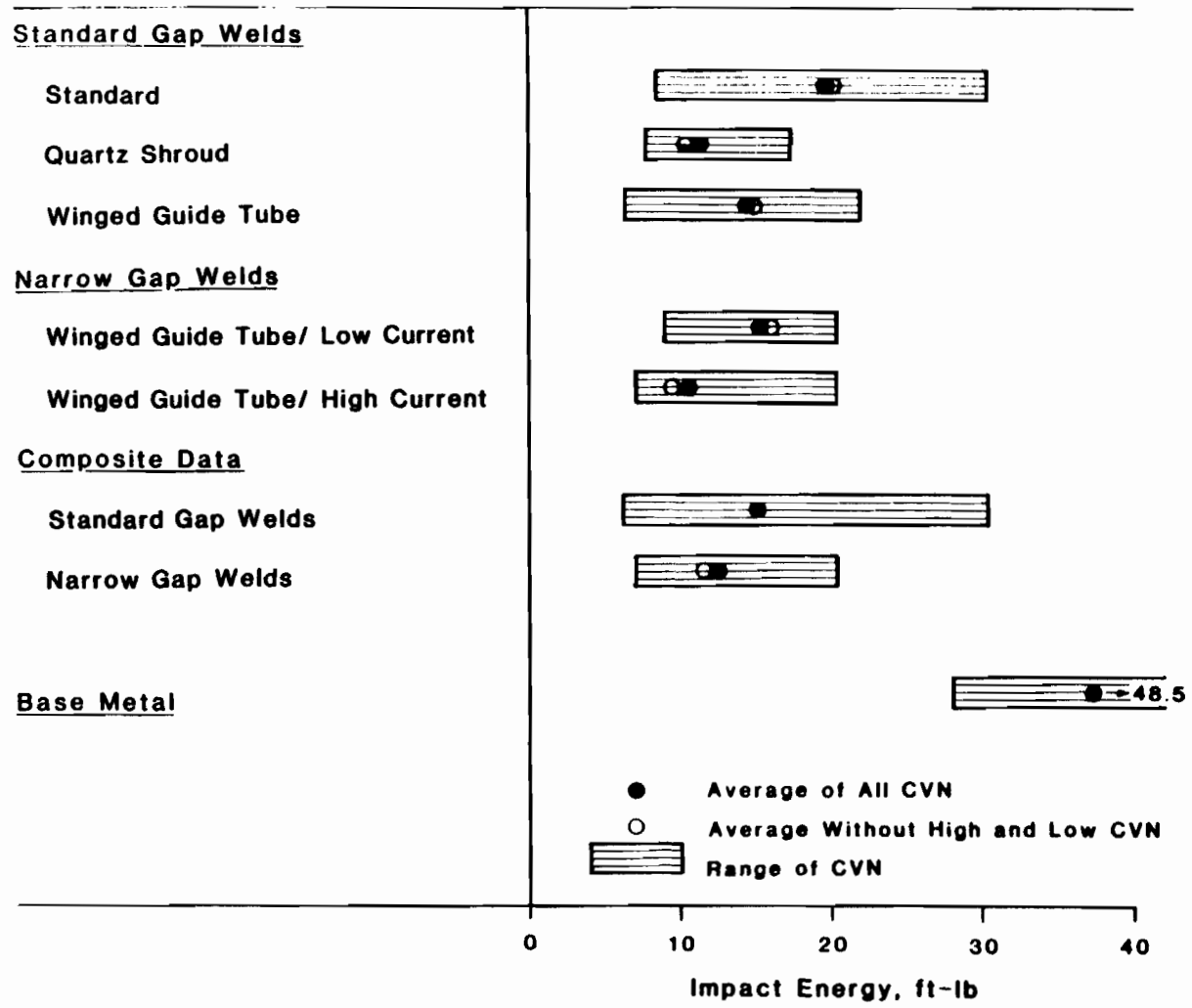
Figure 91. HAZ 0°F CVN TOUGHNESS DATA FOR VARIOUS ES WELDS PREPARED IN THE INVESTIGATION.
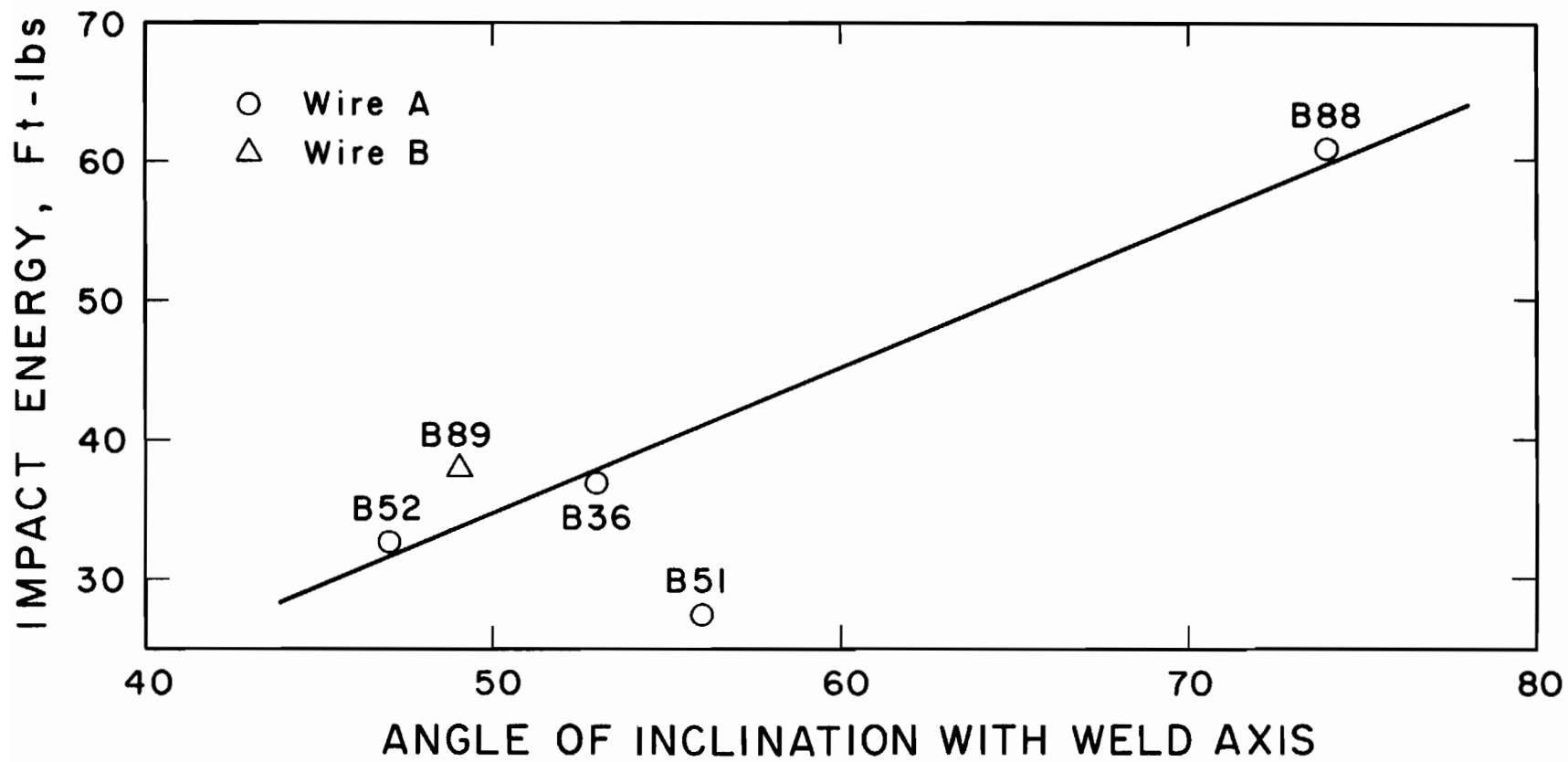
Figure 92. RELATIONSHIP BETWEEN THE ANGLE OF INCLINATION OF CCGS WITH WELD AXIS AND THE 0°F CVN TOUGHNESS IN ES WELDS.

across the fracture plane due to the unusual grain size. This may not represent the behavior of the weld zone under practical loading conditions. Larger fracture mechanics based specimens or full thickness dynamic tear specimens should be tested for proper toughness evaluation of the weld zone.

The average CVN toughness values for the WCL zone of ES welds made using wire A ranged from 4 to 11 ft.lbs. There is a wide difference between the CCG and WCL zone average toughness values. Culp[4] has suggested the difference in fracture morphology in these zones due to the directional weld microstructures to be responsible for the toughness variations. In WCL specimens, TCGs were aligned parallel to the crack propagation direction causing an intergranular failure along the brittle ferrite phase, whereas in CCG zone specimens, CCGs were inclined to the fracture plane causing transgranular failure and higher toughness values. Grain orientation, microstructure and impurity segregation at WCL led to a 4 ft.lbs. average CVN toughness in standard welds. On the other hand, the refined WCL grain structure in high current/narrow gap/winged guide welds achieved through lower specific heat input and faster cooling rates provided for 11 ft.lbs. average impact toughness.

In both standard and grain refined welds, prior austenite grain boundaries were decorated with proeutectoid ferrite films. The "quartz weld" contained more ferrite due to increased nucleation sites and silicon content of the weld metal. Several investigators have shown that proeutectoid ferrite films along grain boundaries are detrimental to

mechanical properties.[4,6,23,53] Thus, the advantages of the refined grains can be offset by increased proeutectoid ferrite. This accounts for the drop in toughness of the grain refined weld zone representative of the CCG zone in the standard weld. As-welded grain refinement also resulted in a 100% improvement in the average CVN impact toughness at the WCL as compared to the standard weld even though there were no apparent microstructural differences. The improvement should have occurred from the intense stirring action present in weld metal which limited the segregation at the weld center. In fact, uniform weld toughness was achieved throughout the entire fusion zone.

Welds made with elemental molybdenum additions possessed improved WCL average toughness values ranging between 9 and 14 ft.lbs. Elimination of proeutectoid ferrite along grain boundaries in alloy welds eliminated the least tough, intergranular crack paths, thus improving WCL toughness properties. The CCG average toughness values for these welds were between 14 and 19 ft.lbs., considerably lower than that of standard welds. Alloy additions generally increased the strength and the hardness of the weld metal. Therefore, with larger amounts of alloy additions, the improvement in weld toughness may be negated by increased weld metal hardness and strength. In CCG zone, fracture occurs in a transgranular mode. Therefore, even in the absence of proeutectoid ferrite along grain boundaries, the increased weld hardness decreased the CCG zone toughness compared to standard welds. In fact, a decreasing toughness trend was observed with increasing molybdenum content. Variations between the CCG and WCL average toughness values were considerably reduced.

Standard ES welds made using wire E (Cr-Mo) possessed 12 and 15 ft.lbs. average CVN impact toughness values for WCL and CCG zones, respectively. Again, the complete elimination of proeutectoid ferrite phase and the presence of a bainitic ferrite structure with finely dispersed carbides improved the WCL toughness, while the increase in the weld hardness limited the toughness of the CCG zone in which transgranular fracture occurred. The high current/narrow gap/winged guide tube made using wire E contained lower alloy contents than the standard wire E weld due to increased base metal dilution. This led to a slight reduction in weld metal hardness, while retaining the improved microstructure. As a result, both WCL and CCG average CVN toughness values were improved to 17 to 19 ft.lbs., respectively.

Both CCG and WCL zones of the standard weld made using wire B possessed toughness values comparable to that of the standard wire A weld. Microstructures of these welds were similar. Meanwhile, standard welds made using wire D possessed 3 and 7 ft.lbs. average CVN toughness values for WCL and CCG zones, respectively. Alloy additions in this weld were not sufficient to eliminate the proeutectoid ferrite phase. The severe drop in the CCG average toughness was not evident from the weld microstructure, however. Trace elements present in wire D may have caused the toughness decrease. Benter et al.[6] have reported elements such as arsenic to have an adverse affect on impact toughness. But, analyses of residual elements were not carried out in this investigation.

Ductile-brittle transition temperatures obtained from precracked CVN toughness data were well above 0°F for ES welds tested,(Table XIII).The SEM

Table XIII.

DUCTILE-BRITTLE TRANSITION TEMPERATURE OF ES WELDS AND BASE METAL

#	Weld ID	Welding Conditions	Transition Temperature °F (approximate)		
			WCL	CCG	HAZ
1	B36	Standard--cylindrical guide, 42 volts, 600 amps, 1-1/4" gap, wire A	80	40	80
2	B51	Winged guide, 36 volts, 700 amps, 1-1/4" gap, wire A	80	40	100
3	B52	Winged guide, 40 volts, 600 amps, 1-1/4" gap, wire A	60	40	100
4	B47	Quartz shielded guide, 48 volts, 600 amps, 1-1/4" gap, wire A	60	60*	80
5	Base Metal	--	——— 100 ———		

Note: *Weld metal adjacent to fusion line.

fractographic analyses of standard CVN specimens tested at 0°F also revealed a quasi cleavage fracture mode. However, transition temperatures of fusion zone were lower than that of base metal. As indicated by Pense et al.,[70] post-weld heat treatment would be necessary to decrease the transition temperature.

4.5. Overview and Recommendations for Future Work

The importance of plate grounding and electrode position in the joint gap on controlling the weld symmetry has been well established in this investigation. A technique for slag level maintenance during welding has been devised. Interrelationships between process variables, weld microstructure, and mechanical properties have been determined, Table XIV.

As-welded grain refinement provided a fairly uniform impact toughness for the entire fusion zone. Increase in the amount of proeutectoid ferrite should have restricted the toughness improvement in these welds. Alloy design considerations should effectively control the occurrence of proeutectoid ferrite films and enhance the toughness of these fine-grained zones. The WCL region of the grain refined welds had higher toughness as well as greater resistance to cracking than the conventional weld even though the microstructure did not show any significant differences. Further analyses of the fundamental solidification mechanisms and subsequent chemical segregation differences that may occur at the weld center, which is the last to solidify, are required in order to fully understand the

Table XIV.

SUMMARY OF ES WELD CHARACTERISTICS

Filler Electrode	Weld Zone	Characteristics	Weld Type		
			Standard Cyl. Guide (42V, 600A, 1-1/4" gap)	Narrow Gap/Wing Guide (40V, 1000A, 3/4" gap)	Quartz Shielded Guide (48V, 600A, 1-1/4" gap)
Wire A (mild steel)	WCL	CVN Tough.ft.lbs.	4	11	8
		Fracture Mode	Intergranular	Intergranular	Intergranular
		Microstructure	Continuous ferrite films	Discontinuous ferrite films	Continuous ferrite films (solute redistribution)
	CCG	CVN Tough.ft.lbs.	37	61	9
		Fracture Mode	Transgranular	Transgranular	Transgranular
		Microstructure	Coarse grains Inclined grains	Coarse grains Change in grain inclination	Refined grains Increased ferrite films
Wire E (Cr, Mo)	WCL	CVN Tough.ft.lbs.	12	17	
		Fracture Mode	Intergranular	Intergranular	
		Microstructure	Absence of ferrite films	Absence of ferrite films	
	CCG	CVN Tough.ft.lbs.	15	19	
		Fracture Mode	Transgranular	Transgranular	
		Microstructure	Coarse grains Harder weld	Coarse grains (limited) Harder weld	

WCL--weld centerline   CCG--coarse columnar grains   CVN--Charpy V-notch

underlying mechanisms responsible for the as-welded grain refinement and increased toughness in the WCL.

The quartz-guide tube shielding technique did not accommodate the use of a narrow joint spacing (3/4") without specially fabricated quartz shielding. The guide tube shielding technique required a higher welding voltage even while using a standard joint spacing (1-1/4") to preserve the side wall fusion. Its use in the narrow joint spacing led to slag freezing near the top of the pool terminating the process. Better shielding design of the winged guide tube assembly must also be developed in order to utilize the advantages of the winged guide tube design as well as the grain refinement.

The high current/narrow gap/winged guide ES welds made using wire E possessed 17 ft.lbs. WCL toughness. However, the alloy additions significantly increased the weld metal hardness, which decreased the average CCG toughness property. The minimum amount of alloy additions required to achieve the maximum improvement in weld microstructure and mechanical properties should be determined to limit the hardening effect, which can be achieved by welding with fabricated metal cored alloyed filler wires of suitable compositions.

The high current/narrow gap/winged guide welds resulted in a 50% reduction in the coarse grain HAZ width. However, the HAZ of those high speed welds possessed the least toughness of the entire joint and restricts their use in the as-welded condition. Efforts to improve the HAZ toughness properties should be made by modifying the base metal chemistry to prevent

prior austenite grain growth, and the Widmanstatten ferrite structure formation. Previous investigators have shown certain improvements through microprecipitation of titanium and aluminum nitrides,[80-81] and additions of rare earth metals and boron to aid fine ferrite formation.[82] With an improvement in HAZ toughness, the high current/narrow gap/winged guide tube/alloy additive ES welding technique should enable the safe use of ES welds in the as-welded condition.

5. SUMMARY AND CONCLUSIONS

1. Plate grounding and electrode position in the weld gap were criti-
cal in order to control the weld symmetry. Grounding of both
plates and positioning the electrode within 1/16 inch from the
geometric center of the joint gap provided a symmetrical weld about
the weld axis with equal penetration into both plates.

2. Proper slag level was required to control the process stability and
weld microstructure. Grain coarsening at the weld center was ob-
served with the use of a depleted slag pool (1/2 inch). On the
other hand, an excessive slag (3 inches and above) delayed the proc-
ess stabilization. A slag depth of 1-1/2 inches resulted in optimum
welding conditions.

3. Periodic current fluctuations caused by intermittent guide tube
melt off resulted in solute band formation.

4. Large fluctuations in welding voltage led to slag entrapment at the
fusion boundaries.

5. Winged guide tubes enabled lower welding voltages (34 to 36V) with
complete penetration, whereas the standard 1/2 inch diameter cylin-
drical guide tube required a minimum of 42V to achieve complete
side wall fusion.

6. Generally, narrow gap welds (3/4 inch) resulted in higher base metal
dilution than standard gap welds (1-1/4 inches). At any given

voltage, the narrow gap/winged guide tube welds possessed maximum base metal dilution, while the standard gap/cylindrical guide tube welds contained the minimum base metal contribution.

7. The welding current had minimal influence on base metal dilution of the weld.

8. The base metal dilution increased linearly with decreased joint spacing.

9. The joint spacing had minimum influence on the weld form factor.

10. The welding current vs. wire feed rate relationship was influenced by the guide tube design and joint spacing. For a given current value, narrow gap welds utilized lower wire feed rates compared to standard gap welds, and for a given current and joint spacing, winged guide tubes utilized lower wire feed rates than cylindrical guide tubes.

11. The welding current vs. wire feed rate relationship resulted in decreased filler melting efficiency using a narrow gap and winged guide tube. However, higher welding speeds were obtained using narrow gap for any current setting due to the reduced filler volume required.

12. Increased current was required with winged guide tubes to achieve a specific weld heat input reduction. This guide tube design also

eliminated the need for electrode oscillation during welding thicker
sections and minimized the errors involved in electrode positioning.

13. The high current/narrow gap/winged guide technique resulted in a
weld with a form factor of 1.3. No centerline cracking was observed.
A 50% reduction in specific heat input was achieved using this
technique, and the welding time was also reduced from 36 minutes
to 12 minutes. The coarse grained heat affected zone width was also
reduced by 50%, and the weld centerline microstructure was slightly
refined.

14. Combination of ceramic guide tube shielding and weld puddle mechani-
cal stirring resulted in a refined as-welded microstructure. The
use of a thin quartz shroud for guide tube shielding eliminated the
need for supplemental mechanical vibration to achieve the grain
refinement. The directed heat input towards the bottom of the slag
pool and intense stirring of the weld metal combined to produce grain
refinement.

15. Elemental molybdenum additions made through molybdenum rods welded
on to the guide tube eliminated the formation of proeutectoid ferrite
films bordering the prior austenite grain boundaries of standard
welds. The matrix structure was of a bainitic ferrite morphology.
However, the weld hardness increased considerably and severe alloy
segregation was observed.

16. Chromium and molybdenum additions through filler wire also eliminated the proeutectoid ferrite phase and gross segregation and produced a bainitic ferrite matrix structure. The weld hardness was considerably higher (28 R_C), but was slightly reduced (25 R_C) by using high current/narrow gap/winged guide tube technique to increase the base metal dilution.

17. Standard welds made using wire A possessed 4 and 37 ft.lbs. average CVN toughness at the WCL and CCG zones, respectively, at mid-thickness locations when tested at 0°F. Proeutectoid ferrite films bordering prior austenite grain boundaries and the grain orientation were responsible for the poor WCL toughness.

18. Standard welds, however, possessed 19 and 36 ft.lbs. CVN toughness at 0°F for the WCL and CCG zones, respectively, at quarter-thickness locations. These welds, therefore, would have met the American Welding Society D 1.1 Structural Code Requirements in spite of having poor toughness at mid-thickness WCL locations.

19. The high current/narrow gap/winged guide welds made with wire A possessed 11 and 61 ft.lbs. CVN toughness at 0°F at the mid-thickness WCL and CCG zones, respectively. The improved WCL toughness was due to a slightly refined microstructure.

20. A linear relationship was observed between the angle of inclination of CCGs with the weld axis and the CVN impact energy.

21. As-welded grain refinement improved the mid-thickness WCL toughness from 4 to 8 ft.lbs. at 0°F, whereas the toughness of the zone representative of the CCG zone of the standard weld dropped from 37 to 9 ft.lbs. at 0°F. Increase in proeutectoid ferrite content limited the CVN toughness in the weld metal.

22. Chromium and molybdenum additions improved the mid-thickness WCL toughness by three fold (12 ft.lbs. at 0°F). The mid-thickness CCG zone toughness, on the other hand, dropped to 15 ft.lbs. due to increased weld metal hardness. The high current/narrow gap/ winged guide welds made with this alloy wire possessed 17 and 19 ft.lbs. average CVN toughness for mid-thickness WCL and CCG zones, respectively, at 0°F.

REFERENCES

1. J. Skirinar: Metals Technical Conference, 1976, Sydney, Australia, International Institute of Welding, 1976.

2. A. L. Liby and D. L. Olson: Quarterly of the Colorado School of Mines, 1974, vol. 1, p. 41.

3. K. E. Dorschu, J. E. Norcross, and C. C. Gage: Welding J., Nov. 1973, vol. 52, 11, pp. 710.

4. J. D. Culp: Electroslag Weldments: Performance and Needed Research, Michigan Department of State Highways and Transportation, Lansing, September 1977.

5. B. E. Paton: Electroslag Welding, 2nd ed., AWS, New York, NY, 1962.

6. W. P. Benter: Acceptance Criteria for Electroslag Weldments in Bridges, Report 201, National Coop. Hwy. Res. Program, National Res. Council, 1979.

7. A. T. D'Annessa: Welding J., Dec. 1966, vol. 45, 12, pp. 569-s.

8. R. D. Thomas: Welding J., Feb. 1960, vol. 39, 2, pp. 111.

9. M. Solari and H. Biloni: Welding J., Sept. 1977, vol. 56, 9, pp. 274-s.

10. H. B. Cary: Portaslag Welding, Troy, Ohio, Hobart Brothers Tech. Center, 1970.

11. R. H. Frost, G. R. Edwards and M. D. Rheinlander: Welding J., Jan. 1981, vol. 60, 1, pp. 1-s.

12. M. G. Kozulin, A. P. Syatishev and V. V. Emel'Yanov: Welding Prod., 1969, 12, pp. 18.

13. J. E. Jones, D. L. Olson and G. P. Martins: Welding J., Sept. 1980, vol. 59, 9, pp. 245-s.

14. M. V. Nolan and R. L. Apps: Welding and Met. Fab., Nov. 1969, pp. 464.

15. M. V. Nolan: Founding, Welding, Production Eng., J., April 1970, pp. 14.

16. H. C. Campbell: Welding Res. Council Bulletin No. 154, Sept. 1970.

17. N. Iwamoto, J. Nose, Y, Naganawa, Y. Tsunawaki and Y. Makino: Trans. of Japan Welding Res. Inst., 1977, vol. 6, 1, pp. 23.

18. N. E. Andersen: Svetsaren, 1973, $\underline{1}$, pp. 9.

19. A. H. Dilawari, T. W. Eager and J. Szekely: Welding J., Jan. 1978, vol. 57, $\underline{1}$, pp. 24-s.

20. T. DebRoy, J. Szekely and T. W. Eager: Heat Generation Patterns and Temperature Profiles in ESW, Massachusetts Inst. of Tech., Cambridge, March 1980.

21. T. Narahari and B. A. Graville: Welding and Met. Fab., June 1976, pp. 350.

22. K. Watanabe, I. Sejima, S. Kokura, G. Taki and H. Miyake: Advanced Welding Technology, Tokyo, Japan Welding Soc., 1975, 1975, pp. 519.

23. E. E. Banks and J. Ritchie: Australian Welding J., Jan./Feb., 1975, pp. 7.

24. T. Kunihiro and H. Nakajima: Proceedings of "Significance of Defects in Welded Structures", Tokyo, Oct. 1973, Univ. of Tokyo press, 1974, pp. 105.

25. J. R. Mitchell, C. H. McGogney and J. Culp: Dunegan/Endevco Tech. Report DE 79-13, San Juan Capistrano, CA, March 1980, pp. 124.

26. G. I. Evstratov: Welding Prod., 1979, $\underline{6}$, pp. 43.

27. B. M. Patchett: Vertical Welding Efficiently with the Consumable Guide Electroslag Process (tech. paper), Soc. of Manufacturing Eng., 1974, AD74-407.

28. V. Vaidya, W. Coulter and B. A. Graville: Welding and Met. Fab., June 1976, pp. 345.

29. A. Ujiie, S. Sata, S. Sakai, and A. Hamanaka: Advanced Welding Technology, Tokyo, Japan Welding Soc., 1975, pp. 543.

30. Y. Ito, M. Ikeda, N. Yamauchi and J. Furuichi: Advanced Welding Technology, Tokyo, Japan Welding Soc., 1975, pp. 513.

31. B. M. Patchett, F. W. Collins and D. Timpson: Cranfield Inst. of Tech., Memo No. 72, June 1972.

32. A. Haslam, R. L. Apps and B. M. Patchett: In "Advances in Welding Process", 3rd International Conf., Harrogate, 1974, pp. 47.

33. R. B. Turpin: M. S. thesis, Oregon Graduate Center, Beaverton, Oregon, 1981.

34. I. I. Sushchuk-Slyusarenko, et. al: Aut. Welding, 1974, $\underline{2}$, pp. 49.

35. G. R. Edwards and R. H. Frost: Report No. DOE/ET/12313-T1, Colorado School of Mines, Golden, Colorado, Sept. 1980, pp. 138.

36. K. R. Venkataramaiah: M. S. Thesis, University of Toronto, 1967.

37. Yu. V. Sharapov: Welding Prod., 1967, 7, pp. 38.

38. E. M. Kuzmak and M. S. Skuditskii: Welding Prod., 1975, vol. 22, 6, pp. 39.

39. A. N. Khakimov, et al.: Welding Prod., 1974, 1, pp. 39.

40. S. A. Smirnov and L. A. Efimenko: Aut. Welding, 1973, 9, pp. 45.

41. F. Eichhorn and P. Hirsch: DVS-BERICHTE, 1974, 31, pp. 37.

42. F. Eichhorn, P. Hirsch, W.-G. Burchard and F.-S. Chen: Schweissen Und Schneiden, 1976, vol. 28, 6, pp. 210.

43. R. G. Garlick and J. F. Wallace: American Foundrymen's Soc. Trans., 1959, vol. 67, pp. 366.

44. A. H. Freedman and J. F. Wallace: Foundry, Nov. 1957, vol. 85, pp. 578.

45. M. D. Coward: J. of Iron and Steel Inst., Aug. 1973, pp. 586.

46. I. P. Trochun and V. P. Chernysh: Welding Prod., 1965, 11, pp. 6.

47. P. G. Shmidt: Steel in the USSR, 1977, (4), pp. 216.

48. Magnetic Stirring of Aluminum Weld Metal: Current Awareness Bulletin, 1979.

49. G. V. Sutyrin: Russian Metallurgy, 1974, (4), pp. 84.

50. H. S. Marr: Iron and Steel International, Feb. 1979, pp. 29.

51. D. C. Brown, F. A. Crossley, J. F. Rudy and H. Schwartzbart: Welding J., June 1962, vol. 41, 6, pp. 241-s.

52. J. Campbell: International Metal Review, 1981, No. 2, pp. 71.

53. I. Sijima, H. Kita, T. Rokutani and T. Wada: Advanced Welding Tech., Tokyo, Japan Welding Soc., 1975, pp. 537.

54. R. L. Apps and E. Smith: In Proc. "Weldability of Heightened and High Stg. Metals", May 1974, Zagreb, Yugoslavia, Assoc. of Yugoslav Welding Soc., Yugoslavia, pp. 163.

55. L. A. de Vedia and B. M. Patchett: Welding and Met. Fab., Jul/Aug. 1977, pp. 365.

56. B. M. Patchett, F. W. Collins and R. L. Apps: In Conf. on Welding Low Temp. Containment Plant, Nov. 1973, London, The Welding Inst., Cambridge, 1973, pp. 117.

57. R. E. Dolby: In Proc. "Mechanic & Physics of Fracture", Jan. 1975, Cambridge, Metals Soc., 1975, pp. 95.

58. Y. Kawaguchi, Y. Yamaguchi, G. Ohtani and S. Watanabe: The Sumitomo Search No. 20, Nov. 1978.

59. B. I. Medovar, L. V. Chekotilo, S. I. German: Welding Prod., 1965, 9, pp. 58.

60. E. Pikna: Zvaranie, 1977, 26, (4), pp. 105.

61. H. Suzuki, et al.: U.S. Patent 3,352,993, (Feb. 7, 1966).

62. Consumable Nozzle Type ESW Process Using Flux Cored Wire, Nippon Steel Corporation, Japan, pp. 105.

63. L. Muncner: Proceedings N.Y., Amer. Soc. Mech. Eng., 1973. Pt. II: Materials, Fabrication & Inspection, paper II-82, pp. 1121.

64. E. Mryka: Aut. Welding, 1974, 1, pp. 23.

65. S. S. Tuliani, K. S. Probert and A. H. Briscoe: In Proc. "Welding & Fab. in the Nuclear Ind.", Apr. 1979, London, British Nuc. Energy Soc., 1979, pp. 327.

66. M. G. Dawes: Welding International Research & Development, 1971, 1, vol. 4.

67. C. E. Jackson: Welding Res. Council Bulletin No. 190, Dec. 1973.

68. D. N. Shakleton: Progress Report, E/59/75, The Welding Inst., Cambridge, Britain, March 1975.

69. D. N. Shakleton: Report 73/1978/PE, The Welding Inst., Cambridge, Britain, Oct. 1978.

70. A. W. Pense, J. B. de S. Ramos and R. D. Stout: Welding J., Jan. 1976, vol. 55, 1, pp. 1-s.

71. K. Matsumoto and K. Takai: Tetsu-tor Hagane (J. of The Iron and Steel Inst. of Japan), June 1978, vol. 64, 7, pp. 141.

72. V. A. Soroka: Aut. Welding, 1979, 10, pp. 30.

224.

73. J. F. Lowery: Report P/32/68, The Welding Inst., Cambridge, Britain, July 1968).

74. S. Shankar: Ph.D. Thesis, Oregon Graduate Center, Beaverton, Oregon, 1982.

75. D. S. Clark and W. R. Varney: Physical Metallurgy for Engineers, 2nd ed., D. Van Nostrand Company, New York, 1963.

76. E. C. Bain and H. W. Paxton: Alloying Elements in Steel, 2nd ed., ASM, Ohio, 1966.

77. R. W. K. Honeycombe: Met. Sci., June 1980, vol. 14, 6, pp. 201.

78. J. V. Bee and R. W. K. Honeycombe: Met. Trans., 1978, 9A, pp. 587.

79. Structural Welding Code--Steel, D 1.1-80, AWS, New York, 1980.

80. S. V. Egorova, L. I. Adeeva, B. B. Vinokur, L. V. Khaustova and E. V. Denisevich: Aut. Welding, 1979, 10, pp. 11.

81. S. Kanazawa, A. Nakashima, K. Okamoto and K. Kanaya: Trans. of Iron and Steel Inst. of Japan, 1976, vol. 16, pp. 486.

82. T. Kunakoshi, T. Tanaka, S. Ueda, M. Ishikawa, N. Koshizuka and K. Kobayashi: Trans. of Iron and Steel Inst. of Japan, 1977, vol. 17, pp. 419.

CONVERSION TABLE

1 inch   = 25.4 millimeters

1 micrometer (μm)   = 10^{-6} meters

1 pound (lb.)   = 453.6 grams

1 calorie   = 4.184 Joules

1 foot pound   = 1.3558 Joules

1 Watt Hour   = 3600 Joules

Degree C   = (Degree F – 32) 5/9

Degree F   = (Degree C x 1.8) + 32

Appendix I

HEAT INPUT CALCULATION FOR ES WELDS

The specific heat input for an ES weld is determined from the relation,

$$\text{specific heat input} = \frac{E \times I}{v} \text{ Kilojoules/millimeter}$$

where E is the welding voltage in volts, I is the welding current in amperes, and v is the welding speed expressed in millimeter/second.

For a two-foot long ES weld made using 42 volts and 600 amps over a period of 36 minutes,

$$\text{specific heat input} = \frac{42 \times 600}{(2 \times 25.4)/(36 \times 60)} = 89.3 \text{KJ/mm}.$$

BIOGRAPHICAL NOTE

Srivathsan Venkataraman was born November 23, 1953, in Madras, India. He graduated from P.S. High School, Madras, India, in 1969. He received his Bachelor of Science degree in Chemistry in 1973 from Madras University, Madras, India, and his Bachelor of Engineering degree in Metallurgy in 1976 from Indian Institute of Science, Bangalore, India. He joined the Oregon Graduate Center in the Fall of 1976, and finished the requirements for the degree of Doctor of Philosophy in Materials Science in November, 1981.